Wireless Communication onboard Spacecraft

Draadloze Communicatie aan boord van Ruimtevaartuigen

Amini, Rouzbeh

DOI
10.4233/uuid:ef88dac7-d007-44ae-a48a-f134d6a95cf2

Publication date
2016

Document Version
Final published version

Citation (APA)
Amini, R. (2016). *Wireless Communication onboard Spacecraft: Draadloze Communicatie aan boord van Ruimtevaartuigen.* [Dissertation (TU Delft), Delft University of Technology].
https://doi.org/10.4233/uuid:ef88dac7-d007-44ae-a48a-f134d6a95cf2

Important note
To cite this publication, please use the final published version (if applicable).
Please check the document version above.

Wireless Communication onboard Spacecraft

Rouzbeh Amini

Draadloze Communicatie aan boord van Ruimtevaartuigen

PROEFSCHRIFT

ter verkrijging van de graad van doctor
aan de Technische Universiteit Delft,
op gezag van de Rector Magnificus prof. ir. K.C.A.M. Luyben,
voorzitter van het College voor Promoties,
in het openbaar te verdedigen

op dinsdag 6 september 2016 om 15:00 uur

door

Rouzbeh AMINI
Elektrotechnisch Ingenieur,
Master of Science aan de Aalborg Universiteit, Denemarken
geboren te Ahvaz, Iran

This dissertation has been approved by the promotors:
Prof. dr. E.K.A. Gill *and*
Prof. dr. ir. G.N. Gaydadjiev

Composition of the doctoral committee:

Rector Magnificus	
Prof. dr. E.K.A. Gill,	Delft University of Technology (NL), promotor
Prof. dr. ir. G.N. Gaydadjiev,	Imperial College London (UK), promotor
Independent members:	
Prof. dr. ir. M.H.G. Verhaegen,	Delft University of Technology (NL)
Prof. dr. D.G. Simons,	Delft University of Technology (NL)
Prof. dr. A.V. Veidenbaum,	University of California (USA)
Ir. J. Leijtens,	Lens R&D (NL)
Prof. dr. ir. J.A. Mulder,	Delft University of Technology (NL), reserve member

CIP-DATA KONINKLIJKE BIBLIOTHEEK, DEN HAAG

Amini, Rouzbeh
Wireless Communication onboard Spacecraft
Delft: Technische Universiteit Delft, Faculteit Luchtvaart- en Ruimtevaarttechniek, Afdeling Space Systems Engineering.
Thesis Technische Universiteit Delft. - With index, ref. - With summary in Dutch.
ISBN 978-94-6186-708-7
NUR-code 910
Subject headings: onboard wireless communication, onboard energy management.

This research was funded by *MicroNed program* managed by the Dutch government.

Printed by Uitgeverij BOXPress, Vianen, The Netherlands. First printing, August 2016.
This document has been typeset in LaTeX.

To my Parents

Samenvatting

Dit proefschrift richt zich op draadloze communicatie in ruimtevaartuigen als een oplossing voor het verminderen van de hoeveelheid bekabeling in ruimtevaartuigen. Ondanks de buitengewone vooruitgang in de lucht- en ruimtevaart zijn de kosten om een vaartuig in de ruimte te brengen nog steeds zeer hoog en is de hoeveelheid ingenieurswerk om ruimtevaartuigen te ontwerpen en te ontwikkelen enorm. De belangrijkste elementen die de ontwikkelings- en lanceerkosten van een ruimtevaartuig verhogen zijn de omvang, de massa en de noodzaak van een voor iedere missie op maat gemaakt ontwerp. Onderzoeken tonen aan dat het aandeel van on-board bekabeling in de massa van het ruimtevaartuig ongeveer 6% tot 10% bedraagt. Iedere poging om de bekabeling te verminderen kan direct leiden tot verlaging van de lanceerkosten en tot een flexibeler en meer modulair ontwerp.

Dit proefschrift tracht een antwoord te geven op de volgende vragen:

1. Welke problemen zijn inherent aan ingebouwde bedrade standaarden en wat zijn de voordelen en kenmerken van een draadloos netwerk in een ruimtevaartuig?
2. Welke subsystemen in ruimtevaartuigen zouden vooral kunnen profiteren van een draadloos on-board communicatieparadigma?
3. Wat is de grootste uitdaging met betrekking tot het gebruik van een draadloze standaard aan boord van ruimtevaartuigen?
4. Hoe kunnen we de aanwijsbare uitdaging van een ontwerp op systeemniveau oplossen?

Voor een antwoord op deze vragen worden in dit proefschrift de bestaande bedrade databusstandaarden in ruimtevaartuigen en grote commerciële kant-en-klare (COTS) draadloze communicatieoplossingen beoordeeld om de architectuur ervan vast te stellen en te karakteriseren. Deze draadloze standaarden zijn Wi-Fi, Bluetooth en ZigBee. Het karakteriseren van verschillende

on-board gegevenstypen helpt bij het bepalen van een geschikte COTS draadloze communicatieoplossing voor alle soorten toepassingen. Vooral sensoren voor standbepalings- en controlesystemen (ADCS) kunnen enorm profiteren van een energiezuinige draadloze communicatieoplossing met een lage transmissiesnelheid, zoals ZigBee. Maar de grootste uitdaging is de vermindering van het energieverbruik van sensoren om een draadloze architectuur mogelijk te maken en de levensduur van accu's te optimaliseren zonder de prestaties van het systeem te beïnvloeden.

Dit proefschrift stelt twee ingebouwde, op basis van sensor planningsschema's werkende energiemanagers voor om de uitdaging op het gebied van energiebesparing aan te pakken. Deze oplossingen zijn afgestemd op ADCS-sensoren en hebben als doel het totale ADCS energieverbruik te verlagen zonder de nauwkeurigheid van standbepaling te beïnvloeden. Beide energiemanagers maken gebruik van vergelijkbare ontwerpelementen en beslissingsalgoritmes, maar een ervan geeft een gecentraliseerd schema weer en de ander maakt gebruik van een gedecentraliseerde architectuur. Een uniek kenmerk van deze ontwerpen is dat de energiebeheeroplossing volledig is geïntegreerd met het on-board standbepalingssysteem van het ruimtevaartuig. Uit de resultaten van een simulatie blijkt dat het inzetten van energiemanagers een totale energiebesparing oplevert van 20.9% tot 51% (afhankelijk van het scenario) zonder de nauwkeurigheid van standbepaling te beïnvloeden.

Abstract

This dissertation focuses on intra-spacecraft wireless communication as a solution for reducing the spacecraft onboard harness. Despite outstanding advances in aerospace industry, the cost of accessing space is still very high and the amount of engineering work required for spacecraft design and development is enormous. The key elements which increase the development and launch cost of a spacecraft are size, mass, and the necessity of a tailored design for each mission. Studies show that the contribution of onboard harness to spacecraft mass is about 6% to 10%. Any effort to reduce harness can directly result in reducing the launch cost and arriving to a more modular and flexible design.

This thesis aims to answer the following questions:

1. What are the problems of onboard wired standards and what are the benefits and characteristics of wireless network onboard spacecraft?
2. Which spacecraft subsystems could benefit most from a wireless onboard communication paradigm?
3. What is the major challenge regarding employing a wireless standard onboard a spacecraft?
4. How can we solve the identified system level design challenge?

To answer these questions, this dissertation reviews the existing wired spacecraft data bus standards and major commercial off the shelf (COTS) wireless communication solutions to identify and characterize their architectures. These wireless standards are Wi-Fi, Bluetooth and ZigBee. Categorizing different onboard data types aids to identify a suitable COTS wireless communication solution for each application category. Specifically, sensors of attitude determination and control system (ADCS) can greatly benefit from a low power and low data rate wireless communication solution such as ZigBee, however, the major challenge is conserving energy on the sensors to enable a wireless

architecture and achieve an adequate battery life without compromising the system performance. This dissertation proposes two onboard energy managers based on sensor scheduling schemes to tackle the energy conservation challenge. These solutions are tailored to ADCS and aim to reduce the overall ADCS energy consumption without affecting the required accuracy of attitude determination. Both energy managers use similar design elements and decision making algorithms while one of them presents a centralized scheme and the other one employs a decentralized architecture. A unique characteristic of these designs is that the energy management solution is fully integrated with the onboard attitude determination system of the spacecraft. Simulation results show that enabling the energy managers result in total energy saving between 20.9% to 51% (depending on the scenario) without compromoising accuracy of attitude determination.

Acknowledgement

This thesis is the result of my work at the Chair of Space Systems Engineering at the Faculty of Aerospace Engineering of Delft University of Technology.

One of the joys of completion is to look and remember all the friends and family who have helped and supported me along this long but fulfilling road.

I would like to express my heartfelt gratitude to Prof. Dr. Eberhard Gill and Prof. Dr. Georgi Gaydadjiev who were not only promoters and mentors but dear friends. I could not have asked for better role models. They were both very inspirational, supportive, and extremely patient.

I would also like to thank my examiners. Reviewing a PhD dissertation is no easy task, and I am grateful for their thoughtful and detailed comments.

This thesis was funded by The MicroNed program which is a huge research program managed by the Dutch government aiming at investments to improve and strengthen the knowledge infrastructure of the Netherlands. I would like to thank this organization for their generous support.

Next, I wish to thank the other people who made this work directly possible. I would like to thank Dr. Wim Jongkind who made this research possible by accomplishing the MISAT cluster proposal within the MicroNed program. I would like to give my special thanks and regards to Robbert Hamann whose help really made a difference for me in many occasions, and Barry Zandbergen for always being available to listen to me when I was feeling frustrated. Thanks to Geert Brouwer, Arash Noroozi and Daan Maessen who shared a room with me during past years and Hans Kuiper who motivated me directly or indirectly in several occasions to accelerate my work. Other colleagues without the help of whom this work would have not been the same are Jasper Bouwmeester, Prem Sundaramoorthy, Rui Sun, Steven Engelen and Debby van der Sande at the SSE chair. I want to specially mention Paolo Massioni, Napoleon Cornejo, Arvin Emadi, Wouter Jan Ubbels, Amir Agah, Kamran Souri, Gerard Aalbers, Ali Bahrami Sharif, Dan Torczynski, Stefan Brak and my fellows at the Computer Engineering laboratory of TU Delft, specially Marius Enachescu.

To the staff and students at ACCESS Linnaeus Center of KTH University in Stockholm specially Prof. Dr. Karl-Henrik Johansson, I am grateful for the chance to visit and be a part of the laboratory team during Summer 2010. Thank you for welcoming me as a friend and helping me to develop the ideas in this thesis.

I would not have contemplated this road if not for my parents, Nahid and Mohammad, who instilled within me a love of creative pursuits, science and language, all of which finds a place in this thesis. To my parents, thank you. My siblings, Laleh and Zhaleh, have also been the best of friends along this journey.

Rouzbeh Amini

Contents

List of Tables

List of Figures

Standard Notations

Standard notation developed and used through the dissertation is given below.

Type Styles

A scalar is denoted by capital or lowercase italic face	q
A vector is denoted by lowercase bold and italic face	$\boldsymbol{q}$
A quaternion is denoted by bold Sans-serif non-italic face with a curved arrow on top	$\mathbf{q}$
A matrix is denoted by capital bold and non-italic face	$\mathbf{M}$
A unit vector is denoted by bold San-serif non-italic face	$\vec{\mathbf{n}}$
A basis unit vector of a frame $\mathfrak{A}$ is denoted by bold Sans-serif non-italic	${}^{\mathfrak{A}}\vec{\mathbf{e}}$
A unit vector or vector in reference frame $\mathfrak{A}$ is denoted by	${}^{\mathfrak{A}}\boldsymbol{v}, {}^{\mathfrak{A}}\mathsf{v}$
A map from reference frame $\mathfrak{B}$ to reference frame $\mathfrak{A}$ is denoted by quaternion or a matrix	${}^{\mathfrak{A}}_{\mathfrak{B}}\mathbf{q}, {}^{\mathfrak{A}}_{\mathfrak{B}}\mathbf{A}$

Abbreviations

ADCS	Attitude Determination and Control System
ADS	Attitude Determination System
AFF	Autonomous Formation Flying
AIT	Assembly, Integration and Test
AOCS	Attitude and Orbital Control Systems
APSS	Active Pixel Sun Sensor
AWGN	Additive White Gaussian Noise
BC	Bus Controller
BM	Bus Monitor
BO	Beacon Order

BVDI	Balanced Voltage Digital Interface
CAN	Controller Area Network
CAS	Contention Access Period
CCK	Complementary Code Keying
CCSDS	Consultative Committee for Space Data Systems
CDHS	Command and Data Handling System
CDMU	Central Data Management Unit
CFP	Contention Free Period
CMOS	Complementary Metal-Oxide Semiconductor
COTS	Commercial Off-The-Shelf
CSMA-CA	Carrier Sense Multiple Access with Collision Avoidance
CSMA-CD	Carrier Sense Multiple Access with Collision Detection
DC	Direct Current
ECI	Earth Centered Inertial
ECEF	Earth Centered Earth Fixed
EDR	Extended Data Rate
EKF	Extended Kalman Filter
EMC	Electromagnetic Compatibility
EMI	Electromagnetic Interference
EPS	Electrical Power System
ESA	European Space Agency
FF	Fill Factor
FFD	Full-Function Device
FHSS	Frequency Hopping Spread Spectrum
FPGA	Field Programmable Gate Arrays
Gbps	Giga bit per Second
GFSK	Gaussian Frequency Shift Keying
GPS	Global Positioning System
GOCI	Gravity field and steady-state Ocean Circulation Explorer
GTS	Guaranteed Time Slot
ICB	Instrument Control Bus
IEE	Institution of Electrical Engineers
IEEE	The Institute of Electrical and Electronics Engineers
IGRF	International Geomagnetic Reference Field
INTA	Institute for Aerospace Technique of Spain
ISO	International Organization for Standardization
ISS	International Space Station
Kbps	Kilo bit per Second
LAN	Local Area Network
LEO	Low Earth Orbit
LQR	Linear Quadratic Regulator
MAC	Media Access Control
MACS	Modular Attitude Control System

MANET	Mobile Ad hoc Network
MAS	Manipulator Arm System
MAE	Mean Absolute Error
Mbps	Mega bit per Second
MEMS	Micro Electro Mechanical Systems
NASA	National Astronautic and Space Administration
NLR	Nationaal Lucht- en Ruimtevaartlaboratorium
NORAD	North American Aerospace Defense
OBC	Onboard Computer
OBDH	Onboard Data Handling
OFDM	Orthogonal Frequency Division Multiplexing
OQPSK	Offset Quadrature Phase-shift Keying
OWLS	Optical Wireless Links for Intra-spacecraft Communications
OWSAN	Onboard Wireless Sensor and Actuator Network
PAN	Personal Area Network
PLME-ED	Physical Layer Management Entity - Energy Detection
PnP	Plug and Play
PTU	Power Transfer Unit
PVDF	Polyvinylidene Fluoride
RF	Radio Frequency
RFID	Radio Frequency Identification
RMSE	Root Mean Square Error
RFD	Reduced Function Device
RT	Remote Terminal
RTD	Resistance Temperature Detector
SAE	Society of Automotive Engineers
SCB	Spacecraft Body
SDST	Small Deep-Space Transponder
SEU	Single Event Upset
SGP4	Standard General Perturbations Satellite Orbit Model 4
SNR	Signal to Noise Ratio
SO	Super-frame Order
SOC	System on Chip
TAS	Thales Alenia Space
TCEU	Thermal Control Electronics Unit
TCP	Transmission Control Protocol
TDMA	Time Division Multiple Access Schemes
TLE	Two Line Elements
TSB	Telecommunication Support Board
UDP	User Datagram Protocol
USD	United States Dollar
VIIRS	Visible/Infrared Imaged and Radiometer Suite
WPAN	Wireless Personal Network

WSAN	Wireless Sensor and Actuator Network
WSN	Wireless Sensor Network

Chapter 1

Introduction

I do not think that the wireless waves I have discovered will have any practical application.

– Heinrich Rudolf Hertz[1]

The recent advancements in electronics and micro technologies have provided the possibility of creating miniature and intelligent units which can improve the modularity and reconfigurability of spacecraft onboard architectures. Smart use and integration of these units can ease spacecraft integration and decrease the development and launch costs. These potentials trigger the need to re-think the design process and the architecture of onboard systems and components. The challenge is to solve the associated problems of employing new technologies without compromising spacecraft performance.

The scope of this thesis is to study the possibilities and challenges of using a commercial-off-the-shelf (COTS) wireless standard as a tool for reducing spacecraft mass and increasing design flexibility. Furthermore, the objective is to formulate a system level solution which implements an energy efficient approach for onboard wireless sensors and verify it.

1.1 Motivation

Space activities have gradually developed into a multi-billion dollar business with steadily growing number of applications such as communication, navigation and earth observation. Despite outstanding advances in aerospace

[1] Heinrich Rudolf Hertz (Feb. 22, 1857 - Jan. 1, 1894) a German physicist who clarified and expanded the electromagnetic theory of light and devised a transmitting oscillator radiating electric waves.

Table 1.1: Average price per pound (USD) for Low Earth Orbit (LEO) launch vehicles by year 2000 [Futron Corp. 2002, Thorpe and Labs 2009]

Launch vehicle	Country	Launch capacity [kg]	Total launch cost [USD]	Payload cost yr 2000 [USD/kg]	Payload cost yr 2007 [USD/kg]
Cosmos	Russia	1485	13M	8666	8888
Dneper	Russia	4361	15M	3406	4723
Delta 2	USA	5098	55M	10679	8184
Soyuz	Russia	6938	37.5M	5350	5962
Atlas 2AS	USA	8542	97.5M	11300	N/A
Long March 2E	China	91194	50M	5427	N/A
Ariane 44L	Europe	10106	112.5M	11015	N/A
Zenit 3SL	Multinational	15736	85M	5348	4591
Ariane 5G	Europe	17842	165M	9156	8116
Proton	Russia	19586	85M	4297	3326

industry, the cost of accessing space and Low Earth Orbit (LEO) is still very high and the amount and complexity of engineering work required for spacecraft design and development is enormous. The high cost is due to several reasons. The key elements which increase the development cost of a spacecraft are size, mass and the necessity for a tailored design for each mission. Table 1.1 compares average price per kilogram for different launch vehicles by year 2000 and 2007. The information indicates that although the non-western launchers are significantly cheaper, the overall launch cost has not significantly decreased over time at least for the most of the launchers. A simple calculation shows that launch cost of a 100 kg micro-satellite exceeds 500,000 USD if a western launcher is used. Traditionally, spacecraft are built according to the requirements of their particular mission. As a consequence the designed units can not be reused for other missions without major modifications. Each mission presents a set of unique requirements that have to be met by the design team. The concepts of a plug-and-play architecture or reconfigurable design are not considered in traditional spacecraft design [Miler et al. 2002]. The solution for a basic problem such as data interfacing between subsystems is generally approached by redesigning the interfaces one by one, careful cable routing, extensive considerations for electromagnetic compatibility/interference (EMC/EMI), allocating necessary shields and mounting hundreds of meters of cables to practice the connections between units. For example, the Cassini spacecraft (the orbiter) which was 6.8 meters high and about 4 meters wide, had a mass of 2150 kilograms and more than 1630 interconnected electronic components, 22000 wire connectors and more than 12 kilometers of cabling [Meltzer 2015]. If we assume that each meter of cabling including shields and connectors has a mass of about 20 grams[1], we

[1] This is a valid assumption for MIL-STD-1553b bus cables.

Table 1.2: Harness mass relative to spacecraft dry mass [Magness 2003].

Spacecraft	Dry mass [kg]	Harness mass [kg]	Proportion [%]
Envisat	8500	850	10.0
GOCE	740	60	8.0
Cluster II	540	33.4	6.2
MarsExpress	450	28	6.2
SMART-1	280	22.1	8.0
Proba	100	7.6	7.6

can conclude that only cabling accounted for about 240 kilograms of Cassini spacecraft's mass with cost of about 1.5 million USD. Table 1.2 presents similar information for other space vehicles.

During the past years, space agencies such as ESA and NASA have taken steps for reusing parts of a design and moving toward modular plug-and-play architectures. For example, the INTEGRAL spacecraft reused parts of XMM Newton vehicle and Mars Express spacecraft has used some designs which were made for the Rosetta mission. Considering the reduction of the space exploration budget in USA and Europe, certainly the future trend of space vehicle development will target employing lighter and more intelligent units to achieve lower mission cost by reducing the required development time and the overall spacecraft volume and mass [Smith et al. 2003].

Furthermore, as spacecraft systems become smaller in volume and mass, the wiring harness and connectors become a dominant limiting factor in miniaturizing spacecraft units. This trend is not limited to spacecraft only but it is also evident in other application areas where micro systems technology is applied. In general, architecture paradigm shifts are taking place which will require a major rethinking of design methodologies in the future. Traditionally, most architectures were and are integral product architectures. They feature a close coupling among the different elements and modules. The elements are in a close spatial proximity, perform many integrated functions, require a central device to control them, and are tightly synchronized. Examples of such architectures are found in spacecraft, airplanes, medical applications and cars. A modular and plug-and-play scheme requires to rethink the system architecture towards a decentralized, reconfigurable and scalable solution. It is believed that using wireless communication can vastly contribute to realizing an architecture for a modular plug-and-play spacecraft bus. This technology can contribute to mass reduction, maximizing reuse of components, easy integration, enabling a scalable design, and reconfiguring spacecraft for a multitude of tasks and missions. Furthermore, it can be an important step in enabling

new perspectives in developing fractionated spacecraft[2], inflatable space structures, swarm of femto-satellites, satellite on chip and even fly-by wireless for aircrafts [Gill et al. 2010, Sundaramoorthy et al. 2010].

1.2 Contribution to the Field

Academic research around employing wireless technology onboard spacecraft has become interesting a decade ago. In 2003, ESA and NASA started co-organizing a work-group to sponsor a number of young industrial and academic activities [Magness et al. 2004]. This activity was later merged into Consultative Committee for Space Data Systems (CCSDS). Since then, various research activities were conducted by space agencies, industry and academy to evaluate the potential applications and to solve the related challenges. Examples of these researches are numerous e.g. [Wilson and Juarez 2014, Wilson and Atkinson 2013, CCSDS Secretariat 2013].

In this section, first we will review the most relevant results in the field and then we will define the objectives of this thesis work and its contributions.

1.2.1 Relevant Work in the Field

Detailed studies show that the mass of cables, interfacing hardware and connectors together is around 5%-10% of the spacecraft dry mass [Lappas et al. 2006, Magness 2003] (Table 1.2). The harness mass includes the power distribution cables (25%), data transfer cables (55%) and mechanical fasteners and shielding (20%) [Plummer and Planck 2001]. Furthermore, there are other problems with the harness that need to be addressed, such as difficult and labor intensive manufacturing, cost of space grade harness and interfaces, difficulty of assembling, cost of integration and test (AIT), and difficult post-integration testing.

In 1999, the National Institute for Aerospace Technique of Spain (INTA) proposed optical communication as a solution for interconnections between micro/nano devices [Guerrero 2003] and named it OWLS which stands for Optical Wireless Links for intra-Spacecraft communications. Between 2002 and 2005, EADS Astrium and Thales Alenia Space (TAS) started working on optical onboard communication. Some results such as the report by Gayrard *et al.* [Gayrard et al. 2003] and the contribution by Pelissou which validated the performance of onboard optical communication by experiments [Pelissou et al.

[2] Fractionated spacecraft is a space system that distributes its functionalities, such as computation, communication, data storage, payload and even power generation, over several independent spacecraft that share those functionalities through a wireless network [CHU 2015]

2005] were results of these studies. Although the optical solution presents a clear benefit due to the natural elimination of EMC/EMI concerns, the need for careful placing of repeaters to route the optical beam to compensate for multi-path dispersion and the requirement for line-of-sight can be exhaustive. Optical communication can be very promising where a high data rate is required, for example for transmitting payload measurements. Similarly, some studies tried to adapt infrared links for intra spacecraft communication [Walts et al. 2001, Santamaria et al. 2003]. However, this category of techniques can not support a flexible plug-and-play architecture and rapid integration.

Radio Frequency (RF) communication can potentially solve the limitations of optical communication. Although there is no RF communication standard designed or officially approved for space applications, several types of wireless devices and sensors have already flown on space missions, e.g., wireless LAN onboard International Space Station (ISS), simple wireless RF sensors [Champaigne 2003], wireless sun senor onboard the Delfi-C3 CubeSat [Ubbels et al. 2005], etc. Magness provides a comprehensive list of recent activities related to using the wireless devices in space applications [Magness 2006].

Recently a few research groups have focused on adopting commercial off-the-shelf (COTS) wireless standards for a spacecraft bus. Most of these works stay at a very high level of design and study the pros and cons of employing intra-spacecraft wireless communication such as the work by Shaobin [Li et al. 2009]. Some others take a step further and present laboratory experiments to implement and test a wireless bus. For example Ravichandran presents a design and development of a telecommand and telemetry subsystem for spacecraft using the ZigBee protocol [Ravichandran et al. 2009]. Most of these works, however, do not provide a realistic scenario for integrating the wireless bus system with spacecraft sensors based on the sensors purposes and application. In similar recent works, the performance of the ZigBee is evaluated and reported too [Xie 2014, Stone et al. 2012, Wagner and Barton 2012].

The results of almost all of these studies prove the feasibility of employing RF transmitters onboard spacecraft for data communication either for telemetry/telecommand or for payloads. In both cases, the effect of limited availability of energy onboard a spacecraft is however not considered. Also no research on employing wireless communication for attitude determination and control system (ADCS) has been done to the best of the author's knowledge. Besides, no attempt to apply onboard energy management schemes is available in the literature to tackle the energy limitation and its link to ADCS performance. An energy management scheme can reduce the energy consumption, improve the life time of sensors and improve the overall spacecraft performance (because more energy remains available for other tasks). In the wireless sensor network domain, different energy management techniques have been proposed to reduce the energy consumption of battery powered devices [Chung et al.

1999, Zuquim et al. 2003, Sinha and Chandrakasan 2001]. Some of the available techniques rely on approximate querying which exploits the natural trade-off between energy consumption and data accuracy [Han et al. 2004, Silberstein et al. 2006]. This technique basically relies on the applications specific error bound which are disseminated to each sensor node along with the query. Here a measurement is sent to the base station if the change of two consecutive sensor values exceeds a user-defined error bound. There are also other approaches which exploit sleep scheduling. However they mostly lack the explicit interaction with the application layer modules [Keshavarzian et al. 2006, Santini and Römer 2006].

1.2.2 Scope and Contribution

Application constraints play an important role in designing onboard wireless architectures. The design requirements can vary tremendously depending on whether housekeeping sensors, ADCS sensors or a payload system are involved. Also the design challenges vary based on the type of specific type of sensors and their use.

In this thesis, we try to answer the following research questions:

1. What are the problems of onboard wired standards and what are the benefits and characteristics of wireless network onboard spacecraft?
2. Which spacecraft subsystems could benefit most from a wireless onboard communication paradigm?
3. What is the major challenge regarding employing a wireless standard onboard a spacecraft?
4. How can we solve the identified system level design challenge?

The first three questions are closely connected. To answer the first question we will review the existing wired spacecraft data bus standards to identify and characterize their architectures and design. Then we will present the characteristics of COTS wireless data communication standards and carefully evaluate them. Thereafter we categorize different onboard data types and identify a suitable COTS wireless standard for each application category. This evaluation will enable us to answer the second question. To answer the third question, we will study the design challenges of wireless communication and map it to specific requirements of space vehicles design. To answer the last question we will systematically analyze and model the problem identified in question 3, develop a mathematical framework which is analytically solved and verified by numerical simulations, and evaluate it by simulations.

1.3 Thesis Structure

This thesis is divided in two parts. The first part is entitled Intra-spacecraft Wireless Network which contains Chapters 2 and 3. Chapter 2 is dedicated to an extensive study of spacecraft bus standards for command and data handling systems (CDHS) and justifies the necessity for reducing the harness. Also it introduces different wireless standards and identifies the most suitable subsystems which can benefit from an onboard wireless communication. It also identifies the main system level design challenge.

Chapter 3 takes the result of Chapter 2 and dives into the details of wireless communication architectures. This Chapter reviews major available wireless communication services which are widely used on the ground and compares their specifications with characteristics of an intra-spacecraft wireless network. This will lead the discussion to introducing an onboard wireless sensor actuator network (OWSAN) as a new category for describing spacecraft onboard wireless nodes. In addition, this Chapter qualitatively evaluates potential solutions for the identified system level design challenge.

The second part of this thesis is entitled Onboard Energy Management and is dedicated on answering question 4 in depth and verifying the solution. This part is composed of Chapters 4 and 5. In Chapter 4, we provide a mathematical framework to model the identified design challenge. Different subcomponents of the design are modeled and presented in details. This Chapter is concluded by two discrete analytical solutions and algorithms for implementing them.

Chapter 5 is dedicated to simulating the proposed solutions through two extensive simulation scenarios. Also details of modeling the space environment and related spacecraft subsystems are presented. In this Chapter the algorithms which were suggested in Chapter 5 are implemented and their performances are evaluated by different simulation scenarios.

The thesis is concluded in Chapter 6 and a summary of the thesis is provided together with a future research road map.

Part I

Intra-spacecraft Wireless Network

Chapter 2

Onboard Data Communication

Absence of understanding does not warrant absence of existence.

– Ibn Sina [1]

Traditionally, spacecraft featured custom electrical and mechanical designs based on the mission requirements. Therefore the spacecraft manufacturers had to go through the general requirements and functions for every new mission and instrument. The spacecraft industry has gone through an interesting trend. In early years of space exploration, the capability of launch was limited therefore most of the early launched spacecraft were in the class of microsatellites (10 to 100 kg) and minisatellites (100 kg - 500 kg).

In 1980's, the launcher capabilities were already significantly improved. Thus we see much larger, heavier and more complex space vehicles emerge in those years. The next coming technology wave was the advancement of electronics. The electronic circuits became much more dense and integration of subsystems became a daily and creative practice after the 1980's. However the new complexity brought higher demands for reliability and quality assurance. The result was increasing the development time and reduction of number of launches per year. Many projects were re-planned, extended or postponed due to such issues, for example ENVISAT project which took almost a decade to finalize the development [ESA 1998]. Surrey Satellite Technology Ltd (SSTL) started rethinking the situation in 1980s and introduced microsatellites. The emphasized characteristics of this class of satellites are the following: modular and flexible platform and instruments, looking for new functionality concepts, new services, reducing the development and launch costs. This idea was aligned with

[1] Ibn Sina (980 - 1037) was a Persian philosopher, physician, mathematician and astronomer. He wrote about 450 treatises on a wide range of subjects, of which around 240 have survived. In particular, 150 of his surviving treatises concentrate on philosophy and 40 of them concentrate on medicine.

the technology trend toward miniaturization of solid-state electronics, optics, sensors, miniaturized actuators, and later micro electro-mechanical systems (MEMS) and systems on chip (SoC).

Spacecraft bus and data handling subsystems of spacecraft, which provide the interfaces and data links between all other subsystems such as payload, telecommunication, on-board computer, etc., are also affected by technology advancements in the last decades. Technology advances in electronics and micro-mechanics have already provided the possibility of integrating more hardware and software functions in a smaller volume.

Current satellites and launch vehicles adopt microprocessor-based systems together with a data bus as the Command and Data Handling Subsystem (CDHS). Generally CDHS provides the means for decoding, storing, transmitting and distributing the commands between spacecraft subsystems. Typically these signals and data can be any of the the following:

- Attitude determination and control data which are transmitted to or from sensors and actuators to other subsystems;
- Commands initiated by the ground station and sent to a specific subsystem (or set of subsystems) onboard;
- Timing information needed for communication synchronization;
- Commands and signals generated by the spacecraft onboard processing system to control different subsystems;
- Commands or data generated by the spacecraft payload and need to be stored or transmitted to the spacecraft onboard processing unit;
- Housekeeping data which is generated by onboard sensors to monitor the health, performance or functionality of the spacecraft.

With the growing demand for CDHS's capabilities, it has become an essential part of most of many space vehicles. CDHS typically consists of processor(s), RAM, ROM, data storage and onboard software. The performance and features of this subsystem are very essential to optimize the overall spacecraft system performance and to process the available data for onboard use or transmit it to the ground station. Therefore, the design requirements for CDHS can be very extensive and demanding. Such design requirements mainly concern reliability, low mass, low latency and low energy consumption. Later in this Chapter, these requirements will be introduced in further detail.

An essential part of CDHS is the data bus. CDHS uses the data bus (data cables and connectors) for transmitting data to and from the spacecraft units. This data path may be a group of electrical lines that transports signals back

and forth in parallel with each other. The physical carrier may be metal wires or a wireless (RF or optical) channel that carries the information serially [Bever 1991]. Data may be time-multiplexed or modulated on different frequencies and sent concurrently. The bus system together with the connectors and power distribution lines are composing the harness of a spacecraft. Most of the time, spacecraft wiring harnesses and hardware/software interfaces are customized for each vehicle. In addition, the incorporation of commodity components (defined as the spacecraft subsystems and components that are reused) requires the development of many custom interfaces and interface converters. These customized and often unique interfaces and wiring harnesses increase the cost, complexity and time to develop, fabricate and integrate satellites. Also based on the required data connections between nodes, different network topologies are typically implemented.

In this Chapter a short overview on the different network topologies is presented. Then to give an overview of the state of the CDHS technology the commonly used wired bus standards are reviewed. Next, wireless standards are introduced and different design considerations are discussed. It is immediately identified that the limited amount of available energy is the biggest design challenge for enabling a fully plug-and-play wireless architecture. Thereafter different types of data which are communicated through spacecraft data bus are enlisted and major COTS wireless standards (Wi-Fi, Bluetooth and ZigBee) are mapped into these data types to identify the most suitable standard for each application.

2.1 Network Topologies

Network topology is the pattern of interconnecting all different elements of a network. These elements include nodes and links. Here nodes represent onboard subsystems and units such as spacecraft onboard computer, onboard sensors, payload. Topology shows the overall shape and structure of the network without showing the details of units. There are two basic categories of network topologies: physical topologies and logical topologies. The shape of the cabling layout (or communication for wireless systems) which links the nodes is called physical topology of the network. In contrast, logical topology is usually described by the protocols and is closely associated with Media Access Control (MAC) methods and standards. The design of MAC methods are out of the scope of this work. In wired network standards, the physical topology of the network is implemented by the electrical distribution system or cable harness. Harness forms the important link between different subsystems of the spacecraft. The spacecraft harness includes all interconnecting cables that interface with each of the spacecraft subsystems.

Point to Point Topology

Point to point topology is the simplest topology which can be arranged to provide a link between nodes of a network. It provides a link between node pairs in the network. These links can be permanent or temporary (switched). Permanent links usage can increase the reliability of the network but can drastically grow the required harness.

Bus Network Topology

In the bus network topology, all network nodes are connected by a shared cable which is called network backbone. The transmitting node broadcasts the message to all other nodes but only the desired recipient picks up and processes the message. However all other nodes have physical access to the message too. The required cabling in this topology is minimized and failure of one of the network nodes does not physically effect the network connectivity. Also if some nodes are not active (sleep mode), the network connectivity will not be affected. The messages sent by one node can be seen by all other nodes almost at the same time, therefore the communication delay is not usually changing for different nodes. The major disadvantage is that if the backbone infrastructure fails the entire network communication stops.

Ring Network Topology

In a ring network topology, each node is connected to two other neighbor nodes. The messages travel from the originator node to the destination node via several intermediate nodes. Therefore the intermediate nodes act as repeaters for the messages which are intended for other nodes. If the ring is not bi-directional, the common direction of traveling the message in the ring network can be predefined as either clockwise or counterclockwise. In bi-directional rings the messages flow in either directions, but there might be two cables between each two neighboring nodes. If a package is not consumed by any node in the ring, it can fall in to an infinite loop. In such cases blocking devices are required on the ring to stop packet storming. A disadvantage of ring network topology can be relatively long transmission time between nodes compared to the bus network. Here the propagation delay of relaying nodes accumulates and the communication delay between different nodes can be inhomogeneous. Failure of communication between two nodes can disable the entire network communication. Bi-directional ring networks which use two connection lines between the neighbor nodes can show a higher degree of reliability in such situations.

Star Network Topology

Star network topology assumes that one of the nodes can be a central top level node to manage the communication of all other nodes. This top level node can be a central computer of the spacecraft or just a simple data switch or connection point. The messages which are received by this top level can either be relayed to the other nodes or the a specific node which is the desired destination. A connection failure between one of the nodes and the top level node will not disrupt the whole network communication and communication delays are minimized and equalized because all nodes are interconnected with exactly one medium. The disadvantage is that if the top level node fails the whole network will become unusable.

Tree Network Topology

Tree network topology can be constructed in two ways. One approach is to make a set of star network topologies subordinate to a central node. The other possibility is to link a set of star networks together directly through a bus. Therefore, the functionality of the central node is distributed among several star network top level nodes. A tree network has at least three levels of hierarchy, otherwise it will be a star network. In such a network, a message can meet different levels of network hierarchy before arriving to the destination. One major advantage of such a network is its scalability. Adding an additional star network to the bus can expand the network without changing the order of the hierarchy. A failure in one of the links can not disable the whole network, however if a star network top level node fails then the entire lower level network section will lose its connection to the rest of the system.

Mesh Network Topology

Mesh network topology is developed based on path redundancy. Such network can be very efficient if the communication traffic volume is large because a subset of nodes have multiple paths to a destination node. This topology and the bidirectional ring are the only ones which can provide inherent redundancy for network communication to mitigate link failures. In a mesh network it is usually possible to determine the best route to the destination from each node. A full mesh network is described as each node being directly connected to all other nodes in the network. This topology can consume a lot of harness when cables are used as the links.

2.2 Onboard Wired Communication

Every spacecraft is composed of a number of different subsystems and units together with a large number of sensors and actuators which send or receive the data. The bus system is responsible for transferring the data between the units or delivering the data to the processing units or controllers. Different bus standards are being developed due to emerging new requirements on data transfer speed, ease of units integration, flexibility of design, reducing the cost of test and verification, etc. Most of these buses are naturally transferring the data serially. To give a better insight into these architectures, a number of major CDHS standards are reviewed in this Section.

Most of the architectures described in this Section have extensive aerospace or aeronautic deployment history. Almost all of them are deployed in existing space vehicles and most of them are still strong CDHS candidates in designing spacecraft. However there are many more standards which are either variants of the existing ones or are custom-designed for specific applications. In addition, there are several industrial communication architectures which are used in industries and automation for process and control purposes. For example similar communication architectures can be used to control the lighting, elevator services in building or automation systems in factories. The design requirements for each of these architectures and their application fields are different. For instance, the requirements for manned and robotic space vehicles differ significantly from those for low earth orbit (LEO) spacecraft and from those for industrial applications. It will be not feasible to use one standard and architecture readily for all of these different applications. However in the past years there was a significant movement towards use off-the-shelf standards and components as much as possible to reduce the development costs and minimize the changes needed in designing a new system. On the other hand, those communication architectures developed for use in space applications and robotic missions are usually being adopted by to the industry on the ground. This is naturally due to their higher degree of reliability, safety and performance which are key requirements in spacecraft development procedures.

2.2.1 MACS

In late eighties, ESA used Modular Attitude Control System (MACS) bus as a serial data bus for linking the elements of attitude and orbit control systems. The MACS bus was supposed to become the ESA standard for bus and onboard data handling. However this did not happen and MACS standard is now obsolete. It was one of the first onboard bus architectures which was developed to be modular and reusable in different systems. The number of the

elements connected to the bus was limited to 32 because of the address range of the protocol. The physical transmission media consisted of two standby redundant buses, each compromising two twisted wire pairs (clock and data). MACS bus operates from 125 Kbps to 500 Kbps over a maximum distance of 30 meters. The MACS bus concept allows for a true multi-master system. This calls for some method of contention such that only one user wins the access to the bus at any instance of time to minimize the possibility of conflicts and glitches. In MACS bus, all units on the bus use the same clock and are synchronized to a source. Each user consists of at least a bus head and a control ASIC. The original MACS system was dual redundant which apparently doubles the harnessing and mass per node. As an example, MACS bus was used in Manipulator Arm System (MAS) which was designed by Fokker in the Netherlands. It was shown by Hamann that MACS can fully satisfy the design requirements of a complex space robotic system [Hamann 1985]. Figure 2.1 shows the MACS bus onboard MAS. It is enabling the data communication between SJTS (Stowage, Jettison and Thermal Control Subsystem), EES (Standard Effector Subsystem), SAFS (Safeguard Subsystem), ESSS (External State Sensor Subsystem), TPS (Task Processing Subsystem), ADCS (Attitude Determination and Control Subsystem), PDCS (Power Conversion and Distribution Subsystem), CMS 1&2 (Central Management Subsystem) and MRA (Monitor and Reconfiguration Assembly).

Similarly, the XMM-newton spacecraft which was designed by NLR (Nationaal Lucht- en Ruimtevaartlaboratorium) in the Netherlands used MACS bus [NLR 1993, van Ingen Schenau et al. 1998]. Modularity, plug-and-play features and reconfigurability of the design were of a less concern in these projects therefore MACS bus architecture was not followed in other missions [ESA 1983]. NASA used MACS for some missions too e.g., as Instrument Control Bus (ICB) for UVOT telescope in the Swift mission [Roming et al. 2005] and also for the attitude control system onboard SOHO mission [Bouffard et al. 1995]. Figure 2.1 demonstrates an example of onboard architecture based on MACS as it was used in the MAS project. A very detailed design example is reported by Brouwer *et al.* which demonstrates the integration of MACS and ESA OBDH standards [Brouwer et al. 2000].

Another purpose was to establish a minimum acceptable end-to-end performance for data transmitted via the data handling subsystem onboard ESA spacecraft. This standard has a single master and a number of connected devices which behave as slaves. The design specifications for OBDH contain power distribution details too. The first revision of OBDH was composed of telemetry channels, telecommand channels, and data bus. The data bus is a full duplex system with two separate lines, one for each direction. Telemetry channels can facilitate both analogue and digital (serial) acquisitions. The telecommand outputs are generated from a 24-bit data field. Data acquisition

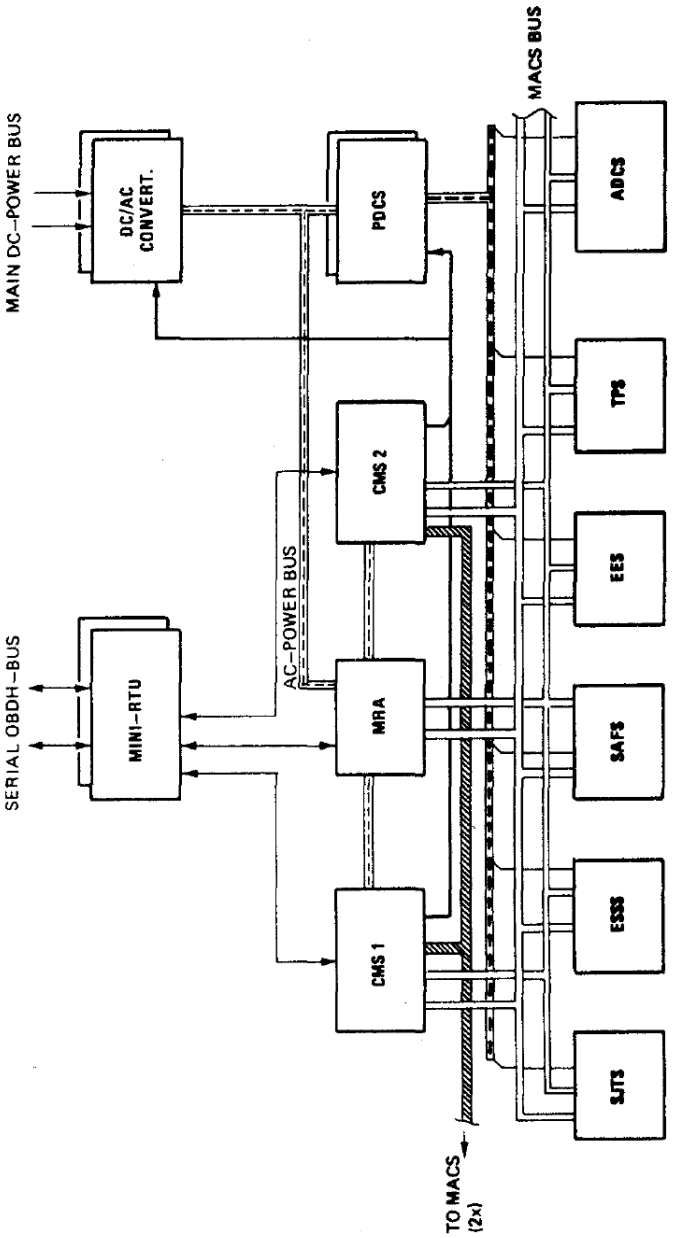

Figure 2.1: An example of using MACS bus architecture onboard Manipulator Arm System (MAS) by Fokker [Hamann 1985].

rate can be set to maximum 125 Kbps. The bus operates on 5 Volts and it can bear an over voltage of 16 Volts which improves the reliability and flexibility perspective [ESA 1979]. Later in middle 1990s, ESA attempted to upgrade this standard with some modifications to comply with the new design requirements and introduced OBDH-9x.

2.2.2 ESA OBDH

OBDH stands for Onboard Data Handling and ESA internally refers to it as TTC-B-01. This standard was developed to unify the data handling interfaces onboard an ESA spacecraft. The justifications were made mainly to meet some new requirements for future missions and supporting diagnostic at a subsystem and unit level. ESA continued the modifications on OBDH until the latest revision of this standard was released (and is referred to) as 4-255 Data Bus [Plummer 1996]. The 4-255 standard is slightly different from the baseline OBDH. Among many upgrades, the 4-255 OBDH bus provides a higher bus speed at 524 Kbps full duplex data transmission, possibility of extending the harness to 60 meter, increasing the maximum allowed number of connected devices to the bus to 63, adding a Reconfiguration Module Service (RMS) for fault and failure detection, accommodation of various data sources (synchronous, periodic, asynchronous), and efficient terminal to terminal communication procedure. Figure 2.2 shows the bus architecture and main elements of ESA OBDH 4-255 version. The main elements of this design are Interrogation Bus (I-Bus), Response Bus (R-Bus) and Block Transfer Bus (BT-Bus). I-Bus was to

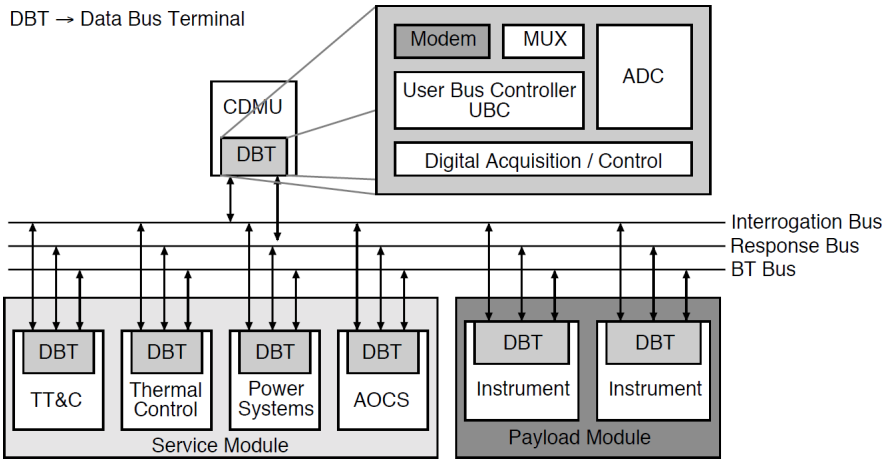

Figure 2.2: Block diagram of ESA OBDH (4-255 version) [Boi et al. 2005]

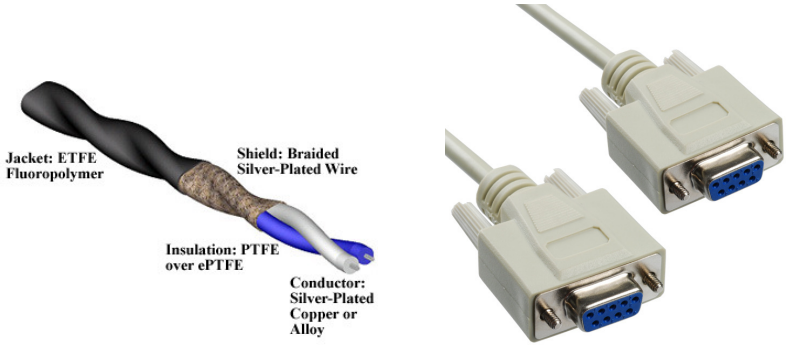

(a) Shielded twisted pair wires (b) 9-pin D type female connectors

Figure 2.3: Typical harness used for the ESA OBDH standard

broadcast interrogation words from Central Data Management Unit (CDMU) to different terminals, where R-Bus and BT-Bus were used to transmit and receive response words and large data blocks respectively. In addition, some directions were introduced to decrease the onboard harness comparing to the traditional OBDH standard [Maeusli 1994]. The bus consists of two component buses called the Interrogation Bus and the Response Bus. Also there is an optional Block Transfer Bus which can be used to exchange blocks of data between terminals and is a multiple access bus. Figure 2.2 shows an sample configuration of this standard in practice [Boi et al. 2005]. The recommended cable for interrogation and response buses is shielded twisted pair and the connectors are 9-pin D connectors. Variant 24 of SCC 3901/002 cable was regularly used in this standard which has a mass of about 10.5 grams per meter [AXON 2008] (see Figure 2.3). OBDH standard family is used in numerous projects and missions such as MINISAT, SOHO, Cluster-1& 2, Integral, Rosetta, Mars Express, ERS-1 & 2, MSG, Envisat, METOP-1, Artemis, and more. Interestingly to mention that the Japanese satellite data bus standard SDB was also derived from ESA OBDH standard.

2.2.3 MIL-STD-1553B

MIL-STD-1553B is a DoD military standard currently in revision B. This standard is perhaps the most famous and cited cabling standard in the history of space and aviation industry. The first draft of this standard was developed in 1968 by the Aerospace Branch of the Society of Automotive Engineers (SAE) which laid the foundation for the first version of MIL-STD-1553 at the US Air Force in 1973. The modifications were developed later as MIL-STD-1553A in

1975 and then MIL-STD-1553B in 1978 and where used in F-16 and AH-64A Apache Attack Helicopter. The latest revision of MIL-STD-1553B (Notice 2) was released in 1986 which is not updated thereafter. It is widely used by NASA, ESA and other space agencies in various missions and projects. During the past years, it has been always used as baseline of many command and data handling design projects [Elias 2000, Kim and Han 2000, Lockheed Martin 1998, Larson and Wertz 1992].

MIL-STD-1553B defines mechanical, electrical and functional characteristics of the data bus. It describes the methods of communication that correspond to the physical and data-link layers. This standard defines a dual-redundant, bi-directional, Manchester II encoded data bus with a very high bit error reliability. A main bus controller initiates and controls all of the bus communications as a master. In general, three type of hardware can be connected to a bus: bus controller (BC), remote terminal (RT) and bus monitor (BM). The data bus is a twisted shielded redundant transmission line made up of a main bus and a number of attached stubs. The bus operates at 1 Mbps and interconnects up to 31 remote terminals, using a command/respond method. Each remote terminal can have 31 sub-addresses and it can work as a bridge between two MIL-STD-1553B data buses. The redundant data bus operates in a cold redundant configuration. The length of the bus is not limited in the specifications. Figure 2.5(a) shows the bus topology and Figure 2.5(b) shows an example of a possible bus implementation. The redundant architecture facilitates an extremely low error rate of one word fault per 10 million words which means the implies an extremely high communication reliability. There is an error detection and recovery mechanism implemented in the bus controller which keeps a history of the errors. A bus controller and an optional bus monitor are also connected to the bus [Condor Engineering Inc. 2004]. Usually concentric twin-axial or

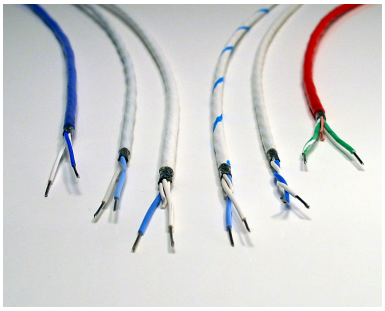

(a) MIL-STD-1553B cables

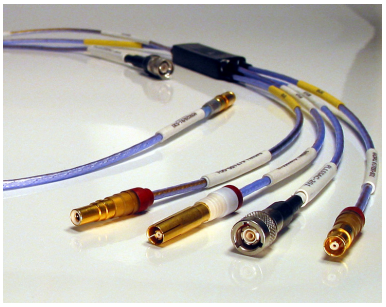

(b) MIL-STD-1553B connectors

Figure 2.4: MIL-STD-1553B harness

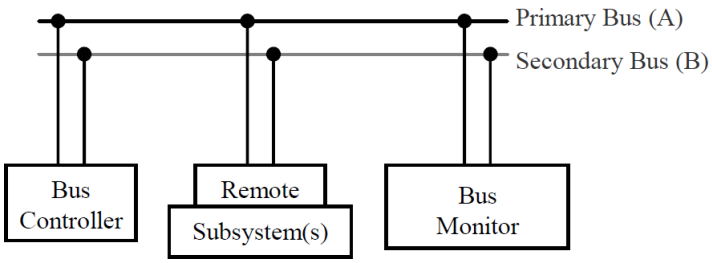

(a) The major elements of MIL-STD-1553B bus.

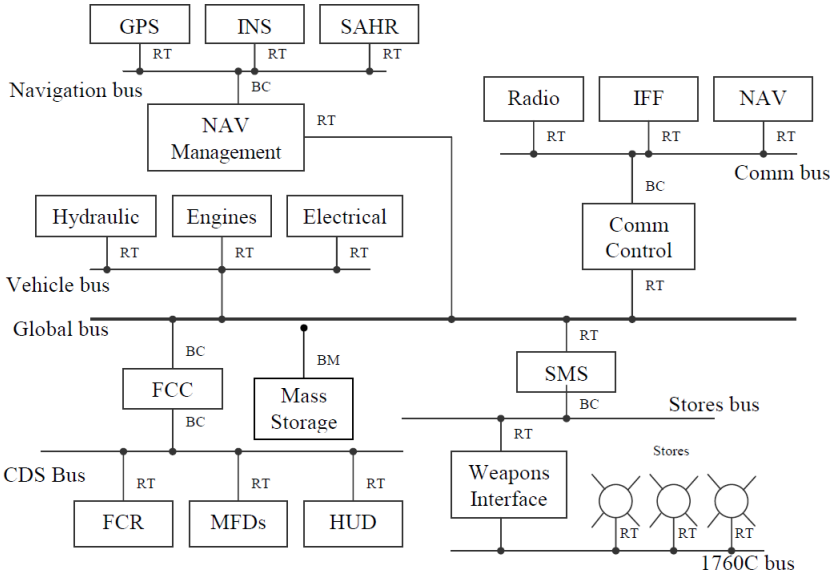

(b) A configuration example for MIL-STD-1553B bus standard.

Figure 2.5: MIL-STD-1553B bus architecture is shown in this figure. Data bus can be extended by using bus controllers as bridges [Condor Engineering Inc. 2004].

tri-axial cables and connectors are used for MIL-STD-1553. Each connector (without the harness) has a mass of about 1 gram and the required harness mass is about 20 grams per meter (Figure 2.4).

2.2.4 RS-422

This bus standard was developed in 1978 for Balanced Voltage Digital Interface (BVDI) circuits. It is a serial bus very similar to RS-232 where only the electrical characteristics are defined in the standard. Therefore it can be combined with

other standards which define higher levels of the design. For example it is possible to use RS-422 as the physical layer for ESA OBDH standard. The interface consists of a transmitter and up to ten receivers. Therefore, every subsystem which needs to transmit the data must have two interfaces. Between each pair of transmitter-receiver a paired cable has to be used. Therefore four wires are needed for bidirectional communication between each two nodes. Practically a ground signal is necessary too, which brings the total number of needed cables to five (See Figure 2.6).

Usually 24 AWG[1] twisted-pair telephone cables are used for this standard which are not as heavy as the ones for MIL-STD-1553B. RS-422 harness is shown in Figure 2.7. RS-422 is a balanced, or differential, transmission system. Neither of its transmission wires are tied to the ground reference at either end. Therefore the transmission system is less sensitive to common mode disturbances and consequently less sensitive to noise. The transmission rate is up to 10 Mbps at line lengths up to 1219.2 meters (4000 ft). To achieve higher data rates, multiple busses could be used which increases the cost and the effort for test and integration. If custom software is designed, custom-built test equipments will also be necessary which again increases the cost and debugging time. However, still the simplicity and reliability of this bus makes it interesting for harsh environments such as space. It is usually a strong candidate when onboard point-to-point communication is needed. RS-422 is used onboard many missions solely or in combination with other data bus standards which define the physical layer. Thermal Control Electronics Unit (TCEU) onboard GOCE uses RS-422 links to communicate with the onboard computer [Johannessen and Aguirre-Martinez 1999]. It is also used onboard Mars Exploration

[1] American Wire Gauge (AWG) is a U.S. standard set of non-ferrous wire conductor sizes. The "gauge" means the diameter.

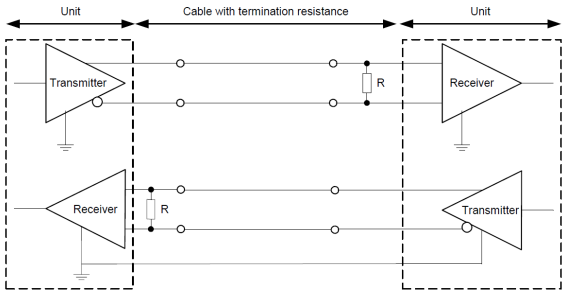

Figure 2.6: RS-422 standard is a differential transmission system therefore four wires are necessary to establish a bidirectional connection between two devices [Soltero et al. 2002].

(a) RS-422 wire (b) RS-422 point to point cable

Figure 2.7: RS-422 cables include five wires for a point-to-point connection.

rover for communication between the Small Deep-Space Transponder (SDST) and Telecommunication Support Board (TSB) [Taylor et al. 2005]. Another interesting example is the usage of RS-422 onboard PROBA-2 where RS-422 is used in combination with OBDH (TC-B-01 version) as the data bus standard for the onboard data and power management system [Gantois et al. 2006].

2.2.5 CAN Bus

The development of the CAN bus was initiated in 1983 by Robert Bosch GmbH in Germany. The purpose of this development was to create a faster and more interference-resistant data network. The specification of CAN bus data link layer and physical layer are specified in ISO11898 Part 1 standard [ISO11898 2003]. There are some fundamental drawbacks in traditional data buses like ESA OBDH and MIL-STD-1553B such as inherent single master topology, high energy consumption and costly development support which motivates the application of CAN bus in spacecraft onboard data handling [Lopez et al. 2004]. The CAN protocol provides an asynchronous multi-master architecture, where any node can arbitrarily transmit a message on the network. This can happen when the network is free at the time when the transmission commences. Traditional data bus standards use node labeling while CAN bus uses content labeling. If two nodes on the network transmit messages simultaneously the messages are not destroyed. The CAN bus standard is using a technique called non-destructive bitwise arbitration to resolve this type of transmission conflicts [ECSS 2005]. CAN bus features include prioritizing messages, configuration flexibility, system wide data consistency, and automatic retransmission of corrupted messages. A CAN bus system usually consists of a bus wire, bus terminations and a bus station. The bus station includes a micro-controller, the bus controller and the bus driver. An example of CAN bus architecture in avionics is shown in Figure 2.8. This figure shows that in CAN bus it is

possible to connect a device to two separated bus lines. This means that multi drop and daisy chain configurations are both feasible. Twisted cable or coaxial cable are usually used as the cable composing the bus, but the cable specifications are not included in the standard. Due to the multi-master configuration, there is no separated bus controller for CAN systems on the network (unlike MIL-STD-1553B). Whenever a unit wins the bus and starts the communication, the other units automatically become receiver [Plummer et al. 2003, Etschberge 2001]. The maximum transmission speed is 1 Mbps with a 50 meters long bus cable. It is possible to extend the bus length but the recommended speed declines for longer bus cables. For a bus length of 500 meters, the recommended speed is defined 125 Kbps in the standard. Since the automotive industry heavily uses this standard, the commercial-off-the-shelf equipments are widely available at low prices [Emrich 2005]. Later on, SSTL developed RadCAN standard based on CAN bus as a more robust and radiation tolerant standard for deep space and non-LEO missions [Woodroffe and Madle 2004]. RadCAN hardware is much more expensive, bigger, heavier and consumes slightly more energy comparing to the standard version. CAN bus standard is used onboard FASat-Alpha/Bravo experimental microsatellite, SNAP-1, ALSAT-1, ChinaSAT, GEMINI, CFESAT and many other missions. CAN bus has many other variants for different applications such as MilCAN for military applications, TJA 1054 for low power and low speed usage, TTCAN which is a time-triggered CAN architecture, AU5790 standard which is a single

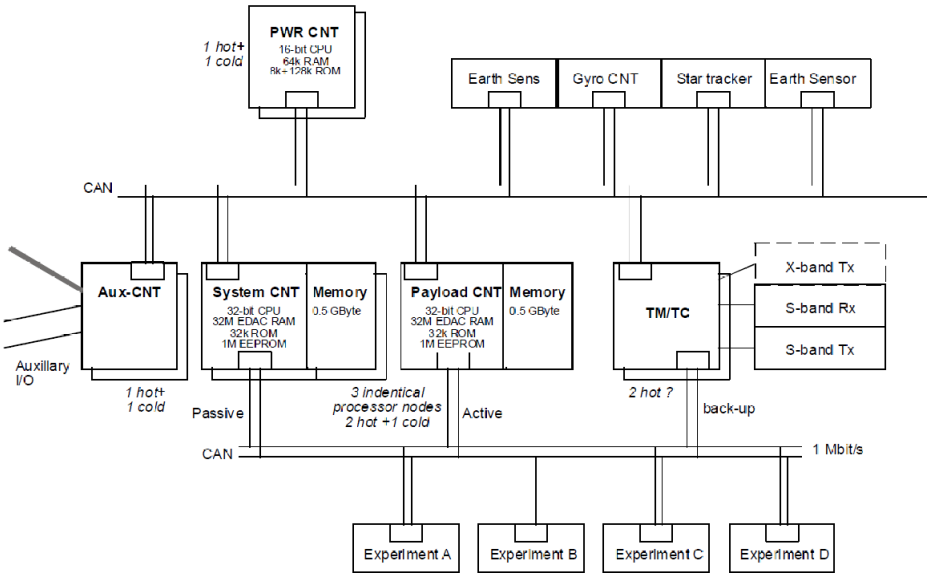

Figure 2.8: Block level sketch of CAN BUS for SMART-1 satellite [Emrich 2005]

(a) Twisted pair wires

(b) CAN bus harness

(c) CAN bus with coaxial cables

Figure 2.9: Twisted pair cables or coaxial cables can be used for CAN bus. Based on the interfacing requirements different types of connectors can be used.

wire CAN bus, and many more.

2.2.6 I^2C

By emerging the new system on chip devices, new integrated bus standards have been recently developed. In the case of I^2C bus standard, the history goes back to 1980's when Phillips Semiconductor intended to develop an easy interfacing way to connect the CPU to peripherals. I^2C performs chip-to-chip communications using only two wires as a serial interface. The standard provides a flexible multi-master configuration. The data rate could be 100 Kbps, 400 Kbps or 3.4 Mbps. The bus can not be longer than 3 meters, but the standard does not specify the type of cables or connectors. Therefore very different types of harness exists for I^2C. This bus standard is very popular in industry yet it is not inherently providing a means of error detection. Although each byte should be acknowledged by the receiver, this does not guarantee the error free transmission of the byte. However, I^2C uses a collision avoidance mechanism to resolve conflicts between master nodes which want to access the bus at the same time instance [Philips Semiconductor 2000]. Comparing to

other space qualified standards such as SpaceWire and CAN, this is a drawback. There are some attempts by different groups to compensate for this issue by combining I^2C with other standards. For example in X2000 project at JPL CAN bus is integrated with IEEE 1394 [Chau et al. 1999]. This bus standard has received a lot of attention in the recent years. Its popularity is due to the recent trends in applying COTS components and standards to reduce the cost of space exploration programs. This bus is used in a number of CubeSat projects such as Delfi-C3 [Aalbers et al. 2006], AAUSAT-I [Alminde et al. 2004], COMPASS-2 and ALMASat-1. It is also promoted by a number of companies such as Pumpkin Inc. which provide CubeSat kits and technologies for rapid development of small satellites.

2.2.7 Ethernet

The most widely used data communication standard for computer networks is Ethernet. The first prototype of Ethernet standard was developed by Robert Metcalf in 1973 at Xerox Palo Alto Research Center (PARC). This standard was evolved and improved until it was approved in 1984 International Organization for Standardization (ISO) and titled as IEEE 802.3bg standard and the most recent revision is published in 2011 and is an amendment to IEEE 802.3 published in 2008. Ethernet provides data transmission rate of 10 Mbps to 40 Gbps. There are different requirements and recommendations for the physical layer and type of cables based on the data communication speed and communication distance. For 10 Mbps and 100 Mbps unshielded twisted pair cables can be used with maximum length of 100 meters. For 1 Gbps data rate, shielded twisted pair cables for short range and fiber optic for longer distances are used. For speeds higher than 1 Gbps multi-mode fiber cables are recommended [IEEE 2010]. It supports half-duplex and full-duplex modes of operation. In half-duplex mode CSMA/CD (Carrier Sense Multiple Access with Collision Detection) manages the channel sharing between nodes, which means that a node can access the channel when the line is idle. If two nodes initiate the transmission at the same time, the transmission is ceased and the nodes should choose another random wait time before reclaiming the line. In full-duplex mode the nodes are connected to the switch which is responsible for routing the messages to the intended receivers. Usually Ethernet is used in combination with transmission control protocol (TCP) or user datagram protocol (UDP). In principle, UDP does not guarantee arrival of the message to the destination but it adds very small overhead to the communicated data. TCP provides a reliable connection but adds significant overhead to the communicated data. Among other features, it also provides flow control and sequential transmission. Ethernet has found various military and aerospace applications. For example it is currently used on the International Space Station (ISS) [Webb

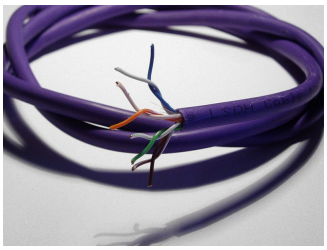

(a) Ethernet twisted pair wires

(b) Ethernet cable and connectors

(c) Ethernet fiber cable and connectors

Figure 2.10: Twisted pair cables (shielded and unshielded) fiber cables are used for Ethernet standard. The type of the cable follows the given recommendations based on the data communication speed and link distance.

2002]. Figure 2.10 presents an overview of cables and connectors which are used for Ethernet communication.

2.2.8 IEEE 1394 (FireWire)

IEEE 1394 standard introduces a high speed bidirectional serial data bus which uses point-to-point connections in a tree topology. It was derived from Apple Computer's commercially developed FireWire standard. The standard is well matured and developed by the IEEE work groups [FireWire 2008]. It is very widely used in industry, computer market and audio/video technology. It is a well developed, well tested and well supported standard. As it is shown in Figure 2.11 it needs four wires to enable communication between two nodes (and two extra cables for power). The data rate can be up to 100 Mbps. No loops are allowed in a FireWire network. Upon power up, all connected nodes participate in an automatic configuration of the network via tree identification and self-identification. This standard has two modes of operation. Isochronous and Asynchronous. The first one emphasizes on guaranteeing on-time data

delivery without giving an error free communication guarantee. In contrast, asynchronous transfer mode guarantees data delivery and assures an error free operation but can not guarantee real-time communication. A single 1394 bus can support up to 63 nodes. By bridging between buses (up to 1024 buses) maximum 64000 nodes can be connected to the bus. Each IEEE 1394 cable can not be longer than 4.5 meters. With nodes acting as repeater (maximum 16 hops) the length can be extended to maximum 72 meters, however this will cause extra communication delay. IEEE 1394 provides a truly plug-and-play data bus. When a new node is connected to the network, the network automatically reconfigures itself and recognizes the new member [IEEE 2000, Anderson 1998]. COTS hardware and software are very widely available for this standard. Tai has shown that the reliability of a FireWire LAN can be highly increased (close to 1) even in a long term mission [Tai et al. 1999]. Also some successful attempts are reported to make it radiation hardened [Wolfram and Bloom 2004]. There are two revisions to FireWire standard. In IEEE 1394a, the number of wires is reduced to 4 (power and ground wires are removed). In IEEE 1394b released in 2002, higher data rate up to 3200 Mbps and longer cable length up to 100 meters with glass optical fiber are supported. This standard is mostly used in NASA missions and projects. It was shadowed in Europe by the reputation of SpaceWire standard. For example the Pluto Rover is using FireWire to establish the connection of the onboard cameras and the onboard computer and the VIIRS (Visible/Infrared Imaged and Radiometer Suite) instrument onboard NPOESS spacecraft are using the IEEE 1394 standard for communicating the information [NASA 2009].

(a) Firewire cable structure (b) Typical Firewire connectors

Figure 2.11: For Firewire, two pair of cables for signal transmission and one pair for power transmission are used. Shielded or unshielded twisted pair cables can be used.

2.2.9 SpaceWire

One of the latest developed space qualified bus technologies is SpaceWire which is developed in Europe. SpaceWire is a point to point serial data link bus standard which is specially designed for space applications as a high speed bus with high level of reliability. It is very popular for space engineering applications [Rakow et al. 2006]. A SpaceWire network is made up of links, nodes and routing switches. Any subsystem onboard can be one of the SpaceWire nodes. Nodes can be connected directly by links or via routing switches. Usually a node can support a maximum of six links which limits the number of direct connection between nodes. To connect more nodes, routing switches are used. They can connect many nodes and provide a means of routing packets from one node to one of many other possible nodes as shown in Figure 2.13. The physical interconnection and the protocol are defined in the standard. The standard evolved from IEEE 1355 by improving the ruggedness, energy consumption and EMC characteristics [IEEE 1996]. It uses two differential signal pairs in each direction i.e. it has eight signal wires (four separately shielded twisted wires) (Figure 2.12). The maximum bus length is 10 meters and it operates from 2 to 400 Mbps data rate. SpaceWire introduces very low energy consumption level and low electromagnetic interference. Reliability and fault tolerance are achieved by using cross-switches and routers which increases the complexity of the system architecture and integration. SpaceWire network can be extended to include more devices by creating cascades of hubs or switches to route the messages. Because of the bus system architecture, each additional data route from a node increases data bandwidth of the system since simultaneous communication is possible on multiple paths. This be-

Figure 2.12: SpaceWire harness

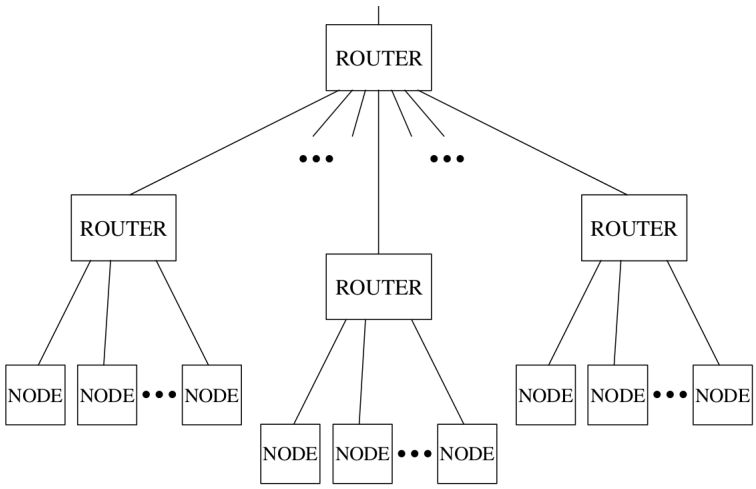

Figure 2.13: Architecture of a typical SpaceWire bus

comes non-effective if multiple nodes are addressing a single node, i.e. when the subsystems are sending data to the main processing unit or data storage unit [ECSS 2008].

2.3 Bus Standards Comparison

Table 2.1 compares important features of the presented standards. There are many other bus standards such as SAFEbus, TTP/C, FlexRay, AFDX, FibreChannel, SPIDER, Profibus, etc. which are not popular in space applications.

The communication standards which were reviewed include event-triggered and time-triggered standards. In event-triggered class, the messages are generated only based on the need to transmit a new piece of information.

For example Ethernet is event-triggered and is used for communication between computers in office networks. In Ethernet the messages are sent over the network when one of the nodes requests for information. Only then another node may respond to the request and start a communication. These requests can happen in any time without being synchronized with another source or an arranged timing. On the contrary, time-triggered communication architectures are based on specified time slots arranged by global agreements. These communications are scheduled in the time domain and each node of the network is given a finite amount of time for transmitting a message.

Table 2.1: Comparison of technical features for major spacecraft onboard data handling standards

Feature	MACS	ESA-OBDH	MIL-STD-1553B	CAN	Ethernet	IEEE-1394B	SpaceWire
Application field	Space industry	Space industry	Military aircraft / Spacecraft	Automotive drive-by-wire	Mostly LAN applications, ISS	Consumer electronics / Space	Space industry
Communication control	time-triggered	time-triggered	event-triggered	time- and event-triggered	Event based	time-triggered	event-triggered
Maximum data date	500 Kbps	524 Kbps (additional 534 Kbps on a separated half-duplex bus)	1 Mbps	1 Mbps (not fault tolerant) & 125Kbps (fault tolerant)	10/100 Mbps up to 40 Gbps	3200 Mbps (limited by cable length, etc.)	400 Mbps
Maximum number of nodes on single bus	32	63	31	120	1024	63 (up to 1023 by extensions)	224 (up to 224 × 224)
Physical layer length	30 meters	60 meters	no limits	30 meters for 1 Mbps	100 m for 10/100Mbps version	4.5 meters point to point	10 meters
Extensibility	N/A	N/A	depends on implementation	requires redesign or reconfiguration	Easy	Easy	requires reconfiguration
Network topology	multi-drop & multi-master	multi-drop and point-to-point	multi drop	multi drop	Spanning tree & point to point	peer-to-peer	point-to-point
Redundancy	dual redundant	dual redundant	dual redundant	No	No	No	No
Message failure detection	N/A	application layer (Litton coding)	Yes (status bit)	yes (in hardware)	Collision detection at physical later, delivery ack. for TCP	yes in **asynchronous mode (in hardware)**	yes
Node failure detection	N/A	yes (time-out)	only for terminals (RTs)	yes	No	yes	yes

These moments of time are predefined as referenced to a global time base. The global time base is generated either by the network master node and communicated to the other nodes, or it is made by combining the clock messages from several nodes.

If there is no global base for time available, an abstract time that is based on the order of messages sent and received across the interfaces of a node can be used. However if the relationship between the physical time and the abstract time is not readily accessible by nodes, then this model can be imprecise. A sample situation is when it is necessary to determine the precise state of a system at an instant of physical time [Kopetz and Bauer 2003]. If there is no unique master node, the communication architecture will be more robust because there is no single point of failure.

Usually standards which use time-triggered protocols are considered to provide a higher degree of reliability and be more suitable for safety critical distributed systems. This is because the bus loading, message latency and jitter are known and rather predictable [Rushby 2003]. The down side is that such standards need a significant amount of design to create the message schedule models and coordinate it with the timing of tasks at different nodes. Therefore adding new nodes to the network without redesigning the message and task scheduling is not allowed or is not directly feasible. But this restriction does not apply to event-triggered architectures. New nodes can be added to the network without adding a new time schedule. This configuration can be even more efficient when the amount of data in a given period of time is sparse and the nodes occasionally need to send messages without being asked from the master node. This inherently needs more autonomy and smartness in the nodes to decide about their time of communication based on external or internal events. Also when the amount of data to be transmitted is very large, time-triggered standards might be inefficient.

In a time-triggered network, it is often required to split the data to small packages and transmit it over several transmission cycles, which is unacceptable for some applications such as video/audio streaming. Of course such architectures might not be able to ensure a guaranteed real-time performance. Video/audio streaming application is interesting in the sense that usually users can accept non-guaranteed real-time performance and delays as long as the stream is not broken to different pieces in time domain.

The properties of event-triggered and time-triggered architectures are discussed by Kopetz in one of his earlier works [Kopetz 1991] and these criteria are very important to be taken into account to analyze spacecraft data bus standards. In principle the selection of a bus standard is not very crucial as long as the bus standard meets the communication requirements and application deadlines. But reviewing these criteria which can generally influence the decision can give

insight into the evaluation of the research challenges and obstacles. Scheler and Schröder-Preikschat have already provided the criteria for comparing time-triggered and event-triggered communication standards which can be used for our purpose [Scheler and Schröder-Preikschat 2006]:

Analyzability: Given temporal constraints, schedulability of tasks for a time-triggered system to find an appropriate schedule is usually performed statistically in an off-line manner beforehand [Schild and Würtz 1997]. For event-triggered systems this can be done with a careful response time analysis [Liu 2000] to guarantee that deadlines can be met.

Predictability: The nature of time-triggered systems allows prediction of the system status at any a given time. This can be done statistically based on the communication schedule. However for an event triggered system it is impossible to compute the specific event of the system in the time domain. On the other hand, predictability is not a requirement for a real-time systems. Practically if the communication duration is much smaller than the time-out then the performance can still be guaranteed for an event-triggered system.

Testability: Verifying the timing constraints can be done for both systems by testing the performance in the worst case. These testing techniques exist for both time triggered and event triggered systems.

Extensibility: In principle event triggered architecture can show advantages over a time-triggered architecture when it comes to adding new nodes or extending the system. For a time-triggered system, the response analysis should be performed again which limits its flexibility. This analysis might be much easier for an event triggered system, but still the real-time deadlines should also be guaranteed for an event-triggered system. Otherwise the systems performance will degrade after adding the extension. Therefore, event-triggered systems are not readily extensible if certain requirements are not met by the extension.

Fault tolerance: Inherently, a fault tolerant system needs replica determinism. Replica determinism means that redundant nodes can take the same decision in (almost) the same time. For example, two sensors can measure the same phenomena at the same time and report the results to the fusion center together. This is easy to achieve in a time-triggered system but can not be readily achievable for an event triggered system. As a result of this problem, guaranteeing fault tolerance in an event-triggered system such as CAN bus is not easy without extra communication between the nodes which will use extra resources.

Resource utilization: In most real-time systems, the majority of events are not periodic. In fact most of the real-time systems exhibit a rather event-based behavior. Therefore it can be difficult (if not impossible) to calculate the exact polling period of nodes in such systems. Sensors of spacecraft attitude determination system show perfect examples of this concept. The requirements on sensors sampling frequency are very much depending on the undertaken maneuver. Constant polling in a time-triggered manner at high rate in such systems can waste the energy resources easily. Therefore event-triggered systems can be preferred when the occurrence of events are aperiodic and sporadic.

Scheler and Schröder-Preikschat conclude that among the discussed criterion, only fault tolerance and resource utilization can be considered to have substantial impact on the selection of the preferred communication architecture.

We can conclude that for spacecraft data bus applications where reliability demands are high and resources are limited a time triggered communication standard is preferred only when regular communication is in demand. Otherwise, the communication should be initiated in an even-triggered manner.

2.4 Bus Harness Reduction

Missions costs are essentially proportional to the total mass of the spacecraft. Several studies have been carried out in Europe and United States on the effect of mass on the development cost and final cost of a spacecraft including launch [Lao et al. 1998, Mahr and Richardson 2003, Koelle 1984]. Some of these studies provide estimation methods to relate the mass and cost of the satellite, and some of them suggest approaches to lower the satellite dry mass. Havard and Armon conduct a detailed study on the impact of decreasing size, mass and energy consumption of individual onboard subsystems on the overall onboard size, mass and energy consumption [Havard et al. 2008]. The goal of their research is to achieve overall reduction of space vehicle mass by a factor of 4. Detailed studies show that the mass of cables, interfacing hardware and connectors together is around 15% of the spacecraft dry mass [Lappas et al. 2006]. This is due to the large number of units, subsystems, sensors, actuators and interfaces which are used onboard spacecraft. Onboard electrical interconnections require a high level of assembly, integration and testing which increases the development time too. Some of these units may need point-to-point communication which requires even more customization. The harness distributes the electrical power, exchanges the data between units and connects the sensors and actuators to the controllers. The harness mass includes the power distribution cables (25%), data transfer cables (55%) and mechanical

Table 2.2: Harness mass relative to spacecraft dry mass [Plummer and Planck 2001]

Spacecraft	Dry mass [kg]	Harness mass [kg]	Proportion [kg]
Envisat	8500	850	10.0%
GOCE	740	60	8.0%
Cluster II	540	33.4	6.2%
MarsExpress	450	28	6.2%
SMART-1	280	22.1	8.0%
Proba	100	7.6	7.6%

fasteners and shielding (20%) [Plummer and Planck 2001]. To account for this mass overhead of the data bus and interfacing mechanism, two solution can be identified: a) unit miniaturization and b) enabling wireless communication onboard the satellite. Both solutions need to be taken in parallel and will be discussed in further details in the following sections.

2.4.1 Unit Miniaturization

Electronics advancement and miniaturization can have major affects on spacecraft harness reduction. These effects can be identified as follows:

Size and mass reduction: Recent electronics and MEMS technologies have reduced the size of sensors and actuators and consequently their energy consumption. In many cases, the sensors and actuators or the spacecraft unit are able to work with battery for the whole period of mission. With the help of energy scavenging techniques and self powering technologies the life time could be increased [Rouault 2006]. Removing the power cables from the unit reduces the harness.

Increasing functionality: Miniaturization provides the possibility of integrating more functions into a single unit. Smart packaging techniques can boost miniaturization to produce smaller units which can provide more functions. Hence, energy consumption and data/power bus harness will be reduced. Consequently, the overall size and mass of the spacecraft will be reduced.

Units integration: Development of smart sensors and actuators with the help of miniaturization technologies such as MEMS has brought the possibility of integration of actuation and sensing electronics into a single device. In many cases, the control unit can be integrated as well by using SOC (System On Chip) technology. Reduction of number of subsystems and

electronics elements can increase the reliability and reduce the size, mass and number of interfaces between units.

Easy interfacing: By using the SOC technology, the interfacing unit can be integrated in the sensor. Thus, sensors can directly communicate with each other or with the other units such as the onboard computer. This removes the extra harness due to interfacing electronics.

A smart example which shows the potential of miniaturization for the design and development of space missions is the Jupiter Entry Probe (JEP) by NASA. In this project, the impact of miniaturization of systems through a SOC solution on the overall mass, size, reliability and costs is studied. The approach was to replace the traditional avionic units by a SOC and analyzing the impact on avionics mass, power, volume, complexity, risk and cost of the probe. The results of the study concluded that 5 kg saving in avionics mass is feasible by the SOC solution which also leads to a further 15 kg saving on other subsystems (power, structure, batteries, etc.) without a significant risk increase. The authors estimate that the mass saving practice will save 4% of project costs during project phases [Trautner et al. 2008].

To get the most out of miniaturization, creative solutions should be employed for onboard data communication too. For example, the mass of a microthruster such as the work presented by Zhang *et al.* is reported 21.4 grams including the propellant [Zhang et al. 2004], while the mass of one meter of cable used for MIL-STD-1553B communication standards with its connectors can exceed 25 grams. Thus, miniaturization should be combined with smarter communication techniques such as wireless communication standards which can directly reduce the required mass budget for intra-spacecraft communication.

2.5 Onboard Wireless Communication

Among the different available techniques to address data bus harness reduction (e.g., fiber optics bus usage, data through power lines [Oria et al. 2006]), wireless interfaces appear to be the most interesting option. Wireless interfaces offer the possibility of eliminating cables and reducing the harness from the data bus. Wireless bus architecture could be based on optical or radio frequency (RF) communication techniques.

Wireless radio frequency links: wireless RF communication uses omnidirectional, short-range radio links between units. The major benefit of wireless RF interfaces over an optical interface is that all data traffic on the links can be monitored very easily during the integration and

testing. Furthermore, integration is greatly simplified because the units need only be within range of the RF links in order to operate. Therefore the spacecraft units could be operated on the bench during check-out. Later they can be progressively integrated into the spacecraft without the need for any special harness. One disadvantage of wireless RF interfaces is that they may be susceptible to RF interference from external sources. Also they may interfere with other equipment or each other. Among the different wireless communication standards, developments based on the IEEE 802.15.4 and Bluetooth for limited distances and low data rates are the preferred options. Among these two, the IEEE 802.15.4 standard which features a sleep mode has attracted more attention. Also the family of IEEE 802.15.3 (WiMedia) standard seems to be very promising for high data rate and short range intra-spacecraft communication. For longer range communication (i.e. inter-spacecraft communication in close distances), IEEE 802.11 family of standards (specially revision 'n') suits the application. These standards will be introduced in further details later in this Chapter. Network topology, bandwidth, energy consumption, EMC requirements, intrinsic robustness and implementation complexity are the factors to be considered before using any of the wireless standards for onboard applications.

Wireless optical links: Optical wireless interfaces could be divided to two classes: line-of-sight and diffuse. The line-of-sight technique is a point-to-point data transmission method which requires a clear line of sight between the communication parties. This technique is less flexible for monitoring the data, however its data rate could be very high, can be very long-range and will relax the EMC requirements. Careful aiming of the receiver and transmitter is also required. The diffuse technique is more flexible. However its range of operation is shorter and transmission is not guided. Thus, this method is a point-to-multipoint communication technique [Bevan et al. 2003, Sakano et al. 1991, Kim et al. 2000, Li et al. 1992, Gfeller and Bapst 1979]. Monitoring the traffic of diffuse optical links inside the spacecraft for test and verification purposes is easy but not as easy as the case of wireless RF interfaces. Walts *et al.* present an example of designing an infrared bus for a small spacecraft [Walts et al. 2001]. Likewise, Pelissou *et al.* report validation of a wireless optical communication architecture for data communication onboard spacecraft [Pelissou et al. 2005].

Comparing to wired communication, RF and optical wireless interfaces sound unreliable but on the other hand they offer many benefits and features which are out of reach of wired communication standards. To overcome the reliability issue it might be necessary to develop or use special protocols which can

ensure a higher degree of reliability in wireless communication for onboard applications. However the main benefits of a wireless communication structure are not bound to the protocol.

The main motivations and benefits for developing a wireless data communication system onboard spacecraft can be summarized as the following:

- Reducing the time and cost of assembly, integration and testing (AIT);
- Inherently providing galvanic isolation;
- Simplifying integration tests and verification;
- Reducing the harness and the complexity of connections;
- Reducing the harness of cable connectors;
- Removing the risk of mechanical damage to interfaces during test;
- Possibility of monitoring the data communication without adding new units and cables to the data bus;
- Flexibility in upgrading and replacing the units;
- Flexibility in designing deployable parts and moving subsystems;
- Possibility of integrating with new power scavenging techniques for designing totally wireless and autonomous modules (i.e. AWSS experiment onboard Delfi-C3 CubeSat - see [Ubbels et al. 2005]);
- Possibility of reusing the same hardware design and interface for other missions.

On the other hand, there are some drawbacks concerning the security and EMC issues of wireless interfaces. Almost all of the available wireless interfacing standards are designed to operate in relatively open environment such as home or office, and not a closed environment such as the area within a spacecraft. It is important to make sure that the wireless interfaces are not sensitive to disturbances made by other on-board electronics, and also are not interfering with other equipment. Different studies have reported no meaningful EMC concern connected to using COTS wireless standards onboard spacecraft. For example Yuanyuan studies EMC effects of Mica2 WSN nodes operating in 903 MHz and 927 MHz frequency range in a spacecraft mock up and reports no EMC effect or communication problem [Yuanyuan et al. 2008]. Likewise Narvaez has studied several frequency bands between 14 kHz and 8.445 GHz inside a spacecraft and has found no anomaly [Narvaez 2003]. Several types of wireless devices and sensors have already flown on space missions. For example implementing a wireless LAN in International Space Station (ISS), simple

wireless RF sensors [Champaigne 2003], or soon will be flown [Arruego et al. 2003]. Magness provides a comprehensive list of current activities in using the wireless devices in space applications [Magness 2006]. In fact, migration from current bus standards to a wireless standard has begun and will become smoother in the upcoming years.

2.5.1 Design Considerations

A systematic observation of the bus development over the past years shows that the general development direction has been towards increasing the bus speed, reducing harness, increasing reliability and fault tolerance and reducing mass. Technology advancements has brought the opportunity of developing higher speed bus standards, i.e., SpaceWire which is not only providing a high speed communication link, but also introduces advanced features for increasing the reliability and fault tolerance [Parkes 2001]. Increasing the rate of data communication on the bus usually reduces the harness and mass, because with a higher speed data handling system, fewer conductor pairs are required in transferring larger volumes of data, thus less point-to-point links are necessary. Use of fiber optics instead of wire could be another way of saving mass and reducing EMC effects [Barnes et al. 2002]. Miniaturization has brought the possibility of developing smaller embedded systems as the drivers of high speed bus systems. Because of the advances in the chip design and electronics, it is possible to use more advanced algorithms for fault detection and correction for CDHS. The impacts of technology advances on the reliability and performance of the bus architecture become clearly visible by systematically comparing the features of SpaceWire with other standards (see Table 2.1). Observing the development of data bus standards, reviewed in Section 2.2, highlights the following trends in design requirements and drivers:

Higher data rates: In earth observation science and remote sensing, acquiring more data is always beneficial because it provides higher resolution information about the phenomena. Also a higher bandwidth can generally guarantee a real-time communication and smaller delay. CDHS should be able to communicate the information to spacecraft units with the lowest needed delay and latency;

Higher processing power: Availability of a higher volume of data onboard brings a higher demand for onboard pre-processing and logging. It is generally much more efficient to pre-process onboard data before communicating to the ground station. Data compression and pre-processing needs more onboard processing power. Although this is rather a requirement on CDHS in general, the onboard communication standard can

be affected too. For example CAN bus micro controllers are much more powerful than ESA OBDH or MIL-STD-1553B;

Lower energy consumption: The availability of electrical energy onboard spacecraft is usually very limited, and the cost of generating energy in terms of spacecraft mass is very high. Therefore low energy consumption is essential at all levels (communication, processing, synchronization, etc.);

Lower cost: the cost of spacecraft launch is directly proportional to the spacecraft mass. Parametric cost models which are made for spacecraft clearly demonstrate this direct relationship [Department of Defense (DoD) 1999]. Also, standardization of interfaces, modules and building blocks allows savings due to the re-use of the elements. This means that customization is not a cost friendly exercise. This requirement shows the potential of COTS devices in reducing the cost of space exploration.

2.5.2 Scientific Research Challenges

An intra-spacecraft wireless network enables wireless data communication between different nodes onboard the spacecraft. These nodes can be sensors, actuators, payloads or spacecraft subsystems. Onboard wireless communication eliminates the mass and occupied space of cables for data and possibly power. The inherent untethered operation also makes them much easier to provision during test, development and inspection, particularly after the spacecraft is built, because the need for additional cabling is minimized or eliminated. As it was discussed before, benefits of wireless communication for intra-spacecraft communication include reduced mass, mechanical and electrical isolation, communication redundancy, easiness of adding, deleting, or re-purposing circuits during the design. However, it is very important to consider the design constraints and the performance potential that can be made to identify the major research challenges. Major research challenges for onboard intra-spacecraft communication are:

Real-time communication: In some specific cases of payload, real time data delivery plays a key role. A permanent or temporary real time data transmission delivery may be required by such nodes while other subsystems, such as attitude determination sensors, may not demand this. In addition, on the system level the priorities of different nodes may change over time. Most of the existing communication standards either ignore real-time needs or simply attempt to increase the data processing power to approach the real time requirements. Solutions to dynamic prioritizing

of the nodes' traffic demands and design of true real-time protocols are considered to be the two major research challenges in this field.

Energy management: Limited processor bandwidth and memory are two constraints which are disappearing with the new advances in miniaturization and electronics. However energy constraints are unlikely to be abandoned in a near future. WSAN nodes can be self-powered or spacecraft-powered. The self-powered nodes should rely on a local battery or energy harvesting mechanisms. A solution could be adding more intelligence to the nodes to reduce the data transmission rate upon energy shortage [Bandyopadhyay and Coyle 2005, Willett et al. 2004]. If the sensor is self-powering, it can become intelligent enough to change its resolution to sustain its performance. In this case, algorithms will be needed to reconfigure the transmission strategy or the sampling rate of the sensor front end [Kho et al. 2007, Marbini and Sacks 2003].

Interference: A number of WSAN problems and research topics are dealing with real world factors. For example, effects of signal reflection, scattering and fading. Presence of walls and holes in the body of the spacecraft and different electronic systems have influences on the signals. The electromagnetic waves produced by nodes may be harmful for some of the sensitive devices. Optimizing the location of the nodes (if possible) to achieve the highest signal to noise ratio (SNR) and efficiency should be done during the design [Feriencik et al. 2006]. If necessary, relays can be added. The number of relays and their locations and gains are to be analyzed. However no harmful interference effect is reported in the literature [Yuanyuan et al. 2008, Narvaez 2003].

Distributed task accomplishing: To realize most of the potentials of onboard wireless communication, the onboard WSAN can be used to implement a distributed task strategy. For example, sensors and actuators of ADCS may communicate to each other directly in a point-to-multipoint configuration. If the control can be accomplished by different actuators, algorithms can be developed to trade off time and precision vs. energy consumption to identify the most optimum actuator. In case of a failure in an actuator or power shortage, the network should be able to reconfigure and update its decision.

All these challenges are important and should be addressed in case of developing a new approach or choosing a COTS standard for spacecraft onboard wireless communication. Among these challenges energy management is the most important one which is a major issue in all space related designs and technologies.

In the next Section we focus on choosing a COTS standard instead of developing a new one. Some COTS standards present unique features related to their operation modes, network topology and energy consumption. Thus, this selection has an impact on approaching the energy management problem. Later in Chapter 3, the energy management problem will be further discussed and different solutions will be introduced. In the second part of this dissertation, (Chapters 4 and 5) energy management algorithms are developed to approach this challenge for sensors of spacecraft ADCS.

2.5.3 Onboard Wireless Nodes

The intra-spacecraft wireless network provides wireless link between various nodes inside the spacecraft. In a typical satellite, the wireless network is in charge of handling the following data traffic types:

a. House-keeping information: this data type is usually sent from the sensors to the main computer for monitoring the spacecraft itself or the environment around it. The commands which are sent from spacecraft onboard computer to subsystems for maintaining spacecraft operation fits in this category as well;

b. Payload data: payload data is usually sent from the payload to the main computer for further processing or communication to the ground station;

c. The ADCS data: this information is usually sent from sensors to onboard computer and from onboard computer to actuators for spacecraft navigation and control.

House-keeping information may include data from small wireless temperature sensors [Eckerley et al. 2005] or the messages communicated between the microprocessors on different subsystems to maintain the operation of the spacecraft. Payload data is usually coming from a single or multiple devices onboard the spacecraft such as optical camera, radar, etc. ADCS information may contain several data types generated by different sensors and actuators, e.g., magnetometer, GPS, star camera, reaction wheels, magnetorquers, etc. The nodes involved in handling of the above three data types can be self-powered (by a battery or local energy scavenging techniques) or powered by the spacecraft power subsystem. In both cases the main engineering objective is reducing the wiring harness and improving flexibility of interfacing.

The different data traffic types impose various requirements to the design of spacecraft data handling. The following parameters are chosen as criteria for selecting the most suitable wireless RF standard for intra-spacecraft communication:

Table 2.3: Requirements on network features for different systems in a typical micro-satellite

Data type	Data rate	Data robustness	Fault tolerance	Reconfigurability
Payload data	High (>10 Mbps)	Low	High	Low
Monitoring & House keeping	Low(<50 kpbs)	Low	Low	Medium
ADCS	Medium (50 Kbps - 1 Mbps)	Medium	High	High

a. Data rate: presents the maximum data bandwidth required by the wireless nodes;

b. Data robustness: a requirement for higher data robustness means that the impact of data loss during the communication is severe;

c. Fault tolerance: represents the requirement on graceful degradation and data recovery. The cause of failure can be temporary power loss or interference;

d. Reconfigurability: presents the ability of the network to reconfigure itself in presence of a permanent power loss of some nodes, e.g., maintaining ADCS in case of a sensor failure.

Table 2.3, depicts the aforementioned requirements for the three typical data types for a typical satellite. The presented data is gathered after evaluating recent micro-satellite projects such as BIRD [Lorenz et al. 2004], PRISMA [Gill et al. 2006] and Ørsted [Hoffmeyer 2000]. For example, the BIRD micro-satellite ADCS uses a GEM-S GPS receiver which communicates its data at maximum 76800 bps [Gill et al. 2001, Rockwell Collins 1997]. BIRD spacecraft carries three main science payloads. The payloads communicate their data with a maximum rate of 4790 Kbps [Schuster et al. 2002].

2.5.4 Wireless RF Standards

In this Section, an overview of selected COTS wireless standards is given. Potentially, the spacecraft bus harness could be reduced by using any of these wireless transmitters instead of wired data communication standards. Thereafter, the features of these standards are evaluated to select the most suitable candidate among them.

Bluetooth ™

Bluetooth is designed as a wireless communication standard for short-range and low cost devices to replace cables of computer peripherals. This range of applications is called wireless personal network (WPAN). This protocol is maintained by the Bluetooth special interest group (Bluetooth SIG) which was originally founded by Ericsson, IBM, Intel, Nokia and Toshiba. IEEE 802.15.1 was derived from Bluetooth v1.1, however later versions were not standardized by IEEE. Bluetooth operates in the frequency range of 2402 Ghz - 2490 Ghz of free ISM band [2]. Using Frequency Hopping Spread Spectrum (FHSS), the available frequency range is divided into 79 channels of 1 Mhz, where data is modulated using Gaussian Frequency Shift Keying (GFSK). A Bluetooth transmitter switches between these channels at up to 1600 Hz which provides added security, reduced interference with other devices, and decreased noise on the network. Bluetooth was designed for real-time data and voice applications. Bluetooth version 2.0 with Extended Data Rate (EDR) is capable of data throughput of up to 2.1 Mbps (maximum transfer rate of 3.0 Mbps). Bluetooth devices can be categorized into three classes according to energy consumption and effective range. Classes 1, 2, and 3 have transmission ranges of approximately 100 m, 10 m, and 10 cm respectively. Two connectivity topologies are defined in Bluetooth: the piconet and scatternet. A piconet is a WPAN formed by a Bluetooth device serving as a master in the piconet and one or more Bluetooth devices serving as slaves. A slave can also be a master in another piconet resulting in a series of interconnected piconets, referred to as scatternets. A frequency-hopping channel based on the address of the master defines each piconet. All devices participating in communications in a given piconet are synchronized using the clock of the master. Slaves communicate only with their master in a point-to-point fashion under master control. The master's transmissions may be either point-to-point or point-to-multipoint. Also, besides in an active mode, a slave device can be in the parked or standby modes so as to reduce energy consumptions. A scatternet is a collection of operational Bluetooth piconets overlapping in time and space. Two piconets can be connected to form a scatternet. A Bluetooth device may participate in several piconets at the same time, thus allowing for the possibility that information could flow beyond the coverage area of the single piconet. A device in a scatternet could be a slave in several piconets, but master in only one of them. This standard is capable of addressing a maximum of seven active

[2] The ISM (Industrial, Scientific and Medical) bands are open frequency bands, varying by region, that allow for operation without a license. These are also know as the unlicensed bands. In North America, these bands are the 260 Mhz to 470 MHz, 902 Mhz to 928 MHz, and 2.4GHz, among others. The 2.4 GHz band is also utilized for worldwide operation. As a basis for unlicensed operation, these bands are often hosts for standardized and proprietary protocols such as Wi-Fi, Bluetooth, ZigBee, Z-Wave, etc.

(and up to 255 inactive) slave devices in a piconet. Any device that is powered can query to find and establish connections with other devices. Given a security pass key, a device can communicate with any other device, allowing full Plug-and-Play (PnP) capability. For secure data communication, this pass key can be refreshed regularly. Three low power states have also been integrated into Bluetooth: sniff, park and sleep. These states allow moderating the energy consumption according to link activity.

ZigBee ™

ZigBee is a WPAN network standard which is regulated by ZigBee Alliance. It defines a communication at level 3 in the OSI model build on top of IEEE 802.15.4 which defines a level 2 OSI layer. It is designed to provide extremely energy efficient connections between devices that use small packets. For this reason it is only capable of supporting a maximum data rate of 250 Kbps in a distance of 10 meters. In addition to its power efficiency, this standard provides security by means of data encryption, frame integrity, and access control. ZigBee can function in one of the three ranges of the unlicensed ISM band, specifically 2.4 GHz - 2.48 GHz, 902.0 MHz - 928.0 Mhz or 868.0 Mhz - 868.6 MHz. Another consequence of ZigBee 's low energy consumption is that data processing on either end of a communication channel is kept to a minimum. This reduces the overhead on each packet, but makes the protocol readily prone to interference and blockage in closed environments. ZigBee is an industry standard supported by multiple solution providers, making COTS available at cost effective levels.

IEEE 802.15.4 based communication family performs very well against noise because they use direct sequence spread specturm (DSSS) to modulate the information before being sent to the physical layer. Each bit of information is modulated to 4 different signals. Thus, the total information to be transmitted requires a larger bandwidth but uses a lower spectral power density for each signal. This brings less interference in the frequency bands and a better signal to noise ratio (SNR) in the receiver. Furthermore, IEEE 802.15.4 family uses carrier sense multiple access collision avoidance (CSMA-CA) and also guaranteed time slots (GTS) which both reward higher robustness against interferences. One of the functionalities implemented in IEEE 802.15.4 is the channel energy scan feature (PLME-ED) request. The idea is to determine how much energy (activity, noise or interference) is available in the communication channels before selecting one. This enables inherent energy saving in transmission of the information.

ZigBee provides self-organized, multi-hop, and reliable mesh networking with long battery lifetime. Two different device types can participate in a low rate WPAN network: a full-function device (FFD) and a reduced-function device

(RFD). The FFD can operate in three modes serving as a PAN coordinator, a coordinator, or a device. Each FFD can talk to RFDs or other FFDs, while a RFD can talk only to a FFD. A RFD is intended for applications that are extremely simple, such as a light switch or a passive infrared sensor. They do not have the need to send large amounts of data and may only associate with a single FFD at a time. Consequently, the RFD can be implemented using minimal resources and memory capacity. After a FFD is activated for the first time, it may establish its own network and become the PAN coordinator. All star networks operate independently from all other star networks currently in operation. This is achieved by choosing a PAN identifier, which is not currently used by any other network within the radio sphere of influence. Once the PAN identifier is chosen, the PAN coordinator can allow other devices to join its network. An RFD may connect to a cluster tree network as a leave node at the end of a branch, because it may only associate with one FFD at a time. Any of the FFDs may act as a coordinator and provide synchronization services to other devices or other coordinators. Only one of these coordinators can be the overall PAN coordinator, which may have greater computational resources than any other device in the PAN.

IEEE 802.11 (Wi-Fi)

IEEE 802.11 is a wireless LAN (WLAN) communication protocol which is also referred to as Wi-Fi, and is introduced and maintained by Wi-Fi Alliance. The revisions of this standard currently available include 802.11a, 802.11b, 802.11g and 802.11n. This standard defines the medium access control and several physical layer protocols of the OSI model for wireless communication. IEEE 802.11 can be setup on either a mesh or star topology. Due to elimination of wires, these architectures have reduced complexity of design, while maintaining their high data throughputs. The main difference between these three standards is their operating carrier frequency and their data transmission rates. While the 802.11b and c are on the 2.4GHz ISM band, the 802.11a runs on the 5 GHz and 3.7 GHz signals. Also since IEEE 802.11g was based on 802.11a and 802.11b was not, the a and g share other qualities such as higher data transmission rates. IEEE 802.11g revision uses orthogonal frequency division multiplexing (OFDM), however can revert to complementary code keying (CCK) to maintain backward compatibility with IEEE 802.11a. the 802.11g type has an effective range of up to 100 meters depending on the construction of its surrounding environment. This distance can be extended by employing a range extender which will increase the energy consumption of the system. The major advantage of Wi-Fi is the ease of Plug and Play and hot swapping of peripheral devices. The major disadvantage is that the energy consumption is much higher than Bluetooth and ZigBee.

2.6 Discussion

Adding wireless connectivity feature to a sensor or actuator can increases mass, computation overhead and energy consumption of the node. For example equipping a very simple and small pressure or temperature sensor with a wireless transmitter is too expensive and hence not intended. Thus, the number of wireless nodes in a microsatellite is not expected to be very high. It should be mentioned that a microsatellite typically has a mass of less than 100 kg and can generate a limited amount of energy due to the restricted size of its solar panels. Therefore, not only mass reduction is a key requirement in the design but low energy consumption is very important too, even if the wireless enabled module is not self-powered. Thus, given the design requirements which were presented in Section 2 and the characteristics of onboard data types presented in Table 2.3, one can conclude that a low power, reliable and fault tolerant communication protocol which supports low to medium data rates can fulfill most of the intra-spacecraft communication requirements. As it is shown in Table 2.4, ZigBee and Bluetooth both can meet this need but ZigBee consumes less current and has lower system complexity.

ZigBee is categorized as a low rate data transferring standard as well as Bluetooth. However ZigBee and Bluetooth have very similar specifications, they are two different technologies with different areas of application and different means of designing for those applications. While ZigBee is focused on control and automation, Bluetooth is focused on connectivity for data communication between laptops, PDAs and it is designed for reducing harness and cable replacement. If the network size is important, ZigBee networks can accommodate more nodes than a Bluetooth network. Because of these differences, the technologies are not only geared toward different applications, they do

Table 2.4: Specifications of COTS wireless standards which can be used for intra-spacecraft wireless communication

Criteria	**Bluetooth (802.15.1)**	**Wi-Fi (802.11b)**	**Wi-Fi (802.11a)**	**Wi-Fi (802.11g)**	**ZigBee (802.15.4)**
Max data rate [Mbps]	0.72	11	54	54	0.25
TX power [mW]	1	100	100	100	0.1-10
Network topology	Ad-hoc piconets	Point to Multipoint	Point to Multipoint	Point to Multipoint	Ad-hoc, Star, Mesh
System complexity	Medium	High	High	High	Low
Typical current consumption [mA]	<150	<400	<500	<400	<60

not have the capability to extend to other applications. As an example, for its applications, Bluetooth must rely on fairly frequent battery recharging, while ZigBee is designed for devices which need long lasting battery life and infrequent data communication. In timing-critical applications, ZigBee is designed to respond quickly, while Bluetooth takes much longer and could be detrimental to the application. Therefore, a user could easily decide which technology suits the application and choose between Bluetooth and ZigBee for the onboard data communication. It could be suggested that ZigBee is more suitable for house keeping and low data rate ADCS sensors while Bluetooth suits high data rate sensors and actuator. However, where a higher data rate is necessary for a payload, other types of wireless communication standards such as Wi-Fi could be considered. In such a case, care should be taken in selection of the standard since a higher data rate translates into a higher energy consumption. To accommodate this issue, system level energy management techniques can be employed which will be discussed later in this dissertation.

Another reason for selecting ZigBee as a strong candidate is hidden in two unique features of this standard. The IEEE 802.15.4 which is the core of ZigBee defines *sleep mode* for wireless transmitters hardware. In this mode the transmitter operates in a very low power state but it is ready to wake up and transmit the information almost immediately. The nodes stay in sleep mode and wait until they receive the beacon from the network coordinator. The beacons wake up other nodes to check whether there is any incoming message. If there is none, both the nodes and the coordinators go back to sleep. In other wireless standards, the transmitter shall stay awake all the time to initiate a communication which results in a high energy consumption. The second benefit is hidden in capability of this standard in organizing a fully connected mesh network. This feature enables a decentralized architecture for ADCS nodes which can increases the robustness and modularity of the system.

Chapter 3

Onboard Wireless Sensor and Actuator Network

Science never solves a problem without creating ten more.

– George Bernard Shaw [1]

Wireless communication is one of the biggest engineering achievements during the past decades. The scientific and economical impacts of this technology and its applications have been enormous. Technology advancements in automation and monitoring has brought up the rapid growth in the number of computers, peripherals, sensors and electronics for indoor use in offices, manufacturing floors, shopping areas, warehouses, hospitals, etc. To avoid cable routing to every foreseeable location and to provide flexibility, wireless communication for indoor applications is very appealing. These days it is not easy to find an office, house or shopping center without a type of wireless communication system, either for Internet, telephony or monitoring. Two approaches have always been in focus to implement this concept: infrared radiation, or spread spectrum microwave technology (radio frequency, i.e. RF). Between these two, infrared technology is not very much encouraged for office and house hold appliances because of its limitation due to multi path, ambient lights and transient time of the light emitting diodes (LED) [Carruthers and Kahn 1998]. However, wireless devices based on RF technology are widely used nowadays. They are resistant to multi path fading, interception and interferences. In RF technology, it is possible to provide simultaneous access to a communication

[1] George Bernard Shaw (Jul. 26, 1856 - Nov. 2, 1950) was an Irish playwright and a co-founder of the London School of Economics. He is the only person to have been awarded both a Nobel Prize in Literature and an Oscar.

channel for a number of devices.

This Chapter shortly reviews major available wireless communication services which are widely used commercially. Then it compares these services with an intra-spacecraft wireless network. This will to introducing onboard wireless sensor actuator network (OWSAN) as a new category for describing spacecraft onboard wireless nodes. Thereafter the problem of energy conservation for ADS nodes of an OWSAN will be discussed and suitable energy management methods will be presented. Finally, a basic idea for designing an energy manager is presented.

3.1 Wireless Networking

Several services were developed over the past 30 years based on wireless RF communication and they have had broad applications in our environment. Some of these services have found their applications in our houses, offices and daily life. These services are reviewed in this section to gain a better understanding of possible architectures for onboard wireless communication.

Broadcast: The first introduced wireless service was broadcast radio. In broadcast radio the information is transmitted to different users in one direction. This means that only broadcast station sends the information and users only listen and receive them. This information is the same for all users and it is sent usually continuously. Sometimes multiple transmitters are used to send the same information. Usual European TV and radio broadcast is an example of such a wireless system. In this configuration the transmitters do not need to have prior knowledge about the receivers. Here, duplex channels are not necessary to establish a two-way communication path. Also the number of receivers (or active receivers) does not change the structure of the transmitter station as it sends the same information for all receiver nodes. Such unidirectional communication configurations can be used onboard a spacecraft if receiving data or feedback from the target are not required.

Paging: Paging systems are similar to broadcasting in the sense that they are unidirectional wireless communication systems. However, the information is intended only for a single user. The amount of transmitted data is usually very small and temporally scarce. In most of paging systems, the received information is only a single bit of information which can be translated into an alert or emergency note. Sophisticated paging allows transmission of short messages but still the amount of information is rather limited. Therefore the required bandwidth for this service can be very low and the service can work in very low carrier frequencies, e.g.

150 MHz. Pagers were very popular during 1980s for specific group of professionals such as doctors to enable fast reactions upon emergency situations [Russek 1994]. However the success of cellular telephony has considerably changed the popularity of such wireless pager systems. Still, the strong advantage of pager systems lies in the large coverage area that they can achieve due to their low carrier frequencies. Such configuration can not be beneficial onboard a spacecraft not only because the communication channel is unidirectional from the base station to the nodes, but also due to the quite low bandwidth.

Cellular telephony: Cellular telephony is an important type of wireless communication. The information flow in cellular telephony is bi-directional. Each user can transmit and receive the information at the same time. The location of the user within the network coverage is not important and the user can be highly mobile during the communication. Information transmission can be initiated by the user or the network but a call is always initiated for a single user and the other users can not freely listen to the communicated information. Usually in such networks the available bandwidth is limited and is dynamically shared between users. Therefore the number of active users at each instant of time is usually limited but there are different techniques to lift this limit such as using the cellular principle [Lee 2005]. This architecture is too sophisticated for spacecraft and it is not mainly designed for short range distances. However, offering the functionality to establish on-demand communication is relevant to onboard communication.

Trunking radio: A variant of cellular telephony network is trunking radio system. It is used as a communication service between closed user groups. In these systems, a communication can be sent to a number of users at the same time or conference can be set up between multiple users. Such systems usually serve on a *first-come, first-serve* basis. Thus, when a call is established it can not be interrupted by other users. However, it is possible to prioritize the calls to allow dropping a low-priority call to serve a high-priority one. In such systems, the range of the network can be extended by using each wireless node as a relay station. Such system can even use multiple relays to reach the base station. Example of trunking radio systems is the communication network which is used for police, taxi services, fire fighters or similar closed group of users [Chen and Trajkovic 2004]. The on demand priority based functionality of trunking radio systems is interesting for spacecraft onboard communication but the trunking radio hardware is not intended for low-power short-range communication.

Cordless telephony: Such system describes a wireless link between a handset

and a base station which is directly connected to a larger network. The main difference between this system and a cellular telephony is that cordless telephone is usually communicating with only a single base station. No mobile switching center exists and mobility is limited. In this system, the base station does not need to know the location of the mobile node while it is located within the covered area. An example of this system is cordless phones in offices or apartments [Harte and Ofrane 2006]. A cordless telephony system is very similar to the type of communication which is needed onboard a spacecraft if a star communication architecture is sought. Such configuration can be implemented with ZigBee and Bluetooth.

Wireless local area network (WLAN): Wireless local area networks are very similar to cordless phones. These networks connect a single user device to a public network system. Examples of users of this system can be a laptop computer and the public network can be the Internet. A major difference between WLAN and cordless telephony is the required data rate. Cordless phones usually transmit only digitized speech which needs a data rate about 64 Kbps while WLANs facilitate a higher data rate over a relatively large distance (usually up to 100 meters). To meet the need for a higher data rate, different standard for WLAN are developed which mostly carry the identifier IEEE 802.11 [Roshan 2004]. WLAN devices can connect to any base station which uses the same standard however it is possible to enable security settings to limit the access for undesired users. A variant of WLANs are fixed wireless access systems. These systems are replacing a dedicated wired connection between the user and the public land-line system. In this case, the user has no mobility but placement of a wire can cause mechanical, safety or security issues. WLAN is not meant for short range application such as spacecraft onboard network.

Personal area network (PAN): Personal Area Network (PAN) is used when a smaller coverage area than that of WLANs is needed. These networks are mostly used for simple *cable replacement* purposes. For example devices which are enabled with Bluetooth wireless transmitters allow connection of a hands-free headset to a phone, or a keyboard to a computer which is located in the vicinity of the keyboard without using a cable. In such cases the distance between the base station and the wireless device is less than few meters. In most of these applications the required data rates are fairly low (less than 1 Mbps) [Misic and Misic 2008]. A variant of PAN is body area network (BAN) which is for even shorter distances and enables communications between devices located on a user's body. PANs application is rapidly increasing mostly in health monitoring for patients and recently for military uses [Quwaider and Biswas 2010]. Most of these systems use a point to point or star topology but they can potentially

enable point to multi point connections. ZigBee and Bluetooth are very popular wireless communication standard for these type of systems. The flexibility, features and architecture of PAN and BAN are similar to that of a spacecraft onboard wireless network, specially because these standards and topologies are designed for low power sensing and communication in short distances in star and mesh configurations.

Ad hoc network: In ad hoc networks, instead of arranging a network infrastructure, networking nodes establish network connections in an ad hoc manner on demand. No infrastructure and base station is needed. Usually ad hoc network are made for a special purpose which can be emergency situations [Murthy and Manoj 2004]. In the simplest case of an ad hoc network, all nodes are in direct communication range of each other and make a single-hop network. In all more complex cases, data must be delivered through multiple nodes. Such multi hop routing needs dynamic path identification and management. Limited communication range of the nodes can increase the complexity of the problem. The single hop configuration usually is not practical due to the distances and obstacles. All nodes in ad hoc network must provide network data forwarding and routing capability next to their application dependent features, which means more local processing power is required. This duality is unique in ad hoc network, since each node is participating as an end system and also as a router. Each node of an ad hoc network can have unique and pre-configured identifier, i.e. an address. This address remains fixed during the operation time and location. Then the network needs to use these identifiers to detect the topology of the network and establish the routes. Ad hoc networks are perfect example of mesh network topology. Since no base station is present, self-organization is the key to establish a true ad hoc network. Due to these characteristics, an ad hoc network is truly plug and play and expandable. Although, adding each new node to the network increases the processing load on all nodes to understand the network topology and routing paths. A more complex scenario is realized when the ad hoc network nodes can move around. This type of ad hoc network is called mobile ad hoc network (MANET). Here the quality of network depends on the speed of the nodes to adapt themselves to the new topology. Each node needs to recognize the neighbors and re-establish the connections and re-understand the topology of available routes. An ad hoc network can be a hybrid configuration of mobile and fixed nodes. Although ad hoc networks can be very interesting for space applications such as inter spacecraft communication, due to the limited number of onboard nodes and fixed physical location of the nodes, the rich features of ad hoc networking are not very relevant to intra-spacecraft wireless networking.

Wireless sensor network (WSN): a wireless sensor network is made of a collection of nodes which are organized into a cooperation network [Hill et al. 2000]. The basic idea of WSN is to transmit the measurements of physical values to a base station for data fusion and further processing. Therefore in a WSN the network nodes are required to perform sensing and transmission of data. In addition, several kinds of preprocessing activities can be applied on the measured data locally on the nodes. Sensors data can be transmitted directly to the data fusion center (*sink*) without passing through any hub, or can be delivered via multi hops. WSN can have a single sink or multiple sinks. The sink can be connected to other networks, for example the Internet, to deliver the information to the end customer or control center. A single sink WSN can be very practical for a small WSN, but for bigger networks with huge number of nodes multi sink configuration can be more energy efficient and responsive specially in multi hop configurations. The bigger network size, the higher amount of data should be gathered by the sink and sometimes clustering is designing such networks. [Guo et al. 2009, Hou et al. 2009]. Figure 3.1(a) shows the overall architecture of WSN in a multi hop configuration with multi sinks. A WSN can be used to monitor an environment with battery powered sensors. For example a WSN with large number of battery powered nodes can be deployed to monitor a structure such as bridge or building, or in a forest to measure the temperature or humidity [Zhang et al. 2009]. Specific type of WSNs can be used to monitor animals behavior in nature, which introduces mobile wireless sensor network and adds extra complexity in designing and analyzing the network [Andonovic et al. 2010, Guo et al. 2006].

Wireless sensor and actuator networks (WSAN): In WSAN, actuators are introduced to WSN. Actuators are by definition the devices which are able to manipulate the environment, while sensors only observe it. WSANs are made of sensors, actuators and data sinks (Figure 3.1(b)). Adding actuators to the network is not just a simple extension of WSN. The flow of information in WSAN network is partly reversed because actuators need to receive data. The data can be received either directly from the sensors or from the sinks. Therefore a WSAN protocol should be able to arrange many-to-one communications when sensors provide data, and one-to-many when an actuator needs to receive information. Also one-to-one communication might be needed when data should be transmitted from a sensor to a specific actuator (or sink) [Morita et al. 2007, Cayirci et al. 2005]. In most WSANs, the number of sensors is much higher than the number of actuators and sinks. In most WSAN applications, battery-powered devices are used to make the deployment of such nodes easier. To let the system work with required performance requirements

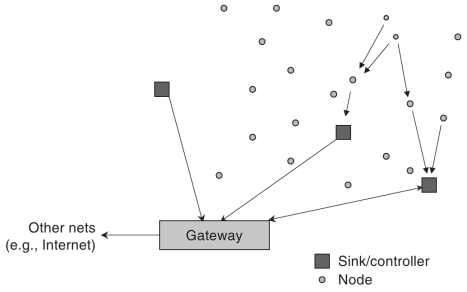

(a) A multi-hop multi-sink WSN

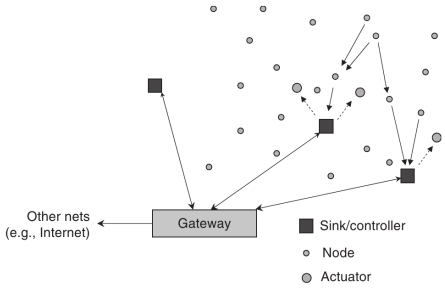

(b) multi hop WSAN

Figure 3.1: A sink is where data fusion, data aggregation or data logging takes place. If the network is onboard spacecraft then the onboard computer can represent the sink.

during the network lifetime, the nodes must be capable of staying alive for a sufficiently long period by using the energy provided by their local battery. In many applications the battery can not renewed during the lifetime of the system [Umehira et al. 2008]. For example if the nodes are deployed in nature in large number, the cost of recapturing them and replacing their batteries will be practically high. This highlights the importance of energy efficiency of all tasks performed by a node in a WSAN.

Spacecraft onboard wireless communication shows many similarities to the aforementioned services. Specially, properties of WSN and WSAN are very relevant an onboard communication scheme. The next Section discusses these opportunities in further details.

3.2 Intra-office vs. Intra-spacecraft WLAN

A modern office environment has similarities to a spacecraft. Although the design of spacecraft onboard electronics follows tougher reliability requirements, the nature of the majority of communications requirements are similar. Usually a modern office is equipped with many computers and peripherals. Similarly, there are many subsystems available inside a spacecraft. In both cases, these devices need point to point connections to interchange information. For example a mouse or keyboards is connected to a computer with a point to point communication link. Similarly, payload measurements are usually transmitted to the spacecraft onboard computer (OBC) with a direct point to point connection. Some office equipment need to access or share common services which are available locally or globally, e.g., accessing a network printer or the Internet. The same type of connection needs exist on spacecraft. An onboard point to point connection can be the link between a health monitoring temperature sensor with onboard computer. As a shared onboard service, sensors can use a centralized logging system on the onboard computer. Another example could be the communication between between an actuator and several sensors which provide the feedback. In a decentralized onboard architecture, several point to multi-point communications can be established.

On the other hand, we observe that the rising need for portability, productivity, interchangeability, safety and plug and play features has introduced different wireless communication solutions and techniques for office environments. For example to avoid extra cabling of computer peripherals, Bluetooth enabled mouse and keyboards are very popular. Wi-Fi networks exist in almost all offices to enable fast and easy Internet access for laptops, netpads, netbooks and PDAs. Similar needs and requirements have emerged the ideas of intra-spacecraft wireless networking which was presented in Chapter 2.

An intra-spacecraft wireless network can potentially support wireless sensors which monitor the environmental or structural health of a spacecraft or are used for attitude determination and control sensors and actuators. Each of these wireless nodes can be powered either by a battery in its package (and possibly an energy harvester) or receives energy the spacecraft electrical power subsystem through cables. Either way, replacing the wired harness with wireless transceiver front end for sensor nodes eliminates the cable and connectors' mass and frees the occupied space of the data communication harness. If the sensor is equipped with local energy harvesting the power cables are removed too and additional reduction is achieved. However mass reduction is not the only benefit of wireless onboard technology. The untethered operation of different sensors also makes them much easier to be used for provision and tests particularly after the spacecraft has been built or is operational. Thus

additional cabling on the subsystems for performing tests and monitoring the data transmission is minimized or completely eliminated. If the node is battery powered then one of the primary design objective is to maximize the amount of measurements and data which is successfully transmitted from the network before the batteries expire. In practice even if the nodes are spacecraft-powered it is essential to increase the energy efficiency of the system without sacrificing the performance.

PAN and WLAN networks are widely used for intra-office communication and the correspondent standards and hardware are widely tested and available at low cost. This has been the motivation for several studies which are conducted on the possible usage of COTS components and office communication standards for space applications [Kayali 2002, Haebel 2004, Underwood 2003]. In a systematic approach Krishnan and Mazzuchi have proposed a procedure for evaluating the uncertainty in the reliability of an electronics component and modeling its effect on the overall system reliability [Krishnan and Mazzuchi 2001]. These reliability concerns are mostly motivated by the effects of ionization radiation on the electronics COTS components. For low earth orbits, the ionization radiation is mainly caused by trapped electrons, trapped protons and galactic cosmic rays [Howard and Hardage 1999]. The effect of other sources such as neutrons and X-rays in producing radiation dose effects and single event effects (SSE) are negligible.

The major SSEs which are related to today's COTS technologies are single event upset (SEU) and latch-up (LU). SEU is an unintentional change in the state of a digital electronics device which can result in erroneous data or control. This effect is not permanently damaging the device and reprogramming can restore the functionality. Latch-up is the loss of functionality of the device and can be caused by controlled input changes. Usually in such a case the electronics can be restored only by removing and re-applying the power supply. This failure can damage the device if current limiting is not provided for the electronics. The effect of radiation on different COTS electronics is tested and studied in different publications. Layton *et al.* has tested a wide range of electronics such as different types of field programmable gate arrays (FPGA), analog switches, transistors, A/D converters, etc. and has shown that many of these electronics can withstand LEO radiation [Layton et al. 1998]. Other independent studies have drawn similar conclusions too, such as works of Menichelli *et al.* [Menichelli et al. 2000, Menichelli et al. 2002]. Kimura *et al.* has reported successful in-orbit demonstration of a high-performance on-board computer developed by using COTS components in terms of the single-event performance [Kimura et al. 2004] onboard Micro-LabSat Japanese microsatellite. The processor worked and successfully demonstrated its performance under not only normal conditions but also solar flare conditions. In another report, Incledon describes the successful employment of COTS components in the

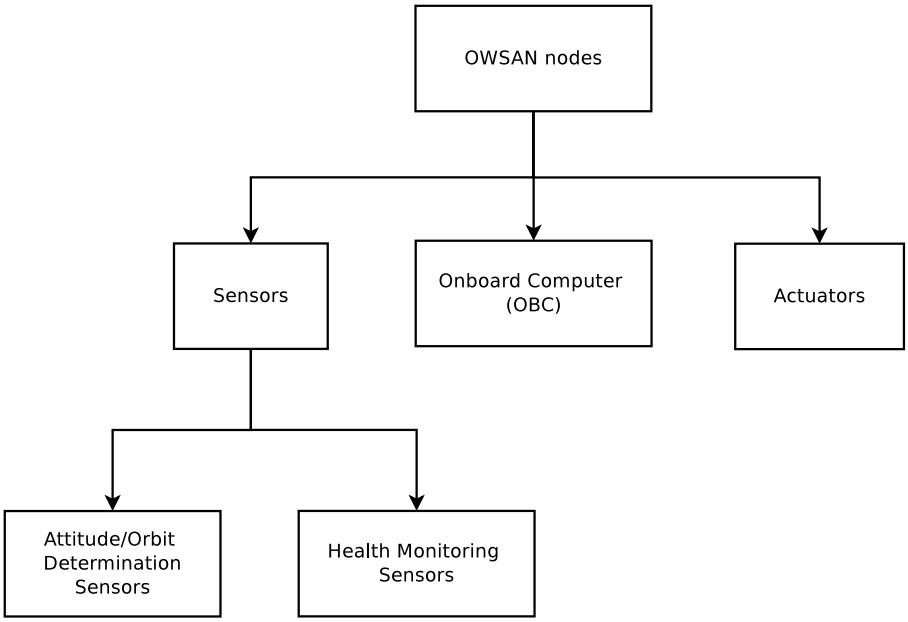

Figure 3.2: Differnet types of OWSAN nodes

Power Transfer Unit (PTU) US space shuttle Orbiter equipment [Incledon 2005]. In addition, success of most university CubeSat spacecrafts which are largely based on COTS electronics shows the high potential of using office standards and electronics for at least LEO space applications.

3.3 Onboard Wireless Sensor and Actuator Network (OWSAN)

From a system design perspective, several criteria can be defined in designing an onboard wireless network and choosing an onboard communication standard. These requirements were discussed in Chapter 2, and it was concluded that onboard wireless communication is feasible with the standards based on IEEE 802.15.4 (such as ZigBee). A typical low power ZigBee transmitter consumes less than 40 mW and has about 2 grams mass. As it is shown in Figure 3.2, an OWSAN architecture can enable the communication between several types of nodes which are detailed as follows:

Onboard computer (OBC): OBC is usually the heart of onboard data handling. It processes the data, records the information and harmonizes the op-

eration of all other subsystems. The onboard computer may collect the payload data, process it and communicate to the ground station through the onboard communication module and vehicle antenna. Depending on the design, attitude determination and control algorithms may reside on the OBC as it has higher computational power. The OBC receives its required energy from electrical power system (EPS) therefore equipping it with a wireless transceiver will not significantly increase the energy consumption. For example, power consumption of an advanced onboard computer such as Myriade for a CNES microsatellite is about 6 W and has a mass of 3 Kilograms [Carayon et al. 2002]. OBC can operate as a sink in the onboard wireless network in a star topology.

Health monitoring sensors: These sensors provide information about spacecraft health situation or ensure the payload functionality. The information produced by these sensors is usually directly transmitted to OBC to be used for making onboard decisions. Examples of such sensors are temperature measurement devices (e.g. thermistors, thermocouples, resistance temperature detectors (RTDs), temperature bulbs, solid-state temperature sensors, etc.), pressure measurements (piezoelectric, rho-cell, solid-state sensor, bourdon-tube, etc.), status inputs from various elements, position switches and status switches. The measured data might be recorded onboard for later use or transmission to the ground station. Usually no other onboard subsystem needs these measurements. The required bandwidth for these sensors is low and the data rate is very low. A point to point connection in a star network topology can perfectly meet the network requirements of these sensors. In such configuration, the sensors are the nodes of the network and OBC is the sink. Hypothetically, such sensors can be easily equipped with a battery powered wireless ZigBee transceiver and last more than 2 years. For example, MICA2DOT ZigBee wireless mote which can be equipped with a wide variety of health monitoring sensors consumes 3 μW in standby mode and 24 mW in active mode. If it is equipped with a 750 mAh coin battery and works with a duty cycle of 0.10%, it can have a life time of 27780 hours which is equivalent to three years and two months [Lappas et al. 2006]. Practically, adding extra electronics on a tiny health monitoring sensor can significantly increase its mass and overall energy consumption. In specific situations this added mass or size overhead can be compensated by the added design value. For example mounting wireless temperature sensors on solar panels to monitor the temperature variation can be much easier than using tiny wired sensors which add a number of long cables to the design. Thus, depending on the design requirements, performing a trade-off analysis is necessary to make the final decision for each individual health monitoring sensor.

Attitude/orbit determination sensors: These sensors measure specific physical elements in the satellite environment which can be used to reconstruct the attitude of the spacecraft or determine the position in orbit. Usually these sensors transmit the information either directly to the onboard computer or to attitude (or orbit) determination and control unit. There is usually a limited number of them mounted onboard spacecraft in a hot or cold redundant configuration. Size and mass of these sensors are typically much more than that of health monitoring sensors and they transmit more information frequently. For example, ESA active pixel sun sensor (APSS) which will be used onboard LISA mission has a mass of about 380 grams, and power consumption of about 1 Watt. SSTL manufactures a sun sensor which consumes less than 100 mW and has 300 grams mass. A typical gyroscope which was flown onboard TUBSAT has 2 Watts power consumption and its mass is 439 grams. This mass and power consumption characteristics allow adding low power ZigBee wireless transceivers when the duty cycle is low. In a centralized ADCS (or AOCS) architecture, the sensors and OBC are working together in a star configuration.

Attitude/orbit control actuators: Actuators are used to tune spacecraft attitude or position in orbit by converting an available source of energy onboard to mechanical energy. Comparing to sensors, typical actuators have more mass and consume more energy. In practice, the characteristics of an actuator are directly related to the mission requirements, type of maneuvers and the mass of the spacecraft. As an example 10SP-M space qualified 3-axis reaction wheel manufactured by SSTL produces maximum wheel torque of 10 mNm and has 960 grams mass while consumes between 0.65 W to 11.5 W depending on the wheel rotation speed. Comparably, the MTR-5 magnetorquer made by SSTL which has flown on a number of LEO microsatellites consumes 1 Watt power and has mass of 500 grams (Table 3.1). Such actuators usually receive the required energy from the spacecraft electrical power supply. Adding the wireless transceiver module will not introduce a significant mass and power consumption overhead on such actuators. In conventional ADCS and AOCS architecture, almost no processing is happening on the actuators. They usually receive the actuation signals commands from the onboard computer. Thus, the communication needs of a conventional ADCS (or AOCS) can be easily met by OWSAN in a star topology. If more processing power can be put on the actuators, then OWSAN can enable a full mesh topology and actuators can directly receive the feedback signals from the sensors and process it locally.

From the later observations, it can be concluded that typical onboard sensors

Table 3.1: Characteristics of different hardware which can be nodes of an OWSAN

Device	Manufacturer	Hardware type	Size [mm]	Mass [g]	Power [W]
Myriade OBC	CNES	OBC	220×120×125	3000 (no housing)	< 6
OBC750	SSTL	OBC	306×167×30	1500	< 10
10SP-M	SSTL	Reaction wheel	101×109	960	0.65 - 11.5
MicroWheel 200	Dynacon	Reaction wheel	102×94×89	930	0.6 - 3.2
Reaction wheel	Satellite Services Ltd.	Reaction wheel	102×102×105 (diameter)	1550	1.4 - 4.2
MTR-5	SSTL	Magnetorquer	251×30×66	500	1
MTR-30	SSTL	Magnetorquer	378×74×49	1800	1
Magnetorquer	Satellite Services Ltd.	Magnetorquer	Length: 80 to 600	< 55	1
A-STR	SelexGalileo	Star tracker	195×175×288	3000 (with baffle)	8.9 - 13.5
ALTAIR HB+	SSTL	Star tracker	316×178×33 (no baffle)	2200 (no baffle)	12
μASC	DTU	Star tracker	120×100×40	555	3.6
Phoenix GPS	DLR	GPS receiver	70×47×15	20	0.85
SGR-05P GPS	SSTL	GPS receiver	105×65×12	60	1
3-axis gyroscope	SunSpace	Gyroscope	99×117×31	439	2
IRES-NE	SelexGalileo	Earth sensor	170×164×156	< 2500	< 4
DSS	DLR	Sun sensor	65×55×25	120	< 0.5
μDSS	TNO	Sun sensor	40×40×10	30	Self powered
2-axisSun sensor	SSTL	Sun sensor	107×95×35	300	< 0.1
Magnetometer	Satellite Services Ltd.	Magnetometer	90×90×20 sensor : 10×10×10	150 sensor: 15	0.4

and actuators of ADCS (or AOCS) can be equipped with wireless data communication. Also the OBC can be enabled as a sink for OWSAN. The OWSAN can be extended to health monitoring sensors too. Usually health monitoring sensors only report a measurement at fixed time intervals and do not need a bidirectional communication with the OBC. Therefore the integration of wireless transmitter on these sensors is straight forward. In a decentralized configuration where sensors have higher level of autonomy and smartness, a mesh configuration can be sought. Here the nodes will be sensors and actuators and can freely communicate and transfer the data without relaying it through the OBC. Nevertheless, a decentralized configuration will be more computation hungry which highlights the importance of onboard energy management. Also it can be concluded that wireless transceivers' mass overhead is not a design issue for majority of the nodes but its energy consumption can introduce design challenges for ADCS sensors. State of the art ZigBee modules are very low power but the majority of ADCS sensors also consume low amount of energy. For some sensors, specially sun sensors and magnetometers, the wireless transceiver energy consumption overhead is comparable to that of the sensor. To analyze this issue the second part of this dissertation (Chapters 4 and 5) focuses on the attitude determination sensors of OWSAN

and presents a solution for lowering the overall energy consumption of these sensors.

Furthermore, taking a closer look into the properties of OWSAN shows interesting characteristics which distinguishes it from available WSAN and wireless ad-hoc networks on the ground. Table 3.2 summarizes the characteristics of OWSAN and compares it with WSAN and Wireless ad-hoc Networks. The key characteristics of OWSAN can be enlisted as follows:

- In OWSAN usually the number of nodes is very limited even if redundant components are considered. The nodes are placed in close proximity and the locations are known. Therefore data routing is not an issue;
- Unlike WSAN, the nodes are usually not prone to failure because the designed reliability for space applications is usually very high;
- The nodes usually transmit the measurement data (with or without pre-processing) to a central processing unit which may use the sensor data to manage the actuators. Therefore the type of the communication is point-to-point and not broadcast;
- Each nodes has a local ID on the spacecraft and this ID is pre-designed and known to other nodes. After spacecraft launch, new nodes are not added to the system;
- The nodes are not physically moving so the configuration of the network is not changing over time. Mobility of nodes is not an issue for OWSAN;
- There is a high correlation between data points in an OWSAN because the sensors are measuring the attitude of the satellite which evolves with a very slow dynamics. This correlation is very useful to reconstruct the lost data and increase the fault tolerant aspects of OWSAN;
- The ultimate design goal is to have completely wireless nodes. Therefore the nodes must be equipped with a local battery and possibly a local energy harvester. Thus, the sensors and actuators will have limited energy available. Nevertheless, some of the nodes such as the Sun Sensors can be equipped with an energy harvester. Also, the close proximity of the sensors may enable the sharing of energy harvester between two or more sensors. This can be achieved by packaging those sensors together.

The available power on each node should be shared between the sensor and the radio transceiver. The question is how to use the available energy in an intelligent way to extend the life-time and maintain the performance of the ADCS. To address this issue, it is necessary to understand all feasible methods for energy conservation on a sensor node.

Table 3.2: Comparison of Onboard Wireless Sensor Actuator Network (OWSAN) with WSN and Wireless Ad-hoc Network

	WSN	Wireless Ad-hoc Network	OWSAN
Number of nodes	>100 (1000s)	10-100	<10
Deployment	densely	relatively sparsely	closely
Failure	prone to failure	not prone to failure	not prone to failure
Communication	broadcast	point-to-point	point-to-point / mesh
Topology change	almost steady	frequent	steady
Power	limited	rechargeable	rechargeable but limited
Identity	local ID	global ID	Local ID
Data correlation	low-medium	no / low	high correlation

3.4 OWSAN Energy Management

Based on the discussion in the previous Chapter and according to various literatures, energy efficiency is key for most wireless sensors applications [Seah et al. 2009,Akyildiz et al. 2002,Alippi et al. 2009]. To maximize the autonomy, it is very important to keep network lifetime as long as necessary. The definition of life time depends on the application and mission, but normally it can be determined by the moment when the battery of the sensor node is no longer able to provide the required energy for sensing, processing or communication. An extended lifetime can be achieved by two clear approaches: conserving the available energy on the node, and adding energy scavenging techniques to the node to recharge the battery simultaneously.

These two approaches will be presented briefly in this Section to provide a deeper understanding for designing a system level energy management in later Chapters.

3.4.1 Energy Conservation

As shown in Figure 3.3, a sensor node is usually composed of the sensor and ADC, a microprocessor and memory module, and the transceiver. Ideally, a sensor node of OWSAN can be equipped with a battery, otherwise it receives the energy from an external energy source. Concerning OWSAN energy management, the following properties of an OWSAN node can be quickly observed from this architecture:

Transceiver energy efficiency: When the node is transmitting, the transceiver consumes much more current than the microprocessor or the memory module. This ratio between the energy needed for transmitting and for processing one bit of information is usually much larger than one. In most commercial platforms this ratio can be larger than a thousand.

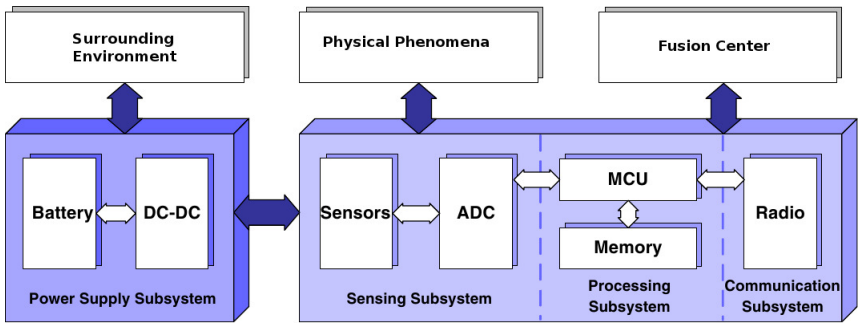

Figure 3.3: Hardware diagram of a WSN node

Therefore, the communication protocols communication strategy should be designed according to energy-efficient paradigms. Since there is no chance to access the sensor node in space and recharge the battery or redesign the communication pattern, design of energy efficient protocols becomes even more important for OWSAN. WSAN shows the same design requirement for many applications too. The majority of literatures on WSANs deal with the design of energy efficient protocols, without much emphasis on the role of the processor inside the node in consuming energy [Verdone 2004, Xu et al. 2001, Ye et al. 2002]. It can be rapidly concluded that between these two, transceiver is the part responsible for the consumption of most energy and any attempt to decrease the energy consumption of this part yields sensible benefit in the overall energy efficiency. In fact onboard communication can be traded for onboard computation [Rahimi et al. 2005].

Transceiver states: different states of the wireless transceiver do not consume the same amount of energy. The transceiver can be in any of listening, transmitting, sleeping or switched-off modes. Intuitively, the transmit and receive states are the most energy consuming state, because both baseband and RF part of the transceiver are active. When the transceiver is in sleep or off mode it drains much smaller current from the energy source. Therefore, it is very effective to put the transceiver in sleep state often. During such sleep periods, a data burst sent to the node can not be detected. Therefore, the radio should be switched sleep mode (or turned off) as frequently as possible. Logically, the transceiver must be kept in those two states for the shortest possible percentage of time [Mutazono et al. 2010]. Switching to the transmit state is needed only when a data burst should be transmitted. Shorter data length and less

frequent transmission increase the lifetime of a wireless node. A very straight conclusion is to avoid protocols and standards based on complex handshakes. If proper scheduling of transmission periods is not arranged then a transceiver might need to stay in receive mode for longer periods of time.

Onboard communication channel: the environment inside a spacecraft is rather quiet and predictable and the characteristics of the wireless channels can be very well analyzed beforehand. It is possible to set the transmit power of the wireless transceivers at the minimum level needed to allow signal correct detection at the receiver. This technique is often used in wireless networks to reduce the impact of interference emissions of radio waves with large power. Of course setting a proper power level requires information about the channel gain. This calculation might be challenging but it is not as complicated as the case of WSAN on the ground because the intra-spacecraft environment does not change and the nodes do not move so the distances are fixed. Looking at the technical data-sheet of CHIPCON (Texas Instruments) CC2420 ZigBee transceiver which is widely used in many COTS WSAN platforms, highlights this conclusion. When this transceiver is transmitting at the highest power level (0 dBm), it drains about 17 mA from the energy source. However, at the minimum transmit power (-25 dBm), the drained current is 8.5 mA [CC2420].

The sensory part: the sensor system on the node is energy consumer. Depending on the application the energy consumption properties of this component can vary [Raghunathan et al. 2002]. If the sensors needs a long time to acquire the data, then the sensor can consume even more energy than the radio [Alippi et al. 2009]. This implies that sensor's energy consumption should be reduced too. This can be achieved by designing low power sensor systems, and also switching off the sensor whenever it is not needed.

The lifetime of OWSAN can be even more extended by applying different techniques together. Energy efficient protocols can be used to ensure low energy consumption of node components (transceiver, microprocessor, etc.) during different states of operation. At the same time, a system level energy management scheme can be applied to switch off the nodes or their components or putting them in sleep mode when they are not temporarily needed. Similar solutions are widely used for WSN and WSAN systems which can be very relevant for reducing energy consumption of sensors node in OWSAN.

Duty Cycling

Duty cycling techniques focus on putting the radio transceiver in the low power mode when the transmission is not required. This low power state can be sleep mode or switched-off. Therefore the node alternates between active and sleep periods. Here *duty cycle* is the fraction of time which nodes are active during the lifetime. The decision making for putting the transceiver to a specific operation mode can be made in a centralized or decentralized way. For OWSAN, duty cycling can reduce the energy consumption in two ways. Different ADS sensor measurements have strong correlation therefore unneeded samples will not be transmitted which reduces the duty cycle of the transceiver. Furthermore, it can reduce the duty cycle of the sensor part of the node, which further reduces the overall energy consumption on the node. Duty cycling can be achieved through different approaches.

Topology control protocols: These approaches use node redundancy and select a minimum subset of nodes which need to remain active to ensure the required performance. For example. it might not be necessary to use all ADS sensors to achieve the required pointing accuracy for all spacecraft maneuvers. Topology control is vastly employed in WSN for monitoring the environment but it mainly targets applications where a large number of nodes are deployed. The topology of the network can be controlled based on location of the sensors [Xu et al. 2001] or the network connectivity [Chen et al. 2002]. Designing routing protocols and using graph theory are the main characteristics of these approaches. Such techniques can be used for OWSAN when certain nodes are not required based on the required maneuver or certain conditions during the mission. In such situation the CDHS can put the node in sleep mode and schedule its later activity.

Sleep/wakeup protocols: This type of technique deals with the operation status of each node rather than the topology of the network. These protocols provide either *on-demand schemes, scheduled rendezvous schemes* or *asynchronous schemes* [Keshavarzian et al. 2006]. On-demand schemes suggest that a node should wake up just when it has to transmit or receive a package from a neighboring node. In scheduled rendezvous schemes, all neighboring nodes wake up at exactly the same time and periodically to check for necessary communications. Finally asynchronous schemes let each node to wake up independently but they guarantee that there is always an overlapped active period within a number of cycles. It is easy to observe that the on-demand protocol is the ideal one. It maximizes the energy efficiency because the node becomes active only when the communication is required. Also it minimizes the latency. However, two different channels are required for this scheme:

a channel for awakening the nodes when needed, and a data channel. An example of the mechanism is described in [Schurgers et al. 2002]. Scheduled rendezvous can be very convenient for data aggregation and broadcast traffic but they require nodes to be synchronized which may need additional protocol overhead for synchronization purposes. Asynchronous schemes are the least energy efficient ones but they are the easiest one to implement. They wake up the nodes more frequently to avoid synchronization issues [Zheng et al. 2003].

MAC protocols: Various MAC protocols for WSN have been proposed in different literatures which most of them design a low duty-cycle scheme for power management [Ye and Heidemann 2004, Naik and Sivalingam 2004]. These MAC protocols can be time division multiple access schemes (TDMA), contention-based protocols or a hybrid of these two. In TDMA-based schemes, time is divided into periodic frames where each frame consists of certain number of time slots. Every node is assigned to one or more slots of each frame and uses these slots for establishing its communication with other nodes. In most cases the nodes are clustered and a cluster-head assigns and schedules the slots to the nodes of its own cluster. For example ZigBee is a TDMA protocol. Contention-based MAC protocols are also known as random access protocols. These protocols do not require coordination among the nodes to access the channel. Colliding nodes back off for a random period and then try to access the channel again until they succeed. Examples of such protocols are B-MAC and S-MAC [Ye et al. 2004, Polastre et al. 2004]. These protocols can apparently cause collisions but there are solutions to stabilize and minimize them [Busch et al. 2004]. The hybrid MAC protocols try to switch the protocol behavior between TDMA and CSMA based on the level of contention. A TDMA based scheme is inherently more energy efficient because a node's radio is turned on only during the allocated time slot and sleeps for the rest of the period. Also, such a protocol can minimize the interference possibility. Unfortunately, they have limited flexibility and scalability when the network size grows or the topology changes [Rhee et al. 2005]. But this is not an issue for an OWSAN because the topology and network size are fixed. Also they are sensitive to interference and synchronization. A solution to this issue can be achieved by using a central coordination [Haartsen 2000]. Such a centralized coordinator can be implemented on an onboard computer or another CDHS node. If the network traffic is very low, then TDMA methods can be less efficient than contention-based protocols. Contention-based MAC protocols offer more flexibility and robustness but can waste more energy due to collisions and contention. Hybrid techniques can present the best of both techniques but their implementation can be rather complex.

Data-driven Approaches

These types of techniques try to either remove the unneeded data samples or to decrease the energy spent by the sensing electronics of the node. These approaches are very relevant to the application and use of the sensor data.

Data prediction: A data prediction approach tries to build a model instead of actually sensing the data. Data prediction can be done by different ways depending on the application. In a stochastic approach, the characteristics of the phenomenon is exploit so that a probabilistic method can be built and used to predict the sensor measurements. An example of this approach is presented by Che *et al.* [Chu et al. 2006]. They introduce a few models which reside in the sensor nodes and in the central node. A probabilistic base model is obtained after a training phase with a set of measurements. This model is used to predict the sensor measurements later on and when no longer valid a new phase of training starts with a new set of measurements to define a new model. Using time series for forecasting is another prediction approach. These method are typically characterized by using moving average, auto-regressive or an auto-regressive moving average model, e.g, PAQ method in the work of Tulone and Madden [Tulone and Madden 2006]. These methods can be representative enough for some very simple WSN applications. This category of data prediction methods do not tune the sampling rate of the sensor.

Energy efficient data acquisition: This category of solutions suggest approaches to reduce the energy consumption of the sensor head on the node. For example adaptive sampling can use the correlation between the measurements and reduce the sample rate of the sensor, therefore less data will be available to communicate to the base station [Vuran et al. 2004]. As an example, temporal analysis of the measurements can be used to suggest an adaptive sampling scheme for predictive monitoring [Alippi et al. 2007]. Alippi *et al.* present a technique to analyze the measurements in the base station and and notify the nodes to change the sampling rate. Another example is the work of Willet *et al.* where spatial correlation is used for adaptive filtering. In this approach, first a small subset of the wireless sensors communicate their information to a fusion center. This provides an initial estimate of the environment being sensed, and guides the allocation of additional network resources [Willett et al. 2004].

Hierarchical sampling is another approach in this category. Here the nodes are equipped with different type of sensors which have different performance characteristics, e.g. energy consumption and accuracy. The

simple sensors have limited accuracy but high energy efficiency. However more complex sensors present a better accuracy and resolution while consuming more energy. The low power sensors can be used to get a coarse understanding about the phenomena or detecting specific events. Then at the right moment, the less energy efficient sensors can be activated to acquire more accurate information. A good example of this approach is presented by Araujo *et al.* for target localization with an ultrasound sensor and a web-camera [Araujo et al. 2009].

3.4.2 Energy Harvesting

An OWSAN node receives its energy either from the spacecraft electrical power system (EPS), or from a local battery. To fully exploit the capabilities of OWSAN and enable a plug and play configuration, it is essential to use local energy sources on the nodes to remove the power cables. Either each node can be equipped with a proper scavenging system, or a number of nodes can be clustered in a package and use a central energy scavenging unit to save volume and mass. Applying the aforementioned techniques in the previous Section can improve the lifetime of the network, but supplementing the local energy source with an energy scavenger can extend the endurance and robustness of the design. This dissertation does not focus the design of the energy scavenger, but provides a short overview on the start of the art and available technologies from a systems engineering perspective.

An energy scavenging device usually consists of three parts: energy collection element, electronics for conditioning/processing, and energy conversion hardware. The scavenged energy should be converted to electricity energy, then it can be conditioned to a proper form for recharging the batteries. Power output per unit mass or volume is the key performance measure for the energy collection element.

Photonic Energy

Photonic energy can be converted directly to electrical energy using photovoltaic cells (solar cells) made from semiconductor materials. A photovoltaic cell is a semiconductor diode with a large *p-n* junction in the plane of the cell which is positioned close to the top surface. The maximum voltage produced by a typical photovoltaic cell is about half volt. At lower voltages, the produced current is almost independent of voltage but it varies with the intensity of solar radiation. There are two important quality attributes which describe the the efficiency of a photovoltaic cell. The first one is the Fill Factor (FF) which describes the quality of the cell production. A higher FF shows

that the current-voltage characteristics of a given photovoltaic cell is closer to the ideal case. It can range from zero (poor quality) to 100% (excellent quality) [Goetzberger and Hoffmann 2005]. Usually commercial solar cells have values around 70% to 80%. More important is the solar cells conversion efficiency. Commercial solar cells have a conversion efficiencies range from 8% to 30%. The latest experimental technology which is reported has achieved is 41% which is reported by Wojtczuk *et al.* [Wojtczuk et al. 2010]. Several factors are important in designing a photovoltaic energy scavenging system. These factors are the radiation intensity and ambient temperature, radiation incident angle, and load matching to ensure the maximum power output. The maximum power output point of the cell depends on the number of cells which are connected in series and their temperature. Arranging more cells in parallel can increase the total output current. Lower operating temperature can increase the output power too. It is estimated that power output decreases by 0.45% for every 1°C temperature increase for a typical solar cell [Patel 1999]. Higher radiation intensity and smaller incident angle increase the output current of the cell. On a spacecraft, the Sun's radiation and the Earth's albedo are the main sources of electricity generation by a photovoltaic cell. However, the contribution of Earth albedo is much less in comparison to the Sun.

Thermal Energy

Thermal energy scavenging can be performed by using thermal gradient or thermal variation. In thermal gradient based methods, existence of temperature differential is enough to extract energy from a thermal reservoir. There are several methods to create electrical current from a thermal gradient [Culp 1979]: thermoelectric, thermionic, thermomagnetic, ferroelectricity, and the Nernst effect. Among them thermo-electric conversion is the most effective of these processes. Thermo-electricity technology uses the Seebeck, Peltier and Thomson effects [Nolas et al. 2001]. A typical thermo-electric transducer is constructed from P-type and N-type thermo-elements which are often referred to as thermoelectric couples. These elements are connected electrically in series and thermally in parallel. Electric current is generated by a voltage difference which is created within each element of the thermo-electric couple when subjected to a temperature gradient. When these couples are put in series configuration the resultant voltage is equal to the sum of the individual thermo-couple voltages and the resultant current is equal to the smallest individual thermo-couple current. A wide variety of thermo-electric devices are commercially available but they are mostly used for cooling rather than electrical energy generation. The couple of bismuth-telluride has the highest efficiency among the commercial products, but its temperature range is rather limited ($<250°C$). Another efficient couple is lead-telluride which can operate

in a temperature range (<500°C). The efficiency of thermo-electric devices are in the range of 5% to 10% when operated at their highest temperature limits [Nuwayhid and Hamade 2005]. But the results for experimental modules are very promising. Carlson *et al.* has presented a switched mode DC-DC converter with digital control for thermo-electric energy harvesting from human body. The whole required circuit can be fabricated with 0.13 μm CMOS process. The converter reaches the thermal equilibrium in 10 minutes. At equilibrium, the generator produces 34 mV (unloaded voltage) and the converter can deliver 34 μW at 1 Volt [Carlson et al. 2010]. Also Carmo *et al.* has reported an output power of about 18 μW by using 1 cm^2 thin films of bismuth and antimony tellurides in room temperature and temperature gradient of about 10°C [Carmo et al. 2010]. Energy scavenging based on temperature variation is performed based on pyroelectric effect. The pyroelectric effect is known as a release of electric charge at the surface of the material when subjected to temperature changes [Mane et al. 2011]. For example, studies by Gyomar *et al.* have shown that a pyroelectric harvester composed of 8 grams of PVDF can produce 0.32 mW power with 7°C temperature amplitude and 0.2 Hz frequency [Guyomar et al. 2009]. Such temperature variation with high frequency usually does not exist on a OWSAN nodes and generated energy is very small, therefore using this technique may be less beneficial.

Electromagnetic Energy

Electromagnetic radiation covers microwave communication, visible light, X-ray, gamma rays, cosmic rays, etc. Electromagnetic radiation energy can be harvested by an appropriately designed antenna and power conditioning circuitry. This type of energy harvesting is based on the electromagnetic induction law of Faraday. An interesting example is the work of Berland *et al.* which describes the theoretical design of a *rectenna* to convert solar radiations in Terra Hertz frequency range directly into DC electricity with efficiency higher than 85% [Berland 2003]. Although this work is not demonstrated yet due to hardware constrains it shows the potential of this energy harvesting method. Commercial example of using rectenna for electromagnetic energy harvesting is RFID technology which works in RF frequency range and. In RFID enabled systems, the sensor is powered by the external electromagnetic field which can be induced by the RFID reader. RFID is already tested and used in space applications by NASA onboard ISS to track the cargo supplies. Experimental results are reported by Arrawatia *et al.* which works in 877 MHz to 998 MHz range and can produce 2.78 V at a distance of 10 meters [Arrawatia et al. 2011]. Also harvesting the electromagnetic energy at 2.4 GHz frequency with 31% efficiency is reported by other researchers *et al.* [Gao et al. 2011].

3.5 Discussion

From the presented results and information about energy conservation, the characteristics of OWSAN and by considering the properties of ZigBee as a strong candidate for onboard wireless communication standard, several key results can be concluded for ADS sensors of OWSAN. First of all, the environment inside the spacecraft should be well studied to select the minimum possible transmission power for each sensor transceiver. This is an engineering task which should be taken care of during prototyping spacecraft engineering model. Also, the electronics of the sensor head of the nodes should be designed such that they can be easily switched off and on without needing recalibration. On the nodes, the design goal is to put the wireless transceiver in sleep or off mode as frequent as possible. This can be achieved by allowing extra computation and data processing. This extra processing power can be employed either on the nodes or on the onboard computer. Due to the inherent characteristics of ADS sensor nodes of OWSAN, a hybrid energy management algorithm can be designed to improve the energy efficiency. This hybrid approach can use model based prediction to forecast sensor measurements. The energy manager can supervise the operation of the network by mixing three techniques: deciding which nodes should be working to ensure the required ADS accuracy, scheduling the sleep and active modes of the transceivers and tuning the measurement rate of sensor heads on the nodes. This supervision can be implemented either in a centralized manner by the onboard computer, or in a decentralized scheme on the nodes. Finally to increase the reliability of the transmission and avoid extra computation overhead on the nodes, a TDMA based communication scheme should be used which can be coordinated by one of the onboard nodes. The onboard computer is a good candidate for this coordination task because comparing to the sensors nodes it has more energy resources available, however, any other node can overtake this responsibility when needed.

Part II

Onboard Energy Management

Chapter 4

System Modeling

A hair devides what is false and true.

– Omar Khayyam[1]

Novel technologies drive the miniaturization of spacecraft and enable more efficient and autonomous on board subsystems. The application of onboard wireless communication between spacecraft subsystems allows overall mass reduction and additional flexibility in the spacecraft development. In Chapter 3 we shouwed that ADCS sensors are strong candidates to be equipped with a low-power wireless data transmission technology such as ZigBee. This is due to low to medium data rates of ADCS sensors' measurements and the correlation between the attitude determination measurements. The communication data rate can be even further reduced when the spacecraft is not performing high precision maneuvers [Szerdahelyi 2003].

A typical ADCS wireless sensor node is integrated with a battery, a power harvesting solution and a wireless transmitter module. To enable more functionality, a smart sensor can be equipped with microprocessor to enable local data processing and decision making. At the hardware level, the electronic circuits, communication protocol, and sensing must all be energy efficient. In addition, an energy management scheme at the software level can additionally reduce the energy consumption and improve the life time of the node.

Different energy management techniques have been proposed to reduce the energy consumption in battery powered devices [Chung et al. 1999, Zuquim et al. 2003, Sinha and Chandrakasan 2001]. Some of the available techniques

[1] Omar Khayyam (1048-1131) was a Persian mathematician, astronomer, philosopher and poet. He wrote one of the most important books in mathematics, *Treatise on Demonstration of Problems of Algebra* from which most algebraic principles have been drawn from.

rely on approximate querying which exploits the natural trade-off between energy consumption and data accuracy [Han et al. 2004], [Silberstein et al. 2006]. This technique basically relies on the application specific error bound which is disseminated to each sensor node along with the query. A measurement is sent to the base station if the change of two consecutive sensor values exceeds a user-defined error bound. There are also other approaches which exploit sleep scheduling but they mostly lack the explicit interaction with the application layer modules [Keshavarzian et al. 2006, Santini and Römer 2006].

Application constraints play a great role in designing efficient power management mechanisms specifically for ADCS sensors because the information about vehicle attitude which is provided by different sensors is correlated in time and the trajectory of the spacecraft can be estimated by mathematical models. The problem is to maintain the performance of ADCS without degrading the availability of OWSAN nodes.

In a fully modular onboard wireless network, sensor nodes are required to operate on limited energy budgets. Energy management can prolong the lifetime of a sensor network and conserve scarce energy resources. However, inefficient management could result in severe performance degradation. In this Chapter, the modeling of an onboard attitude determination system which is composed of sensor nodes and a fusion center (onboard computer) is studied. Each sensor node can use a local energy harvesting and storage unit, therefore it has limited available energy.

The available energy on each node should be shared between the sensor head, microcontroller and the wireless transmitter. The goal of the energy manager is to reduce the energy consumption of the sensor nodes which have limited energy availability. A system level design for sensor scheduling can contribute to this goal by reducing the wireless communication frequency of the sensor nodes. This energy management scheme is a type of decision making which can be implemented either centralized in the fusion center or decentralized.

In this Chapter we suggest two different designs for an onboard energy manager and in the next Chapter both design will be implemented and tested in a simulation environment. A unique characteristic of our design is that it is fully integrated with the onboard attitude determination system of the spacecraft and therefore the computation overhead of the energy manager is very small. Thus, spacecraft attitude determination needs to be fully understood to facilitate the energy manager formulation.

4.1 Spacecraft Attitude

Spacecraft attitude can be calculated onboard by employing models of the environment, the spacecraft kinematic and dynamic analytical models and sensor measurements.

4.1.1 Orbit Model

Predicting the orbital motion of a spacecraft to a sufficient level of accuracy is one of the key steps for modeling and simulation of a space vehicle. An orbit propagator is a mathematical algorithm which predicts the future position and velocity of a spacecraft in an orbit given some initial conditions and assumptions on the spacecraft dynamics. Different orbit propagation techniques have been developed which provide different accuracy for various applications.

In general, a system consisting of two bodies orbiting each other is considered as a two-point-mass system. The *two-body equation of motion* describes the acceleration vector $\ddot{\boldsymbol{r}}_{\oplus}$ of an Earth orbiting spacecraft is written as

$$\ddot{\boldsymbol{r}}_{\oplus} = -GM_{\oplus}\frac{\boldsymbol{r}_{\oplus}}{r_{\oplus}^{-3}} = \mathbf{0} \tag{4.1}$$

where G is the universal constant of gravitation, $M_{\oplus}$ is the mass of the Earth, $\boldsymbol{r}_{\oplus}$ is the distance vector from the center of the Earth to the center of spacecraft and $r_{\oplus} = \|\boldsymbol{r}_{\oplus}\|$. In this work the Simplified General Perturbations model 4 (SGP4) is used to predict the spacecraft position in the Earth orbit [Lane and Hoots 1979]. SGP4 is based on an extensive analytical theory which was developed by Lane *et al.* [Lane and Murphy 1962]. The SGP4 can use Two Line Elements (TLE) generated by NORAD which is a set of two ASCII records with 69 characters each. The SGP4 model accounts for the perturbations caused by atmospheric drag and non-spherical mass distribution of the Earth on the spacecraft motion. The SGP4 model offers an efficient way of computing the spacecraft position and velocity to an accuracy of about 1 to 2 kilometers which is sufficient in the context of this thesis.

4.1.2 Reference Frames

A set of three mutually orthogonal unit length vectors which are linearly independent can span the vector space $\mathbb{R}^3$. These vectors can form a orthonormal *basis* or *coordinate system*. A *reference frame* is a term to describe a right-handed three dimensional Cartesian coordinate system which is described by three mutually orthogonal unit vectors $\{\vec{\mathbf{e}}_1, \vec{\mathbf{e}}_2, \vec{\mathbf{e}}_3\}$ such that

$$\vec{\mathbf{e}}_1 \times \vec{\mathbf{e}}_2 = \vec{\mathbf{e}}_3. \tag{4.2}$$

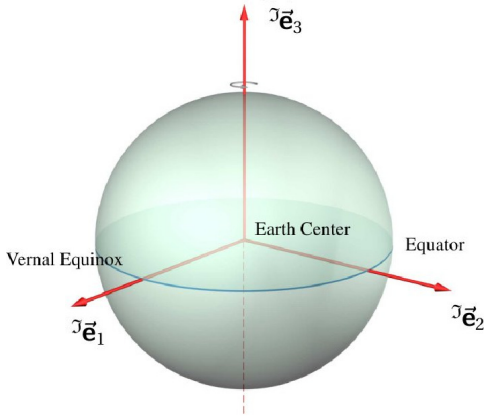

Figure 4.1: ECI frame

Three different reference frames are used in this thesis which are briefly introduced in this section and will be extensively used later on.

Earth-Centered Inertial Reference Frame (ECI)

The motion of spacecraft in an Earth orbit is described in this frame to simplify the orbital equations of motion. The center of this reference frame is placed in the Earth center of mass and is defined by its basis vectors set, $\mathcal{I} = \{ {}^{\mathcal{I}}\vec{e}_1, {}^{\mathcal{I}}\vec{e}_2, {}^{\mathcal{I}}\vec{e}_3 \}$. Here symbol $\mathcal{I}$ is to denote the ECI frame. ${}^{\mathcal{I}}\vec{e}_1$ is in the direction of Vernal Equinox which is the direction of the vector from the Earth center of mass to the Sun when the Sun crosses the Earth equatorial plane from South to North. This direction changes due to the nutation of the Earth's spin axis in time, therefore the Vernal Equinox of epoch J2000 is used here which is the direction of the Vernal Equinox at 12:00 Terrestrial Time on 1

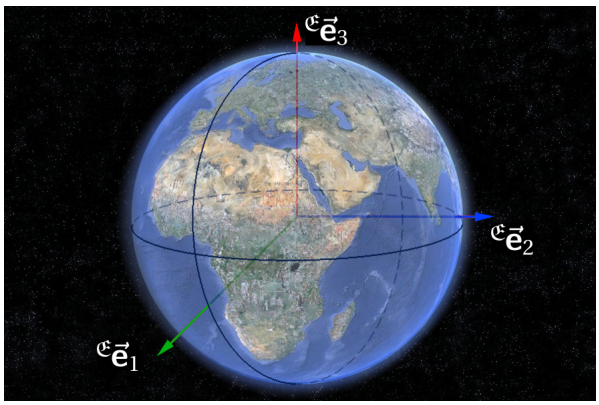

Figure 4.2: ECEF frame

January 2000. ${}^{\mathfrak{I}}\vec{\mathbf{e}}_3$ axis is aligned with the Earth's spin or celestial North Pole. ${}^{\mathfrak{I}}\vec{\mathbf{e}}_2$ is rotated by 90° East about the celestial equator (Figure 4.1). Therefore the plane spanned by ${}^{\mathfrak{I}}\vec{\mathbf{e}}_1$ and ${}^{\mathfrak{I}}\vec{\mathbf{e}}_2$ is aligned with the Earth equatorial plane [Montenbruck and Eberhard 2000].

Earth-Centered Earth Fixed Reference Frame (ECEF)

The ECEF, also termed *conventional terrestrial coordinate system* is fixed relative to the Earth surface. Therefore it can be used for defining certain physical properties of the Earth such as Earth's magnetic field. The center of the ECEF is on the Earth's center of mass. This frame is defined by $\mathfrak{E} = \{ {}^{\mathfrak{E}}\vec{\mathbf{e}}_1, {}^{\mathfrak{E}}\vec{\mathbf{e}}_2, {}^{\mathfrak{E}}\vec{\mathbf{e}}_3\}$ basis vectors. Symbol $\mathfrak{E}$ is to denote the ECEF later on. ${}^{\mathfrak{E}}\vec{\mathbf{e}}_1$ is in the direction of Greenwich Prime Meridian, ${}^{\mathfrak{E}}\vec{\mathbf{e}}_3$ is in the direction of the North Pole similar to ECI frame, and ${}^{\mathfrak{E}}\vec{\mathbf{e}}_2$ is such that it makes a right-handed orthogonal frame with ${}^{\mathfrak{E}}\vec{\mathbf{e}}_1$ and ${}^{\mathfrak{E}}\vec{\mathbf{e}}_3$ as it is shown in Figure 4.2. This frame is Earth fixed so it rotates relative to ECI frame with Earth's angular velocity.

Spacecraft Body Reference Frame (SCB)

This frame is used for onboard sensors to relate the orientation of the spacecraft in the orbit to the sensor measurements. This reference frame is defined by $\mathfrak{B} = \{ {}^{\mathfrak{B}}\vec{\mathbf{e}}_1, {}^{\mathfrak{B}}\vec{\mathbf{e}}_2, {}^{\mathfrak{B}}\vec{\mathbf{e}}_3\}$ and is aligned with the spacecraft principal axes. Here symbol $\mathfrak{B}$ is to denote the SCB frame. The definition of this frame depends on the spacecraft design but usually ${}^{\mathfrak{B}}\vec{\mathbf{e}}_3$ is aligned with the principal axis of the smallest inertia.

4.1.3 Rotation and Attitude

The term *spacecraft attitude* denotes the orientation of an spacecraft SCB frame relative to a known reference frame such as the ECI. An illustration is shown in Figure 4.3 which shows a spacecraft SCB and ECI frames with their own corresponding basis vectors. Also an arbitrary vector $\boldsymbol{v}$ is presented which can be defined in SCB and ECI frames by ${}^{\mathfrak{B}}\boldsymbol{v}$ and ${}^{\mathfrak{I}}\boldsymbol{v}$ respectively. The attitude determination problem is to find the transformation between the two coordinate systems which brings the axes of ECI to the axes of SCB. Such a transformation will also transform ${}^{\mathfrak{I}}\boldsymbol{v}$ to ${}^{\mathfrak{B}}\boldsymbol{v}$. Onboard a spacecraft, ${}^{\mathfrak{B}}\boldsymbol{v}$ can be found from the sensor measurements and ${}^{\mathfrak{I}}\boldsymbol{v}$ can be calculated from the mathematical models of the environment. Determining this transformation matrix is equivalent to describing the attitude of the satellite in ECI frame. According to Euler's theorem , the general displacement of a rigid body with one point fixed is a rotation about an axis through that point [Goldstein 1950].

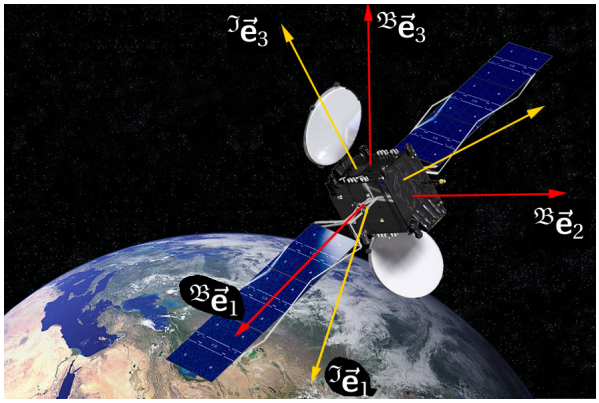

Figure 4.3: Rotation of SCB frame in ECI frame

The Euler's formula states that for every given pair of vectors such as $\boldsymbol{a}$ and $\boldsymbol{b}$ with the same magnitude there is a linear transformation which transforms $\boldsymbol{a}$ to $\boldsymbol{b}$ through an angle of rotation about a physical axis of rotation. Therefore the same type of transformation should exist for $^{\mathcal{B}}\vec{\mathbf{e}}_i$ and $^{\mathcal{I}}\vec{\mathbf{e}}_i$ such that

$$^{\mathcal{B}}\vec{\mathbf{e}}_i = (\cos\theta)\,^{\mathcal{I}}\vec{\mathbf{e}}_i + (1-\cos\theta)(\vec{\mathbf{n}}\cdot\,^{\mathcal{I}}\vec{\mathbf{e}}_i)\vec{\mathbf{n}} + (\sin\theta)\vec{\mathbf{n}}\times\,^{\mathcal{I}}\vec{\mathbf{e}}_i \qquad i=1,2,3. \tag{4.3}$$

where θ is the angle of rotation and $\vec{\mathbf{n}}$ is the axis of rotation.

For any set of two orthonormal bases such as $\mathfrak{A} = \{\vec{\mathbf{a}}_1, \vec{\mathbf{a}}_2, \vec{\mathbf{a}}_3\}$ and $\mathfrak{A}' = \{\vec{\mathbf{a}}'_1, \vec{\mathbf{a}}'_2, \vec{\mathbf{a}}'_3\}$ a *direction cosine matrix*, $^{\mathfrak{A}'}_{\mathfrak{A}}\mathbf{C}$, exists which maps the basis of frame $\mathfrak{A}$ to the basis of frame $\mathfrak{A}'$

$$\begin{pmatrix} \boldsymbol{a}'_1 \\ \boldsymbol{a}'_2 \\ \boldsymbol{a}'_3 \end{pmatrix} = {}^{\mathfrak{A}'}_{\mathfrak{A}}\mathbf{C} \begin{pmatrix} \boldsymbol{a}_1 \\ \boldsymbol{a}_2 \\ \boldsymbol{a}_3 \end{pmatrix}. \tag{4.4}$$

It can be easily deduced that

$$^{A'}_{A}\mathrm{c}_{i,j} = \boldsymbol{a}_i \cdot \boldsymbol{a}'_j \quad , \quad i,j=1,2,3. \tag{4.5}$$

where elements denoted by $^{\mathfrak{A}'}_{\mathfrak{A}}\mathbf{c_{i,j}}$ are the components of $^{\mathfrak{A}'}_{\mathfrak{A}}\mathbf{C}$. The direction cosine matrix can be used in a cascading manner

$$^{\mathfrak{A}''}_{\mathfrak{A}}\mathbf{C} = {}^{\mathfrak{A}''}_{\mathfrak{A}'}\mathbf{C}\,{}^{\mathfrak{A}'}_{\mathfrak{A}}\mathbf{C}. \tag{4.6}$$

When both sets of bases are orthonormal and right-handed, the resulting matrix is called a *rotation matrix* . Usually for spacecraft, the rotation matrix from the inertial reference frame ECI to spacecraft body frame SCB is called the *attitude matrix*, $^{\mathcal{B}}_{\mathcal{I}}\mathbf{A}$ [van der Ha and Shuster 2009]. $^{\mathcal{B}}_{\mathcal{I}}\mathbf{A}$ is the attitude matrix which maps a vector in ECI frame such as $^{\mathcal{I}}\boldsymbol{v}$ to SCB frame

$$^{\mathcal{B}}\boldsymbol{v} = {}^{\mathcal{B}}_{\mathcal{I}}\mathbf{A}\,{}^{\mathcal{I}}\boldsymbol{v}. \tag{4.7}$$

By using (4.3) and (4.5), the attitude matrix for a rotation of θ around rotation axis $\vec{\mathbf{n}}$ can be formulated as the following

$$\begin{aligned} {}^{\mathfrak{B}}_{\mathfrak{I}}\mathbf{A}(\vec{\mathbf{n}},\theta) &= (\cos\theta)\mathbf{I}_{3\times3} + (1-\cos\theta)\vec{\mathbf{n}}\vec{\mathbf{n}}^{\mathsf{T}} - (\sin\theta)\mathfrak{S}\langle\vec{\mathbf{n}}\rangle && (4.8)\\ &= \mathbf{I}_{3\times3} - (\sin\theta)\mathfrak{S}\langle\vec{\mathbf{n}}\rangle + (1-\cos\theta)\mathfrak{S}\langle\vec{\mathbf{n}}\rangle^2 && (4.9)\end{aligned}$$

with $\mathbf{I}_{3\times3}$ being the 3×3 identity matrix and $\mathfrak{S}\langle\vec{\mathbf{n}}\rangle$ the antisymmetric matrix for a vector $\vec{\mathbf{n}}_{3\times1}$, which are defined as the following

$$\mathbf{I}_{3\times3} := \begin{pmatrix} 1 & 0 & 0 \\ 0 & 1 & 0 \\ 0 & 0 & 1 \end{pmatrix} \quad , \quad \mathfrak{S}\langle\vec{\mathbf{n}}\rangle := \begin{pmatrix} 0 & -n_3 & n_2 \\ n_3 & 0 & -n_1 \\ -n_2 & n_1 & 0 \end{pmatrix}. \tag{4.10}$$

It can be shown that ${}^{\mathfrak{B}}_{\mathfrak{I}}\mathbf{A}\,{}^{\mathfrak{B}}_{\mathfrak{I}}\mathbf{A}^{\mathsf{T}} = \mathbf{I}_{3\times3}$ and $\det({}^{\mathfrak{B}}_{\mathfrak{I}}\mathbf{A}) = \det({}^{\mathfrak{B}}_{\mathfrak{I}}\mathbf{A}^{\mathsf{T}}) = \pm1$. The space of matrices which satisfy the later requirements is called *special orthogonal group* and denoted by SO(3). Furthermore, these equations imply six constraints on ${}^{\mathfrak{B}}_{\mathfrak{I}}\mathbf{A}$ and leave three degrees of freedom for attitude matrix. In another words, six out of nine elements of the attitude matrix are redundant elements. Stuelpnagel showed that there is no non-singular three-parameter representations of SO(3) [Stuelpnagel 1964]. The rotation matrix singularity can be visualized when Euler angles are used to represent the rotation. Singla *et al.* have analyzed of this phenomena and prescribed techniques to avoid it [Singla et al. 2004]. This singularity problem has led to employing higher-dimensional non-singular parameterization for attitude determination which are described in various literature [Shuster 1993]. One of the most widely used methods is applying a four-component quaternion [Paulson et al. 1969, Bar-Itzhack and Oshman 1985].

4.1.4 Quaternions

A quaternion has the lowest possible dimensionality for a global non-singular representation of SO(3) [Markley 2004]. Another advantages of using a quaternion is its linear kinematic equations which will be shown later. Quaternion is also known as hyper complex numbers and represented by $\mathbb{H}$. The quaternion four dimensional space $\mathbb{H}$ is spanned by a set of three mutually perpendicular unit vectors orthogonal to the fourth scalar part. Orthonormal a real axis and a set of three orthogonal axes. The orthogonal axes, $\boldsymbol{i}$, $\boldsymbol{j}$ and $\boldsymbol{k}$ are called *principal imaginaries* which follow Hamilton's rules

$$\vec{\mathbf{i}}^2 = \vec{\mathbf{j}}^2 = \vec{\mathbf{k}}^2 = \vec{\mathbf{i}}\vec{\mathbf{j}}\vec{\mathbf{k}} = -1. \tag{4.11}$$

A quaternion is defined as $\mathbf{q} = q_s + q_1\vec{\mathbf{i}} + q_2\vec{\mathbf{j}} + q_3\vec{\mathbf{k}}$ which is made of a *real* part q_s and a *pure* part $\boldsymbol{q} = q_1\vec{\mathbf{i}} + q_2\vec{\mathbf{j}} + q_3\vec{\mathbf{k}}$ [Hamilton 1844]. A quaternion with zero

real part ($q_s = 0$) is called *pure quaternion* which can also be represented as a column vector $\boldsymbol{q} = (q_1 \quad q_2 \quad q_3)^\intercal$. Using later notations, we have the following form for a quaternion which is more interesting for our application in attitude determination

$$\mathbf{q} = \begin{pmatrix} \boldsymbol{q} \\ q_s \end{pmatrix}. \tag{4.12}$$

The four components of quaternion known as *Euler symmetric parameters* first appeared in a paper by Euler [Euler 1770]. Later Hamilton[1] presented them as an abstract mathematical object [Hamilton 1844]. The use of quaternion is also present in an unpublished work of Gauss[1] [Gauss 1900].

Conjugate, 2-norm and inverse of a quaternion $\mathbf{q}$ are respectively defined as

$$\mathbf{q}^* = (-\boldsymbol{q} \quad q)^\intercal \tag{4.13}$$

$$\|\mathbf{q}\| = \sqrt{q_1^2 + q_2^2 + q_3^2 + q_s^2} \tag{4.14}$$

$$\mathbf{q}^{-1} = \frac{\mathbf{q}^*}{|\mathbf{q}|^2}. \tag{4.15}$$

Multiplication of two quaternions $\mathbf{p}$ and $\mathbf{q}$ and also operator matrix $[\mathbf{q}\otimes]$ is defined by

$$\mathbf{s} = \mathbf{q} \otimes \mathbf{p} = [\mathbf{q}\otimes]\mathbf{p} = \underbrace{\begin{pmatrix} q_s & q_3 & -q_2 & q_1 \\ -q_3 & q_s & q_1 & q_2 \\ q_2 & -q_1 & q_s & q_3 \\ -q_1 & -q_2 & -q_3 & q_s \end{pmatrix}}_{[\mathbf{q}\otimes]} \begin{pmatrix} p_1 \\ p_2 \\ p_3 \\ p_s \end{pmatrix}. \tag{4.16}$$

If $\|\mathbf{q}\| = 1$, the quaternion is called *unit quaternion*. It is easy to show that for unit quaternion $\mathbf{q}$ we have

$$\mathbf{q} \otimes \mathbf{q}^* = \mathbf{q} \otimes \mathbf{q}^{-1} = (0 \quad 0 \quad 0 \quad 1). \tag{4.17}$$

For unit quaternions, the quaternion product corresponds to the attitude matrix product

$$\mathbf{s} = \mathbf{p} \otimes \mathbf{q} \longleftrightarrow \mathbf{A_r} = \mathbf{A_p}\mathbf{A_q} \tag{4.18}$$

which means that a consecutive (cascading) rotation can be represented by multiplication of corresponding unit quaternions.

[1] Sir William Rowan Hamilton (1805 - 1865) was an Irish physicist, astronomer, and mathematician. He made important contributions to classical mechanics, optics, and algebra. His greatest contribution is perhaps the reformulation of Newtonian mechanics, now called Hamiltonian mechanics.

[1] Johann Carl Friedrich Gauss (1777 - 1855) was a German scientist who contributed significantly to many fields, including mathematics, geodesy, geometry, electrostatics, astronomy and optical physics.

For a rotation angle of θ around a unit vector $\vec{\mathbf{n}}$ as the axis of rotation, we can derive the following expression for the corresponding unit quaternion

$$\mathbf{q}\{\vec{\mathbf{n}}, \frac{1}{2}\theta\} = \begin{pmatrix} \vec{\mathbf{n}}\sin(\frac{\theta}{2}) \\ \cos(\frac{\theta}{2}) \end{pmatrix}. \tag{4.19}$$

which can be alternatively shown as

$$\mathbf{q}\{\vec{\mathbf{n}}, \frac{1}{2}\theta\} = \cos(\frac{\theta}{2}) + \vec{\mathbf{n}}\sin(\frac{\theta}{2}) \tag{4.20}$$

$$= \exp(\vec{\mathbf{n}}\frac{\theta}{2}). \tag{4.21}$$

Furthermore, the attitude matrix can be constructed from a quaternion through the following equation

$$\mathbf{A}(\mathbf{q}) = \begin{pmatrix} q_1^2 - q_2^2 - q_3^2 + q_s^2 & 2(q_1q_2 + q_3q_s) & 2(q_1q_3 - q_2q_s) \\ 2(q_1q_2 - q_3q_s) & -q_1^2 + q_2^2 - q_3^2 + q_s^2 & 2(q_2q_3 + q_1q_s) \\ 2(q_1q_3 + q_2q_s) & 2(q_2q_3 - q_1q_s) & -q_1^2 - q_2^2 + q_3^2 + q_s^2 \end{pmatrix} \tag{4.22}$$

$$= (q_s^2 - |\boldsymbol{q}|^2)\mathbf{I}_{3\times3} + 2\boldsymbol{q}\boldsymbol{q}^\intercal - 2q_s\mathfrak{S}\langle\boldsymbol{q}\rangle \tag{4.23}$$

with $\mathfrak{S}\langle\boldsymbol{q}\rangle$ being the antisymmetric matrix for $\boldsymbol{q}$ as defined in (4.10). Finally for a given vector ${}^{\mathfrak{I}}\boldsymbol{v}$ in frame $\mathfrak{I}$, if quaternion ${}^{\mathfrak{B}}_{\mathfrak{I}}\mathbf{q}$ represents the attitude of frame $\mathfrak{B}$ with respect to frame $\mathfrak{I}$, then ${}^{\mathfrak{I}}\boldsymbol{v}$ is transformed to SCB frame by

$${}^{\mathfrak{B}}\mathbf{v} = {}^{\mathfrak{B}}_{\mathfrak{I}}\mathbf{q} \otimes {}^{\mathfrak{I}}\mathbf{v} \otimes {}^{\mathfrak{B}}_{\mathfrak{I}}\mathbf{q}^*. \tag{4.24}$$

where ${}^{\mathfrak{B}}\mathbf{v} = \begin{pmatrix} {}^{\mathfrak{B}}\boldsymbol{v} \\ 0 \end{pmatrix}$ and ${}^{\mathfrak{I}}\mathbf{v} = \begin{pmatrix} {}^{\mathfrak{I}}\boldsymbol{v} \\ 0 \end{pmatrix}$. This rotation can be equivalently described by attitude matrix in the following form

$$\begin{pmatrix} {}^{\mathfrak{B}}\boldsymbol{v} \\ 0 \end{pmatrix} = \begin{pmatrix} \mathbf{A}_\mathbf{q} & \mathbf{0}_{3\times1} \\ \mathbf{0}_{1\times3} & 1 \end{pmatrix} \begin{pmatrix} {}^{\mathfrak{I}}\boldsymbol{v} \\ 0 \end{pmatrix}. \tag{4.25}$$

4.1.5 Equations of Attitude

The equations of spacecraft attitude are split into kinematic equation of attitude and and dynamic equation of attitude. The kinematic equation studies the change in the attitude without considering the cause i.e. external forces. On the other hand, the dynamic equation describes the attitude parameters which change in time as functions of external forces.

Spacecraft Attitude Kinematics

Kinematics describes the motion of objects. A change in the spacecraft attitude can be described with two quaternions. If $\mathbf{q}(t)$ is the attitude of a spacecraft

at time t, and $\mathbf{q}(t+\Delta t)$ is the attitude at time $t+\Delta t$, then we can write

$$\mathbf{q}(t+\Delta t)=\mathbf{q}\{\vec{\mathbf{n}}(t),\frac{1}{2}\theta(t)\}\otimes\mathbf{q}(t) \tag{4.26}$$

which means the spacecraft has undergone a rotation with angle of rotation θ around axis of rotation $\vec{\mathbf{n}}$ (see (4.19)). If this rotation is small enough according to (4.21) we have

$$\mathbf{q}\{\vec{\mathbf{n}},\frac{\theta}{2}\}=\exp(\vec{\mathbf{n}}\frac{\theta}{2})=\sum_{m=0}^{\infty}\frac{1}{m!}(\vec{\mathbf{n}}\theta)^m \tag{4.27}$$

$$=\mathbf{I}+\vec{\mathbf{n}}\frac{\theta}{2}-\frac{\theta^2}{8}+\ldots \tag{4.28}$$

which results in

$$\mathbf{q}(t+\Delta t)=(\mathbf{I}+\vec{\mathbf{n}}\frac{\theta}{2}-\frac{\theta^2}{8}+\ldots)\otimes\mathbf{q}(t). \tag{4.29}$$

Note that $\mathbf{I}$ is the unit vector. If Δt is small enough, then the rotation angle becomes small enough such that θ^2 is negligible comparing to θ. Thus the series in (4.29) can be approximated to a first order. Therefore we have

$$\frac{1}{\Delta t}\mathbf{q}(t+\Delta t)=\frac{1}{\Delta t}\Big(\mathbf{I}+\vec{\mathbf{n}}(t)\frac{\theta(t)}{2}\Big)\otimes\mathbf{q}(t)+\mathcal{O}(\|\theta\vec{\mathbf{n}}\|^2). \tag{4.30}$$

As Δt converges to zero, angular velocity vector can be defined as follows

$$\boldsymbol{\omega}(t):=\lim_{\Delta t\to 0}\frac{\vec{\mathbf{n}}(t)\theta(t)}{\Delta t} \tag{4.31}$$

and as $\Delta t\to 0$ (4.30) yields

$$\dot{\mathbf{q}}(t)=\frac{\mathrm{d}}{\mathrm{d}t}\mathbf{q}(t)=\frac{1}{2}\underline{\boldsymbol{\Omega}}(t)\mathbf{q}(t) \tag{4.32}$$

where

$$\underline{\boldsymbol{\Omega}}(t)=\begin{pmatrix}0 & \omega_3(t) & -\omega_2(t) & \omega_1(t)\\ -\omega_3(t) & 0 & \omega_1(t) & \omega_2(t)\\ \omega_2(t) & -\omega_1(t) & 0 & \omega_3(t)\\ -\omega_1(t) & -\omega_2(t) & -\omega_3(t) & 0\end{pmatrix}. \tag{4.33}$$

$\underline{\boldsymbol{\Omega}}(t)$ can be written by using the skewsymmeteric form as

$$\underline{\boldsymbol{\Omega}}(t):=\begin{pmatrix}-\mathfrak{S}\big\langle\boldsymbol{\omega}(t)\big\rangle & \boldsymbol{\omega}(t)\\ -\boldsymbol{\omega}^{\intercal}(t) & \mathbf{0}\end{pmatrix}. \tag{4.34}$$

Similarly the kinematics can be represented by using the rotation matrix

$$\frac{\mathrm{d}\mathbf{A}}{\mathrm{d}t}(t)=-\mathfrak{S}\big\langle\boldsymbol{\omega}(t)\big\rangle\mathbf{A}(t). \tag{4.35}$$

Remark 4.1. By comparing (4.33) with quaternion multiplication rule in (4.16) we can deduce the following alternative form for (4.32)

$$\dot{\mathbf{q}}(t)=\frac{1}{2}\mathbf{q}_{\boldsymbol{\omega}}(t)\otimes\mathbf{q}(t) \tag{4.36}$$

where

$$\mathbf{q}_{\boldsymbol{\omega}}(t)=\begin{pmatrix}\boldsymbol{\omega}(t)\\0\end{pmatrix}. \tag{4.37}$$

Spacecraft Attitude Dynamics

Dynamics is concerned about the motion of an object and the torques which cause it. The changes in the angular momentum of spacecraft caused by external torques or actuators yields the dynamic equation. The angular momentum of spacecraft as a rigid body with respect to its center of mass is $\boldsymbol{h}_b(t)\in\mathbb{R}^3$ and described by [Kane et al. 1983]

$${}^{\mathfrak{B}}\boldsymbol{h}(t)=\int {}^{\mathfrak{B}}\boldsymbol{r}(t)\times{}^{\mathfrak{B}}\boldsymbol{v}(t)\,\mathrm{d}\,m=\underline{\mathbf{I}}^{\mathfrak{B}}\boldsymbol{\omega}_{\boldsymbol{b}}(t) \tag{4.38}$$

where $\underline{\mathbf{I}}\in\mathbb{R}^{3\times3}$ is the moment of inertia tensor of spacecraft body about the center of mass of spacecraft, which is a symmetric positive semi-definite matrix. ${}^{\mathfrak{B}}\boldsymbol{r}(t)$ and ${}^{\mathfrak{B}}\boldsymbol{v}(t)$ are the position and velocity of a point of mass in SCB frame. If the spacecraft body is subject to external torques which is originated in the ECI frame and ${}^{\mathfrak{I}}\boldsymbol{h}\in\mathbb{R}^3$ is the angular momentum of spacecraft in ECI frame, then we have the momentum balance equation

$$\frac{\mathrm{d}}{\mathrm{d}t}{}^{\mathfrak{I}}\boldsymbol{h}(t)={}^{\mathfrak{I}}\boldsymbol{n}(t) \tag{4.39}$$

with ${}^{\mathfrak{I}}\boldsymbol{n}(t)$ being the vector sum of external torques. ${}^{\mathfrak{I}}\boldsymbol{h}(t)$ can be transformed to SCB frame with ${}^{\mathfrak{B}}\boldsymbol{h}(t)={}^{\mathfrak{B}}_{\mathfrak{I}}\mathbf{A}\,{}^{\mathfrak{I}}\boldsymbol{h}(t)$. Therefore we get

$$\frac{\mathrm{d}\,{}^{\mathfrak{B}}\boldsymbol{h}(t)}{\mathrm{d}t}=\frac{\mathrm{d}\,{}^{\mathfrak{B}}_{\mathfrak{I}}\mathbf{A}(t)}{\mathrm{d}t}{}^{\mathfrak{I}}\boldsymbol{h}(t)+{}^{\mathfrak{B}}_{\mathfrak{I}}\mathbf{A}(t)\frac{\mathrm{d}\,{}^{\mathfrak{I}}\boldsymbol{h}(t)}{\mathrm{d}t} \tag{4.40}$$

$$=-\mathfrak{S}\left\langle{}^{\mathfrak{B}}\boldsymbol{\omega}(t)\right\rangle{}^{\mathfrak{B}}\boldsymbol{h}(t)+{}^{\mathfrak{B}}\boldsymbol{n}(t) \tag{4.41}$$

and

$$\underline{\mathbf{I}}\frac{\mathrm{d}}{\mathrm{d}t}\mathfrak{S}\left\langle{}^{\mathfrak{B}}\boldsymbol{\omega}(t)\right\rangle=-\mathfrak{S}\left\langle{}^{\mathfrak{B}}\boldsymbol{\omega}(t)\right\rangle\left(\underline{\mathbf{I}}^{\mathfrak{B}}\boldsymbol{\omega}(t)\right)+{}^{\mathfrak{B}}\boldsymbol{n}(t) \tag{4.42}$$

which is the Euler equation [Goldstein 1950]. ${}^{\mathfrak{B}}\boldsymbol{n}(t)$ is composed of all external torques which are either the control torques, $\boldsymbol{n}_c(t)$, or the disturbance torques,

$\boldsymbol{n}_d(t)$. The kinematic and dynamic differential equations presented in (4.32) and (4.42) together form the nonlinear equation of spacecraft attitude

$$\underbrace{\begin{pmatrix} \dot{\mathbf{q}}(t) \\ \dot{\boldsymbol{\omega}}(t) \end{pmatrix}}_{\dot{\boldsymbol{x}}} = \underbrace{\begin{pmatrix} \frac{1}{2}\underline{\boldsymbol{\Omega}}(t)\mathbf{q}(t) \\ \underline{\mathbf{I}}^{-1}\Big(-\mathfrak{S}\big\langle\boldsymbol{\omega}(t)\big\rangle\big(\underline{\mathbf{I}}\boldsymbol{\omega}(t)\big)+\boldsymbol{n}_c(t)+\boldsymbol{n}_d(t)\Big) \end{pmatrix}}_{f(\boldsymbol{x},\boldsymbol{w},t)}. \tag{4.43}$$

Since the elements of this set of equations are all in the body frame, the notation $\mathfrak{B}$ denoting SCB frame is intentionally dropped.

External Torques

The external torques are dominated by control torque $\boldsymbol{n}_c(t)$ from actuators, and external disturbances torque $\boldsymbol{n}_d(t)$ which is a sum of gravity gradient torques, aerodynamic drag torques and the torque caused by residual magnetic dipole moments. Control torque is known during the design. The model of other external torques are briefly presented hereafter.

Earth's gravitational field: Due to the Earth's gravitational field, any spacecraft is subject to gravitational torque in orbit. The gravity torque vector $\boldsymbol{n}_g$ in SCB frame can be found as

$$^{\mathfrak{B}}\boldsymbol{n}_g(t) = \frac{3\mu}{r_E(t)^3}\Big(^{\mathfrak{B}}\vec{\mathbf{r}}_E(t) \times \underline{\mathbf{I}}\,^{\mathfrak{B}}\vec{\mathbf{r}}_E(t)\Big). \tag{4.44}$$

Here $\underline{\mathbf{I}}$ is the moment of inertia tensor of the spacecraft, $^{\mathfrak{B}}\vec{\mathbf{r}}_E(t)$ is the unit vector pointing from the Earth's center of mass to the spacecraft's center of mass and μ is the Earth's gravitational constant and r is the distance to the center of the Earth.

Aerodynamic drag: This disturbance is originated by the impact of atmospheric molecules on the spacecraft body in LEO. Clearly at higher altitudes this impact converges to zero but for LEO should be considered. This impact introduces a torque about the spacecraft center of mass. If we approximate the spacecraft body by a collection of small geometrical elements the the aerodynamic torque in SCB frame, $^{\mathfrak{B}}\boldsymbol{n}_a$, can be formulated as

$$^{\mathfrak{B}}\boldsymbol{n}_a(t) = \frac{1}{2}C_D\rho(t)\|^{\mathfrak{B}}\vec{\mathbf{v}}(t)\|^2\sum_{i=1}^{k}A_i\Big(^{\mathfrak{B}}\vec{\mathbf{n}}\cdot{}^{\mathfrak{B}}\vec{\mathbf{v}}(t)\Big)^{\mathfrak{B}}\vec{\mathbf{n}}\times\vec{\mathbf{r}}_{SP,i}(t) \tag{4.45}$$

where C_D is the drag coefficient, ρ is the atmospheric density, A_i is the surface area of the ith element of the body, $^{\mathfrak{B}}\vec{\mathbf{n}}_{\boldsymbol{i}}$ is the normal vector of element ith which points outward, $^{\mathfrak{B}}\vec{\mathbf{v}}$ is a unit vector in the direction of the translational velocity in SCB frame and $\vec{\mathbf{r}}_{SP,i}$ is the vector from spacecraft center of mass to the center of pressure of the ith element.

Residual magnetic dipole moment: Sources of magnetic disturbance torques include permanent magnetism onboard a spacecraft, magnetism induced by external fields, spacecraft generated current loops and currents induced by external fields. Onboard current loops and onboard materials which are subject to permanent or induced magnetism are the main sources of magnetic torques, but eddy currents and hysteresis effects can cause such disturbance too, specially when the spacecraft is rapidly rotating in the Earth magnetic field. Understanding the source and effect of this disturbance is usually very essential in designing spacecraft ADCS, specially sizing the actuators [Blackburn et al. 1969]. The residual magnetic torque in SCB frame ${}^{\mathfrak{B}}\boldsymbol{n}_m$ can be formulated as

$$ {}^{\mathfrak{B}}\boldsymbol{n}_m(t) = {}^{\mathfrak{B}}\boldsymbol{m}_m(t) \times {}^{\mathfrak{B}}\boldsymbol{b}_E(t) \tag{4.46} $$

where ${}^{\mathfrak{B}}\boldsymbol{m}_m$ is the spacecraft effective magnetic dipole moment in SCB frame and ${}^{\mathfrak{B}}\boldsymbol{b}_E$ is the vector of Earth's magnetic field in SCB frame. The spacecraft magnetic dipole moment is known from measurements made on the flight hardware, or it is estimated based on the measurements made on similar equipments. Also it can be estimated from other similar spacecraft. The magnetic field vector of the Earth at the location of spacecraft can be calculated by mathematical models such as International Geomagnetic Reference Field (IGRF) model.

4.2 Attitude Determination

The problem of attitude determination onboard a spacecraft can be solved in two general ways. The first category of approaches are point-to-point methods which employ only sensor observations in single time instants. The second category employs estimators and filtering methods which combine the sensor measurements with the dynamic and/or kinematic models of the process to compute the attitude.

To design an energy manager for OWSAN we use a data fusion based on estimators which will be described in the next section, but the point-to-point solution can be used for initializing the estimator to establish initial conditions. Also it can be used as a tool for verifying the operations of the stochastic solution in attitude determination. Here we present a simple deterministic approach which will be used later in the design of the energy manager and also gives a better insight into attitude determination.

In an ideal situation the sensor measurements would be always available and error free. Then there would be no need for using any attitude determination approach. A point-to-point solution can be employed in the data fusion where

all sensor measurements arrive. Such as solution aim to use multiple observations from different sensors to find a rotation matrix $\mathbf{A}$ (or a quaternion $\mathbf{q}$) which describes an estimate of the spacecraft attitude. The problem of attitude determination based on only vector observations is formulated by Wahba as constrained minimization of a loss function [Wahba 1965]

$$\boldsymbol{J}(\mathbf{A}) := \frac{1}{2}\sum_{i=1}^{n} a_i \| {}^{\mathfrak{B}}\vec{\mathbf{b}}_i - \mathbf{A}\,{}^{\mathfrak{I}}\vec{\mathbf{b}}_i \|^2 \quad i \geq 2. \tag{4.47}$$

$\mathbf{A}$ is a proper orthogonal rotation matrix which was explained in Section 4.1.4 and a_i are individual non-negative weights which are assigned to each vector set of ${}^{\mathfrak{B}}\vec{\mathbf{b}}_i$ and ${}^{\mathfrak{I}}\vec{\mathbf{b}}_i$. For example they can be chosen as the inverse variance of measurement noise. ${}^{\mathfrak{B}}\vec{\mathbf{b}}_i$ is a unit vector in SCB frame, and ${}^{\mathfrak{I}}\vec{\mathbf{b}}_i$ is the corresponding unit vector in ECI frame. For example ${}^{\mathfrak{B}}\vec{\mathbf{b}}_i$ can be a unit vector to the Sun in SCB frame whilst ${}^{\mathfrak{I}}\vec{\mathbf{b}}_i$ is the Sun unit vector in ECI frame. In ideal situations where the sensor measurement are error free, there is no need for calculating this loss function because $\mathbf{A} = {}^{\mathfrak{B}}_{\mathfrak{I}}\mathbf{A}$ and we have ${}^{\mathfrak{B}}_{\mathfrak{I}}\mathbf{A}\,{}^{\mathfrak{I}}\vec{\mathbf{b}}_i = {}^{\mathfrak{B}}\vec{\mathbf{b}}_i$ for all i and the loss function is zero. Different solutions to this problem are given in various literatures [Farrel and Stuelpnagel 1966, Markley 1993, Shuster 2006].

The last equation can be re-written as

$$\boldsymbol{J}(\mathbf{A}) = \frac{1}{2}\sum_{i=1}^{n} a_i - \text{trace}(\mathbf{A}\mathbf{B}^{\intercal}) \tag{4.48}$$

where

$$\mathbf{B} = \sum_{i=1}^{n} a_i\, {}^{\mathfrak{B}}\vec{\mathbf{b}}_i\, {}^{\mathfrak{I}}\vec{\mathbf{b}}_i^{\intercal}. \tag{4.49}$$

To minimize the loss function in (4.48), the trace of the matrix production should be maximized. We need to find the optimum $\underline{\mathbf{A}}$ which maximizes the trace. From matrix algebra we have

$$\text{trace}(\mathbf{A}\mathbf{B}^{\intercal}) = \text{trace}\Big(\mathbf{U}^{\intercal}\mathbf{A}\mathbf{V}\,\text{diag}\{\lambda_{11}, \lambda_{22}, \lambda_{33}\}\Big) \tag{4.50}$$

λ_1, λ_2 and λ_3 are the eigenvalues of $\mathbf{B}$, and $\mathbf{U}$ and $\mathbf{V}$ are proper orthogonal matrices which can be found by singular value decomposition of $\mathbf{B}$. Finally the optimum value for $\mathbf{A}$ will be the following

$$\underline{\mathbf{A}} = \mathbf{U}\,\text{diag}\{1, 1, \det(\mathbf{U}), \det(\mathbf{V})\}\mathbf{V}^{\intercal}. \tag{4.51}$$

Also a covariance matrix $\underline{\mathbf{P}}$ can be defined as a measure of the rotation matrix calculation [Markley 1988]

$$\mathbf{P}_{\underline{\mathbf{A}}} = \mathbf{U}\,\text{diag}\{(s_2 + s_3)^{-1}, (s_3 + s_1)^{-1}, (s_1 + s_2)^{-1}\}\mathbf{U}^{\intercal} \tag{4.52}$$

with the following definitions

$$s_1 := \lambda_{11} \quad , \quad s_2 := \lambda_{22} \quad , \quad s_3 := \det(\mathbf{U})\det(\mathbf{V})\lambda_{33}. \tag{4.53}$$

Remark 4.2. A point-to-point attitude determination approach can be used only when at least two observation vectors related to the same rotation matrix are available. Clearly this condition does not hold for all combinations of ADCS sensors onboard a spacecraft. For example a combination of magnetometer and sun sensor fails when the spacecraft is in eclipse or when the observation vectors are parallel. In such case, the rotation matrix can be still calculated from the magnetometer measurements with a lower precision than the optimal solution.

4.2.1 ADCS Sensors

As discussed in Section 4.2, attitude measurements in SCB frame are necessary to derive the quaternion which describes the rotation of SCB frame relative to ECI. Practically, different type of sensors and their combinations can be used to achieve this goal. In this dissertation three different type of sensors are chosen in the implementation and evaluation of the energy management system for OWSAN. These sensors are a three-axis gyroscope, a three-axis magnetometer and a Sun sensor . This set is carefully chosen because of their popularity in various missions. On the other hand, these sensors generally consume low energy for operations which make them good candidates for OWSAN. These sensors provide information in SCB frame and system level model of these sensors are not complex.

A gyro simply provides the vector of spacecraft rotation rate in SCB frame which is ${}^{\mathfrak{B}}\boldsymbol{\omega} = [\omega_1 \quad \omega_2 \quad \omega_3]^\intercal$. A magnetometer returns a full three dimensional vector measurement of Earth's magnet field in its frame which is known relative to SCB frame, ${}^{\mathfrak{B}}\boldsymbol{m} = [m_1 \quad m_2 \quad m_3]^\intercal$. By comparing this vector with the Earth's IGRF model we can construct the corresponding quaternion which provides spacecraft attitude information in ECI frame. A simple Sun sensor is typically made of a small photocell. It is electrically designed in short circuit mode to make sure that the output current of the sensor is only a function of the incoming Sun radiation flux. Although in theory it seems to be possible to employ solar panels as Sun sensors, in practice the varying electrical load on the output of the cells makes the modeling of the output current very complex. The output current of Sun sensor i_{ss}, depends on the performance of the cell and the angle of the incidence of Sun radiation

$$i_{ss}(\alpha) = i_{ss,\max}\cos(\alpha). \tag{4.54}$$

In this equation, $i_{ss,\max} = i_{ss}(0)$ and α is the angle between the sun-senor normal vector ${}^{\mathfrak{B}}\vec{\mathbf{n}}_{ss}$ and ${}^{\mathfrak{B}}\vec{\mathbf{r}}_{\boxtimes\odot}$ (see Fig. 4.4). Therefore, calculation of the Sun

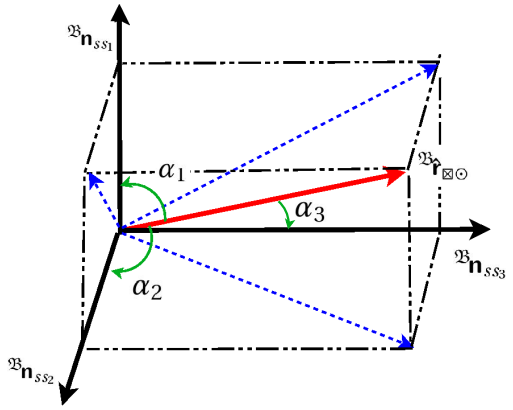

Figure 4.4: Sun-sensor model

incidence angle on each side of the cube shape spacecraft is straight forward. For example for α_1

$$\alpha = \arccos(^{\mathfrak{B}}\hat{\vec{\mathbf{r}}}_{\boxtimes\odot} \cdot {}^{\mathfrak{B}}\vec{\mathbf{n}}_{ss_1}). \tag{4.55}$$

Similarly, α_2 and α_3 can be calculated. Thus $^{\mathfrak{B}}\boldsymbol{r}_{\boxtimes\odot}$ the vector from spacecraft to the Sun in the spacecraft body frame can be found. If a four-quadrant Sun sensor is used then measurements of one Sun sensor will be adequate to calculate the Sun vector when the Sun is in field of view (FOV) of the sensor [Lee et al. 2003, Xing et al. 2008]. A four quadrant Sun sensor can determine the Sun ray elevation α and azimuth β in the Sun sensor body coordinates. With this information calculating the unit vector $^{\mathfrak{B}}\vec{\mathbf{r}}_{\boxtimes\odot}$ yields

$$^{\mathfrak{B}}\vec{\mathbf{r}}_{\boxtimes\odot} = \begin{bmatrix} \cos\alpha\cos\beta \\ \sin\alpha\cos\beta \\ -\sin\beta \end{bmatrix}. \tag{4.56}$$

4.3 Data Fusion

We consider a system with m sensors and a fusion center. Therefore the observation vector is $\boldsymbol{z} = \{\boldsymbol{z}_1, \boldsymbol{z}_2, \ldots, \boldsymbol{z}_m\}$. Each sensor can communicate the information to the fusion center. For the ith sensor we have

$$\boldsymbol{z}_i = \boldsymbol{h}_i(\boldsymbol{x}) + \boldsymbol{w}_i \tag{4.57}$$

where $\boldsymbol{z}_i$ is the vector of observations, $\boldsymbol{x}$ is the true state of the system which shall be estimated and $\boldsymbol{w}_i$ is the corresponding noise vector with covariance matrix $\mathbf{R}_i$. On this sensor node, $\hat{\boldsymbol{x}}_i$ is defined as the the local estimate of $\boldsymbol{x}$.

The covariance of this local $\mathbf{P}_i$ estimate can be calculated from of the local estimation error $\tilde{\boldsymbol{x}}_i = \boldsymbol{x} - \hat{\boldsymbol{x}}_i$.

At the fusion center where all data is gathered, we define $\hat{\boldsymbol{x}}$ as the estimation of the true state vector and $\mathbf{P}$ as the covariance matrix of the sensor fusion estimation error $\tilde{\boldsymbol{x}} = \boldsymbol{x} - \hat{\boldsymbol{x}}$. We define $\boldsymbol{y} = \{\boldsymbol{y}_1, \boldsymbol{y}_2, \ldots, \boldsymbol{y}_m\}$ as the vector of all available information in the fusion center. With this model three different architectures can be sought

1. Centralized fusion where $\boldsymbol{y} = \boldsymbol{z}$ and all data and measurements are communicated to the fusion center without any processing;
2. Decentralized fusion where the processed data and information are communicated and the raw measurements are not presented to the fusion center. Thus $\boldsymbol{y} = \{\boldsymbol{g}_1(\boldsymbol{z}_1), \boldsymbol{g}_2(\boldsymbol{z}_2), \ldots, \boldsymbol{g}_m(\boldsymbol{z}_m)\}$;
3. Hybrid data fusion where the fusion center received both processed and unprocessed information.

In our application, measurements are not the only means for estimating the state of the spacecraft. Availability of the spacecraft attitude dynamic and kinematic equations which was presented in Section 4.1.5 enables possibility of using Kalman filter based technique for the data fusion.

4.3.1 Centralized Data Fusion

A centralized data fusion scheme is shown in Figure 4.5. Each sensor obtains measurements from the environment and forwards it to the central fusion node. The central fusion node collects all the information and has an overall view of the system. Onboard a spacecraft a data fusion based on Kalman filter can be used which employs the sensor measurements and the spacecraft model which is described as a stochastic process.

To develop and employ a Kalman filter, the dynamic model of a system (stochastic process) must be transformed to state space representation. The dynamic relations between n states of a stochastic process in time domain consists of a set of n first order differential equations driven by random input noise

$$\begin{cases} \dot{\boldsymbol{x}}(t) = \boldsymbol{f}(\boldsymbol{x}(t), \boldsymbol{u}(t), t) + \boldsymbol{v}(t) \\ \boldsymbol{x}(t_0) = \boldsymbol{x}_0 \end{cases} . \tag{4.58}$$

Here $\boldsymbol{x}(t)$ is the vector of n system states at time t with initial condition $\boldsymbol{x}_0$, $\boldsymbol{f}$ is a $n \times 1$ function vector, $\boldsymbol{u}(t)$ is the vector of deterministic control inputs, $\boldsymbol{v}(t)$ is additive noise vector with dimension $n \times 1$. The additive noise vector here

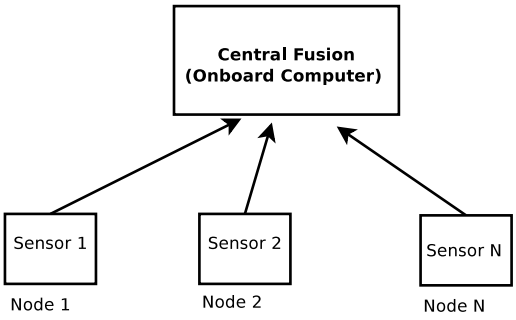

Figure 4.5: Centralized data fusion scheme

represents the modeling uncertainty. The initial condition in (4.58) assumed to have Gaussian distribution with known mean $\hat{\boldsymbol{x}}_0$ and covariance $\mathbf{P}_0$

$$\boldsymbol{x}_0 \sim \mathcal{N}\{\hat{\boldsymbol{x}}_0, \mathbf{P}_0\}. \tag{4.59}$$

Hereafter the $\mathcal{N}$ operator denotes a Gaussian distribution. In this system formulation, the sequence of the system state is a Gauss-Markov process and the additive noise $\boldsymbol{v}(t_k)$ is a zero mean white Gaussian noise with a known covariance which is not correlated with $\boldsymbol{x}(t_k)$. Also the mean and covariance of the initial state $\boldsymbol{x}(t_0)$ are assumed to be known[1]. Thus the following relations hold for the noise vector

$$\mathrm{E}\{\boldsymbol{v}(t)\} = \mathbf{0} \quad , \quad \mathrm{E}\big\{\boldsymbol{v}(t)\boldsymbol{v}^{\mathsf{T}}(t+\tau)\big\} = \mathbf{Q}(t)\delta(\tau) \tag{4.60}$$

$$\therefore \quad \boldsymbol{v}(t_k) \sim \mathcal{N}\big\{0, \mathbf{Q}(t_k)\big\}. \tag{4.61}$$

Note that the E operator denotes the expectation calculation. In (4.60), $\mathbf{Q}(t)$ is the covariance matrix of the noise vector which is a positive semi definite matrix and $\delta(t)$ is the Kronecker delta function.

Furthermore, the state space model which describes the relation between sensor measurements at time t_k and state of the system is

$$\boldsymbol{z}(t_k) = \boldsymbol{h}(\boldsymbol{x}_k, t_k) + \boldsymbol{w}_k. \tag{4.62}$$

Unlike (4.58), this formulation is presented in discrete time domain because the sensors measurements are available discretely. In (4.62), $\boldsymbol{w}_k$ is a white Gaussian discrete time sequence which describes the existing uncertainties in the models of the sensors at time t_k, hence

$$\mathrm{E}\{\boldsymbol{w}_i\} = \mathbf{0} \quad , \quad \mathrm{E}\{\boldsymbol{w}_i \boldsymbol{w}_j^{\mathsf{T}}\} = \mathbf{R}(i)\delta_{i,j} \tag{4.63}$$

$$\therefore \quad \boldsymbol{w}(t_k) \sim \mathcal{N}\big\{0, \mathbf{R}(t_k)\big\} \tag{4.64}$$

[1] Satisfying this assumption onboard spacecraft is not difficult because a first guess for the spacecraft state can be achieved by deterministic attitude determination methods which only use the sensor measurements to reconstruct the attitude matrix.

where $\mathbf{R}(t_k)$ is the covariance matrix corresponding to $\boldsymbol{w}(t_k)$.

Kalman Filter

The Kalman filter provides an estimate of the states of the stochastic process based on the model of the process, models of the sensors, the properties of the uncertainties in the models and the measurements made by the sensors. The conditional mean and covariance of states can be introduced as

$$\hat{\boldsymbol{x}}_{i|j}(t) := \mathrm{E}\{\boldsymbol{x}_i(t)|Z[t_j]\} \tag{4.65}$$

$$\mathbf{P}_{i|j}(t) := \mathrm{E}\big\{(\boldsymbol{x}_i(t)-\hat{\boldsymbol{x}}_{i|j}(t))(\boldsymbol{x}_i(t)-\hat{\boldsymbol{x}}_{i|j}(t))^{\mathsf{T}}\big\} \tag{4.66}$$

where

$$Z[t_j] = \{\boldsymbol{z}_(t_1), \boldsymbol{z}_(t_2) \cdots, \boldsymbol{z}_(t_j)\}. \tag{4.67}$$

$Z[t_j]$ is the set of all sensor measurement (observations) up to time t_j, . At time t_k, two state estimates can be distinguished. The first one is $\hat{\boldsymbol{x}}_{k|k}(t_k)$ which is an estimate based on the model of the process in (4.58) and all observation history up to time t_k. The second estimate is $\hat{\boldsymbol{x}}_{k|k-1}(t_k)$ which is an estimate using the observation history only up to the previous sampling time t_{k-1}, therefore the new observations made by sensor at t_k are not used in computation of $\hat{\boldsymbol{x}}_{k|k-1}(t_k)$. Thus

$$\hat{\boldsymbol{x}}_{k|k}(t_k) = \mathrm{E}\{\boldsymbol{x}(t_k)|Z[t_k]\} \tag{4.68}$$

$$\hat{\boldsymbol{x}}_{k|k-1}(t_k) = \mathrm{E}\{\boldsymbol{x}(t_k)|Z[t_{k-1}])\}. \tag{4.69}$$

At time t_k, the errors corresponding to these estimates are defined as

$$\tilde{\boldsymbol{x}}_{k|k-1}(t_k) = \boldsymbol{x}(t_k) - \hat{\boldsymbol{x}}_{k|k-1}(t_k) \tag{4.70}$$

$$\tilde{\boldsymbol{x}}_{k|k}(t_k) = \boldsymbol{x}(t_k) - \hat{\boldsymbol{x}}_{k|k-1}(t_k). \tag{4.71}$$

here $\hat{\boldsymbol{x}}_{k|k}(t_k)$ is the true value of system state vector at time t_k. The covariance of errors in (4.70) and (4.71) can be derived as the following

$$\begin{aligned}\mathbf{P}_{k|k}(t_k) &= \mathrm{E}\big\{\tilde{\boldsymbol{x}}_{k|k}(t_k)\tilde{\boldsymbol{x}}^{\mathsf{T}}_{k|k}(t_k)\big\} \\ &= \mathrm{E}\big\{\big(\boldsymbol{x}(t_k)-\hat{\boldsymbol{x}}_{k|k}(t_k)\big)\big(\boldsymbol{x}(t_k)-\hat{\boldsymbol{x}}_{k|k}(t_k)\big)^{\mathsf{T}}\big\} \qquad (4.72)\\ \mathbf{P}_{k|k-1}(t_k) &= \mathrm{E}\big\{\tilde{\boldsymbol{x}}_{k|k-1}(t_k)\tilde{\boldsymbol{x}}^{\mathsf{T}}_{k|k-1}(t_k)\big\} \\ &= \mathrm{E}\big\{\big(\boldsymbol{x}(t_k)-\hat{\boldsymbol{x}}_{k|k-1}(t_k)\big)\big(\boldsymbol{x}(t_k)-\hat{\boldsymbol{x}}_{k|k-1}(t_k)\big)^{\mathsf{T}}\big\}. \qquad (4.73)\end{aligned}$$

Likewise, the predicted observation vector $\hat{\boldsymbol{z}}_{k|k-1}(t_k)$ is

$$\hat{\boldsymbol{z}}_{k|k-1}(t_k) = \mathrm{E}\{\boldsymbol{z}(t_k)|Z_{k-1}\} \tag{4.74}$$

Based on this definition, the difference between the real observation vector and value can be defined as *innovation* and formulated as

$$\boldsymbol{\epsilon}_k(t_k) := \boldsymbol{z}(t_k) - \hat{\boldsymbol{z}}_{k|k-1}(t_k). \tag{4.75}$$

With these understandings, a standard Kalman filter for a linear stochastic process can be derived.

A Kalman filter is a state estimator and it is not involved in the controller. Thus, the control input is not considered later on in the state space model of the system which is used in the development of Kalman filter.

Linear Kalman Filter

For a system with linear process and observations models, a direct and close form for Kalman filter can be derived. Linear state space formulation for a system with state vector $\boldsymbol{x}_{n\times 1}$ and $\boldsymbol{z}_{m\times 1}$ sensor measurement vector in discrete form is

$$\begin{cases} \boldsymbol{x}(t_k) &= \mathbf{F}(t_{k-1})\boldsymbol{x}(t_{k-1}) + \boldsymbol{v}(t_{k-1}) \\ \boldsymbol{z}(t_k) &= \mathbf{H}(t_k)\boldsymbol{x}(t_k) + \boldsymbol{w}(t_k) \end{cases}. \tag{4.76}$$

Here $\mathbf{F}(t_k)$ is a $n \times n$ matrix, $\mathbf{H}(t_k)$ is a $m \times n$ measurement matrix. $\boldsymbol{v}(t_k)$ and $\boldsymbol{w}(t_k)$ are noise vectors as introduced before. The predicted state and measurement vectors at time t_k can be computed through (4.73) and (4.76) as

$$\hat{\boldsymbol{x}}_{k|k-1}(t_k) = \mathbf{F}(t_{k-1})\boldsymbol{x}_{k-1|k-1}(t_{k-1}) \tag{4.77}$$

$$\hat{\boldsymbol{z}}_{k|k-1}(t_k) = \mathbf{H}(t_k)\hat{\boldsymbol{x}}_{k|k-1}(t_k) \tag{4.78}$$

and the predicted covariance according to (4.73) and (4.60) is

$$\begin{aligned} \mathbf{P}_{k|k-1}(t_k) &= \mathrm{E}\Big\{\big(\mathbf{F}(t_{k-1})\tilde{\boldsymbol{x}}_{k-1|k-1}(t_{k-1}) + \boldsymbol{v}(t_{k-1})\big) \\ &\qquad \big(\mathbf{F}(t_{k-1})\tilde{\boldsymbol{x}}_{k-1|k-1}(t_{k-1}) + \boldsymbol{v}(t_{k-1})\big)^{\mathsf{T}}\Big\} \\ &= \mathbf{F}(t_{k-1})\mathbf{P}_{k-1|k-1}(t_{k-1})\mathbf{F}^{\mathsf{T}}(t_{k-1}) + \mathbf{Q}(t_{k-1}) \end{aligned} \tag{4.79}$$

because the measurements of time t_k are not yet incorporated in the formulation, thus logically $\mathbf{Q}(t_{k-1})$ appears in the later equation.

The innovation vector which was defined by (4.75) follows

$$\boldsymbol{\epsilon}(t_k) = \mathbf{H}(t_k)\tilde{\boldsymbol{x}}_{k|k-1}(t_k) + \boldsymbol{w}(t_k) \tag{4.80}$$

and the covariance of the innovation vector can be found

$$\begin{aligned} \mathbf{S}(t_k) &= \mathrm{E}\{\boldsymbol{\epsilon}(t_k)\boldsymbol{\epsilon}^{\mathsf{T}}(t_k)\} \\ &= \mathbf{H}(t_k)\mathbf{P}_{k|k-1}(t_k)\mathbf{H}^{\mathsf{T}}(t_k) + \mathbf{R}(t_k) \end{aligned} \tag{4.81}$$

at time t_k, Kalman gain matrix $\mathbf{K}(t_k)$ can be found such that the measurement vector $\boldsymbol{z}(t_k)$ updates the prior state estimate $\hat{\boldsymbol{x}}_{k|k-1}(t_k)$ to a better estimate $\hat{\boldsymbol{x}}_{k|k}(t_k)$. Therefore we have

$$\hat{\boldsymbol{x}}_{k|k}(t_k) = \hat{\boldsymbol{x}}_{k|k-1}(t_k) + \mathbf{K}(t_k)\boldsymbol{\epsilon}(t_k) \tag{4.82}$$

thus we can find the available error in the state estimate at time t_k by

$$\begin{aligned}
\tilde{\boldsymbol{x}}_{k|k}(t_k) &= \boldsymbol{x}(t_k) - \hat{\boldsymbol{x}}_{k|k}(t_k) \\
&= \boldsymbol{x}(t_k) - \big(\hat{\boldsymbol{x}}_{k|k-1}(t_k) + \mathbf{K}(t_k)\boldsymbol{\epsilon}(t_k)\big) \\
&= \tilde{\boldsymbol{x}}_{k|k-1}(t_k) - \mathbf{K}(t_k)\boldsymbol{\epsilon})(t_k) && (4.83) \\
&= \tilde{\boldsymbol{x}}_{k|k-1}(t_k) - \mathbf{K}(t_k)\big(\mathbf{H}(t_k)\tilde{\boldsymbol{x}}_{k|k-1}(t_k) + \boldsymbol{w}(t_k)\big) && (4.84) \\
&= \big(\mathbf{I}_{n\times n} - \mathbf{K}(t_k)\mathbf{H}(t_k)\big)\tilde{\boldsymbol{x}}_{k|k-1}(t_k) - \mathbf{K}(t_k)\boldsymbol{w}(t_k). && (4.85)
\end{aligned}$$

By using (4.72) covariance matrix of this state estimate error vector can be found

$$\begin{aligned}
\mathbf{P}_{k|k}(t_k) &= \mathrm{E}\big\{\tilde{\boldsymbol{x}}_{k|k}(t_k)\tilde{\boldsymbol{x}}_{k|k}^{\mathsf{T}}(t_k)\big\} \\
&= \big(\mathbf{I}_{n\times n} - \mathbf{K}(t_k)\mathbf{H}(t_k)\big)\mathbf{P}_{k|k-1}(t_k)\big(\mathbf{I}_{n\times n} - \mathbf{K}(t_k)\mathbf{H}(t_k)\big)^{\mathsf{T}} \\
&\quad + \mathbf{K}(t_k)\mathbf{R}(t_k)\mathbf{K}^{\mathsf{T}}(t_k) && (4.86)
\end{aligned}$$

Equation (4.86) is known as the *Joseph form* for state error covariance matrix.

The matrix $\mathbf{K}(t_k)$ should be chosen such that the mean squared error of the covariance of state estimation error $\mathbf{P}_{k|k}(t_k)$ is minimized. The solution which meets this requirement is [Kalman 1960, Maybeck 1979]

$$\mathbf{K}(t_k) = \mathbf{P}_{k|k-1}(t_k)\mathbf{H}^{\mathsf{T}}(t_k)\mathbf{S}^{-1}(t_k) \tag{4.87}$$

with this result for the Kalman gain, the state estimation error covariance matrix can be simplified into

$$\mathbf{P}_{k|k}(t_k) = \big(\mathbf{I}_{n\times n} - \mathbf{K}(t_k)\mathbf{H}(t_k)\big)\mathbf{P}_{k|k-1}(t_k) \tag{4.88}$$

or by using the covariance matrix of innovation

$$\mathbf{P}_{k|k}(t_k) = \mathbf{P}_{k|k-1}(t_k) - \mathbf{K}(t_k)\mathbf{S}(t_k)\mathbf{K}^{\mathsf{T}}(t_k). \tag{4.89}$$

Algorithm 1 summarizes the linear Kalman filtering procedure. The Kalman filter equations can be converted to *information filter* form which bring numerical advantages for decentralized data fusion. The term information here is applied in the *Fisher* sense and the formulation is expressed in term of the information measure about the states of the system rather than the direct state

Algorithm 1 Linear Kalman filter algorithm

1. Initialization:
   $$\hat{\boldsymbol{x}}(t_0)=\boldsymbol{x}_0,\quad \mathbf{P}(t_0)=\mathbf{P}_0.$$
2. Prediction:
   1. Project the system state ahead:
      $$\hat{\boldsymbol{x}}_{k|k-1}(t_k)=\mathbf{F}(t_{k-1})\hat{\boldsymbol{x}}_{k|k}(t_{k-1}).$$
   2. Project the error covariance ahead:
      $$\mathbf{P}_{k|k-1}(t_k)=\mathbf{F}(t_{k-1})\mathbf{P}_{k-1|k-1}(t_{k-1})\mathbf{F}(t_{k-1})^{\intercal}+\mathbf{Q}(t_{k-1}).$$
3. Correction:
   1. Compute the innovation:
      $$\boldsymbol{\epsilon}(t_k)=\boldsymbol{z}(t_k)-\mathbf{H}(t_k)\hat{\boldsymbol{x}}_{k|k-1}(t_k);$$
      $$\mathbf{S}(t_k)=\mathbf{H}(t_k)\mathbf{P}_{k|k-1}(t_k)\mathbf{H}^{\intercal}(t_k)+\mathbf{R}(t_k).$$
   2. Compute the Kalman filter gain:
      $$\mathbf{K}(t_k)=\mathbf{P}_{k|k-1}(t_k)\mathbf{H}^{\intercal}(t_k)\mathbf{S}^{-1}(t_k).$$
   3. Update the state estimate with measurement $\boldsymbol{z}_(t_k)$:
      $$\hat{\boldsymbol{x}}_{k|k}(t_k)=\hat{\boldsymbol{x}}_{k|k-1}(t_k)+\mathbf{K}(t_k)\epsilon(t_k).$$
   4. Update the error covariance matrix:
      $$\hat{\boldsymbol{x}}_{k|k}(t_k)=\hat{\boldsymbol{x}}_{k|k-1}+\gamma_k\mathbf{K}(t_k)\big(\boldsymbol{z}(t_k)-\mathbf{H}(t_k)\hat{\boldsymbol{x}}_{k|k-1}(t_k)\big).$$

estimation and its covariance. The formulation is based on reformulation of Kalman filter using the following defined variables

$$\begin{cases}\mathbf{Y}_{k_1|k_2}(t_k):=\mathbf{P}^{-1}_{k_1|k_2}(t_k)\\ \hat{\boldsymbol{y}}_{k_1|k_2}(t_k):=\mathbf{P}^{-1}_{k_1|k_2}(t_k)\hat{\boldsymbol{x}}_{k_1|k_2}(t_k)\\ \boldsymbol{i}(t_k):=\mathbf{H}^{\intercal}(t_k)\mathbf{R}^{-1}(t_k)\boldsymbol{z}(t_k)\\ \mathbf{I}(t_k):=\mathbf{H}^{\intercal}(t_k)\mathbf{R}^{-1}(t_k)\mathbf{H}(t_k)\end{cases}. \tag{4.90}$$

Here $\hat{\boldsymbol{y}}_{k_1|k_2}$ is called the information state vector, and $\mathbf{Y}_{k_1|k_2}$ is information matrix, and $\boldsymbol{i}(t_k)$ is information state contribution from an observation $\boldsymbol{z}(t_k)$ and and $\mathbf{I}(t_k)$ is its associated information matrix. With these definition linear information filter algorithm is shown by Algorithm 2.

Remark 4.3. Due to numerical errors, the state error covariance matrix calculated by (4.88) and (4.89) can not guarantee the positive definiteness of $\mathbf{P}_{k|k}(t_k)$ when the Kalman gain is not the optimal value. However, the Joseph form presented in (4.86) can give this assurance for all values of $\mathbf{K}(t_k)$ and therefore should be used in practice.

Remark 4.4. By observing the algorithm we can understand that the correction equations of the information filter is computationally easier than that of Kalman filter. This property can be used later in decentralizing the data fusion.

Algorithm 2 Linear Information filter algorithm

1. Initialization:
$$\mathbf{Y}(t_0)=\mathbf{P}_0^{-1},\quad \hat{\boldsymbol{y}}(t_0)=\mathbf{Y}(t_0)\boldsymbol{x}_0.$$
2. Prediction:
   1. Project the information state vector:
$$\hat{\boldsymbol{y}}_{k|k-1}(t_k)=\mathbf{Y}_{k|k-1}(t_k)\mathbf{F}(t_{k-1})\mathbf{Y}^{-1}_{k-1|k-1}(t_{k-1})\hat{\boldsymbol{y}}_{k-1|k-1}(t_{k-1}).$$
   2. Project the information matrix:
$$\mathbf{Y}_{k|k-1}(t_k)=\big(\mathbf{F}(t_{k-1})\mathbf{Y}^{-1}_{k-1|k-1}(t_k)\mathbf{F}^{\intercal}(t_k)+\mathbf{Q}(t_k)\big)^{-1}.$$
3. Correction:
   1. Compute the information state update:
$$\hat{\boldsymbol{y}}_{k|k}(t_k)=\hat{\boldsymbol{y}}_{k|k-1}(t_k)+\boldsymbol{i}(t_k).$$
   2. Compute the information matrix update:
$$\mathbf{Y}_{k|k}(t_k)=\mathbf{Y}_{k|k-1}(t_k)+\mathbf{I}(t_k).$$

Also it can be seen that there is no gain and innovation covariance matrix involved in the computation. Also unlike the Kalman filter, the initial condition for the information state vector and information matrix can be set to zero information. This can be performed by using a diagonal matrix with small non-zero elements on the diagonal as the initial condition for the information matrix.

Remark 4.5. It can be shown that the measurements innovation vector and state estimate error are both Gaussian random processes with zero mean. Therefore the following normalized quadratic functions have χ^2 distribution

$$\mathbf{N}_{\boldsymbol{\epsilon}}(t_k)=\boldsymbol{\epsilon}^{\intercal}(t_k)\mathbf{S}^{-1}(t_k)\boldsymbol{\epsilon}(t_k) \tag{4.91}$$
$$\mathbf{N}_{\tilde{\boldsymbol{x}}}(t_k)=\big(\boldsymbol{x}(t_k)-\hat{\boldsymbol{x}}_{k|k}(t_k)\big)^{\intercal}\mathbf{P}^{\intercal}_{k|k}(t_k)\big(\boldsymbol{x}(t_k)-\hat{\boldsymbol{x}}_{k|k}(t_k)\big). \tag{4.92}$$

$\mathbf{N}_{\boldsymbol{\epsilon}}(t_k)$ is an indication for the inconsistency of the measurements and has m degrees of freedom with m being the number of the independent measurements, while $\mathbf{N}_{\tilde{\boldsymbol{x}}}(t_k)$ is a measure of the uncertainty level in estimating the states and has n degrees of freedom with n being the number of the states.

Remark 4.6. Observing the covariance matrix $\mathbf{P}_{k|k}(t_k)$ during the operation of the Kalman filter can provide valuable information about the validity level of state estimate $\hat{\boldsymbol{x}}_{k|k}(t_k)$. The uncertainty of state estimation can be explained by the following normalized equation

$$\big(\boldsymbol{x}(t_k)-\hat{\boldsymbol{x}}_{k|k}(t_k)\big)^{\intercal}\mathbf{P}^{\intercal}_{k|k}(t_k)\big(\boldsymbol{x}(t_k)-\hat{\boldsymbol{x}}_{k|k}(t_k)\big)=1 \tag{4.93}$$

which represents an n dimensional ellipsoid. By applying singular value de-

composition to $\mathbf{P}_{k|k}(t_k)$ as it is introduced Bierman [Bierman 1977] we get

$$\left(\mathbf{U}^{-1}(t_k)\tilde{\boldsymbol{x}}_{k|k}(t_k)\right)^{\mathsf{T}}\mathbf{D}(t_k)^{-1}\left(\mathbf{U}^{-1}(t_k)\tilde{\boldsymbol{x}}_{k|k}(t_k)\right)=1 \tag{4.94}$$

where $\mathbf{U}(t_k)$ is the matrix composed of left singular vectors of the covariance matrix and $\mathbf{D}(t_k)$ is a diagonal matrix composed of the singular values of the covariance matrix at time t_k. These two are found by singular value decomposition of $\mathbf{P}_{k|k}(t_k)$, such that

$$\mathbf{P}_{k|k}(t_k)=\mathbf{U}(t_k)\mathbf{D}(t_k)\mathbf{V}^{\mathsf{T}}(t_k). \tag{4.95}$$

The rank of $\mathbf{D}$ is equal to the number of non-zero singular values of the covariance matrix. These singular values are the lengths of the axes of the ellipsoid in n dimensional space. The columns of are singular vectors which build the orthogonal basis of the state space of the system. More uncertainty in the computation of states corresponds to larger singular values. Therefore if the estimation of the states converges to the true value, the n-dimensional ellipsoid starts shrinking in all directions.

Remark 4.7. It can be shown that the innovation sequence has zero mean and is white. Also the state estimate error sequence has zero mean when the Kalman filter is stabilized. These properties can be used for the energy manager decision making based on observing the properties of Kalman filter parameters.

Extended Kalman Filter

Although the linear Kalman filter provides the tool for estimating the states of the system, the process model of spacecraft is non-linear and does not follow the form presented in (4.76). A non-linear process model without considering the input signals can be written as

$$\begin{cases}\boldsymbol{x}(t_k)=\boldsymbol{f}(\boldsymbol{x}(t_{k-1}))+\boldsymbol{v}(t_{k-1})\\ \boldsymbol{z}(t_k)=\boldsymbol{h}(\boldsymbol{x}(t_k))+\boldsymbol{w}(t_k)\end{cases} \tag{4.96}$$

where both $\boldsymbol{f}(\boldsymbol{x}(t_k))$ and $\boldsymbol{h}(\boldsymbol{x}(t_k))$ are known non-linear vector functions. These nonlinear models should be linearized before applying the Kalman filter solution. The linearizion can be performed either around the pre-computed nominal trajectory, or about an estimated trajectory which is update online and during the operation of the filter. The first linearizion method does not need the measurements and can be done in an off-line manner which results in a linear Kalman filter formulation which was described previously. This approach can not be used on board a spacecraft because the spacecraft maneuvers are not pre-computable. The second linearizion method is suitable for our application and results in Extended Kalman filter form.

During the operation of the system, the best available estimate of the states of the system up to t_k is $\hat{\boldsymbol{x}}_{k-1|k-1}(t_{k-1})$, which is accompanied with the estimation error $\tilde{\boldsymbol{x}}_{k-1|k-1}(t_{k-1})$ defined by

$$\tilde{\boldsymbol{x}}_{k-1|k-1}(t_{k-1}) = \boldsymbol{x}(t_{k-1}) - \hat{\boldsymbol{x}}_{k-1|k-1}(t_{k-1}). \tag{4.97}$$

At this point, a new prediction for states and measurements vectors can be made through the non-linear equations solely based on the models

$$\begin{cases} \hat{\boldsymbol{x}}_{k|k-1}(t_k) = \boldsymbol{f}\big(\hat{\boldsymbol{x}}_{k-1|k-1}(t_{k-1})\big) \\ \hat{\boldsymbol{z}}_{k|k-1}(t_k) = \boldsymbol{h}\big(\hat{\boldsymbol{x}}_{k|k-1}(t_k)\big) \end{cases} \tag{4.98}$$

and the prediction error for this estimate is

$$\begin{cases} \tilde{\boldsymbol{x}}_{k|k-1}(t_k) = \boldsymbol{x}(t_k) - \hat{\boldsymbol{x}}_{k|k-1}(t_k) \\ \boldsymbol{\epsilon}(t_k) = \boldsymbol{z}(t_k) - \hat{\boldsymbol{z}}_{k|k-1}(t_k) \end{cases} . \tag{4.99}$$

To linearize the state space model we can approximate $\boldsymbol{x}(t_k)$ in (4.96) by using a Taylor series expansion around $\hat{\boldsymbol{x}}_{k-1|k-1}(t_{k-1})$ which is the best available estimate of the trajectory at time until t_k. This approximation is formulated as

$$\begin{aligned} \boldsymbol{x}(t_k) = {} & \boldsymbol{f}(\hat{\boldsymbol{x}}_{k-1|k-1}(t_{k-1})) \\ & + \boldsymbol{\Phi}\big(\hat{\boldsymbol{x}}_{k-1|k-1}(t_{k-1})\big) \underbrace{\big(\boldsymbol{x}(t_{k-1}) - \hat{\boldsymbol{x}}_{k-1|k-1}(t_{k-1})\big)}_{\tilde{\boldsymbol{x}}_{k-1|k-1}(t_{k-1})} + \cdots + \boldsymbol{v}(t) \end{aligned} \tag{4.100}$$

where $\boldsymbol{\Phi}\big(\hat{\boldsymbol{x}}_{k-1|k-1}(t_{k-1})\big)$ is the Jacobian matrix

$$\boldsymbol{\Phi}\big(\hat{\boldsymbol{x}}_{k-1|k-1}((t_{k-1}))\big) = \frac{\partial \boldsymbol{f}\big(\boldsymbol{x}(t_{k-1})\big)}{\partial \boldsymbol{x}(t)}\Big|_{\boldsymbol{x}(t)=\hat{\boldsymbol{x}}_{k-1|k-1}(t_{k-1})}. \tag{4.101}$$

By substituting $\hat{\boldsymbol{x}}_{k|k-1}(t_k)$ from (4.98) into (4.100) and considering (4.99) we can find a linear form for $\tilde{\boldsymbol{x}}_{k|k-1}(t_k)$

$$\tilde{\boldsymbol{x}}_{k|k-1}(t_k) = \boldsymbol{\Phi}\big(\hat{\boldsymbol{x}}_{k-1|k-1}(t_{k-1})\big)\tilde{\boldsymbol{x}}_{k-1|k-1}(t_{k-1}) + \boldsymbol{v}(t_{k-1}). \tag{4.102}$$

The Taylor expansion in (4.101) is truncated which will naturally introduce higher order errors. In practice, the power of noise signal $\boldsymbol{v}(t)$ can be increased to account for this modeling error.

The equation for measurements in (4.96) can be similarly linearized around $\hat{\boldsymbol{x}}_{k|k-1}(t_k)$ which gives

$$\boldsymbol{z}(t_k) \simeq \boldsymbol{h}(\hat{\boldsymbol{x}}_{k|k-1}(t_k)) + \boldsymbol{\Upsilon}(\hat{\boldsymbol{x}}_{k|k-1}(t_k))\tilde{\boldsymbol{x}}_{k|k-1}(t_k) + \boldsymbol{w}(t_k) \tag{4.103}$$

with $\boldsymbol{\Upsilon}(\hat{\boldsymbol{x}}_{k|k-1}(t_k))$ being

$$\boldsymbol{\Upsilon}\big(\hat{\boldsymbol{x}}_{k|k-1}(t_k)\big) = \frac{\partial \boldsymbol{h}\big(x(t_k), t_k\big)}{\partial \boldsymbol{x}}\Big|_{\boldsymbol{x}(t_k)=\hat{\boldsymbol{x}}_{k|k-1}(t_k)} \tag{4.104}$$

Note that the Jacobian matrix for measurements model is built around the predicted state vector which is obtained from the nonlinear space state model of the process. Finally by substituting $\hat{\boldsymbol{z}}_{k|k-1}(t_k)$ from (4.98) into (4.103) and accepting the error of Taylor series truncation we get the following linear equation for the measurement innovation

$$\begin{aligned}\boldsymbol{\epsilon}(t_k) &= \boldsymbol{z}(t_k) - \boldsymbol{h}\big(\hat{\boldsymbol{x}}_{k|k-1}(t_k)\big) \\ &= \boldsymbol{\Upsilon}(\hat{\boldsymbol{x}}_{k|k-1}(t_k))\tilde{\boldsymbol{x}}_{k|k-1}(t_k) + \boldsymbol{w}(t_k).\end{aligned} \tag{4.105}$$

From (4.102) the correspondent error covariance matrix for state estimation

$$\begin{aligned}\mathbf{P}_{k|k-1}(t_k) = \boldsymbol{\Phi}\big(\hat{\boldsymbol{x}}_{k-1|k-1}(t_{k-1})\big)\mathbf{P}_{k-1|k-1}(t_{k-1})\boldsymbol{\Phi}^{\intercal}\big(\hat{\boldsymbol{x}}_{k-1|k-1}(t_{k-1})\big) \\ + \mathbf{Q}(t_{k-1})\end{aligned} \tag{4.106}$$

and from (4.103) the error covariance of measurement innovation becomes

$$\mathbf{S}(t_k) = \boldsymbol{\Upsilon}\big(\hat{\boldsymbol{x}}_{k|k-1}(t_k)\big)\mathbf{P}_{k|k-1}(t_k)\boldsymbol{\Upsilon}^{\intercal}\big(\hat{\boldsymbol{x}}_{k|k-1}(t_k)\big) + \mathbf{R}(t_k). \tag{4.107}$$

The rest of the equations follow the standard procedure for linear Kalman filter. Therefore

$$\hat{\boldsymbol{x}}_{k|k}(t_k) = \hat{\boldsymbol{x}}_{k|k-1}(t_k) + \mathbf{K}(t_k)\boldsymbol{\epsilon}(t_k) \tag{4.108}$$

$$\mathbf{P}_{k|k}(t_k) = \mathbf{P}_{k|k-1}(t_k) - \mathbf{K}(t_k)\boldsymbol{\Upsilon}\big(\hat{\boldsymbol{x}}_{k|k-1}(t_k)\big)\mathbf{P}_{k|k-1}(t_k) \tag{4.109}$$

$$\mathbf{K}(t_k) = \mathbf{P}_{k|k-1}(t_k)\boldsymbol{\Upsilon}^{\intercal}\big(\hat{\boldsymbol{x}}_{k|k-1}(t_k)\big)\mathbf{S}^{-1}(t_k). \tag{4.110}$$

These important results will be later used in developing the decision making algorithm for the energy manager.

Remark 4.8. Similar to linear Kalman filter, the information form for EKF can be formulated. The prediction equations are

$$\hat{\boldsymbol{y}}_{k|k}(t_k) = \mathbf{Y}_{k|k-1}(t_k)\boldsymbol{f}(\hat{\boldsymbol{x}}_{k-1|k-1}(t_{k-1})) \tag{4.111}$$

$$\mathbf{Y}_{k|k-1}(t_k) = \Big(\boldsymbol{\Phi}\big(\hat{\boldsymbol{x}}_{k-1|k-1}(t_{k-1})\big)\mathbf{Y}^{-1}_{k-1|k-1}(t_k)\boldsymbol{\Phi}^{\intercal}\big(\hat{\boldsymbol{x}}_{k-1|k-1}(t_{k-1})\big) + \mathbf{Q}(t_k)\Big)^{-1} \tag{4.112}$$

and the correction part is

$$\hat{\boldsymbol{y}}_{k|k}(t_k) = \hat{\boldsymbol{y}}_{k|k-1}(t_k) + \boldsymbol{i}(t_k) \tag{4.113}$$

$$\mathbf{Y}_{k|k}(t_k) = \mathbf{Y}_{k|k-1}(t_k) + \mathbf{I}(t_k). \tag{4.114}$$

Similar to the linear form, the information state vector and its covariance are defined as

$$\mathbf{I}(t_k) = \boldsymbol{\Upsilon}^{\intercal}\big(\hat{\boldsymbol{x}}_{k|k-1}(t_k)\big)\mathbf{R}^{-1}(t_k)\boldsymbol{\Upsilon}(t_k) \tag{4.115}$$

$$\boldsymbol{i}(t_k) = \boldsymbol{\Upsilon}^{\intercal}\big(\hat{\boldsymbol{x}}_{k|k-1}(t_k)\big)\mathbf{R}^{-1}(t_k)\Big(\boldsymbol{\epsilon}(t_k) + \boldsymbol{\Upsilon}\big(\hat{\boldsymbol{x}}_{k|k-1}(t_k)\big)\hat{\boldsymbol{x}}_{k|k-1}(t_k)\Big). \tag{4.116}$$

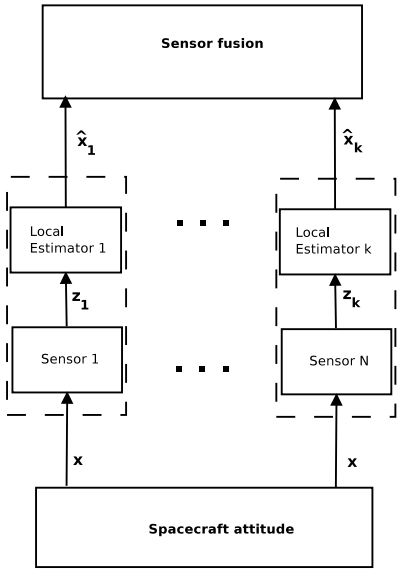

Figure 4.6: Decentralized architecture scheme with local estimators on the sensor nodes

4.3.2 Decentralized Data Fusion

A decentralized sensor fusion scheme is shown in figure 4.6 were N sensor nodes and a central data fusion are integrated. In this scheme $\hat{\boldsymbol{x}}$ is the global estimate of the system state, $\hat{\boldsymbol{x}}_i$ are the local estimates of the system state, $\boldsymbol{z}_i$ are the local measurement vectors, $\mathbf{P}_i$ are the covariances of $\hat{\boldsymbol{x}}_i$, $\mathbf{H}_i$ is the projection matrix of the system states into the measurements and $\boldsymbol{v}_i$ are the measurement noise vectors. Unlike the centralized data fusion, the measurements are not directly communicated to the central node. Instead, each node performs local processing on the data and communicates the results to the center. In this scheme, each sensor S_i is equipped with a local estimator LE_i which processes the measurements before communication. It can be proven that in order to reconstruct the global estimate $\hat{\boldsymbol{x}}$ at the central node it is sufficient to communicate specific statistical properties of the local estimates [Kamgarpour and Tomlin 2008]. The result can be summarized as follows:

Case I: The N local estimators and the global estimator share the same a priori information on vector $\boldsymbol{x}$, i.e. $\boldsymbol{x}$ is assumed to have Gaussian distribution with mean $\bar{\boldsymbol{x}}$ and variance $\mathbf{M}$ which is known to all nodes. Also the local noises are independent Gaussian with zero mean and covari-

ance $\mathbf{R}_i$. Under these conditions we have

$$\mathbf{P}^{-1}(t) = \sum_{i=1}^{N} \mathbf{P}_i^{-1}(t) - (N-1)\mathbf{M}^{-1}(t) \tag{4.117}$$

$$\mathbf{P}^{-1}(t)\hat{\boldsymbol{x}}(t) = \sum_{i=1}^{N} \mathbf{P}_i^{-1}(t)\hat{\boldsymbol{x}}_i(t) - (N-1)\mathbf{M}^{-1}(t)\bar{\boldsymbol{x}}(t) \tag{4.118}$$

which means that to reconstruct the global estimate and its covariance matrix it is sufficient to communicate the local state estimates and their local covariance matrices.

Case II: The N local estimators and the global estimator share the same a priori information similar to case I, but the local measurement noises are correlated. Under these conditions $\hat{\boldsymbol{x}}$ and its covariance matrix can not be calculated without extra knowledge about the measurements.

Case III: The N local estimators and the global estimator have different a priori knowledge about the system state $\boldsymbol{x}$. On the sensor node, $\boldsymbol{x}$ is Gaussian with mean $\bar{\boldsymbol{x}}_i$ and variance $\mathbf{M}_i$ but on the global estimator $\boldsymbol{x}$ has mean $\bar{\boldsymbol{x}}$ and variance $\mathbf{M}$. Also it is assumed that the measurement noises are independent. Under these assumptions we can again find a concrete solution for hierarchical estimation

$$\mathbf{P}^{-1}(t) = \sum_{i=1}^{N} (\mathbf{P}_i^{-1}(t) - \mathbf{M}_i^{-1}(t)) + \mathbf{M}^{-1}(t) \tag{4.119}$$

$$\mathbf{P}^{-1}(t)\hat{\boldsymbol{x}}(t) = \sum_{i=1}^{N} (\mathbf{P}_i^{-1}(t)\hat{\boldsymbol{x}}_i(t) - \mathbf{M}_i(t)^{-1}\bar{\boldsymbol{x}}_i(t)) + \mathbf{M}^{-1}(t)\bar{\boldsymbol{x}}(t). \tag{4.120}$$

Therefore in addition to local estimate and error covariance matrices, mean and variance of the local estimates should be transmitted to the higher level too.

This result is very essential in designing a decentralized energy manager. First of all, it enables a fully decentralized data fusion by designing local estimators on the sensor nodes. Also, it provides a solution to minimize the required calculation for fusion of the data from other nodes. Most importantly, it enables local decision making based on the statistical properties of the local estimations. In a decentralized model for spacecraft data fusion with N sensors and a central node such as the on board computer, a local dynamic model exists on each node. These dynamics together build the global system dynamic. The global dynamic is identical to the one for centralized data fusion presented in (4.76) which is

$$\begin{cases} \boldsymbol{x}(t_k) = \mathbf{F}(t_{k-1})\boldsymbol{x}(t_{k-1}) + \boldsymbol{v}(t_{k-1}) \\ \boldsymbol{z}(t_k) = \mathbf{H}(t_k)\boldsymbol{x}(t_k) + \boldsymbol{w}(t_k) \end{cases} \tag{4.121}$$

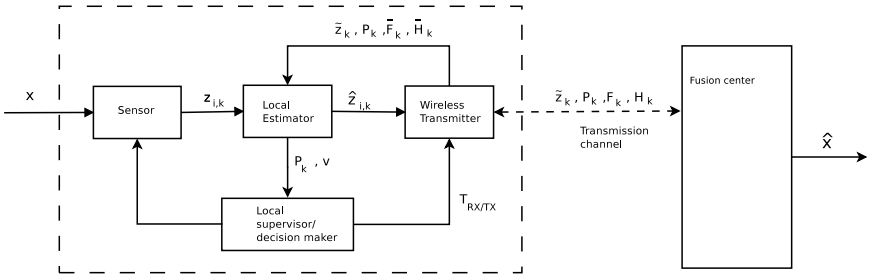

Figure 4.7: Details of a sensor node in a decentralized data fusion architecture where the sensor is equipped with a local decision maker

and a local model on node i, $i \in \{1,2,\ldots,M\}$, the local model is

$$\begin{cases} \boldsymbol{x}_i(t_k) = \mathbf{F}_i(t_{k-1})\boldsymbol{x}_i(t_{k-1}) + \boldsymbol{v}_i(t_{k-1}) \\ \boldsymbol{z}_i(t_k) = \mathbf{H}_i(t_k)\boldsymbol{x}_i(t_k) + \boldsymbol{w}_i(t_k). \end{cases} \tag{4.122}$$

When the sensor systems and their measurements are independent, the global measurement vector, sensor models, measurement noise vectors and their covariance matrices can be partitioned, therefore

$$\boldsymbol{z}(t_k) = \begin{pmatrix} \boldsymbol{z}_1^\intercal(t_k) & \boldsymbol{z}_2^\intercal(t_k) & \ldots & \boldsymbol{z}_M(t_k) \end{pmatrix}^\intercal \tag{4.123}$$

$$\boldsymbol{v}(t_k) = \begin{pmatrix} \boldsymbol{v}_1^\intercal(t_k) & \boldsymbol{v}_2^\intercal(t_k) & \ldots & \boldsymbol{v}_M^\intercal(t_k) \end{pmatrix}^\intercal \tag{4.124}$$

$$\mathbf{H}(t_k) = \begin{pmatrix} \mathbf{H}_1^\intercal(t_k); \mathbf{H}_2^\intercal(t_k) & \ldots & \mathbf{H}_M^\intercal(t_k) \end{pmatrix}^\intercal \tag{4.125}$$

$$\mathbf{R}(t_k) = \text{block diag}\begin{pmatrix} \mathbf{R}_1(t_k) & \mathbf{R}_2(t_k) & \ldots & \mathbf{R}_M(t_k) \end{pmatrix}. \tag{4.126}$$

The term *block diag* represents a matrix that the $\mathbf{R}_i$ matrices are on its diagonal elements and the rest of the elements are zero.

For spacecraft attitude determination, all sensors are observing spacecraft attitude. Therefore, theoretically the state vectors on the local nodes are identical, i.e. $\boldsymbol{x}_i(t_k) = \boldsymbol{x}(t_k)$, and follow identical state equation. At node i, the local observation history up to time t_k is

$$Z_i[t_k] = \{\boldsymbol{z}_i(t_1), z_i(t_2), \ldots, \boldsymbol{z}_i(t_k)\}. \tag{4.127}$$

According to the centralized Kalman filter formulation which was presented before, the best available local estimate of $\boldsymbol{x}(t_k)$ on node i given $Z_i(t_k)$ is

$$\hat{\boldsymbol{x}}_{i,k|k}(t_k) = \big(\mathbf{I}_{n\times n} - \mathbf{K}_i(t_k)\mathbf{H}_i(t_k)\big)\hat{\boldsymbol{x}}_{i,k|k-1}(t_k) + \mathbf{K}_i(t_k)\boldsymbol{z}_i(t_k) \tag{4.128}$$

and the Kalman gain can be found by

$$\mathbf{K}_i(t_k) = \mathbf{P}_{i,k|k-1}(t_k)\mathbf{H}_i^\intercal(t_k)\Big(\underbrace{\mathbf{H}_i(t_k)\mathbf{P}_{i,k|k-1}(t_k)\mathbf{H}_i^\intercal(t_k) + \mathbf{R}_i(t_k)}_{\mathbf{S}_i(t_k)}\Big)^{-1} \tag{4.129}$$

and for covariance

$$\mathbf{P}^{-1}_{i,k|k}(t_k) = \mathbf{P}^{-1}_{i,k|k-1}(t_k) + \mathbf{H}^{\intercal}_i(t_k)\mathbf{R}^{-1}_i(t_k)\mathbf{H}_i(t_k). \tag{4.130}$$

The goal is to calculate the global estimate $\hat{\boldsymbol{x}}(t_k)$ from the local estimates, which can be found as [Hashemipour et al. 1988]

$$\begin{aligned}\hat{\boldsymbol{x}}_{k|k}(t_k) = \mathbf{P}_{k|k}(t_k)\Big(&\mathbf{P}^{-1}_{k|k-1}(t_k)\hat{\boldsymbol{x}}_{k|k-1}(t_k) \\ &+ \sum_{i=1}^{M} \mathbf{P}_{i,k|k}(t_k)^{-1}\hat{\boldsymbol{x}}_{i,k|k}(t_k) - \mathbf{P}^{-1}_{i,k|k-1}(t_k)\hat{\boldsymbol{x}}_{i,k|k-1}(t_k)\Big)\end{aligned} \tag{4.131}$$

with the following covariance matrix

$$\mathbf{P}^{-1}_{k|k}(t_k) = \mathbf{P}^{-1}_{k|k-1}(t_k) + \sum_{i=1}^{M}\Big(\mathbf{P}^{-1}_{i,k|k}(t_k) - \mathbf{P}^{-1}_{i,k|k-1}(t_k)\Big). \tag{4.132}$$

This means that the data fusion needs to receive only the local a priori and a posteriori estimates $\hat{\boldsymbol{x}}_{i,k|k-1}(t_k)$ and $\hat{\boldsymbol{x}}_{i,k|k}(t_k)$, and their covariance matrices $\mathbf{P}_{i,k|k-1}(t_k)$ and $\mathbf{P}_{i,k|k}(t_k)$ to reconstruct the state vector and its covariance in the fusion center.

For OWSAN the communication between nodes can be two-way. Therefore each node can receive partial information about attitude from the other nodes. This is unlike the centralized configuration where sensor nodes only transmit local measurements to the onboard computer.

Considering the scheme presented in Figure 4.8, each node generates its own observation vector and also computes its local prediction of the process model. Therefore the information from observation $\boldsymbol{z}_i(t_k)$ and its associated information matrix for node i are known. According to (4.90) on node i we have

$$\boldsymbol{i}_i(t_k) = \mathbf{H}^{\intercal}_i(t_k)\mathbf{R}^{-1}_i(t_k)\boldsymbol{z}_i(t_k) \tag{4.133}$$

$$\mathbf{I}_i(t_k) = \mathbf{H}^{\intercal}_i(t_k)\mathbf{R}^{-1}_i(t_k)\mathbf{H}_i(t_k). \tag{4.134}$$

Also the prediction equations for node i will be similar to the linear information filter and can be expressed as

$$\hat{\boldsymbol{y}}_{i,k|k-1}(t_k) = \mathbf{L}_{i,k|k-1}(t_k)\hat{\boldsymbol{y}}_{i,k|k-1}(t_{k-1}) \tag{4.135}$$

$$\mathbf{Y}_{i,k|k-1}(t_k) = \Big(\mathbf{F}(t_{k-1})\mathbf{Y}^{-1}_{i,k-1|k-1}(t_k)\mathbf{F}^{\intercal}(t_{k-1}) + \mathbf{Q}(t_k)\Big)^{-1} \tag{4.136}$$

with $\mathbf{L}_{i,k|k-1}$ being the local propagation coefficient defined as

$$\mathbf{L}_{i,k|k-1}(t_k) = \mathbf{Y}_{i,k|k-1}(t_k)\mathbf{F}(t_{k-1})\mathbf{Y}^{-1}_{i,k|k-1}(t_{k-1}) \tag{4.137}$$

which is independent from all local and global observations. At this point, the *local partial correction* of the information state vector on node i can be immediately found by using the third step of Algorithm 2. It is called local partial

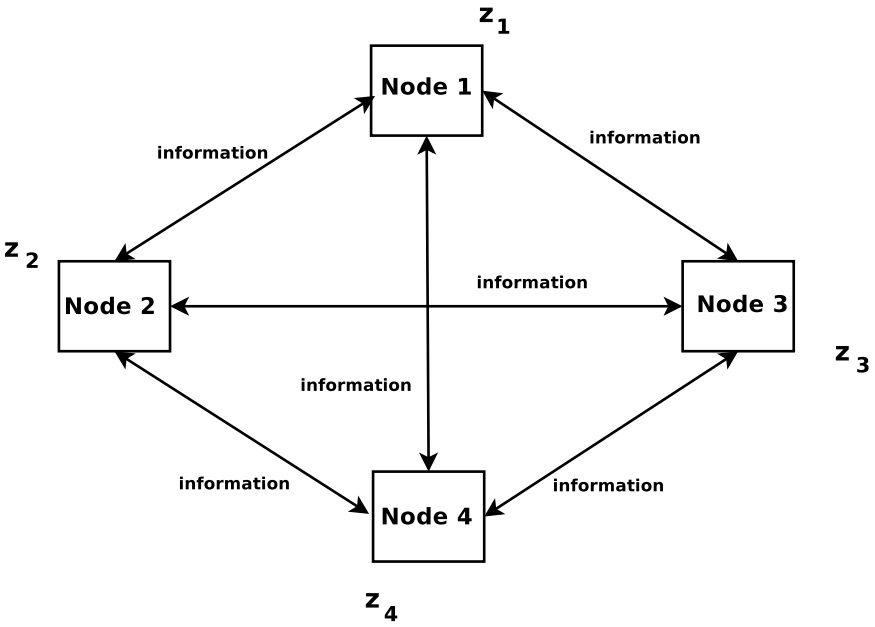

Figure 4.8: Decentralized scheme for OWSAN with two way communication channels

correction because it can be further improved by providing the information communicated from all other nodes. The local partial correction for node i is

$$\check{\boldsymbol{y}}_{i,k|k} = \hat{\boldsymbol{y}}_{i,k|k-1}(t_k) + \boldsymbol{i}_i(t_k) \tag{4.138}$$

$$\check{\mathbf{Y}}_{i,k|k} = \mathbf{Y}_{i,k|k-1}(t_k) + \mathbf{I}_i(t_k). \tag{4.139}$$

After sharing all local partial corrections between nodes, the final local correction on node i becomes

$$\hat{\boldsymbol{y}}_{i,k|k}(t_k) = \hat{\boldsymbol{y}}_{i,k|k-1}(t_k) + \sum_{j=1}^{M} \left(\check{\boldsymbol{y}}_{j,k|k}(t_k) - \hat{\boldsymbol{y}}_{i,k|k-1}(t_k) \right) \tag{4.140}$$

$$\mathbf{Y}_{i,k|k}(t_k) = \mathbf{Y}_{i,k|k-1}(t_k) + \sum_{j=1}^{M} \left(\check{\mathbf{Y}}_{j,k|k}(t_k) - \mathbf{Y}_{i,k|k-1}(t_k) \right). \tag{4.141}$$

Remark 4.9. With identical initial information for all nodes and full communication between the nodes at each time instance, all $\hat{\boldsymbol{y}}_{i,k|k}(t_k)$ and $\mathbf{Y}_{i,k|k}$ become

identical which further simplifies the previous equations to the following

$$\hat{\boldsymbol{y}}_{i,k|k}(t_k) = \hat{\boldsymbol{y}}_{i,k|k-1}(t_k) + \sum_{j=1}^{M} \boldsymbol{i}_j(t_k) \tag{4.142}$$

$$\mathbf{Y}_{i,k|k}(t_k) = \mathbf{Y}_{i,k|k-1}(t_k) + \sum_{j=1}^{M} \mathbf{I}_j(t_k). \tag{4.143}$$

It is obvious that under these conditions the results of decentralized data fusion through information filter will be equal to a centralized information filter.

Remark 4.10. The same methodology can be used to derive the results when the process model is not linear. In this case the local predictions can be calculated by

$$\hat{\boldsymbol{y}}_{i,k|k-1}(t_k) = \mathbf{Y}_{i,k|k-1}(t_k)\boldsymbol{f}(\hat{\boldsymbol{x}}_{i,k-1|k-1}(t_{k-1})) \tag{4.144}$$

$$\mathbf{Y}_{i,k|k-1}(t_k) = \Big(\boldsymbol{\Phi}\big(\hat{\boldsymbol{x}}_{i,k-1|k-1}(t_{k-1})\big)\mathbf{Y}^{-1}_{i,k-1|k-1}(t_k)\boldsymbol{\Phi}^{\intercal}(\hat{\boldsymbol{x}}_{i,k-1|k-1}(t_{k-1})) + \mathbf{Q}(t_k)\Big)^{-1} \tag{4.145}$$

with the same Jacobian matrix which was introduced for EKF.

The local partial correction equations are similar to (4.140) and (4.141), respectively. Also the final correction equations can be calculated by (4.138) and (4.139). (4.111), the local partial corrections will be given by (4.113). However, the local information parameters will change into

$$\mathbf{I}_i(t_k) = \boldsymbol{\Upsilon}_i^{\intercal}\big(\hat{\boldsymbol{x}}_{i,k|k-1}(t_k)\big)\mathbf{R}^{-1}(t_k)\boldsymbol{\Upsilon}_i(t_k) \tag{4.146}$$

$$\boldsymbol{i}_i(t_k) = \boldsymbol{\Upsilon}_i^{\intercal}\big(\hat{\boldsymbol{x}}_{i,k|k-1}(t_k)\big)\mathbf{R}^{-1}(t_k)\Big(\boldsymbol{\epsilon}_i(t_k) + \boldsymbol{\Upsilon}_i\big(\hat{\boldsymbol{x}}_{i,k|k-1}(t_k)\big)\hat{\boldsymbol{x}}_{i,k|k-1}(t_k)\Big) \tag{4.147}$$

where

$$\boldsymbol{\epsilon}_i(t_k) = \boldsymbol{z}_i(t_k) - \boldsymbol{h}_i\big(\hat{\boldsymbol{x}}_{i,k|k-1}(t_k)\big). \tag{4.148}$$

4.4 Missing Measurements

When the Kalman filter is receiving the measurements at full rate, the optimal estimation of the process can be obtained. However when the sensors are scheduled to send measurement (centralized or decentralized) then the optimality and even convergence of the estimator is questionable. We assume a system similar to (4.76) which has linear process and observation models

$$\begin{cases} \boldsymbol{x}(t_k) = \mathbf{F}(t_{k-1})\boldsymbol{x}(t_{k-1}) + \boldsymbol{v}(t_{k-1}) \\ \boldsymbol{z}(t_k) = \mathbf{H}(t_k)\boldsymbol{x}(t_k) + \boldsymbol{w}(t_k) \end{cases}. \tag{4.149}$$

When a sensor scheduling is active, to characterize the availability of measurement vector $\boldsymbol{z}_i(t_k)$ at time t_k, we use a binary decision variable as $\gamma_{i,k}$ such that

$$\gamma_{i,k} = \begin{cases} 1 & , \quad \boldsymbol{z}_i(t_k) \text{ is available;} \\ 0 & , \quad \boldsymbol{z}_i(t_k) \text{ is missing.} \end{cases} \tag{4.150}$$

At time t_k, we assume that $\mathbf{P}_{k|k-1}(t_k)$ from the Kalman filter prediction phase is available (see Algorithm 1). If $\gamma_{i,k} = 1$, then measurement vector is available and Kalman filter can proceed with the correction phase following Joseph's form of covariance matrix from (4.86). However if $\gamma_{i,k} = 0$ then covariance matrix can be extrapolated without being corrected by a measurement vector. For the nominal operation when $\gamma_{i,k} = 1$, we can expand (4.86) to get

$$\mathbf{P}_{k|k} = \mathbf{F}\mathbf{P}\mathbf{F}^{\mathsf{T}} + \mathbf{Q} - \mathbf{F}\mathbf{P}_{k|k-1}\mathbf{H}^{\mathsf{T}}(\mathbf{H}\mathbf{P}_{k|k-1}\mathbf{H}^{\mathsf{T}} + \mathbf{R})^{-1}\mathbf{H}\mathbf{P}_{k|k-1}\mathbf{F}^{\mathsf{T}}. \tag{4.151}$$

Since all matrices and vectors are defined for time t_k, this notation is dropped here to improve readability. Alternatively, we have the following expression for when a measurement is missing

$$\mathbf{P}_{k|k} = \mathbf{F}\mathbf{P}_{k|k-1}\mathbf{F}^{\mathsf{T}} + \mathbf{Q}.$$

We can combine these two equations and derive the following compact form

$$\mathbf{P}_{k|k} = \mathbf{F}\mathbf{P}_{k|k-1}\mathbf{F}^{\mathsf{T}} + \mathbf{Q} - \gamma_{i,k}\mathbf{F}\mathbf{P}_{k|k-1}\mathbf{H}^{\mathsf{T}}(\mathbf{H}\mathbf{P}_{k|k-1}\mathbf{H}^{\mathsf{T}} + \mathbf{R})^{-1}\mathbf{H}\mathbf{P}_{k|k-1}\mathbf{F}^{\mathsf{T}} \tag{4.152}$$

which will result in the following form for state estimate based on the availability of the measurement vector

$$\hat{\boldsymbol{x}}_{k|k}(t_k) = \hat{\boldsymbol{x}}_{k|k-1} + \gamma_{i,k}\mathbf{K}(t_k)\big(\boldsymbol{z}(t_k) - \mathbf{H}(t_k)\hat{\boldsymbol{x}}_{k|k-1}(t_k)\big) \tag{4.153}$$

which means that when the measurements are missing, the state estimate will be solely dependent on the prediction phase based on the state space model of the system. It should be noted that this is a stochastic iteration due to the random loss of observations vector while the classical Kalman filter enjoys deterministic iterations. In practice this is equivalent to receiving a measurement with very high uncertainty which can not be trusted at all, therefore the filter can safely ignore it. Also this implies that the Kalman filter does not know when the next measurement will arrive. Thus $\hat{\boldsymbol{x}}_{k|k}(t_k)$ and $\mathbf{P}_{k|k}(t_k)$ become random variables as a function of $\gamma_{i,k}$ which is also a random variable.

Stability of the Filter

Clearly if the observations do not arrive for a sufficient amount of time, the Kalman filter will start diverging from the optimal solution. The case of missing measurement is equivalent to measurement loss due to communication

problem between sensors and the processor. Similar problem is studied by Faridani [Faridani 1986] and Sinopoli *et al.* [Sinopoli et al. 2003], where the observation vector is lost completely. This idea can be extended when observations arrive with varying rates from various sensors. Without loss of generality we can assume that two sensors are involved. Thus, the observation vector $\boldsymbol{z}(t_k)$ can be partitioned into two parts $\boldsymbol{z}_1(t_k)$ and $\boldsymbol{z}_2(t_k)$. Therefore, the system introduced in (4.76) can be reorganized as the following

$$\boldsymbol{x}(t_k) = \mathbf{F}(t_{k-1})\boldsymbol{x}(t_{k-1}) + \boldsymbol{v}(t_{k-1}) \tag{4.154}$$

$$\begin{pmatrix} \boldsymbol{z}_1(t_k) \\ \boldsymbol{z}(_2\, t_k) \end{pmatrix} = \begin{pmatrix} \mathbf{H}_1(t_k) \\ \mathbf{H}_1(t_k) \end{pmatrix} \boldsymbol{x}(t_k) + \begin{pmatrix} \boldsymbol{w}_1(t_k) \\ \boldsymbol{w}_2(t_k) \end{pmatrix} \tag{4.155}$$

with covariance matrix of the measurements vector represented as

$$\mathbf{R} = \begin{pmatrix} \mathbf{R}_{11} & \mathbf{R}_{12} \\ \mathbf{R}_{21} & \mathbf{R}_{22} \end{pmatrix}. \tag{4.156}$$

If the system $(\mathbf{F}, \mathbf{H})$ is observable then the Kalman filter converges when no measurement is missing. We $\boldsymbol{z}_1(t_k)$ and $\boldsymbol{z}_2(t_k)$ are arriving with varying independent probabilities, $\Lambda_1(t_k)$ and $\Lambda_2(t_k)$. It can be shown that under certain conditions while the pair $(\Lambda_1(t_k), \Lambda_2(t_k))$ falls in a bounded region, the iteration $\mathbf{P}_{k|k} = g_{\Lambda_1,\Lambda_2}(\mathbf{P}_{k|k-1})$ converges to a unique steady state value. Likewise, if $(\Lambda_1(t_k), \Lambda_2(t_k))$ pair falls out of this region, the covariance matrix goes unstable and eventually will explode to infinity [Liu and Goldsmith 2004]. This region can be defind by an upper bound and a lower bound. The result of Liu and Goldsmith can be summarized as following Theorems.

Theorem 4.1. We assume $(\mathbf{P}, \mathbf{Q})$ is controllable and $(\mathbf{F}, \mathbf{H})$ is observable. For a fixed Λ_1, if $\mathrm{E}\{\mathbf{P}_{k|k}|\mathbf{P}_{k|k-1}\} = g_{\Lambda_1,\Lambda_2}(\mathbf{P}_{k|k-1})$ is unstable for $\Lambda_2 = 0$ while stable for $\Lambda_2 = 1$ then $\exists \Lambda_{2c}$ with $0 \le \Lambda_{2c} \le 1$ such that

$$\lim_{k\to\infty} \mathrm{E}\{\mathbf{P}_k\} = +\infty \quad , \quad \forall \Lambda_2 : 0 \le \Lambda_2 \le \Lambda_{2c} \tag{4.157}$$

and there exists a positive semidefinite matrix $\bar{\mathbf{P}}_{\mathbf{P}_0} > 0$ as a function of the initial condition $\mathbf{P}_0 \ge 0$ such that

$$\mathrm{E}\{\mathbf{P}_k\} \le \bar{\mathbf{P}}_{\mathbf{P}_0} \quad \forall k \qquad \Lambda_{2c} \le \Lambda_2 \le 1 \tag{4.158}$$

Theorem 4.2. For a given Λ_1, an upper bound and a lower bound for Λ_2 can be found, such that $\underline{\Lambda}_{2c} < \Lambda_{2c} < \bar{\Lambda}_{2c}$, and

$$\begin{aligned} \underline{\Lambda}_{2c} &= \arg\inf_{\Lambda_2} \{\exists \hat{\mathbf{X}} > 0 | \hat{\mathbf{X}} = (1-\Lambda_1)(1-\Lambda_2)\mathbf{F}\mathbf{X}\mathbf{F}^{\mathsf{T}} + \mathbf{Q}\} \\ &= \max\{1 - \frac{1}{\alpha^2(1-\Lambda_1)}, 0\} \end{aligned} \tag{4.159}$$

where α is the maximum eigenvalue of $\mathbf{F}$, and similarly

$$\bar{\Lambda}_{2c} = \arg\inf_{\Lambda_2} \{\exists \hat{\mathbf{X}} | \hat{\mathbf{X}} > g_{\Lambda_1,\Lambda_2}(\hat{\mathbf{X}})\} \tag{4.160}$$

Theorem 4.3. If $(\mathbf{P}, \mathbf{Q})$ is controllable and $(\mathbf{F}, \mathbf{H})$ is observable, and $\mathbf{F}$ is unstable, for a fixed Λ_1, if $\Lambda_2 > \bar{\Lambda}_{2c}$, then there is positive semidefinite matrices $\mathbf{P}_L \geq 0$ and $\mathbf{P}_U \geq > 0$ such that

$$0 \leq \mathbf{P}_L \leq \lim_{k \to \infty} \mathrm{E}\{\mathbf{P}_k\} \leq \mathbf{P}_U \quad , \quad \forall \mathrm{E}\{\mathbf{P}_0\} \geq 0. \tag{4.161}$$

$\mathbf{P}_L$ and $\mathbf{P}_U$ can be computed by solving following equations

$$\mathbf{P}_L = (1-\Lambda_1)(1-\Lambda_2)\mathbf{F}\mathbf{X}\mathbf{F}^{\mathsf{T}} + \mathbf{Q} \tag{4.162}$$

$$\mathbf{P}_U = g_{\Lambda_1,\Lambda_2}(\mathbf{P}_U). \tag{4.163}$$

Therefore, the transmission rate of sensors can be lowered by the decision maker without endangering the stability of the Kalman filter as long as it is bigger than the lower bound defined by (4.159) in Theorem 4.2.

4.5 Decision Making

Decision making through hypothesis testing is a standard method for many applications such as fault detection. A sudden change in one or more parameters of the system can be detected and used to understand the failures. We can adopt this methodology to our application and integrate it with the centralized or decentralized data fusion which was presented in the previous chapters. Here decision is about incorporating a new measurement from the local node or other nodes in the data fusion or not. The Kalman filter residuals are random vectors with normal distribution with known and pre-computable steady state covariances but the mean values are different. The parameters of their distribution changes if the Kalman filter deviates from the steady state and fail the optimality due to lack of measurements. To understand this change in the distribution model of residuals we need to test different hypotheses. If we stop feeding the filter with real measurements, the operation of the filter will start deviating from the nominal mode and the state prediction error will increase. The Kalman filter algorithm uses process model and sensor models to calculate an expected value and covariance of the sensor measurements. The difference between this prediction and the actual sensor value can provide a measure for the correctness of the Kalman filter estimations.

A test is performed on a hypothesis to examine its correctness. Most hypothesis tests result in a crisp logic, comprising either *zero* (H_0) or *one* (H_1). An answer "zero" means that the hypothesis is true and "one" means that the hypothesis is not valid anymore. Other philosophies for hypothesis testing are also available which incorporate a third aspect such as "'unknown" but they are not considered in our application. In testing the hypotheses, two types of erroneous decisions may be made.

1. Type I: declaring H_1 as true when H_0 is in fact the true hypothesis;
2. Type II: declaring H_0 as true when H_1 is the true statement.

For our application, hypothesis H_0 can be "the filter operation is satisfactory" and hypothesis H_1 is "the filter operation is not satisfactory". The result of Type I test error is a false alarm (FA) resulting in requesting for new sensor measurements. The result of Type II error will be a missed alarm (MA) which causes an increase in the error of the Kalman estimation. To lower the energy consumption it is desired to make the probability of occurrence of Type I error as low as possible.

We have

$$P_{FA} = P(H_1|H_0) = \int_{\aleph_1} p(\zeta|H_0)\,\mathrm{d}\zeta \tag{4.164}$$

$$P_{MA} = P(H_0|H_1) = \int_{\aleph_0} p(\zeta|H_1)\,\mathrm{d}\zeta \tag{4.165}$$

where ζ is representing a test statistics and $p(\zeta|H_0)$ is its conditional probability density. The set $\aleph_0$ is a region containing ζ while hypothesis H_1 holds true. Similarly, set $\aleph_1$ is a region containing ζ while hypothesis H_0 holds true. Sets $\aleph_0$ and $\aleph_1$ partition the observation space together.

Also it can be seen that

$$P_D = P(H_1|H_1) = \int_{\aleph_1} p(\zeta|H_1)\,\mathrm{d}\zeta = 1 - P_{FA}. \tag{4.166}$$

A good decision making algorithm should be able to minimize a wrong decision in both cases which is

$$P_E = P_0 P_{FA} + P_1 P_{MA} \tag{4.167}$$

where P_E is the probability of making an erroneous decision, P_0 is the probability that hypotheses H_0 occurs and P_1 is the probability of H_1 occurrence. From an energy efficiency point of view, P_{FA} is more expensive for the system, therefore a good decision making system should provide a solution to lower the probability of requesting unnecessary measurements. The concept of *confidence interval* is often used which is the probability that a test statistics falls in a known region, and is usually indicated with a certain percentage. For the associated range of a given confidence interval a threshold τ can be defined such that

$$P_{FA}(\tau) = \eta \tag{4.168}$$

here η is expressed as a percentage and denotes the significance level. Then the confidence level becomes $1-\eta$. Therefore a smaller significance level results in a bigger threshold for the hypothesis tests in (4.164).

In OWSAN data fusion, the occurrence probability of either hypotheses are not known beforehand. In such a case we can use the Neyman-Pearson decision making method. The goal is to maximize P_D for an arbitrary probability of P_{FA}. To obtain a trade-off between P_{FA} and P_{MA} we minimize the following cost function

$$F = P_{MA} + \tau(P_{FA} - \eta) = \tau(1-\eta) + \int_{\aleph_0} \big(p(\zeta|H_1) - \tau(\zeta|H_0)\big)\,\mathrm{d}\zeta \tag{4.169}$$

with $\tau \geq 0$ being the Lagrange multiplier [Bertsimas and Tsitsiklis 1997].

The result of minimization and applying the likelihood ratio test leads to the Neyman-Pearson hypotheses test as follows

$$V(\zeta) = \frac{p(\zeta|H_1)}{p(\zeta|H_0)} \underset{H_0}{\overset{H_1}{\gtrless}} \tau\,. \tag{4.170}$$

The threshold is the Lagrange multiplier τ which is chosen such that satisfies the significance level η

$$P_{FA} = \int_{\aleph_1} p(\zeta|H_0)\,\mathrm{d}\zeta = \int_{\tau}^{\infty} p(\zeta|H_0)\,\mathrm{d}\zeta = \eta. \tag{4.171}$$

We can apply this decision making rule to the measurement innovations or state estimate errors to decide about the necessity of a new measurement vector from the a sensor node. To enable this, we need to identify the probability density function $p(\zeta)$ for hypotheses H_0 and H_1. This will enable decision making in the local level and global level for both centralized and decentralized architecture.

For example, let us consider a sequence of one-dimensional n residuals of local Kalman filter on one of OWSAN nodes. This sequence has Gaussian distribution with unknown mean μ but known variance σ^2. The mean, μ, can be either μ_0 (hypothesis H_0) or μ_1 (hypothesis H_1), and $\mu_1 > \mu_0$. The likelihood of the observation is

$$\begin{aligned} p(\zeta|\mu) &= \prod_i \frac{1}{\sqrt{2\pi}\sigma} \exp\left(-\frac{(\zeta_i-\mu)^2}{2\sigma^2}\right) \\ &= \frac{1}{(\sqrt{2\pi})^n \sigma^n} \exp\left(-\frac{\sum_i(\zeta_i-\mu)^2}{2\sigma^2}\right) \\ &= \frac{1}{(\sqrt{2\pi})^n \sigma^n} \exp\left(-\frac{n\mu^2}{2\sigma^2}\right) \exp\left(-\frac{n\mu\bar{\zeta}}{2\sigma^2}\right) \exp\left(-\frac{\sum_i \zeta_i}{2\sigma^2}\right). \end{aligned} \tag{4.172}$$

The ratio of likelihood from Neyman Pearson test is

$$V(\zeta) = \frac{p(\zeta|\mu_1)}{p(\zeta|\mu_0)} = K \exp(\frac{n(\mu_1-\mu_0)\bar{\zeta}}{\sigma^2}). \tag{4.173}$$

Here $\bar{\zeta}$ is the mean of ζ.

According to the Neyman Pearson, H_0 should be rejected if the following condition holds

$$\exp(\frac{n(\mu_1-\mu_0)\bar{\zeta}}{\sigma^2}) > \tau. \tag{4.174}$$

This hypothesis testing approach can be used to design OWSAN energy manager as explained later on.

4.6 OWSAN Energy Manager

In the following, we design the power manager based on estimating ADCS sensor measurements vector. Extensive research has been done on developing efficient and reliable prediction-based energy management techniques for the WSN applications [Jain and Chang 2004, Tang and Cao 2008]. In most of them, the trajectory of the sensor measurements are estimated by exploiting the correlation between the measurements. In most of these works, sensor is locally tuning its sampling rate without a knowledge of the entire system and its dynamics.

4.6.1 Problem Statement

An OWSAN sensor node may be equipped with a sensing head, a local energy harvester, a rechargeable battery, a wireless transmitter such as a ZigBee module and a microprocessor. Therefore, the available local energy should be shared between the wireless transmitter, local microprocessor and the sensing head. A solution to reduce the energy consumption is to put the wireless transmitter on the node to sleep mode. Here, we define three operation modes for an OWSAN node (see Figure 4.9):

- Mode 1: The sensor node is running and the transmitter is communicating the sensor information;
- Mode 2: The sensor and the transmitter are asleep;
- Mode 3: The sensor and the transmitter are both switched off because there is no more energy available in the node.

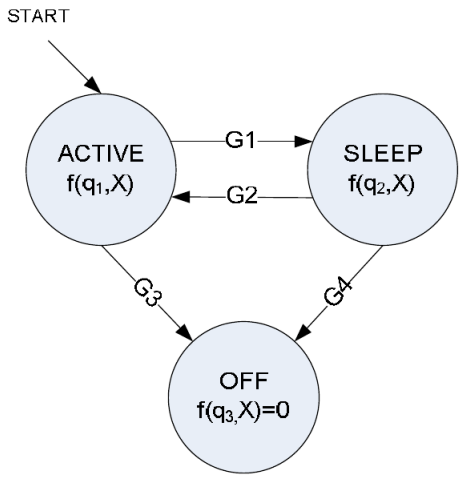

Figure 4.9: State transition diagram of a sensor node

It should be noted that Mode 2 may have two variations based on the type of the sensor: the sensor is switched off and transmitter is asleep, or sensor and transmitter are both asleep. This may depend on the electronic design of the sensor or its boot up time. We consider these variations together as Mode 2, without loss of generality. Mode 3 is not interesting in the power manager design because it is a dead-end. Depending on the necessity and frequency of receiving each measurement, a sensor may visit Mode 1 and 2 frequently. At higher sampling rates, the sensor spend more time in the active mode. The energy consumption of the node will be different in each of these operation modes. The problem here is to decide about the frequency of switching between Mode 1 and Mode 2 for each node and maintain the required attitude determination precision. A smart energy manager algorithm for ADCS is envisioned as an adequate solution for this problem. In this section we design two different architectures for such an energy manager.

4.6.2 Centralized Energy Manager Algorithm

The first architecture is based on centralized data fusion and follows the estimation design approach presented in section 4.3.1 using an extended Kalman filter. OWSAN can be made of several sensor nodes and OBC. In a centralized data fusion architecture, all sensor nodes communicate the measurement information directly to OBC for further processing. The nodes are not equipped with extra computation power to carry local estimators or information about the dynamics of the system. Figure 4.10 shows a simple overview of a centralized scheme. There is no inter-communication between the sensors because there is no reason for it. The energy manager is placed in the OBC where the

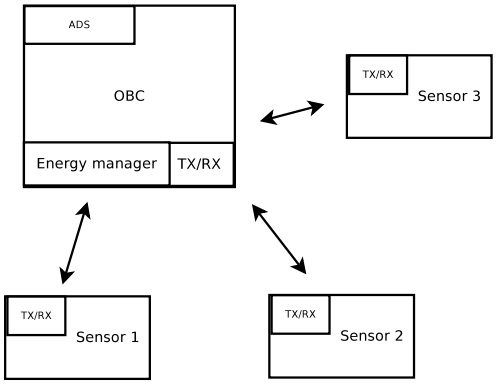

Figure 4.10: A simplified system view of OWSAN with centralized energy management

attitude determination system resides. Thus only one estimator is running in OWSAN which provides the global estimates by using information from the sensor measurements and the dynamics of spacecraft attitude. The energy manager runs as an overhead on the attitude determination algorithm of ADCS so its implementation will be very resource friendly.

In the nominal mode, at time t_k each sensor makes measurements at $f_{i,1}$ samples and provides its observation vector z_i to the onboard computer. The onboard computer processes the information at the same frequency as the samples. When a sample arrives, the extended Kalman filter stars its operation as it was presented previously. It projects the system state and its covariance ahead and computes $\hat{\boldsymbol{x}}_{k|k-1}(t_k)$ and $\mathbf{P}_{k|k-1}(t_k)$. It also calculates its estimate of the observation vector which contains the observation of individual $\hat{\boldsymbol{z}}_{k|k-1}(t_k)$. When the measurement vector $\boldsymbol{z}_i(t_k)$ arrives, the innovation vector $\boldsymbol{\epsilon}_i(t_k)$ and its covariance matrix $\mathbf{S}_i(t_k)$ can be calculated. At this point, the energy manager runs a decision making test on $\boldsymbol{\epsilon}_i(t_k)$ and $\mathbf{S}_i(t_k)$. The results of this test shows the correctness level of $\hat{\boldsymbol{z}}_{k|k-1}(t_k)$ relative to $\boldsymbol{z}_k(t_k)$.

Algorithm 3 Centralized energy manager algorithm

1. Initialization:
   $\hat{\boldsymbol{x}}(t_0)=\boldsymbol{x}_0$, $\mathbf{P}(t_0)=\mathbf{P}_0$, $\gamma_{k,i}=1$ $f_i=f_{i,1}$, $\check{\boldsymbol{z}}(t_0)=\boldsymbol{z}_0$, $\mathbf{R}_i(t_0)=\mathbf{R}_{i,0}$;
   $H_0=$ADS estimation is accurate enough;
   $H_1=$ADS estimation is not accurate enough.
2. Prediction:
   2.1. Project the system state ahead:
   $$\hat{\boldsymbol{x}}_{k|k-1}(t_k)=\mathbf{F}(t_{k-1})\hat{\boldsymbol{x}}_{k|k}(t_{k-1}).$$
   2.2. Project the error covariance ahead:
   $$\mathbf{P}_{k|k-1}(t_k)=\mathbf{F}(t_{k-1})\mathbf{P}_{k-1|k-1}(t_{k-1})\mathbf{F}(t_{k-1})^{\intercal}+\mathbf{Q}(t_{k-1}).$$
   2.3. Project the sensor measurements ahead:
   $$\hat{\boldsymbol{z}}_{i,k|k-1}(t_k)=\mathbf{H}_i(t_k)\hat{\boldsymbol{x}}_{k|k-1}(t_k).$$
3. Decision making and correction:
   3.1. If sensor observation vector $\boldsymbol{z}_{i,k}(t_k)$ is available set $\gamma_{i,k}=1$ and:
      3.3.1. Compute the innovation vector and its covariance:
      $$\boldsymbol{\epsilon}_i(t_k)=\boldsymbol{z}_i(t_k)-\hat{\boldsymbol{z}}_{k|k-1}(t_k);$$
      $$\mathbf{S}_i(t_k)=\mathbf{H}_i(t_k)\mathbf{P}_{k|k-1}(t_k)\mathbf{H}_i^{\intercal}(t_k)+\mathbf{R}_i(t_k).$$
      3.3.2. Run decision maker test and accept H_0 or H_1:
      $$V_{i,k}(\zeta)=\frac{p(\zeta_i|H_1)}{p(\zeta_i|H_0)} \underset{H_0}{\overset{H_1}{\gtrless}} \tau.$$
      3.3.3. Determine the sampling rate for the sensor:
      $$f_i=\begin{cases} f_{i,1} & , \text{ if } H_0 \text{ is true;} \\ f_{i,2} & , \text{ if } H_1 \text{ is true.} \end{cases}$$
      3.3.4. Define arrived measurement vector and its covariance as the true values:
      $$\check{\boldsymbol{z}}_i(t_k)=\boldsymbol{z}_i(t_k);$$
      $$\mathbf{R}_i(t_k)=\mathbf{R}_{i,0}.$$
   3.2. If sensor observation vector $\boldsymbol{z}_{i,k}(t_k)$ is NOT available, set $\gamma_{i,k}=0$, and:
   $$\check{\boldsymbol{z}}_i(t_k)=\hat{\boldsymbol{z}}_{i,k|k-1}(t_k);$$
   $$\mathbf{R}_i(t_k)=\mathbf{R}_{\infty}.$$
   3.3. Compute the Kalman filter gain:
   $$\mathbf{K}(t_k)=\mathbf{P}_{k|k-1}(t_k)\mathbf{H}^{\intercal}(t_k)\mathbf{S}_i^{-1}(t_k)$$
   3.4. Update the state estimate vector:
   $$\hat{\boldsymbol{x}}_{k|k}(t_k)=\hat{\boldsymbol{x}}_{k|k-1}(t_k)+\gamma_{i,k}\mathbf{K}(t_k)\Big(\boldsymbol{z}(t_k)-\mathbf{H}(t_k)\hat{\boldsymbol{x}}_{k|k-1}(t_k)\Big).$$
   3.5. Update the error covariance matrix:
   $$\begin{aligned}\mathbf{P}_{k|k}=&\mathbf{F}(t_k)\mathbf{P}_{k|k-1}(t_k)\mathbf{F}^{\intercal}(t_k)+\mathbf{Q}(t_k)\\&-\gamma_{i,k}\mathbf{F}(t_k)\mathbf{P}_{k|k-1}(t_k)\mathbf{H}^{\intercal}(t_k)\Big(\mathbf{H}(t_k)\mathbf{P}_{k|k-1}(t_k)\mathbf{H}^{\intercal}(t_k)\\&+\mathbf{R}(t_k)\Big)^{-1}\mathbf{H}(t_k)\mathbf{P}_{k|k-1}(t_k)\mathbf{F}^{\intercal}(t_k).\end{aligned}$$

The residuals reflect the discrepancy between the predicted measurement and the actual measurement. A residual of zero means that the two are in complete agreement and an increasing difference between predicted measurement values and real values shows that state estimation error is increasing and the attitude determination is diverging from the optimal attitude results. It is sufficient for the energy manager to check the statistics of the residual periodically and compare it to a threshold. This test can be further improved by using Neyman Pearson decision making which was introduced in (4.170). Based on the result of the statistical test, the decision maker decides either new measurements are necessary (hypothesis H_1) or not (hypothesis H_0). Thus, the sampling rate of the sensor can be updated to $f_{s_i,2}$ or $f_{s_i,3}$ (a lower or higher sampling rate). Obviously this selection of sensor sampling frequency should comply with Nyquist-Shannon. theorem. If new measurements are necessary, the sampling rate will be untouched and the Kalman filter awaits for the next observation vector to run a new test. Meanwhile, the ADS estimation will generate and use measurement prediction vector instead of the real sensor measurement. In the Kalman filter formulation this can be achieved by increasing the measurement vectors covariance $\mathbf{R}_i$ to a matrix with large values, $\mathbf{R}_\infty$. This will imply that measurements are not trustworthy anymore and automatically prevent the correction phase from using the measurement vector.

Algorithm 3 describes the operation of centralized energy manager.

4.6.3 Decentralized Energy Manager Algorithm

To exploit the benefits of a decentralized architecture, different configuration can be employed. In one configuration sensors directly communicate to each other. This configuration can be very energy exhaustive because it naturally decreases the sleep period of the local wireless transmitters. Also this configu-

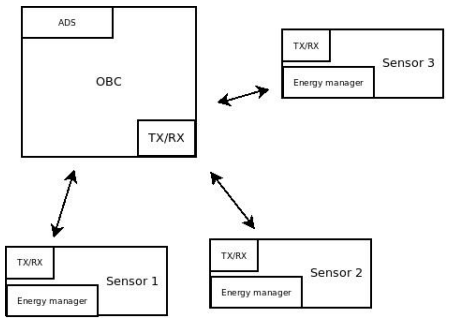

Figure 4.11: A simplified system level view of OWSAN with decentralized energy management

ration does not take benefit of the availability of onboard computer as a node with high computation power and no severe energy constraints. In the second architecture, the communication between sensors is established through the onboard computer. Here the onboard computer contributes as a relay and distributes the information from a node to the other nodes. It waits to receive a request from a node and only then it transmits the latest measurements vector. Also, it is very convenient to accommodate attitude determination algorithms on the fusion center to maintain the global estimate of spacecraft attitude. This enables the onboard computer to provide extra information about spacecraft attitude to the nodes. As a result, the onboard computer always holds the latest valid measurements available from the nodes. Nevertheless, the actual latest measurements can be from different time instances. To ease the explanation but without loosing generality, we consider a system with only two sensor nodes. On the sensor node 1, local measurements are generated with the nominal sampling rate $f_{1,1}$ and immediately communicated to OBC and other node. The local estimator on node 1 maintains a global model of the system and all system statistics and parameters up to time t_k. Therefore it can compute a local prediction of spacecraft states at time t_k with its error covariance matrix which are $\hat{\boldsymbol{x}}_{i,k|k-1}(t_k)$ and $\mathbf{P}_{i,k|k-1}(t_k)$. Furthermore, it can predict its own observation vector $\hat{\boldsymbol{z}}_{1,k|k-1}(t_k)$ and node 2's observation vector $\hat{\boldsymbol{z}}_{2,k|k-1}$. Also it can compute its own local partial information state vector $\check{\boldsymbol{y}}_{1,k|k}$ and its information matrix $\check{\mathbf{Y}}_{1,k|k-1}$ (see section 4.3.2). Each node runs a local energy management algorithm similar to the centralized energy management scheme. In this scheme, the local energy manager on node 1 is only concerned about reducing the sampling rate of sensor 1. It can use a decision making similar to the centralized model to reduce the sampling rate of the sensor when H_0 is true. The correction phase of the algorithm is also similar to the centralized scheme. During the correction phase, the local estimator updates its own state according to (4.140) and (4.141). This algorithm will be performed identically on the fusion center and all sensor nodes. Algorithm 4 presents the operation of decentralized energy manager on an OWSAN node.

Algorithm 4 Decentralized energy manager algorithm

1. Initialization:
   $\hat{\boldsymbol{x}}(t_0)=\boldsymbol{x}_0,\quad \mathbf{P}(t_0)=\mathbf{P}_0,\quad \gamma_{k,i}=1\quad f_i=f_{i,1},\quad \check{\boldsymbol{z}}(t_0)=\boldsymbol{z}_0,\quad \mathbf{R}_i(t_0)=\mathbf{R}_{i,0}$;
   $H_0=$ADS estimation is accurate enough;
   $H_1=$ADS estimation is not accurate enough.
2. Prediction:
   2.1. Project the system state and information state ahead:
   $\hat{\boldsymbol{x}}_{k|k-1}(t_k)=\mathbf{F}(t_{k-1})\hat{\boldsymbol{x}}_{k|k}(t_{k-1})$.
   $\hat{\boldsymbol{y}}_{i,k|k-1}(t_k)=\mathbf{L}_{i,k|k-1}(t_k)\hat{\boldsymbol{y}}_{i,k|k-1}(t_{k-1})$.
   2.2. Project the error covariance and information matrix ahead:
   $\mathbf{P}_{k|k-1}(t_k)=\mathbf{F}(t_{k-1})\mathbf{P}_{k-1|k-1}(t_{k-1})\mathbf{F}(t_{k-1})^{\intercal}+\mathbf{Q}(t_{k-1})$;
   $\mathbf{Y}_{i,k|k-1}(t_k)=\left(\mathbf{F}(t_{k-1})\mathbf{Y}^{-1}_{i,k-1|k-1}(t_k)\mathbf{F}^{\intercal}(t_{k-1})+\mathbf{Q}(t_k)\right)^{-1}$.
   2.3. Project the sensor measurement of the local sensor ahead:
   $\hat{\boldsymbol{z}}_{i,k|k-1}(t_k)=\mathbf{H}_i(t_k)\hat{\boldsymbol{x}}_{k|k-1}(t_k)$.
3. Decision making and correction:
   3.1. If sensor observation vector $\boldsymbol{z}_{i,k}(t_k)$ is available set $\gamma_{i,k}=1$ and:
      3.3.1. Compute the innovation vector and its covariance:
      $\boldsymbol{\epsilon}_i(t_k)=\boldsymbol{z}_i(t_k)-\hat{\boldsymbol{z}}_{k|k-1}(t_k)$;
      $\mathbf{S}_i(t_k)=\mathbf{H}_i(t_k)\mathbf{P}_{k|k-1}(t_k)\mathbf{H}_i^{\intercal}(t_k)+\mathbf{R}_i(t_k)$.
      3.3.2. Run decision maker test and accept H_0 or H_1:
      $$V_{i,k}(\zeta)=\frac{p(\zeta_i|H_1)}{p(\zeta_i|H_0)}\underset{H_0}{\overset{H_1}{\gtrless}}\tau.$$
      3.3.3. Determine the sampling rate for the sensor:
      $$f_i=\begin{cases} f_{i,1} & , \text{ if } H_0 \text{ is true;}\\ f_{i,2} & , \text{ if } H_1 \text{ is true.}\end{cases}$$
      3.3.4. Compute information of the the new measurement:
      $\boldsymbol{i}_i(t_k)=\mathbf{H}_i^{\intercal}(t_k)\mathbf{R}_i^{-1}(t_k)\boldsymbol{z}_i(t_k)$;
      $\mathbf{I}_i(t_k)=\mathbf{H}_i^{\intercal}(t_k)\mathbf{R}_i^{-1}(t_k)\mathbf{H}_i(t_k)$.
   3.2. If sensor observation vector $\boldsymbol{z}_{i,k}(t_k)$ is NOT available:
   $\boldsymbol{i}_i(t_k)=\mathbf{0}\quad,\quad \mathbf{I}_i(t_k)=\mathbf{0}$.
   3.3. Compute the local partial corrections (see (4.138) and (4.139)):
   $\check{\boldsymbol{y}}_{i,k|k}=\hat{\boldsymbol{y}}_{i,k|k-1}(t_k)+\boldsymbol{i}_i(t_k)$;
   $\check{\mathbf{Y}}_{i,k|k}=\mathbf{Y}_{i,k|k-1}(t_k)+\mathbf{I}_i(t_k)$.
   3.4. Interchange the the local partial corrections with other nodes
   3.5. Compute the final local correction:
   $\hat{\boldsymbol{y}}_{i,k|k}(t_k)=\hat{\boldsymbol{y}}_{i,k|k-1}(t_k)+\sum_{j=1}^{M}\left(\check{\boldsymbol{y}}_{j,k|k}(t_k)-\hat{\boldsymbol{y}}_{i,k|k-1}(t_k)\right)$;
   $\mathbf{Y}_{i,k|k}(t_k)=\mathbf{Y}_{i,k|k-1}(t_k)+\sum_{j=1}^{M}\left(\check{\mathbf{Y}}_{j,k|k}(t_k)-\mathbf{Y}_{i,k|k-1}(t_k)\right)$.

Chapter 5

Implementation and Simulation

The most exciting phrase to hear in Science, the one that heralds new discoveries, is not 'Eureka!' but 'That's funny ...'

– Isaac Asimov [1]

In this Chapter the implementation of the centralized and decentralized energy managers are presented and their designs are evaluated. The detailed design of the Extended Kalman Filter for onboard attitude determination is also explained in detail due to its importance and relevance. A set of simulations based on the BIRD spacecraft orbit characteristics are designed to meet the following objectives:

- Demonstrating the impact of employing an energy manager on the performance and energy consumption of ADCS sensors;
- Verification of the algorithms designed in Chapter 4.

The minimum required attitude determination precision is chosen as half degree statistical single axis error. The simulation is executed while the spacecraft is out of eclipse.

The configurations are tested by two independent scenarios. In the first scenario the spacecraft is freely tumbling without involvement of any control system and the aim is to maintain the performance of attitude determination

[1] Isaac Asimov (Jan. 2, 1920 - Apr. 6, 1992) was an American author and professor of biochemistry at Boston University, best known for his works of science fiction and for his popular science books.

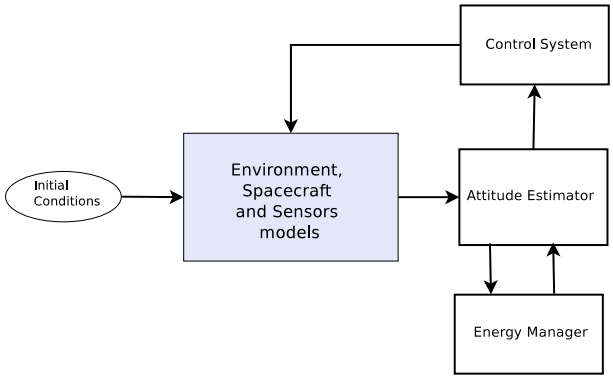

Figure 5.1: System level representation of simulations.

system. The second scenario is much more complicated and evaluates the performance of the design in a pointing scenario, where the spacecraft shall point at a specific direction. A linear-quadratic regulator (LQR) is designed to control the attitude with three reaction wheels. For ADCS sensors, we consider a 3-axis gyroscope, a 3-axis magnetometer and six Sun sensors each of which mounted on one side of the spacecraft cube.

5.1 Simulation Components

Test and simulation of the onboard energy manager has required implementation of an extensive number of spacecraft components. The implementation details of these components are highly relevant to the result of this work. Figure 5.1 shows the overall configuration of simulations. It should be noted that the control system and energy manager components are disabled in some of the scenarios. Hereafter, brief information about the major components of the simulation are detailed.

5.1.1 Quaternion Kalman Filter

As it was described in Section 4.1.2, a quaternion representation of spacecraft attitude is chosen due to the non-singularity in the representation. A quaternion extended Kalman filter (EKF) is desined to simulate the estimator and energy manager.

Filter Design

To enable Kalman filtering, a linearized system equation is needed to present the spacecraft equations of motion and compose the basis of the Kalman filter prediction stage. To do so, attitude quaternion and angular velocity of the spacecraft can be taken as the elements of the system state vector. Thus

$$\boldsymbol{x} = \begin{pmatrix} \mathbf{q} \\ \boldsymbol{\omega} \end{pmatrix}_{[7\times 1]} \tag{5.1}$$

where $\mathbf{q} = [q_1 \quad q_2 \quad q_3 \quad q_s]^\intercal$ is the quaternion which represents the attitude of spacecraft body frame (SCB) in ECI frame, and $\boldsymbol{\omega} = [\omega_1 \quad \omega_2 \quad \omega_3]^\intercal$ is the angular velocity vector in SCB frame. We also define $\boldsymbol{q} = [q_1 \quad q_2 \quad q_3]^\intercal$ to ease the later formulation, thus $\mathbf{q} = [\boldsymbol{q} \quad q_s]^\intercal$.

The spacecraft nonlinear equations of motion which were presented in (4.43) can correlate these state vector elements. These equations need to be linearized for EKF implementation. This linearization can be made by introducing the operation point $\underline{\mathbf{q}}$ and a small transformation $\underset{\sim}{\mathbf{q}}$ around the operating point.

Thus, the attitude of spacecraft body frame with respect to the ECI frame at a given time t can be rewritten as

$$\mathbf{q}(t) = \underset{\sim}{\mathbf{q}}(t) \otimes \underline{\mathbf{q}}(t) \tag{5.2}$$

which means a rotation defined by $\underline{\mathbf{q}}(t)$ followed by a small rotation defined by $\underset{\sim}{\mathbf{q}}(t)$. The symbol $\otimes$ is the quaternion multiplication operator which was introduced previously in (4.16). From the quaternion properties we can conclude that $\underset{\sim}{\mathbf{q}}(t) = \mathbf{q}(t) \otimes \underline{\mathbf{q}}^*(t)$. Respectively, the angular velocity at time t can be defined in terms of the operation point $\underline{\boldsymbol{\omega}}(t)$ and small change $\underset{\sim}{\boldsymbol{\omega}}(t)$

$$\boldsymbol{\omega}(t) = \underline{\boldsymbol{\omega}}(t) + \underset{\sim}{\boldsymbol{\omega}}(t). \tag{5.3}$$

According to Remark 4.1, the kinematics equation can be represented in a quaternion form

$$\dot{\mathbf{q}}(t) = \frac{1}{2}\mathbf{q}_{\boldsymbol{\omega}}(t) \otimes \mathbf{q}(t) \tag{5.4}$$

where

$$\mathbf{q}_{\boldsymbol{\omega}}(t) = \begin{pmatrix} \boldsymbol{\omega}(t) \\ 0 \end{pmatrix} = \begin{pmatrix} \underline{\boldsymbol{\omega}}(t) + \underset{\sim}{\boldsymbol{\omega}}(t) \\ 0 \end{pmatrix} = \mathbf{q}_{\underline{\boldsymbol{\omega}}}(t) + \mathbf{q}_{\underset{\sim}{\boldsymbol{\omega}}}(t). \tag{5.5}$$

Now we can use this result to find the derivative of $\underset{\sim}{\mathbf{q}}(t)$

$$\begin{aligned}
\dot{\underset{\sim}{\mathbf{q}}}(t) &= \mathbf{q}(t)\otimes\dot{\underline{\mathbf{q}}}^*(t)+\dot{\mathbf{q}}(t)\otimes\underline{\mathbf{q}}^*(t)\\
&= \frac{1}{2}\Big(\mathbf{q}(t)\otimes\big(\mathbf{q}_{\tilde{\omega}}(t)\otimes\underline{\mathbf{q}}(t)\big)^*+\big(\mathbf{q}_{\boldsymbol{\omega}}(t)\otimes\mathbf{q}(t)\big)\otimes\underline{\mathbf{q}}^*(t)\Big)\\
&= \frac{1}{2}\Big(-\mathbf{q}(t)\otimes\underline{\mathbf{q}}^*(t)\otimes\mathbf{q}_{\underline{\boldsymbol{\omega}}}(t)+\mathbf{q}_{\boldsymbol{\omega}}(t)\otimes\mathbf{q}(t)\otimes\underline{\mathbf{q}}^*(t)\Big)\\
&= \frac{1}{2}\Big(-\underset{\sim}{\mathbf{q}}(t)\otimes\mathbf{q}_{\underline{\boldsymbol{\omega}}}(t)+\mathbf{q}_{\boldsymbol{\omega}}(t)\otimes\underset{\sim}{\mathbf{q}}(t)\Big)\\
&= \frac{1}{2}\Big(-\underset{\sim}{\mathbf{q}}(t)\otimes\mathbf{q}_{\underline{\boldsymbol{\omega}}}(t)+\mathbf{q}_{\underline{\boldsymbol{\omega}}}(t)\otimes\underset{\sim}{\mathbf{q}}(t)+\mathbf{q}_{\underset{\sim}{\boldsymbol{\omega}}}(t)\otimes\underset{\sim}{\mathbf{q}}(t)\Big). \qquad (5.6)
\end{aligned}$$

Since $\underset{\sim}{\mathbf{q}}(t)$ is assumed to be very small, therefore it can be shown that

$$\mathbf{q}_{\underset{\sim}{\boldsymbol{\omega}}}(t)\otimes\underset{\sim}{\mathbf{q}}(t)\approx\mathbf{q}_{\underset{\sim}{\boldsymbol{\omega}}}(t). \qquad (5.7)$$

Using this result and tedious algebraic manipulation, the linearized kinematics equation for a small change in attitude follows as

$$\dot{\mathbf{q}}(t)=\begin{pmatrix} -\mathfrak{S}\langle\underline{\boldsymbol{\omega}}(t)\rangle & \mathbf{0}_{3\times1}\\ \mathbf{0}_{1\times3} & 0\end{pmatrix}\underset{\sim}{\mathbf{q}}(t)+\frac{1}{2}\mathbf{q}_{\underset{\sim}{\boldsymbol{\omega}}}(t). \qquad (5.8)$$

with $\mathfrak{S}\langle\underline{\boldsymbol{\omega}}(t)\rangle$ being the antisymmetric matrix for vector $\underline{\boldsymbol{\omega}}(t)$ which was introduced in (4.10).

Furthermore the linearized dynamics of the system can be expressed in terms of a small variation in the angular velocity by applying the Jacobian operator

$$\dot{\underset{\sim}{\boldsymbol{\omega}}}(t)\approx-\underline{\mathbf{I}}^{-1}\frac{\mathrm{d}}{\mathrm{d}\boldsymbol{\omega}(t)}\boldsymbol{\omega}(t)\times\underline{\mathbf{I}}\omega(t)\Big|_{\boldsymbol{\omega}(t)=\underline{\boldsymbol{\omega}}(t)}\underset{\sim}{\boldsymbol{\omega}}(t) \qquad (5.9)$$

with $\underline{\mathbf{I}}$ being the spacecraft inertia tensor which results directly in the following simplified form [Bak 1999]

$$\begin{aligned}
\dot{\underset{\sim}{\boldsymbol{\omega}}}(t) &\approx -\underline{\mathbf{I}}^{-1}\frac{\mathrm{d}}{\mathrm{d}\boldsymbol{\omega}(t)}\mathfrak{S}\langle\boldsymbol{\omega}(t)\rangle\underline{\mathbf{I}}\underline{\boldsymbol{\omega}}(t)\Big|_{\boldsymbol{\omega}(t)=\underline{\boldsymbol{\omega}}(t)}\underset{\sim}{\boldsymbol{\omega}}(t)\\
&= \underline{\mathbf{I}}^{-1}\Big(\mathfrak{S}\langle\underline{\mathbf{I}}\,\underline{\boldsymbol{\omega}}(t)\rangle-\mathfrak{S}\langle\underline{\boldsymbol{\omega}}(t)\rangle\underline{\mathbf{I}}\Big)\underset{\sim}{\boldsymbol{\omega}}(t)\Big). \qquad (5.10)
\end{aligned}$$

In existence of control torque $\underset{\sim}{\boldsymbol{n}}_c(t)$ and disturbances $\underset{\sim}{\boldsymbol{n}}_d(t)$, this result can be extended to

$$\dot{\underset{\sim}{\boldsymbol{\omega}}}(t)\approx\underline{\mathbf{I}}^{-1}(\mathfrak{S}\langle\underline{\mathbf{I}}\,\underline{\boldsymbol{\omega}}(t)\rangle-\mathfrak{S}\langle\underline{\boldsymbol{\omega}}(t)\rangle\underline{\mathbf{I}})\underset{\sim}{\boldsymbol{\omega}}(t)\Big)+\underline{\mathbf{I}}^{-1}\Big(\underset{\sim}{\boldsymbol{n}}_c(t)+\underset{\sim}{\boldsymbol{n}}_d(t)\Big). \qquad (5.11)$$

The linearized spacecraft system equations follow from merging (5.8) and (5.10) and result in

$$\begin{aligned}
\dot{\underset{\sim}{\boldsymbol{x}}}(t) &= \mathbf{F}\underset{\sim}{\boldsymbol{x}}(t)\\
&= \begin{pmatrix} -\mathfrak{S}\langle\underline{\boldsymbol{\omega}}(t)\rangle & \mathbf{0}_{3\times1} & \frac{1}{2}\mathbf{1}_{3\times3}\\ \mathbf{0}_{1\times3} & 0 & \mathbf{0}_{1\times3}\\ \mathbf{0}_{3\times3} & \mathbf{0}_{3\times1} & \underline{\mathbf{I}}^{-1}(\mathfrak{S}\langle\underline{\mathbf{I}}\,\underline{\boldsymbol{\omega}}(t)\rangle-\mathfrak{S}\langle\underline{\boldsymbol{\omega}}(t)\rangle\underline{\mathbf{I}})\end{pmatrix}_{[7\times7]}\underset{\sim}{\boldsymbol{x}} \qquad (5.12)
\end{aligned}$$

where $\mathbf{1}_{3\times3}$ is a matrix of ones.

The attitude representation using quaternions is singularity free and the magnitude of the quaternion vector should be unity. Implementing an EKF using quaternions raises two practical problems which need to be addressed: *covariance singularity* and *quaternion unity*.

Due to the quaternion unit norm constraint, the error covariance matrix for the system state vector $\boldsymbol{x}$ is singular. A solution to this problem can be reducing the dimension of the state vector in the correction phase of attitude estimation by the Kalman filter. The scalar element of quaternion vector, q_s, (5.1) can be left out. Therefore the truncated state vector becomes

$$\boldsymbol{x}^{\star}(t_k)=\begin{pmatrix}\boldsymbol{q}\\ \boldsymbol{\omega}\end{pmatrix}_{[6\times1]} \tag{5.13}$$

which is a 6×1 vector. This reduces the dimension of the modified covariance matrix $\mathbf{P}^{\star}_{k}(t_k)$ and the Kalman gain $\mathbf{K}^{\star}_{k}(t_k)$ to 6×6 as well. Since the EKF should be built with the linearized system equations, the a priori reduced-order state estimate can be calculated as

$$\hat{\underset{\sim}{\boldsymbol{x}}}^{\star}_{k|k}(t_k)=\mathbf{K}^{\star}(t_k)\big(\boldsymbol{z}(t_k)-\hat{\boldsymbol{z}}_{k|k-1}(t_k)\big). \tag{5.14}$$

$\boldsymbol{z}$ and $\hat{\boldsymbol{z}}$ are the observation vector and predicted observation vector respectively which were described in Section 4.3.1.

By using the quaternion properties, this a priori reduced estimate can be expanded in order to update the full state vector which is

$$\hat{\underset{\sim}{\boldsymbol{x}}}_{k|k}=\begin{pmatrix}\hat{\underset{\sim}{\boldsymbol{q}}}(t_k)\\ \sqrt{1-\|\hat{\underset{\sim}{\boldsymbol{q}}}(t_k)\|^2}\\ \hat{\underset{\sim}{\boldsymbol{\omega}}}(t_k)\end{pmatrix}. \tag{5.15}$$

This full state vector can be used in EKF to produce the a posteriori state estimate

$$\hat{\boldsymbol{x}}_{k|k}(t_k)=\hat{\boldsymbol{x}}_{k|k-1}(t_k)+\hat{\underset{\sim}{\boldsymbol{x}}}_{k|k}(t_k). \tag{5.16}$$

The EKF should also preserve the unit norm constraint of a quaternion vector. This will ensure the orthogonality of the rotations. However, a standard EKF operates based on unconstrained additive corrections on the state vector. A unit quaternion vector does not belong to a vector space, but is defined on a sphere in $\mathbb{R}^4$. Therefore, the quaternion subspace is not closed with respect to scalar multiplication and scalar addition operations which are used in EKF formulation, such as (5.16). In performing the operation in (5.16), the quaternions part of $\hat{\boldsymbol{x}}_{k|k}(t_k)$ should be calculated by using the quaternions

multiplication rule. Therefore, we have

$$\hat{\boldsymbol{x}}_{k|k}(t_k)=\begin{pmatrix}\hat{\mathbf{q}}_{k|k}(t_k)\\ \hat{\boldsymbol{\omega}}\end{pmatrix}=\begin{pmatrix}\mathbf{q}_{k|k}(t_k)\otimes\hat{\mathbf{q}}_{k|k-1}(t_k)\\ \hat{\underset{\sim}{\boldsymbol{\omega}}}_{k|k-1}(t_k)+\hat{\underset{\sim}{\boldsymbol{\omega}}}_{k|k}(t_k)\end{pmatrix}_{[7\times1]}. \tag{5.17}$$

The correspondent truncated covariance matrix can be calculated from the reduced system state equation which is a truncated form of (5.12). Thus, we have

$$\mathbf{F}^{\star}_{k}(t_k)=\begin{pmatrix}-\mathfrak{S}\langle\underline{\boldsymbol{\omega}}(t)\rangle & \frac{1}{2}\mathbf{1}_{3\times3}\\ \mathbf{0}_{3\times3} & \underline{\mathbf{I}}^{-1}(\mathfrak{S}\langle\underline{\mathbf{I}}\,\underline{\boldsymbol{\omega}}(t)\rangle-\mathfrak{S}\langle\underline{\boldsymbol{\omega}}(t)\rangle\underline{\mathbf{I}})\end{pmatrix}_{[6\times6]}. \tag{5.18}$$

With these modifications, the calculation of the reduced order covariance matrix and the Kalman filter gain follows according to the EKF description in the previous chapter. Therefore, after dropping the time notion (t) for simplicity, the fully linearized state equation for a system without actuators can be presented as

$$\begin{pmatrix}\dot{\underset{\sim}{\mathbf{q}}}\\ \dot{\underset{\sim}{\boldsymbol{\omega}}}\end{pmatrix}=\begin{pmatrix}-\mathfrak{S}\langle\underline{\boldsymbol{\omega}}\rangle & \frac{1}{2}\mathbf{1}_{3\times3}\\ \mathbf{0}_{3\times3} & \underline{\mathbf{I}}^{-1}(\mathfrak{S}\langle\underline{\mathbf{I}}\,\underline{\boldsymbol{\omega}}\rangle-\mathfrak{S}\langle\underline{\boldsymbol{\omega}}\rangle\underline{\mathbf{I}})\end{pmatrix}\begin{pmatrix}\underset{\sim}{\mathbf{q}}\\ \underset{\sim}{\boldsymbol{\omega}}\end{pmatrix}. \tag{5.19}$$

According to the algorithms which were presented in Chapter 4, these system equations can be used to implement the information filter too.

In existence of reaction wheels, this equation can be extended as follows

$$\begin{pmatrix}\dot{\underset{\sim}{\mathbf{q}}}\\ \dot{\underset{\sim}{\boldsymbol{\omega}}}\\ \dot{\underset{\sim}{\boldsymbol{L}}}_m\end{pmatrix}=\begin{pmatrix}-\mathfrak{S}\langle\underline{\boldsymbol{\omega}}\rangle & \frac{1}{2}\mathbf{1}_{3\times3} & \mathbf{0}_{3\times3}\\ \mathbf{0}_{3\times3} & \underline{\mathbf{I}}^{-1}\big(\mathfrak{S}\langle\underline{\mathbf{I}}\,\underline{\boldsymbol{\omega}}\rangle-\mathfrak{S}\langle\underline{\boldsymbol{\omega}}\rangle\underline{\mathbf{I}}+\mathfrak{S}\langle\underline{\boldsymbol{L}}_m\rangle\big) & -\underline{\mathbf{I}}^{-1}\mathfrak{S}\langle\underline{\boldsymbol{\omega}}\rangle\\ \mathbf{0}_{3\times3} & \mathbf{0}_{3\times3} & \mathbf{0}_{3\times3}\end{pmatrix}\begin{pmatrix}\underset{\sim}{\mathbf{q}}\\ \underset{\sim}{\boldsymbol{\omega}}\\ \underset{\sim}{\boldsymbol{L}}_m\end{pmatrix} \tag{5.20}$$

$$+\begin{pmatrix}\mathbf{0}_{3\times3}\\ \underline{\mathbf{I}}^{-1}\\ \mathbf{0}_{3\times3}\end{pmatrix}\underset{\sim}{\boldsymbol{n}}_c$$

where $\boldsymbol{n}_c(t)=\dot{\boldsymbol{L}}_m$. $\boldsymbol{L}_m$ is the angular momentum of reaction wheels which can be measured and $\boldsymbol{n}_c$ is the torque applied to the reaction wheels which is calculated by the controller.

Measurements Incorporation

The Kalman filter requires observations vectors from the sensors. The measurements can not be directly fed into the EKF because it needs linearization of all sensor models. This is a tedious job and introduces additional linearization error to the system. Furthermore, it reduces the autonomy of the design and

dramatically increases the required onboard computation. A different approach is using the nonlinear models of magnetic field and Sun position in ECI frame to generate a state vector mapping such that the magnetic field and Sun vector measurements are expressed in Spacecraft Body (SCB) frame.

For magnetic field measurements, $\boldsymbol{z}_m$, we have

$$\boldsymbol{z}_m(t_k) = \boldsymbol{h}\big(\boldsymbol{x}_k(t_k)\big) + \boldsymbol{w}(t_k) \tag{5.21}$$

$$= {}^{\mathfrak{B}}_{\mathfrak{I}}\mathbf{A}\big(\mathbf{q}(t_k)\big)\,{}^{\mathfrak{I}}\boldsymbol{b}(t_k) + \boldsymbol{w}(t_k) \tag{5.22}$$

where ${}^{\mathfrak{B}}_{\mathfrak{I}}\mathbf{A}\big(\mathbf{q}(t_k)\big)$ is the rotation from the ECI to the SCB frame which corresponds to quaternion $\mathbf{q}(t_k) = [\boldsymbol{q}(t_k) \;\; q_s(t_k)]^{\intercal}$ at time t_k, ${}^{\mathfrak{I}}\boldsymbol{b}$ is the magnetic field vector at the position of the spacecraft in the SCB frame and $\boldsymbol{w}_k$ is a zero mean Gaussian noise with a known covariance $\mathbf{R}_m$. The same applies to Sun sensor measurements $\boldsymbol{z}_s$ and gyro measurements $\boldsymbol{z}_\omega$. Thus we have

$$\boldsymbol{z}(t_k) = \begin{pmatrix} {}^{\mathfrak{B}}\boldsymbol{b}(t_k) \\ {}^{\mathfrak{B}}\boldsymbol{s}(t_k) \\ \boldsymbol{\omega} \end{pmatrix} = \begin{pmatrix} {}^{\mathfrak{B}}_{\mathfrak{I}}\mathbf{A}\big(\mathbf{q}(t_k)\big)\,{}^{\mathfrak{I}}\boldsymbol{b}(t_k) \\ {}^{\mathfrak{B}}_{\mathfrak{I}}\mathbf{A}\big(\mathbf{q}(t_k)\big)\,{}^{\mathfrak{I}}\boldsymbol{s}(t_k) \\ \boldsymbol{\omega} \end{pmatrix}_{[9\times 1]} \tag{5.23}$$

where $\boldsymbol{s}$ is the Sun vector measurement in ECI frame and ${}^{\mathfrak{B}}\boldsymbol{s}$ is the same vector in the SCB frame. This equation should be linearized to be used in EKF formulation. To ease the formulation, the time stamp t_k is dropped later on and the rotation matrix ${}^{\mathfrak{B}}_{\mathfrak{I}}\mathbf{A}$ is simply denoted as $\mathbf{A}$. The attitude matrix can be written as [Wie 1998]

$$\mathbf{A}(\mathbf{q}) = (q_s^2 - \|\boldsymbol{q}\|^2)\mathbf{I}_{3\times 3} + 2\boldsymbol{q}\boldsymbol{q}^{\intercal} - 2q_s\mathfrak{S}\langle\boldsymbol{q}\rangle. \tag{5.24}$$

To linearize this equation, we consider an operation point $\underline{\mathbf{q}}$ with $\underset{\sim}{\mathbf{q}}$ as a small perturbations. For infinitesimal perturbation $\underset{\sim}{\mathbf{q}}$ we have $\underset{\sim}{q}_s \approx 1$, $\|\underset{\sim}{\boldsymbol{q}}\|^2 \approx 0$ and also $\underset{\sim}{\boldsymbol{q}}\underset{\sim}{\boldsymbol{q}}^{\intercal} \approx 0$, therefore

$$\mathbf{A}(\mathbf{q}) = \mathbf{A}(\underline{\mathbf{q}})\mathbf{A}(\underset{\sim}{\mathbf{q}}) \tag{5.25}$$

$$= \mathbf{A}(\underline{\mathbf{q}})(\mathbf{I}_{3\times 3} - 2\mathfrak{S}\langle\underset{\sim}{\boldsymbol{q}}\rangle). \tag{5.26}$$

Thus

$${}^{\mathfrak{B}}\boldsymbol{b} \approx \mathbf{A}(\underline{\mathbf{q}})(\mathbf{I}_{3\times 3} - 2\mathfrak{S}\langle\underset{\sim}{\boldsymbol{q}}\rangle)\,{}^{\mathfrak{I}}\boldsymbol{b} \tag{5.27}$$

$$\approx (\mathbf{I}_{3\times 3} - 2\mathfrak{S}\langle\underset{\sim}{\boldsymbol{q}}\rangle)\,{}^{\mathfrak{B}}\underline{\boldsymbol{b}} \tag{5.28}$$

where ${}^{\mathfrak{B}}\underset{\sim}{\boldsymbol{b}} = {}^{\mathfrak{B}}\boldsymbol{b} - {}^{\mathfrak{B}}\underline{\boldsymbol{b}}$ and ${}^{\mathfrak{B}}\underline{\boldsymbol{b}}$ is the predicted magnetic field measurement in the previous step t_{k-1}. Therefore

$${}^{\mathfrak{B}}\underset{\sim}{\boldsymbol{b}} = {}^{\mathfrak{B}}\boldsymbol{b} - {}^{\mathfrak{B}}\underline{\boldsymbol{b}} \approx -2\mathfrak{S}\langle\underset{\sim}{\boldsymbol{q}}\rangle\,{}^{\mathfrak{B}}\underline{\boldsymbol{b}} \tag{5.29}$$

$$= 2\mathfrak{S}\langle{}^{\mathfrak{B}}\underline{\boldsymbol{b}}\rangle\underset{\sim}{\boldsymbol{q}} \tag{5.30}$$

which is a linear equation. The same approach can be taken for the Sun vector measurements. Therefore, as the result we have

$$\underset{\sim}{z}_k = \mathbf{H}_k \begin{pmatrix} \underset{\sim}{\mathbf{q}} \\ \underset{\sim}{\boldsymbol{\omega}} \end{pmatrix} = \begin{pmatrix} 2\mathfrak{S}\langle^{\mathfrak{B}}\underline{\boldsymbol{b}}\rangle & \mathbf{0}_{3\times3} \\ 2\mathfrak{S}\langle^{\mathfrak{B}}\underline{\boldsymbol{s}}\rangle & \mathbf{0}_{3\times3} \\ \mathbf{0}_{3\times3} & \mathbf{I}_{3\times3} \end{pmatrix} \begin{pmatrix} \underset{\sim}{\mathbf{q}} \\ \underset{\sim}{\boldsymbol{\omega}} \end{pmatrix} \tag{5.31}$$

This equation together with (5.19) completes the state space equation of EKF and information filter. In existence of controller and momentum wheels, the angular momentum of momentum wheels will be added to this measurement vector.

5.1.2 Linear-Quadratic Regulator (LQR)

A linear-quadratic control problem is an optimal control problem. The practical advantages of using LQR for our application is that LQR uses the same spacecraft state space description as derived for the attitude determination in previous section. Thus, incorporating the effect of gyro and reaction wheels and their contribution into the dynamics and kinematics equations is straight forward. A LQR can be designed for discrete systems. Therefore the equation of the system which was introduced in (4.76) shall be transformed to discrete domain. The discrete form of linearized state space with $\mathbf{F}$ and $\boldsymbol{\Gamma}$ is

$$\boldsymbol{x}(k+1) = \mathbf{F}\boldsymbol{x}(k) + \boldsymbol{\Gamma}\boldsymbol{u}(k). \tag{5.32}$$

If the system is controllable and has n states and p inputs then $\mathbf{F}$ will be a $n \times n$ quadratic matrix and $\boldsymbol{\Gamma}$ will be a $n \times p$ matrix. We are considering a finite-horizon discrete-time simulation thus, while the system is controllable, a performance index $\mathbf{J}$ can be defined as

$$\mathbf{J} = \sum_{k=0}^{N} \left(\boldsymbol{x}^{\intercal}(k)\mathbf{Q}_x\boldsymbol{x}(k) + \boldsymbol{u}^{\intercal}(k)\mathbf{Q}_u(k)\boldsymbol{u}(k) \right) \tag{5.33}$$

where $\mathbf{Q}_x$ and $\mathbf{Q}_u$ are quadratic weight matrices of the state and control parameters, respectively. These matrices punish big values in state signals and input signals, respectively.

The simplest control law can be formulated as a linear relation between the control signal and state vector

$$\boldsymbol{u}(k) = -\mathbf{L}(k)\boldsymbol{x}(k) \tag{5.34}$$

where $\mathbf{L}$ is the optimal proportional matrix, given by

$$\mathbf{L}(k) = \left(\mathbf{Q}_u + \boldsymbol{\Gamma}^{\intercal}\mathbf{S}(k+1)\boldsymbol{\Gamma} \right)^{-1} \boldsymbol{\Gamma}^{\intercal}\mathbf{S}(k)\mathbf{F}. \tag{5.35}$$

The value of $\mathbf{S}(k)$ at each step is found by backwards solving the following dynamic Riccati equation (starting from N), assuming $\mathbf{S}(N)=\mathbf{Q}_x$ [Sontag 1998]

$$\mathbf{S}(k-1)=\mathbf{Q}_x+\mathbf{F}^\intercal\big(\mathbf{S}(k)-\mathbf{S}(k)\boldsymbol{\Gamma}(\mathbf{Q}_u+\boldsymbol{\Gamma}^\intercal\mathbf{S}(k)\boldsymbol{\Gamma})^{-1}\boldsymbol{\Gamma}^\intercal\mathbf{S}(k)\big)\mathbf{F}. \tag{5.36}$$

This equation is solved by recursive programming during the simulation.

5.1.3 Onboard Sensors

A set of magnetometers, Sun sensors and gyroscopes is used as the attitude determination sensors for the examined scenarios. These sensors are chosen because they are widely used for attitude determination and typically their precision meets our required ADCS accuracy. In practice, any type of sensor can be selected. Naturally, choosing more accurate sensors such as a star camera can deliver more accurate attitude determination results.

Magnetometer Model

The onboard magnetometer measures the magnetic field vector at the location of the spacecraft in the spacecraft body frame, namely ${}^{\mathcal{B}}\boldsymbol{b}$. Thus ${}^{\mathcal{J}}\boldsymbol{b}={}^{\mathcal{B}}_{\mathcal{J}}\mathbf{A}\,{}^{\mathcal{B}}\boldsymbol{b}$. The Earth magnetic field vector in ECI frame can be calculated by an onboard IGRF model. A seventh order IGRF model is used in the simulations. IGRF model is not accurate enough to precisely model the Earth magnetic field for accurate attitude determination, but its use is justified for our purpose of demonstrating the capabilities of sensor scheduling in attitude reconstruction and energy saving, rather than designing a precise attitude determination system.

A generic model of magnetometer is implemented in the Simulink which delivers the magnetic field data in three dimensions. The model accounts for additive Gaussian noise. An accuracy of $10nT$ with noise level of $100pT/\sqrt{Hz}$ is accounted for simulations which represents a low noise characteristics for the magnetometer.

Table 5.1: Characteristics of onboard sensors which are used in the simulations

Type	Number of units	Accuracy	Noise std.	Drift
Magnetometer	3	10 [nT]	100[pT/$\sqrt{\text{Hz}}$]	N/A
Sun sensor	6	17.0×10^{-4} [rad]	8.0×10^{-5} [rad/sec/$\sqrt{\text{Hz}}$]	N/A
Gyroscope	3	17.0×10^{-4} [rad]	3.5×10^{-3}[rad/sec/$\sqrt{\text{Hz}}$]	1×10^{-2}[rad/sec/°C]

Sun sensor Model

Onboard Sun sensors can provide a vector to the Sun in the spacecraft body frame (${}^{\mathfrak{B}}\boldsymbol{s}$). The simplest type of Sun sensor is made of a single photo diode but it can not provide precision information to reconstruct ${}^{\mathfrak{B}}\boldsymbol{s}$. State-of-the-art Sun sensors are capable of delivering Sun vector in three dimensions. In this thesis a simple configuration of six Sun sensors is used to avoid modeling complications while keeping a generic approach in scope.

We assume that each Sun sensor is placed on one side of the spacecraft cube shape body and can provide two dimensional information about the Sun vector, therefore at least a combination of three sensor measurements is needed to determine the Sun vector. The changes caused by temperature variations and the compensations for dark current are neglected in the Sun sensor model. Sun sensor measurements can not be used when the Sun is in Eclipse. This situation can be detected onboard by combining the information about location of spacecraft in Earth orbit, and the vector from Earth to Sun. A generic Sun sensor model is used for simulations with accuracy of better than 0.1 degree which is an easily achievable accuracy for state of the art Sun sensors [Rhee and Lyou 2012].

Gyroscope Model

Onboard gyroscope measures the rotation rate of the inertial system with respect to the SCB frame which is directly fused with system models in Kalman filter. Gyroscope measurement drift, temperature sensitivity and noise characteristics are implemented in the Simulink model. It is possible to use a Coriolis effect gyroscope to avoid the drift problem but we have used a generic gyro model (see Table 5.1).

5.1.4 Onboard Actuator

Reaction wheels are chosen as the ADCS actuators for our modeling and simulations. Reactions wheels are made by mounting a flywheel on a DC motor. When the rotation speed of DC motor is changed, the spacecraft begins to counter-rotate proportionately through conservation of angular momentum. Reaction wheels can only rotate a spacecraft around its center of mass but cannot cause a translational movement. However, external torques on the spacecraft may require a gradual buildup of reaction wheel rotation speed to maintain the spacecraft in a fixed orientation. The spacecraft is equipped with a set of three momentum wheels which are perpendicular to each other and aligned parallel to the spacecraft body frame (SCB) axis. A generic 3-axis reaction wheel similar to MAI-400 made by Meryland Aerospace is considered

in this work which is usually used for nano and pico satellite. It can produce maximum torque of 0.635×10^{-3} [Nm] per axis [MAI400].

5.1.5 Wireless Communication Channel

As we discussed in Section 2.5.4, ZigBee standard is selected for our OWSAN. ZigBee is a protocol which uses the IEEE 802.15.4 standard as a baseline and adds additional routing and networking functionalities in the application and network layer. IEEE 802.15.4 standard defines characteristics of the MAC and physical layer for low-rate wireless networks. The standard defines two channel access modalities. The first one is the beacon-enabled modality, which uses a slotted CSMA-CA and the optional guaranteed time slot (GTS) allocation mechanism. This mechanism lowers the energy consumption of the Router nodes. The second one is an unslotted CSMA-CA without beacons. The communication scheme uses temporal windows denoted super-frames. The beacon enabled mode which is shown in Figure 5.2 is suitable for designing the centralized energy management scheme in our application. Both methods can be used for the decentralized architecture where each node wakes up and transmits when needed. OBC as the network coordinator periodically sends beacon frames in every beacon interval T_{BI} to identify its PAN and to synchronize nodes that communicate with it. The coordinator and nodes can communicate during the active period, called the super-frame duration T_{SD}, and enter the low-power mode during the inactive period. The structure of the super-frame is defined by two parameters, the beacon order (BO) and the super-frame order (SO), which determine the length of the super-frame and its active period. T_{BI} and T_{SD} can be calculated as follows

$$T_{BI} = T_{BSFD} \times 2^{BO} \tag{5.37}$$

$$T_{SD} = T_{BSD} \times 2^{SO} \tag{5.38}$$

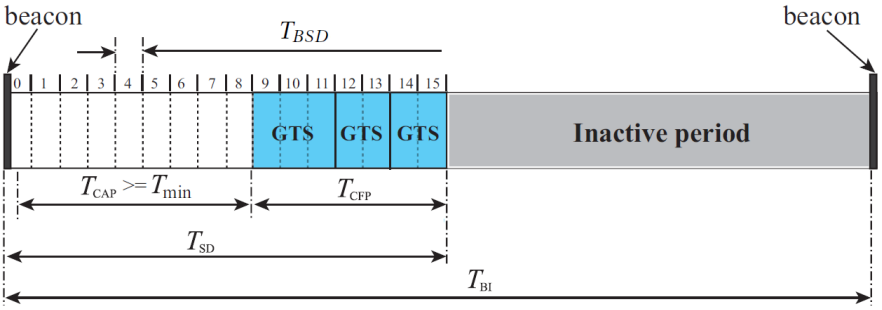

Figure 5.2: The structure of IEEE 802.15.4

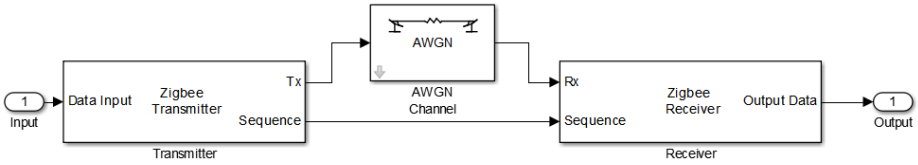

Figure 5.3: Simulink model of ZigBee communication link made in Simulink

where $0 \leq \mathrm{SO} \leq \mathrm{BO} \leq 14$ and T_{BSFD} is the number of symbols forming a super-frame when $SO = 0$. In addition, each super frame is divided to 16 equally sized super frame slots of length T_{BSD}. Each active period can be further divided into a contention access period (CAP) and an optional contention free period (CFP), composed of GTSs. A slotted CSMA-CA mechanism is used to access the channel of non time-critical data frames and GTS requests during the CAP. Further details of the CSMA-CA mechanism of CAP can be found in the work of Park [Park 2011]. Park has extensively studied the use of IEEE 802.15.4 based protocols such as ZigBee for WSN application. Based on Park's work, a Simulink model for ZigBee has been developed in the SpaceTool toolbox to simulate the wireless channels in attitude determination simulation environment (Fig. 5.3). Here ZigBee transmitter, receiver and an Additive White Gaussian Noise (AWGN) channel are modeled. Transmitter uses a PN sequence for the spreading and then the OQPSK modulator is used for modulating the spread bits. The first step on the receiver side is OQPSK demodulation and then the spread bits are de-spread by the delayed version of PN chip sequence.

5.1.6 Simulation Environment

The simulations are carried out with the SpaceTool simulation environment which is a Matlab/Simulink toolbox. Design and development of this toolbox was initiated in 2003 as a simulation tool for AAUSAT-II CubeSat at the Aalborg university by a group of MSc students including the author of this thesis [Amini et al. 2005]. Later on, the toolbox design was revised and extended by the author within the MicroNED MISAT project at the Aerospace Engineering faculty of Delft University of Technology. Previous generations of this tool were used in the design and development of AAUSAT-II and Delfi-C3 CubeSat [Amini et al. 2005]. The majority of the models were verified against EuroSim, designed by Dutch Space BV and the Spacecraft Control Toolbox (SCT), developed by Princeton Satellite Systems. The toolbox contains the following models:

- Different orbit propagation models, including Cowell and SGP4 orbit

propagators;

- Ephemeris blocks to compute the position of the Sun and Moon as functions of Julian date. In this work the effect of Moon on LEO spacecraft is neglected;
- Earth magnetic field block, which uses the IGRF model with configurable precision;
- Configurable disturbances blocks, including solar radiation, atmospheric drag, gravity gradient and magnetic residual which are configurable due to the necessary precision, as well as orbit and the physical characteristics of the satellite;
- Dynamic and kinematics model of rigid body satellites;
- Generic models of various sensors and actuators;
- Generic model of onboard energy harvesting and solar panels;
- Different estimators for attitude determination, including Kalman filter, Extended Kalman filter, Unscented Kalman filter;
- Deterministic attitude determination methods including Q-method, QUEST and REQUEST;
- Transformation routines to transfer between ECI, ECEF and SCB frames;
- Different routines to implement quaternion mathematics.

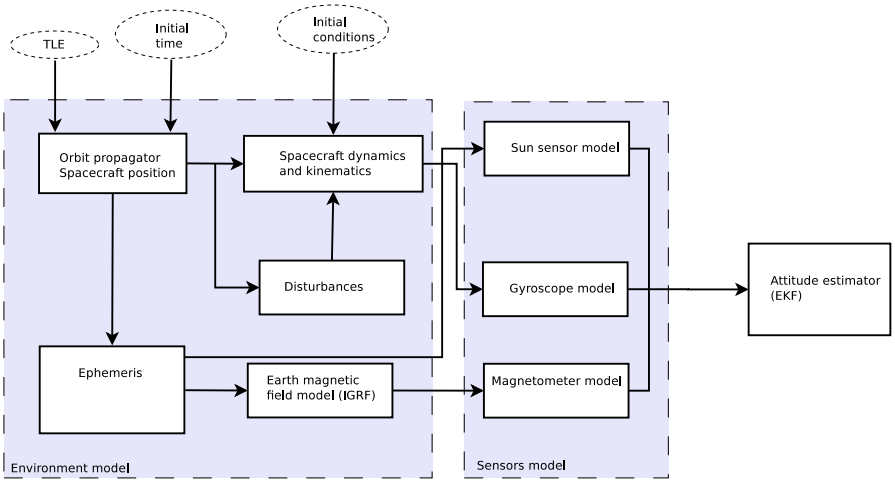

Figure 5.4: Diagram representation of the simulation architecture

Figure 5.4 shows the conceptual block diagram of simulation environment without accounting the energy manager components. It should be noted that the effect of electromagnetic disturbances on magnetometer measurements is not modeled to simplify the models.

5.2 Experimental Results

This Section presents the evaluation results of the energy manager for the attitude determination system. The simulation goal is to demonstrate the possibility of reducing the activation period of wireless sensors without degrading the performance of the attitude determination system below the required threshold.

The simulation scenario is based on a one-unit CubeSat size spacecraft with the BIRD spacecraft orbit characteristics. This assumption is made to simplify the design of attitude controller in pointing scenarios.

The required ADS accuracy is chosen to be better than 0.5 degree (1-sigma, statistical single-axis) which is reasonable considering the chosen sensors. This error is computed as the absolute difference between spacecraft true attitude and the estimated value. The simulation time range is chosen such that the spacecraft is not entering eclipse. The attitude dynamics and estimation is based on quaternions but the result is transformed to Euler angels to ease the comparison. The rotation sequence Z-Y-X (or so called 3-2-1) is chosen for the transformations.

Simulations structure

Three types of simulations are used:

1. Benchmark: The benchmark simulations serve as references for performance comparison. In these tests, the attitude determination and control system is functional but the energy manager is switched off and all measurements are communicated to the central estimator at each simulation step. Two different scenario are designed as benchmark: *free tumbling* and *pointing*.

2. Centralized: In these tests, a centralized energy manager is managing the activities of the sensors. The regulator decides whether each sensor needs to communicate the next measurement vector to the central regulator. Two scenarios are developed and evaluated to cover both free tumbling and pointing operations.

Table 5.2: Simulation parameters for the free tumbling scenario

Parameter	Value	Unit
Simulation step	$T_s = 1$	[s]
Inertia tensor	$\underline{\mathbf{I}} = \begin{pmatrix} 0.002 & 0 & 0 \\ 0 & 0.002 & 0 \\ 0 & 0 & 0.002 \end{pmatrix}$	[kg/m^2]
Initial rotation rate	$\boldsymbol{\omega} = \begin{pmatrix} 0.01 \\ -0.01 \\ 0.01 \end{pmatrix}$	[rad/s]
Initial attitude	$\mathbf{q}_0 = \begin{pmatrix} 0 \\ 0 \\ 0 \\ 1 \end{pmatrix}$	

3. Decentralized: These tests evaluate the performance of a decentralized energy manager. Each sensor individually regulates and schedules its own data transmission. These tests also include two scenarios: free tumbling and pointing.

This structure enables cross comparison between the scenarios.

5.2.1 Benchmark Tests

These scenarios are designed to evaluate the performance of the attitude determination system. In addition, they serve as performance baselines for other tests. Attitude determination and control algorithms are designed by the techniques which were discussed in Chapter 4.

Free tumbling scenario ($\mathrm{REF_T}$)

In this scenario, the spacecraft is freely tumbling with an initial angular rotation rate. The result of this scenario will be used to study the performance of the attitude determination with an energy manager in the loop. In this scenario the controller is not functioning and the reaction wheels are disabled in the simulation. Table 5.2 shows the simulation parameters. The simulator produces the sensor measurements at 1 Hz and feeds them to the EKF. The filter is using the discretized equations of the spacecraft dynamics for the prediction stage and updates this result by using the sensor measurements. It is assumed that the spacecraft is out of Eclipse, therefore Sun sensor measurements are fully employed too. Figure 5.5 shows that the designed EKF satisfies the required accuracy of half a degree. The convergence is complete after about 32 seconds. The fast convergence is mainly due to allocating low

Table 5.3: Parameters of Kalman filter for attitude estimation

Parameter	Value
Initial estimation covariance matrix (P)	$\mathbf{I}_{9\times9}$
Measurements covariance matrix (R)	$\begin{pmatrix} 10^{-10}\mathbf{I}_{3\times3} & \mathbf{0}_{3\times3} & \mathbf{0}_{3\times3} \\ \mathbf{0}_{3\times3} & 8\times10^{-5}\mathbf{I}_{3\times3} & \mathbf{0}_{3\times3} \\ \mathbf{0}_{3\times3} & \mathbf{0}_{3\times3} & 3\times10^{-5}\mathbf{I}_{3\times3} \end{pmatrix}_{9\times9}$
Process covariance matrix (Q)	$10^{-3}\mathbf{I}_{9\times9}$

weight to the systems equations in the Kalman filter. The Kalman filter characteristics are presented in Table 5.3. Table 5.4 shows the characteristics of the attitude estimation. The mean of the estimation error is close to zero for yaw, pitch and roll, which shows that the estimation is rather unbiased and works properly.

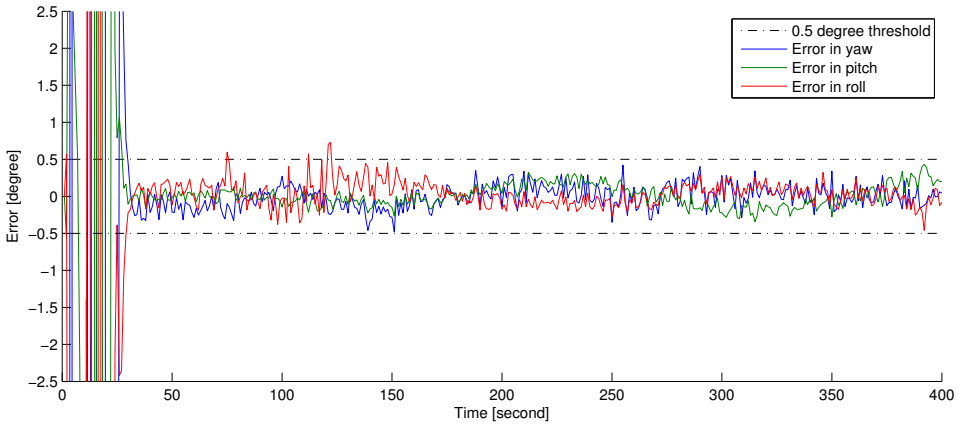

Figure 5.5: EKF error in the benchmark tumbling scenario

Table 5.4: Attitude determination results in benchmark free tumbling scenario. Subscripts y, p and r refer to yaw, pitch and roll respectively

Parameter	Value	Unit
Convergence time	$\tau_y = 32$	[s]
(Error less than half degree)	$\tau_p = 27$	[s]
	$\tau_r = 29$	[s]
Estimation error mean	$\mu_y = -0.01$	[deg]
(after convergence)	$\mu_p = 0.01$	[deg]
	$\mu_r = 0.04$	[deg]
Estimation error 1-sigma	$\sigma_y = 0.16$	[deg]
(after convergence)	$\sigma_p = 0.14$	[deg]
	$\sigma_r = 0.16$	[deg]

Pointing (REF_P)

The second benchmark scenario is designed such that the spacecraft aims to reach a predefined attitude. The result of this scenario will be later used to study the performance of ADS with an energy manager when it interacts with the attitude control system. To design the controller, the system equations are converted into discrete form and a performance index is derived. Then the weight matrices are derived from the performance index and the optimal gain matrices are calculated. The resulting LQR controller is integrated with a model of reaction wheels in the simulation. The target attitude is arbitrary, and it is chosen such that spacecraft performs a $(30^\circ - 15^\circ - 60^\circ)$ maneuver. In this scenario, the LQR controller commands the reaction wheels to rotate the spacecraft to the desired attitude. The EKF is in the feedback loop as observer. Table 5.5 shows the parameters of this simulation.

Figure 5.6 depicts the angular rotation rate of the spacecraft during the maneuver. It is clear that the controller slows down spacecraft rotation rate until it aligns the spacecraft with set point. Since the set point is defined in the ECI frame the spacecraft does not follow a tracking maneuver. Naturally, the inaccuracy of ADS reduces the performance of the controller. Therefore it is expected that the controller will have a steady state error, which is acceptable for the purpose of our work. The ADS estimation error is within the requirements, as shown in Figure 5.7.

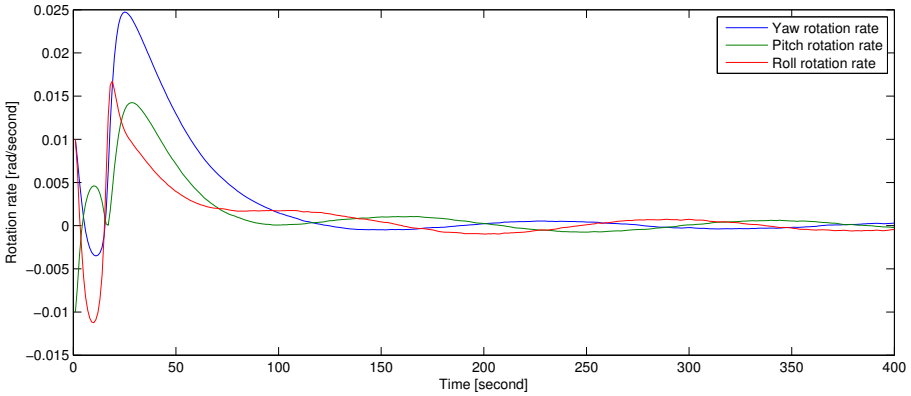

Figure 5.6: The angular rotation rate of spacecraft in benchmark pointing scenario

Table 5.5: Simulation parameters for the benchmark pointing scenario

Parameter	Value	Unit
Simulation step	$T_s = 1$	[s]
Inertia tensor	$\underline{\mathbf{I}} = \begin{pmatrix} 0.002 & 0 & 0 \\ 0 & 0.002 & 0 \\ 0 & 0 & 0.002 \end{pmatrix}$	[kg/m^2]
Initial rotation rate	$\boldsymbol{\omega} = \begin{pmatrix} 0.01 \\ -0.01 \\ 0.01 \end{pmatrix}$	[rad/s]
Initial attitude (in ECI)	$\mathbf{q}_0 = \begin{pmatrix} 0 \\ 0 \\ 0 \\ 1 \end{pmatrix}^T$	-
Target attitude (in ECI)	$\mathbf{q}_{\text{set}} = \begin{pmatrix} 0.4496 \\ 0.2375 \\ 0.1692 \\ 0.8463 \end{pmatrix}$	-

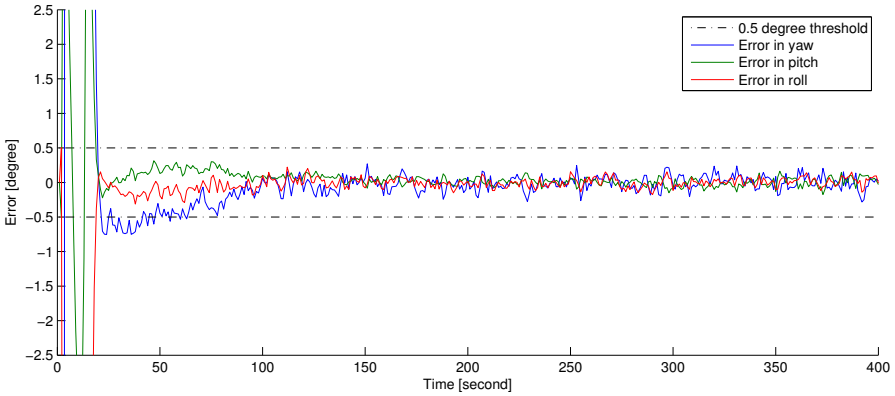

Figure 5.7: Attitude estimation error in benchmark pointing scenario

Table 5.6: Attitude estimation results in benchmark pointing scenario when the energy manager is deactivated but LQR is active. Subscripts y, p and r refer to yaw, pitch and roll respectively

Parameter	Value	Unit
Convergence time	$\tau_y = 42$	[s]
(Error less than 0.5 degree)	$\tau_p = 19$	[s]
	$\tau_r = 19$	[s]
Estimation error mean	$\mu_y = -0.05$	[deg]
(after convergence)	$\mu_p = 0.04$	[deg]
	$\mu_r = -0.01$	[deg]
Estimation error, 1-sigma	$\sigma_y = 0.16$	[deg]
(after convergence)	$\sigma_p = 0.08$	[deg]
	$\sigma_r = 0.08$	[deg]

Table 5.6 presents the characteristics of the attitude estimation in this benchmark scenario. We can directly compare this result with the values in Table 5.4 from the tumbling scenario. This comparison shows that the attitude determination performance is within the design requirements. A closer comparison between Figure 5.7 and Figure 5.5 shows that EKF takes slightly more time to achieve the required precision specially after convergence. This is due to introducing the control torque as a source of external disturbance in the state space equations of the system. This causes an additional error in the prediction phase of Kalman filter from the linearized equations. The estimator does not have any direct measurement from this disturbance. Therefore the extended convergence time is inevitable. The mean estimation error is close

to zero for all three yaw, pitch and roll angles, which shows that the filter estimation is not biased. This is expected because the sensors bias characteristics are neglected and the simulation length is short which lowers the impact of sensors' drift on the end result. To account for drift and bias, the models of bias and drift should be added to the state equations.

5.2.2 Centralized Energy Manager

In the next scenarios a centralized energy manager is added to the system according to the model which was presented in Chapter 4. Its aim is to decrease the activation period of the sensors. The ultimate goal is to show that the attitude determination error is comparable with REF_T and REF_P scenarios while sensors are less frequently used.

Free tumbling (CEN_T)

The first scenario studies attitude determination in free tumbling while the energy manager is supervising the activity of all three sensors and switches them on and off according to the algorithm introduced in Section 4.6.2. The result of this experiment can be compared to REF_T scenario where no energy manager was activated. The setup is similar to REF_T and the initial values are following Table 5.2. The Kalman filter initial conditions are shown in Table 5.3.

It is expected that the energy manager maintains the sensors in the active mode until the required precision is met and reduces their activities thereafter. Figure 5.8 shows the result of attitude determination error. This result shows that the attitude determination error is kept within the precision requirements. The attitude determination error is reduced to less than half a degree which is comparable with REF_T results.

Figure 5.9(a) shows the status of Sun sensor while the energy manager is governing its status. Likewise, 5.9(b) and 5.9(c) show the status of magnetometer and gyro, respectively.

Statistical analysis shows that the Sun sensor and magnetometer are activated for 51.2% and 61% of the simulation time. The gyro is used less often, which is 43.7% of the whole simulation period. The lower duty cycle for gyro means that EKF prediction of spacecraft rate is accurate enough to disregard gyro measurements more often. This can be due to the slow dynamic of the spacecraft and low rotation rate during the simulation time. This result is presented in Table 5.7.

These duty cycles should be compared to 100% duty cycle in REF_T benchmark scenario where the energy manager was not used. It is clear that in the first 50

Table 5.7: Simulation results of centralized energy manager in tumbling scenario in the first 400 seconds of the simulation

Parameter	Value	Unit
Simulation length	400	[s]
Sun sensor total activation period	210	[s]
Sun sensor duty cycle	52.5%	-
Magnetometer total activation period	244	[s]
Magnetometer duty cycle	61%	-
Gyro total activation period	177	[s]
Gyro duty cycle	44.25%	-

seconds of the simulation all three sensors are very frequently used to ensure the quick convergence of EKF.

If we compare Figure 5.8 with Figure 5.5 from REF_T , we can find various spikes and discontinuity in the trend of attitude error. We can guess that this behavior is due to the frequent switching between sensor modes. To further analyze this phenomena, we can superpose Figure 5.8 and Figure 5.9(a) as shown in Figure 5.10. The spikes are mostly happening when energy manager switches the Sun sensor (or other sensors) operation mode. This switching directly affects the correction phase of Kalman filter, each of which introduces a discontinuity in the propagation of the state estimate by the EKF. Removing

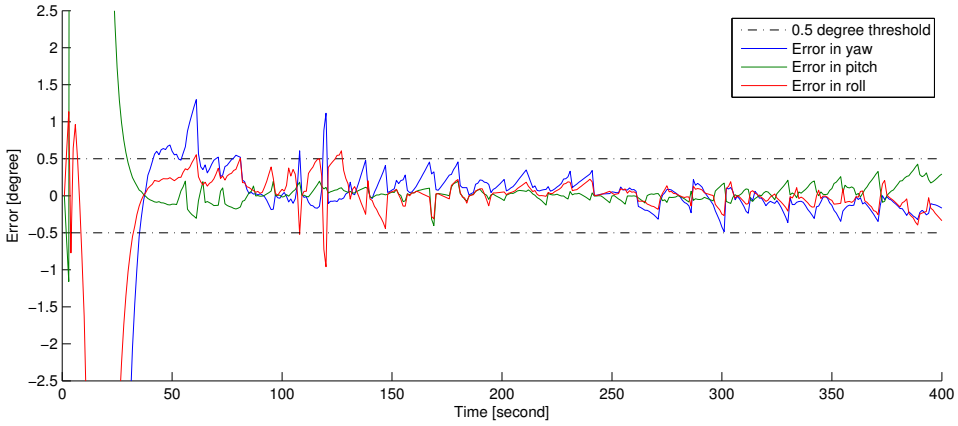

Figure 5.8: Simulation result of attitude determination in tumbling scenario, when the central energy manager is running

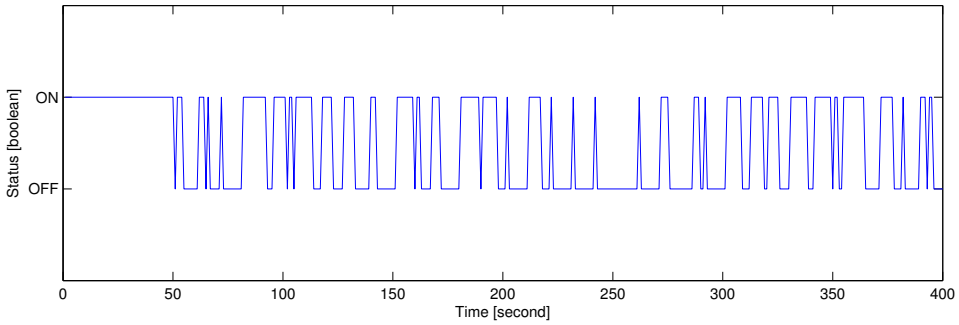

(a) Sun sensor

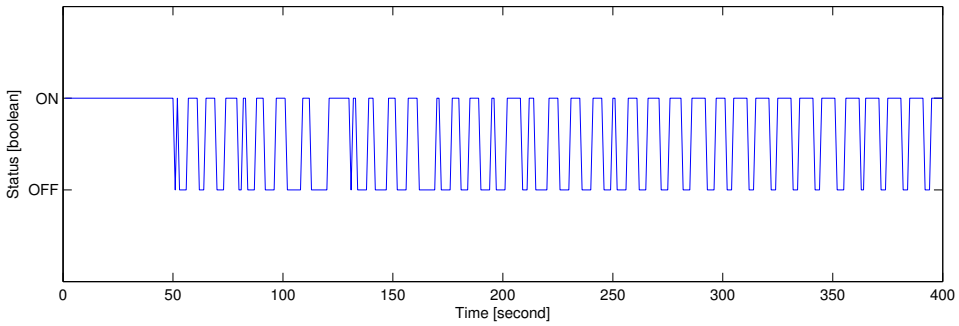

(b) Magnetometer

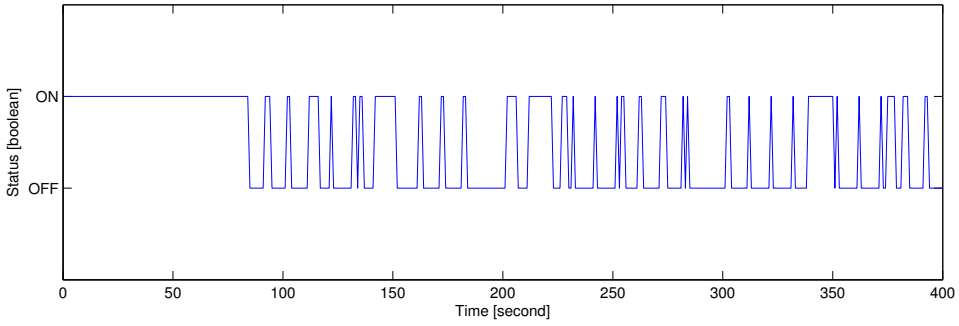

(c) Gyro

Figure 5.9: The sensors statuses are shown for the first 400 seconds of the CEN_T simulation

this discontinuity might be interesting for control applications. This may be approached by applying a low pass filter which is out of the scope of this work.

Table 5.8: ADS performance in centralized tumbling scenario

Parameter	Value	Unit
Convergence time	$\tau_y = 35$	[s]
(Error less than half degree)	$\tau_p = 29$	[s]
	$\tau_r = 32$	[s]
Estimation error mean	$\mu_y = 0.07$	[deg]
(after convergence)	$\mu_p = 0.03$	[deg]
	$\mu_r = 0.04$	[deg]
Estimation error 1-sigma	$\sigma_y = 0.25$	[deg]
(after convergence)	$\sigma_p = 0.10$	[deg]
	$\sigma_r = 0.18$	[deg]

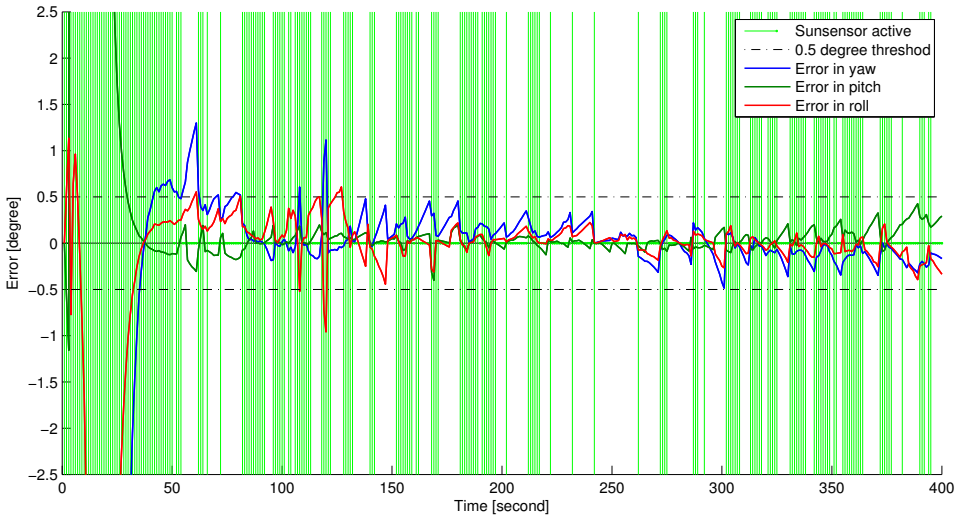

Figure 5.10: Comparing the attitude estimation error and Sun sensor status in CEN_T scenario

Table 5.8 presents an overview of the ADS performance. The result shows that the residuals are still unbiased and the standard deviation is relatively small. We can compare the standard deviation values with the ones for REF_T test. The standard deviation values are slightly increased which means the overall estimation error is relatively higher, however it is still maintained by the energy manager to stay within the precision requirements.

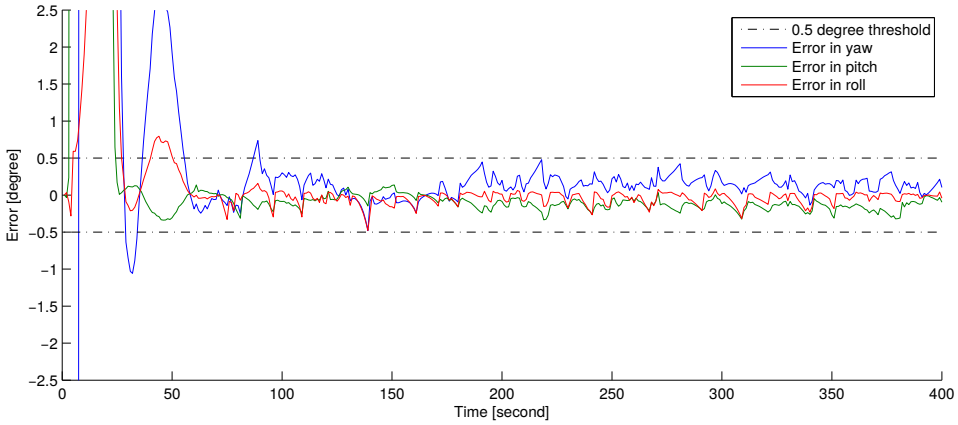

Figure 5.11: Attitude determination error in pointing scenario while central energy manager is enabled

Pointing (CEN_P)

This simulation is using the same initial conditions and parameter as REF_P . The only difference is that energy manager is active and trying to reach the attitude accuracy goal. The setup is similar to REF_T and the initial values are following Table 5.2. The Kalman filter initial conditions are shown in Table 5.3. The energy manager is performing similar to CEN_T and regulates the sensors status. The result of this test shall be compared to REF_P . The maneuver is also the same ($30°-15°-60°$) rotation. The parameters of the LQR controller are not changed or tuned to compare the performance of attitude determination in the loop. Figure 5.11 demonstrates ADS error in the first 400 seconds of simulation. The energy manager decides schedules the next activity of each sensor individually based on the accuracy of its estimated value. The final result is analyzed in Table 5.9. This analysis shows that average ADS error is increased however the standard deviation is slightly decreased. In fact this means that the residuals are biased comparing to REF_P which indicates suboptimal operation of the attitude estimator. This is expected because more measurement packages are missing comparing to the similar benchmark scenario. Convergence time is almost tripled. Observing the status of the sensors provides some hints about the cause of this behaviour. The energy manager has deactivated Sun sensor and the magnetometer as soon as the available estimation of the sensor measurement has been close enough to zero, which is before the completion of attitude estimation convergence comparing to REF_P , thus the dynamic of estimation has changed comparing to Figure 5.7.

Table 5.9: ADS performance in centralized pointing scenario with energy manager

Parameter	Value	Unit
Convergence time	$\tau_y = 55$	[s]
(Error less than 0.5 degree)	$\tau_p = 25$	[s]
	$\tau_r = 50$	[s]
Estimation error mean	$\mu_y = 0.13$	[deg]
(after convergence)	$\mu_p = -0.10$	[deg]
	$\mu_r = -0.03$	[deg]
Estimation error, 1-sigma	$\sigma_y = 0.15$	[deg]
(after convergence)	$\sigma_p = 0.09$	[deg]
	$\sigma_r = 0.08$	[deg]

The statuses of sensors are also showed in Figure 5.12(a), Figure 5.12(b) and Figure 5.12(c) for Sun sensor, magnetometer and gyro respectively. Table 5.10 details the analysis of sensors status. The first 120 seconds of the simulation are neglected in the analysing the results because the convergence is not completed yet and sensors are extensively activated. The result shows a significant reduction of duty cycle for magnetometer and Sun sensor which means close to 45% percent energy saving only for these two sensors. On the other hand, the result does not show any similar improvement for gyro. In fact this shows that the estimator is relying extensively on the gyro measurements to maintain the performance, and uses Sun sensor and magnetometer measurements for corrective actions.

Table 5.10: Simulation results of centralized energy manager in pointing scenario in the first 400 seconds of the simulation after convergence

Parameter	Value	Unit
Simulation length	400	[s]
Sun sensor activation period	280	[s]
Sun sensor duty cycle	70.0%	-
Magnetometer activation period	173	[s]
Magnetometer duty cycle	43.25%	-
Gyro activation period	264	[s]
Gyro duty cycle	66.0%	-

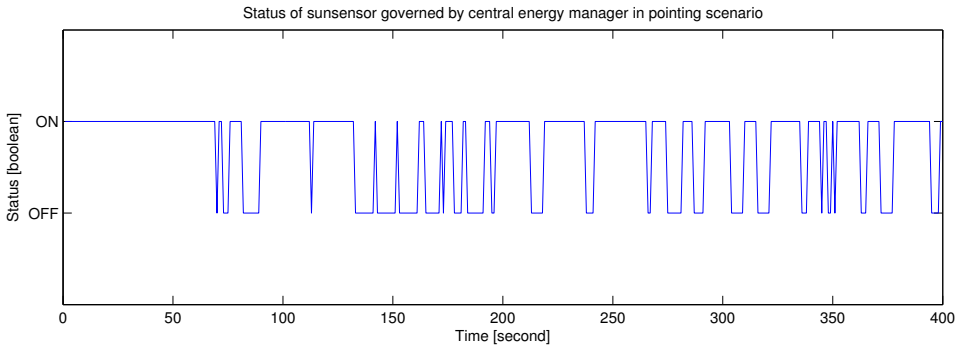

(a) Sun sensor

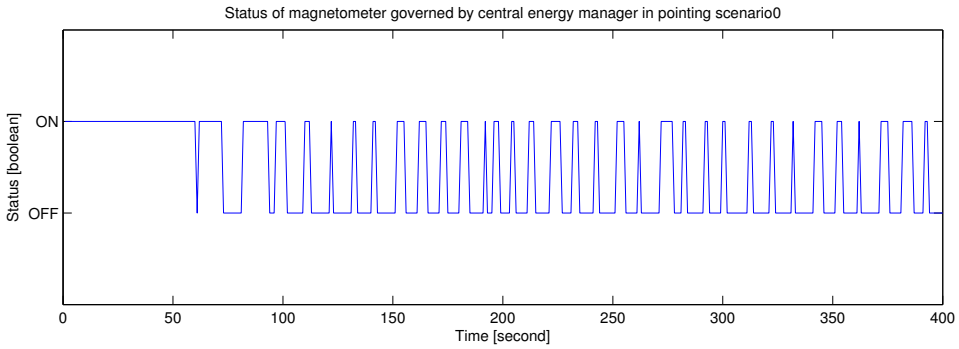

(b) Magnetometer

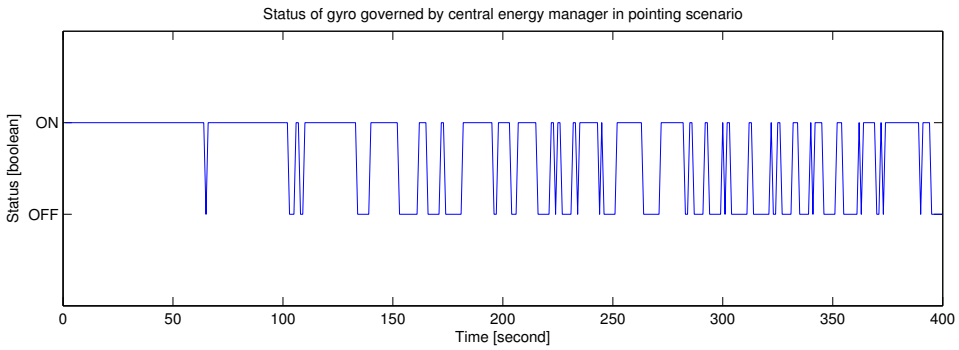

(c) Gyro

Figure 5.12: Sensor statuses in the first 400 seconds of the simulation in CEN_P scenario

Table 5.11: Simulation results in free tumbling scenario with decentralized energy manager

Parameter	Value	Unit
Convergence time	$\tau_{SS,y} = 15$, $\tau_{MM,y} = 15$, $\tau_{G,y} = 14$	[s]
(Error less than 0.5 degree)	$\tau_{SS,p} = 15$, $\tau_{MM,p} = 15$, $\tau_{G,p} = 14$	[s]
	$\tau_{SS,r} = 18$, $\tau_{MM,r} = 17$, $\tau_{G,r} = 17$	[s]
Estimation error mean	$\mu_{SS,y} = 0.00$, $\mu_{MM,y} = 0.00$, $\mu_{G,y} = 0.00$	[deg]
(after convergence)	$\mu_{SS,p} = 0.00$, $\mu_{MM,p} = 0.00$, $\mu_{G,p} = 0.00$	[deg]
	$\mu_{SS,r} = 0.00$, $\mu_{MM,r} = 0.00$, $\mu_{G,r} = 0.00$	[deg]
Estimation error, 1-sigma	$\sigma_{SS,y} = 0.09$, $\sigma_{MM,y} = 0.09$, $\sigma_{G,y} = 0.10$	[deg]
(after convergence)	$\sigma_{SS,p} = 0.08$, $\sigma_{MM,p} = 0.05$, $\sigma_{G,p} = 0.05$	[deg]
	$\sigma_{SS,r} = 0.09$, $\sigma_{MM,r} = 0.08$, $\sigma_{G,r} = 0.10$	[deg]

5.2.3 Decentralized Energy Manager

In the next experiments, a decentralized energy manager scheme is instantiated. Each node computes the local estimation of the attitude with an information filter, performs decision making based on hypothesis tests, and decides on the necessity of transmitting local measurement vectors to the OBC. Here, the OBC plays a relaying role. By each transmission, the local information is transmitted to OBC and the latest information vectors generated by other sensor nodes are acquired from OBC. Also a federated ADCS information filter is placed on OBC to compare the results of the local attitude estimations with the global one.

Free tumbling ($\mathrm{DEC_T}$)

This scenario resembles a free tumbling scenario similar to the one presented in Section 5.2.2 but with a decentralized attitude determination and energy managemer. The results of this test should be compared to $\mathrm{REF_T}$ and $\mathrm{CEN_T}$. The setup is similar to $\mathrm{REF_T}$ and the initial values are following Table 5.2. Table 5.11 presents the attitude determination results of this scenario and Table 5.12 details the analysis of sensors statuses. Figures 5.13, 5.14 and 5.15 present the local attitude estimation results. The figures show that the result is partially within the expected accuracy. The activation status of sensor nodes is presented in Figure 5.16(a), Figure 5.16(b) and Figure 5.16(c). Finally, figure 5.17 shows the reconstructed attitude in OBC from the collected information of sensors. The results of the local estimations are quite comparable to each other and the federated estimation results (see Section 4.3.2). Simulation shows that sensor measurements are very frequently needed which means there is no significant reduction in energy consumption.

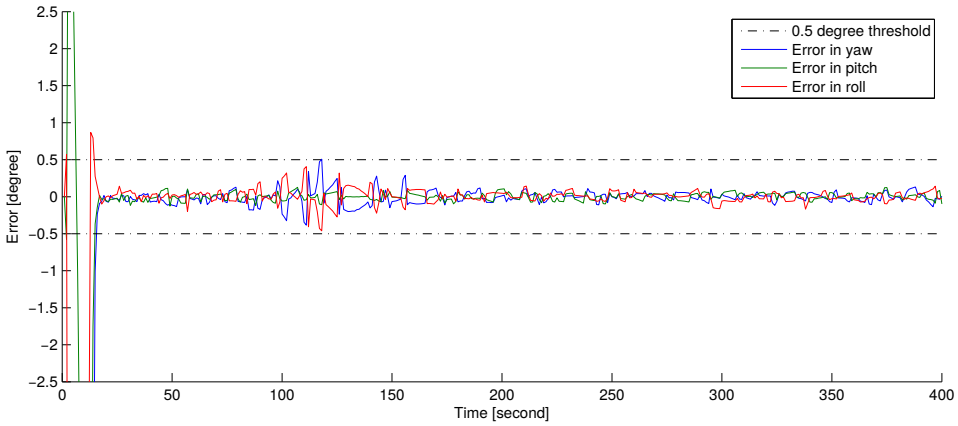

Figure 5.13: Simulation results of local attitude determination at Sun sensor node in tumbling mode while decentralized energy manager scheme is operational

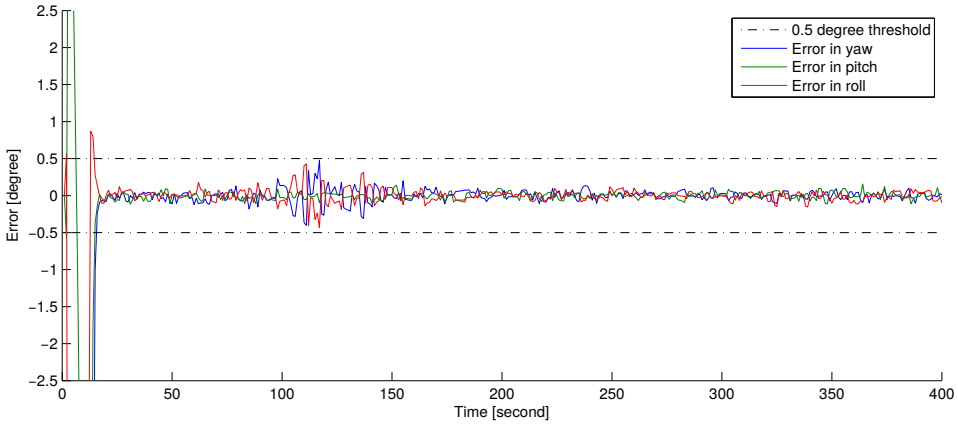

Figure 5.14: Simulation results of local attitude determination at magnetometer node in tumbling mode while decentralized energy manager scheme is operational

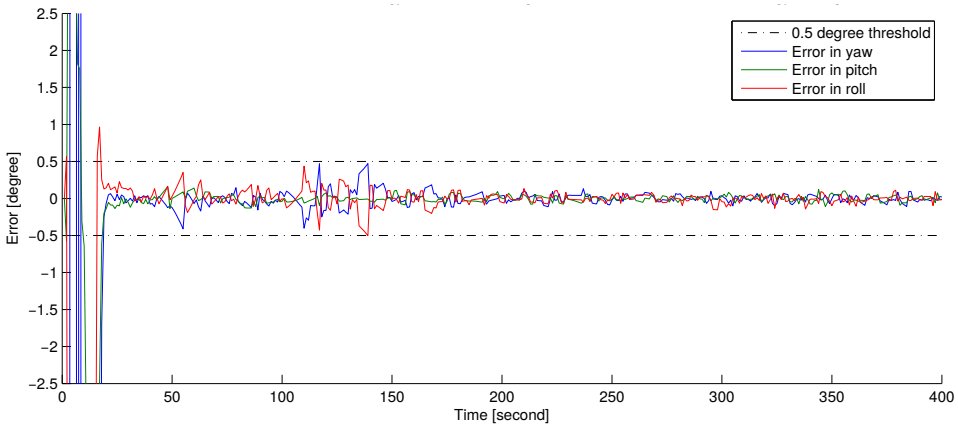

Figure 5.15: Simulation results of local attitude determination at gyro node in tumbling mode while decentralized energy manager scheme is operational

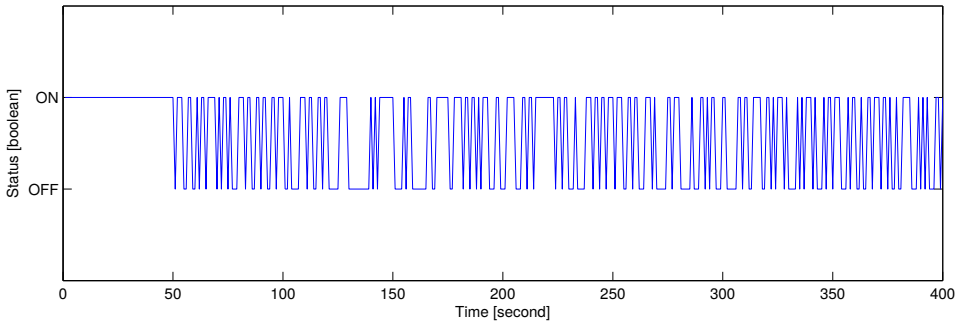

(a) Sun sensor

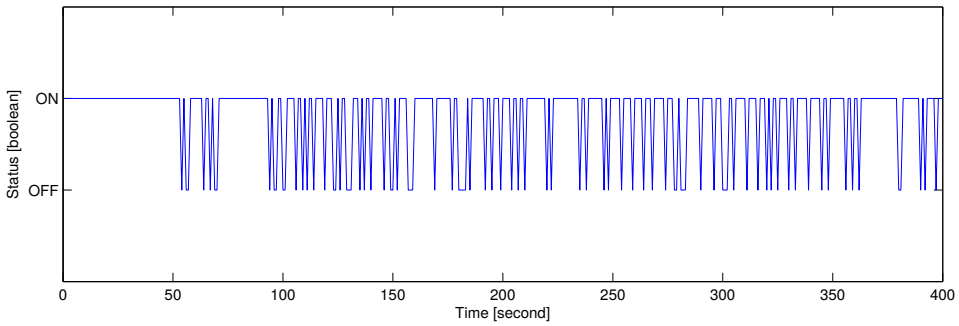

(b) Magnetometer

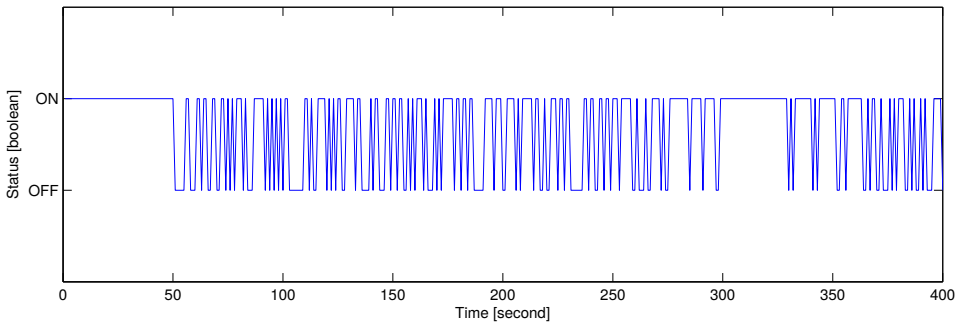

(c) Gyro

Figure 5.16: Sensor statuses in the first 400 seconds of the simulation in free tumbling mode with a decentaralized scheme

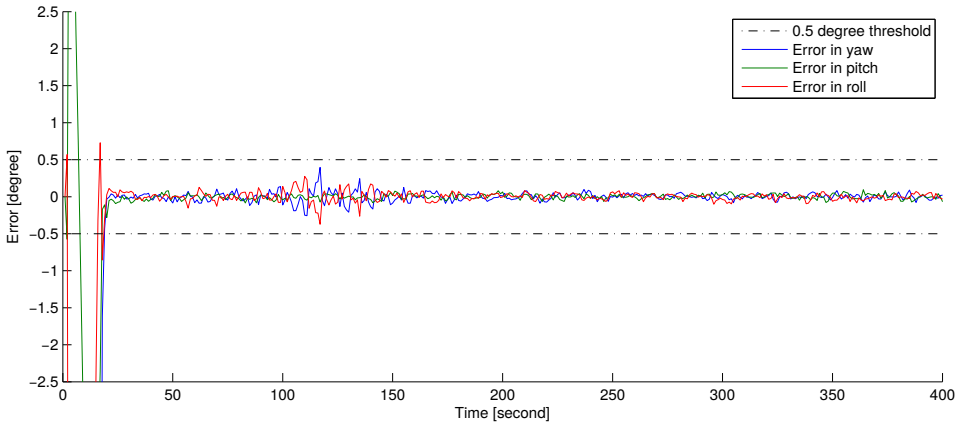

Figure 5.17: Simulation result of attitude determination at OBC in decentralized scenario while spacecraft is tumbling

Table 5.12: Simulation results of decentralized energy manager in free tumbling scenario

Parameter	Value	Unit
Simulation length	400	[s]
Sun sensor activation period	234	[s]
Sun sensor duty cycle	58.5%	-
Magnetometer activation period	314	[s]
Magnetometer duty cycle	78.5%	-
Gyro activation period	266	[s]
Gyro duty cycle	66.5%	-

Pointing (DEC_P)

This scenario presents a spacecraft in pointing mode while a decentralized energy management algorithms are employed. Initial conditions and parameter are similar to REF_P but the energy manager is active and trying to reach the attitude precision goal similar to CEN_P. The result of this test can be compared to REF_P and CEN_P simulations. The maneuver is $(30^\circ - 15^\circ - 60^\circ)$ and the parameters of the controller are not changed. Figures 5.18, 5.19 and 5.20 show the local attitude estimations. Status of each node is presented in Figure 5.21. These results show that the local estimation of spacecraft attitude is within the desired precision on each node. Comparing this results with Figure 5.22 shows that the ADCS performance on each nodes is quite comparable to the federated result at OBC. Also we can see that all estimators show a quick convergence and meet the ADCS accuracy requirements.

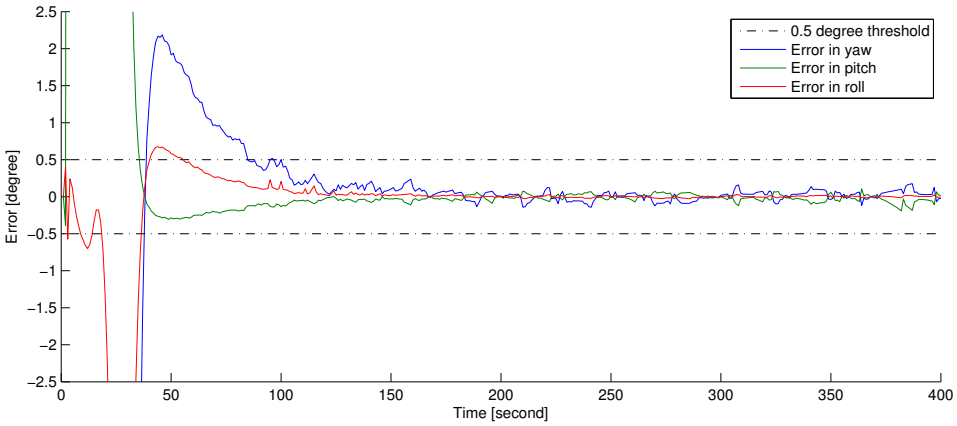

Figure 5.18: Simulation results of local attitude determination in Sun sensor in DEC_p scenarion

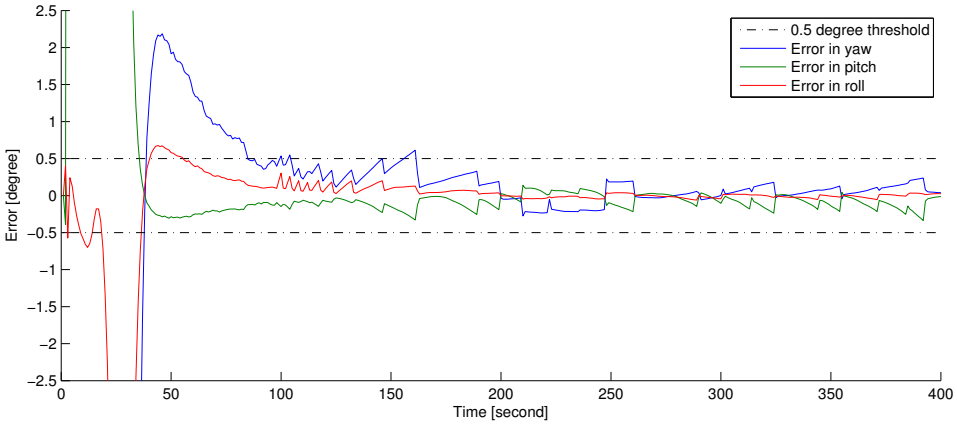

Figure 5.19: Simulation results of local attitude determination at magnetometer node in DEC_p scenarion

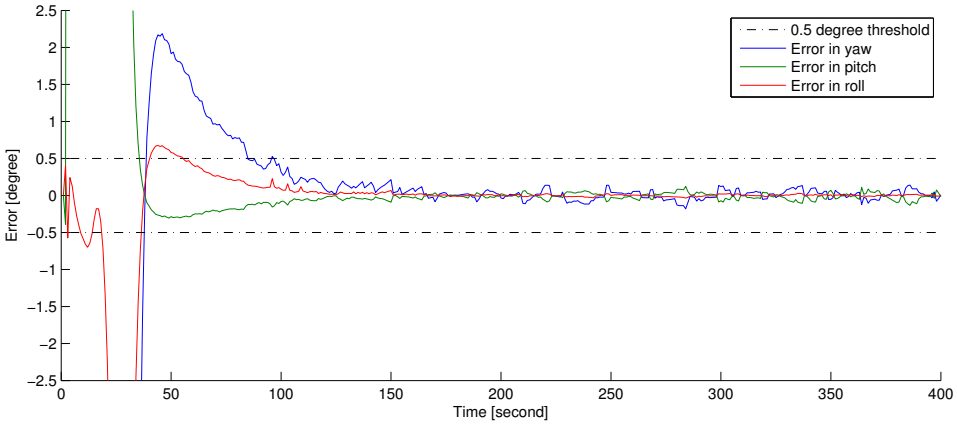

Figure 5.20: Simulation results of local attitude determination at gyro node in DEC_p scenarion

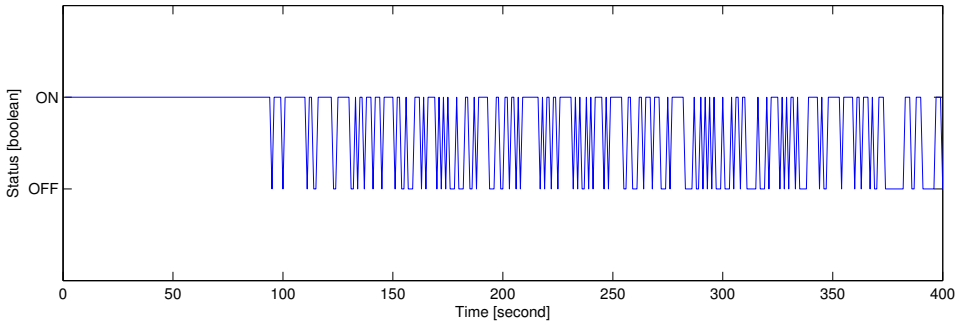

(a) Sun sensor activation status

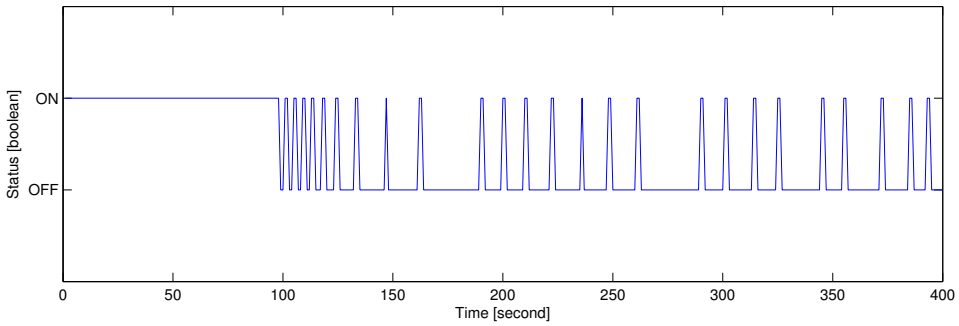

(b) Magnetometer activation status

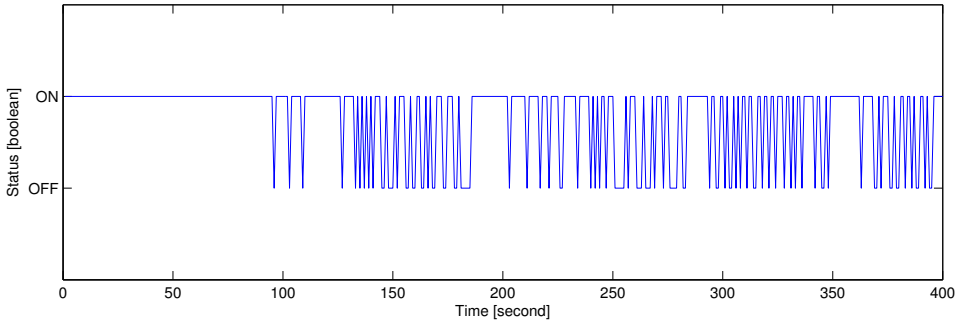

(c) Gyro activation status

Figure 5.21: Sensor statuses are shown here for the first 400 seconds of the simulation DEC_P scenario

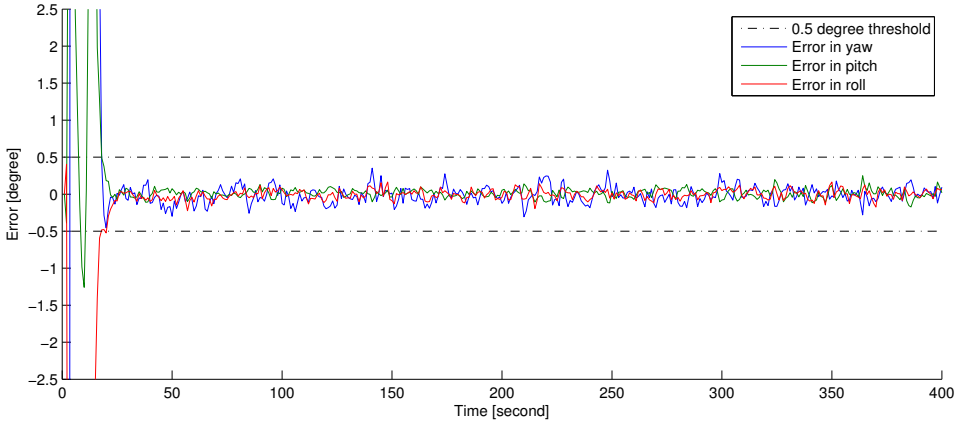

Figure 5.22: Simulation results of attitude determination at OBC for decentralized attitude determination and energy management in a pointing scenario

Table 5.13 presents the characteristics of the local estimators on each node. Similar to the benchmark test, the mean of the estimation residuals are very close to zero for pitch and role which refers to the healthy operation of the estimators. However, the mean of the yaw residuals has significantly deviated from zero comparing to the previous scenarios. This can indicate that the operation of the filter is suboptimal for this estimation mode.

The status of the wireless transmitters is shown in Figure 5.21. Similar to the previous scenarios, 'ON' status means that the sensor's wireless transmitter is activated, while 'OFF' means that it is switched to off or sleep mode. In 'ON' mode, the node makes a local measurement vector, establishes a connection to OBC and transmits the local information vector and local information matrix

Table 5.13: Attitude estimation results in $\mathrm{DEC_P}$ scenario

Parameter	Value	Unit
Convergence time	$\tau_{SS,y}=85$, $\tau_{MM,y}=82$, $\tau_{G,y}=85$	[s]
(Error less than 0.5 degree)	$\tau_{SS,p}=37$, $\tau_{MM,p}=38$, $\tau_{G,p}=38$	[s]
	$\tau_{SS,r}=56$, $\tau_{MM,r}=56$, $\tau_{G,r}=56$	[s]
Estimation error mean	$\mu_{SS,y}=0.22$, $\mu_{MM,y}=0.27$, $\mu_{G,y}=0.21$	[deg]
(after convergence)	$\mu_{SS,p}=0.05$, $\mu_{MM,p}=-0.01$, $\mu_{G,p}=0.05$	[deg]
	$\mu_{SS,r}=0.06$, $\mu_{MM,r}=0.08$, $\mu_{G,r}=0.06$	[deg]
Estimation error, 1-sigma	$\sigma_{SS,y}=0.14$, $\sigma_{MM,y}=0.14$, $\sigma_{G,y}=0.16$	[deg]
(after convergence)	$\sigma_{SS,p}=0.08$, $\sigma_{MM,p}=0.07$, $\sigma_{G,p}=0.07$	[deg]
	$\sigma_{SS,r}=0.09$, $\sigma_{MM,r}=0.08$, $\sigma_{G,r}=0.11$	[deg]

Table 5.14: Simulation results of decentralized energy manager in pointing scenario

Parameter	Value	Unit
Simulation length	400	[s]
Sun sensor activation period	275	[s]
Sun sensor duty cycle	68.8%	-
Magnetometer activation period	146	[s]
Magnetometer duty cycle	36.5%	-
Gyro activation period	299	[s]
Gyro duty cycle	74.7%	-

accordingly. It also receives the relayed information from other sensor nodes. In 'OFF' mode, the local microprocessor continues operation of its information filter without receiving new information vectors from other sensors. We can observe that all sensors are frequently employed during the initial moments of the simulation and then the frequency of activation is remarkably reduced after the convergence of the estimators. It can be observed that the gyro has been switcheded "OFF" mode less often relative to the two other sensors, while magnetometer duty cycle is significantly reduced. This could be due to noise characteristics of the magnetometer which is assumed to be superior to the other two sensors and therefore fewer measurements deliver satisfactory results. We can conclude that by employing more accurate sensors the performance of energy management scheme can be positively affected.

5.3 Discussion

The presented results exhibit that employing an energy management scheme integrated with spacecraft attitude determination allows a very meaningful improvement in efficient use of on-board sensors without compromising the attitude determination accuracy. Comparing the results of centralized and decentralized energy management schemes shows no significant difference between their performance in a tumbling or pointing scenario. This result was expected as in Section 4.3.2 we showed that a central or decentralized scheme will converge to a unique solution given certain conditions. Although removing some of the measurements defects this convergence, the similarity of various suboptimal estimators demonstrates and confirms the theory.

5.3.1 Filter Performance

Usually performance measures such as root mean square error (RMSE) and mean average error (MAE) are used to evaluate the performance of model-produced estimates, such as Kalman filters [Chai and Draxler 2014].

The MAE measures the average magnitude of the errors in a set of forecasts, without considering their direction. It measures accuracy of continuous variables. The MAE is the average over the verification sample of the absolute values of the differences between forecast and the corresponding observation. The MAE is a linear score which means that all the individual differences are weighted equally in the average and is calculated as

$$\mathrm{MAE} = \frac{1}{n}\sum_{i=1}^{n}|e_i|. \tag{5.39}$$

On the other hand, the RMSE is a quadratic scoring rule which measures the average magnitude of the error. Expressing the equation in words, the difference between forecast and corresponding observed values are each squared and then averaged over the sample. Finally, the square root of the average is taken. Since the errors are squared before they are averaged, the RMSE gives a relatively high weight to large errors. This means the RMSE is most useful when large errors are particularly undesirable. RMSE is calculated as

$$\mathrm{RMSE} = \sqrt{\frac{1}{n}\sum_{i=1}^{n}e_i^2}. \tag{5.40}$$

The MAE and the RMSE can be used together to diagnose the variation in the errors in a set of forecasts. The RMSE will always be larger or equal to the MAE; the greater difference between them, the greater the variance in the individual errors in the sample.

Both the MAE and RMSE can range from zero to infinity. They are negatively-oriented scores, thus lower values are better.

Table 5.15 presents performance parameters of simulated scenarios and compares them with the benchmarks. For the decentralized scenarios, some values are marked by star (*) which present the maximum value of the calculated parameter among the sensor nodes.

Observing the values in the table shows that most RMSE and MAE from different simulations are very small and comparable, which means that the estimators are producing consistent results. If the RMSE is equal to MAE, then all the errors are of the same magnitude [Avazpour et al. 2014]. This table shows that the error in yaw calculation has been consistently larger across various simulations comparing to roll and pitch. The cause of this phenomenon is

Table 5.15: Comparison of convergence time, mean average error (MAE) and root mean square error (RMSE) of different energy managers against the benchmarks. The values which are marked by star (*) represent the maximum value of the calculated parameter among the nodes.

	$\mathbf{REF}_T$	$\mathbf{CEN}_T$	$\mathbf{DEC}_T$	$\mathbf{REF}_P$	$\mathbf{CEN}_P$	$\mathbf{DEC}_P$	**Unit**
$\mathbf{max}\{\tau_p, \tau_y, \tau_r\}$	32	35	18	42	55	85	[s]
$\mathbf{MAE}_{\mathbf{yaw}}$	0.12	0.18	0.11*	0.15	0.17	0.32*	[deg]
$\mathbf{MAE}_{\mathbf{pitch}}$	0.11	0.07	0.06*	0.07	0.11	0.11*	[deg]
$\mathbf{MAE}_{\mathbf{roll}}$	0.12	0.13	0.09*	0.06	0.06	0.09*	[deg]
$\mathbf{RMSE}_{\mathbf{yaw}}$	0.03	0.07	0.17*	0.03	0.04	0.31*	[deg]
$\mathbf{RMSE}_{\mathbf{pitch}}$	0.02	0.01	0.10*	0.01	0.02	0.02*	[deg]
$\mathbf{RMSE}_{\mathbf{roll}}$	0.03	0.03	0.14*	0.01	0.01	0.03*	[deg]

not visible due to the nonlinearity of Extended Kalman filter and the mapping between sensor measurements and yaw, pitch and roll estimates. From the maximum convergence time it can be seen that the pointing scenarios generally have a larger convergence time comparing to tumbling scenarios. The reason can be extra nonlinearity which is added to the system equations due to the controller term and related disturbances.

5.3.2 Energy Savings

The presented simulations have shown that enabling the energy manager can significantly reduce the usage of sensor measurements. This will directly translate to less sensor head activation per OWSAN node.

To obtain a characterization of the energy saving potential, a set of standard ADS sensors are chosen and their electrical characteristics are enlisted in Table 5.16. The sensors are typically integrated with an interface harness such as SpaceWire, MIL-STD-1553, RS-422, etc. which is not only heavy and large (see Chapter 2) but adds energy consumption overhead as well. For example BU-67401L which is an ultra low power MIL-STD-1533 transceiver consumes 80mW in idle mode and 500mW in active mode [BU67401L 2011]. These ratings are significantly larger than similar electrical characteristics of a ZigBee transceiver. Instead of a wired data bus controllers, we assume that a standard COTS IEEE 802.15.4 transceiver such as Texas Instruments CC2530 is integrated with each sensor to wirelessly transmit the data to OBC. This chip is capable of running various ZigBee profiles [Texas Instruments 2010]. Depending on the network configuration and topology, some profiles such as ZigBee PRO may introduce a larger control overhead in order to establish and maintain the communica-

Table 5.16: Electrical characteristics of selected sensors and components.

Component	Manufacturer	Power [mW]
Tri-axial gyro (SiRRS01)	Silicon Sensing	250
Tri-axial magnetometer	SSBV	750
ZigBee transceiver (CC2530)	Texas Instruments	TX= 100 Active= 26 Idle= 0.3
Microcontroller (MSP430)	Texas Instruments	Active= 1.8 Idle=0.27

tion between nodes but the impact of this overhead is negligible. There are also some extremely low overhead ZigBee profiles such as RF4CE with less flexibility and features. The selection of the profile is out of the scope of this work and the impact on the results is negligible specially for OWSAN where the number of nodes is limited. The sensor part of the Sun sensor is not consuming energy therefore it is dropped from this discussion. The information in Table 5.16 together with duty cycle information results from the simulation of each scenario allows to calculate the energy consumption of each node. In centralized schemes, the sensor head and RF transceiver can both enter idle mode during the 'OFF' period. The decentralized scheme brings a higher demand for computation and complexity on the sensor nodes but potentially improves the robustness, flexibility and reconfigurability of the architecture. To accommodate this computation demand, we have assumed that a micro controller (MSP430) is also added to the node. This micro controller family is widely used in the industry to run Kalman filters onboard nano and pico spacecraft.

Table 5.17 presents the energy consumption in each scenario. Only the major components are accounted which are sensor head, RF transceiver and micro controller (where needed). Calculation is based on the following assumptions:

1. CC2530 is used only for utilizing the wireless communication with the OBC. No filtering is running on this chip, so the chip can go to idle mode immediately after transmitting the data (or receiving scheduling info from OBC);

2. In decentralized scenarios, MSP430 runs the Kalman filter on the sensor nodes. Therefore it is assumed that this chip is always in active mode;

3. Sensor heads can switch off as soon as the measurement is delivered to CC2530. It is assumed that the sensor head wake up time is less than the sampling period.

Table 5.17: Comparison of total energy consumption of ADS nodes excluding OBC and Sun sensor. In this table E_{RF} is the total energy consumption of RF transceivers and E_{MCU} is the total energy consumption of micro controllers. Total simulation time is 400 seconds.

	REF$_T$ or REF$_P$	**CEN$_T$**	**DEC$_T$**	**CEN$_P$**	**DEC$_P$**	**Unit**
Total Sensors active time	80.00	42.10	58.00	43.70	44.50	[s]
Total RF airtime	1.60	0.84	1.16	0.87	0.89	[s]
Total MCUs active time	-	-	800.00	-	800.00	[s]
Total consumed energy (E)	40.39	22.93	31.92	19.79	20.09	[J]
E_{RF}/E	0.004	0.004	0.004	0.004	0.004	-
E_{MCU}/E	-	-	0.045	-	0.072	-
E_{MCU}/E_{RF}	-	-	11.25	-	18.00	-

4. The startup time of sensors is assumed to be 100 milliseconds. This is the time it takes to go from OFF to ON state and produce a measurement and hand it over to the RF transceiver. It should be considered that the typical startup time of new generations of COTS gyros and magnetometers is much lower than 100 milliseconds.

5. It is assumed that the total air time of RF transceiver per measurement transmission equals to 2 milliseconds. ZigBee nominal communication speed is 250 Kbps. This time window is enough to communicate 500 Bytes of data to the OBC, which is more than enough to meet the bandwidth needed for this application including the measurement overhead.

Reviewing Table 5.17 results leads to a number of important observations.

- The total energy consumption of benchmark simulations, REF_T and REF_P , can be directly compared to other scenarios. The energy saving due to employing the sensor scheduling technique is significant and varying between 20.9% (DEC_T) and 51% (CEN_P).

- Obviously the biggest energy sink is the sensor head. Therefore, reducing sensor head energy consumption and startup time by using advanced electronics or MEMS technology will be very rewarding in reducing overall consumption. Employing the technologies which are used in designing advanced COTS MEMS sensors for improving the characteristics of space qualified sensors can be a direction for future research.

- From the ratio of E_{MCU}/E and Table 5.16 we can conclude that the contribution of MSP430 micro controller to the total energy consumption is very negligible comparing to the sensor head. Thus any effort to reduce the sensors activation periods onboard a spacecraft by adding complex

filtering algorithms can greatly reduce the overall energy consumption. In other words, the trade off between computation power and sensor activation can be very beneficial. However, there is a limit to this because the average energy consumption of a more powerful digital signal processor (DSP) is significantly larger than ultra low power micro controllers such as MSP430.

- It can be seen from the E_{MCU}/E_{RF} ratio that although the RF transceiver airtime has been very limited in both decentralized scenarios, but the total energy consumption of the micro controller and the RF transceiver are rather comparable in comparison with the activation period of these two modules. The design should avoid increasing the RF activities which can quickly explode the total energy consumption.

The most significant conclusion from Table 5.17 is the total energy saving between 20.9% to 51% (depending on the scenario) due to employing the sensor scheduling approach without compromising the accuracy of attitude determination system. The results shows that the total energy consumed in centralized scenarios is lower than decentralized ones. It should be noted that the complexity of hardware and software on each node in a decentralized architecture will be significantly higher than that of a centralized ones.

Chapter 6

Conclusions

6.1 Summary

In this thesis, we have focused on intra-spacecraft wireless communication. This work is motivated by the recent advances in electronics industry which has enabled the possibility of revolutionizing spacecraft design and architecture. As the result, advanced concepts such as modularity, interoperability, plug and play structure, fly-by-wireless can be realized in new space projects. This thesis has shown that wireless technology for onboard communication can be a major step towards spacecraft mass reduction.

In the following, summarized answers to the research questions are provided along with novel contributions of this research to the existing body of knowledge and the list of relevant research publications by the author.

Chapter 2 focuses on answering research questions 1 and 2 which were introduced in the thesis introduction (see Chapter 1, Page 20).

These questions were:

- What are the problems of onboard wired standards and what are the benefits and characteristics of wireless network onboard spacecraft?
- Which spacecraft subsystems could benefit the most from a wireless onboard communication paradigm?

Chapter 2 started with introducing different wired spacecraft command and data handling systems (CDHS) and justified the necessity for reducing bus harness. Thereafter, wireless standards were introduced and different design considerations were discussed. Then, different data types which are transmitted through spacecraft data bus were enlisted and major COTS

wireless standards (Wi-Fi, Bluetooth and ZigBee) were mapped into these data types to identify the most suitable standard for each application. After comparing various characteristics of spacecraft onboard subsystems and their characteristics, the chapter concluded that sensors of the ADCS can greatly benefit from a wireless communication standard such as Zigbee.

Resulting publications:

1. R. Amini, G. T. Aalbers, R. J. Hamann, W. Jongkind. New Generations of Spacecraft Data Handling systems : Less Harness more Reliability. In *Proceedings of the* 57^{th} *International Astronautical Congress*, Valencia, Spain, 2006.

2. G. T. Aalbers, G.G. Gaydadijev, R. Amini. CDHS Design for a University Nanosatellite. In *Proceedings of the* 57^{th} *International Astronautical Congress*, Valencia, Spain, 2006.

3. W. J. Ubbels, A. R. Bonnema, R. J. Hamann, R. Amini, C. J. M. Verhoeven, J. A. P. Leijtens. The Delfi-C3 Student Nanosatellite, an Educational Testbed for Wireless Technology in Space, In *Proceedings of Wireless for Space Applications Workshop*, ESA/ESTEC, Noordwijk, The Netherlands, 2006.

Chapter 3 explained the details of the wireless communication architecture to find an answer to the research question 3 which was:

- What is the major challenge regarding employing a wireless standard onboard a spacecraft?

This Chapter reviewed major available wireless communication services. Then it compared these services with an intra-spacecraft wireless network. As a result, onboard wireless sensor actuator network (OWSAN) was formulated as a new category next to wireless sensors and actuators network (WSAN). In the sequel, the issue of energy conservation for OWSAN nodes was discussed as a major system level challenge in designing a wireless architecture. Finally, the basic design of an energy manager for sensor nodes of OWSAN was drawn and discussed.

Resulting publications:

1. R. Amini, E. K. A. Gill, G. N. Gaydadjiev. The Challenges of Intra-Spacecraft Wireless Data Interfacing. In *Proceedings of the 58th International Astronautical Congress*, Hyderabad, India, 2007.

2. A. A. Vaartjes, R. J. Hamann, R. Amini. Integration and verification of a command and data handling subsystem for nano-satellite projects with critical time constraints: Delfi-C3, In *Proceedings of the* 58^{th} *International Astronautical Congress*, Hyderabad, 2007.

In **Chapter 4**, first we developed the mathematical framework necessary to answer research question 4 which was:

- How can we solve the identified system level design challenge?

As identified in Chapter 3, the major system design challenge is conserving energy in each OWSAN node. To approach this challenge, we proposed two onboard energy managers based on sensor scheduling scheme and tailored to attitude determination and control sensors. Although both energy managers use similar design elements, one of them presented a centralized management scheme while the other one a decentralized architecture. A unique characteristic of these designs was identified as being fully integrated with the onboard attitude determination system of the spacecraft. Thus, spacecraft attitude determination needed to be fully understood and modeled to facilitate the energy manager formalization.

Resulting publications:

1. D. Torczynski, R. Amini, P. Massioni. Magnetorquer Based Attitude Control for a Nanosatellite Test Platform. In *Proceedings of AIAA Infotech@Aerospace Conference*, Atlanta, USA, 2010.
2. N.E. Cornejo, R. Amini, G. N. Gaydadjiev, Model-Based Fault Detection for the DELFI-N3XT Attitude Determination System, *Proceedings of IEEE Aerospace Conference*, Big Sky, USA, 2010.
3. S. Brak, R. Amini, P. Massioni. Student Nano-satellite Development: from Passive Stabilization to Three-Axis Active Attitude Control. In *Proceedings of the* 32^{nd} *Annual AAS Rocky Mountain Guidance and Control Conference*, Breckenridge, USA, 2009.

Chapter 5 sketched two realistic ADCS scenarios and evaluated the performance of the centralized and decentralized energy managers. The scenarios simulated tumbling and pointing modes of a LEO spacecraft. The results showed dramatic reduction in energy consumption of wireless transmitters on the sensor nodes after enabling the energy managers. The simulations showed that the activities of transmitters were reduced by 22% to 55% of the nominal situations depending on the scenario. Later in this chapter (Section 5.3), the energy saving schemes were exercised with actual electronics components.

The results showed that the trade off between computation power and sensor activation can be very beneficial and any attempt to lower the sensors activity can be very rewarding. The results showed total energy savings between 20.9% to 51% (depending on the scenario) without compromising the accuracy of attitude determination system.

Resulting publications:

1. R. Amini, E. K. A. Gill, G. N. Gaydadjiev. Decentralized Energy Management for Spacecraft Attitude Determination. In *Proceedings of the* 2^{nd} *CEAS European Conference on Guidance, Navigation & Control*, Delft, The Netherlands, 2013.

2. R. Amini, G. N. Gaydadjiev, E. K. A. Gill. Smart Power Management for an Onboard Wireless Sensors and Actuators Network. In *Proceedings of AIAA Space Conference & Exposition*, Pasadena, USA, 2009.

In addition, the following patent was filed as the result of this dissertation:

> R. Amini, E. K. A. Gill, G. N. Gaydadjiev. An Attitude Determination System Suitable for a Spacecraft. NL Patent no. 48.293-VB. (Issued Nov. 10, 2010)

6.2 Future Research Directions

The field of intra-spacecraft wireless communication in space applications is still in the early stages of its development. The contribution of this thesis to this field, although significant, does not solve many challenges of intra-spacecraft wireless communication. Here, we focused on the energy management problem which is one of the many challenges. In the following, various promising research directions are provided which can benefit from the results of this research.

- The COTS wireless communication standards which were studied are developed for the office environment and therefore their communication protocols can be significantly simplified for less complex applications such as intra-spacecraft communication. Achieving this goal will require an in-depth study of possibilities and ultimately designing a simplified wireless communication standard for space application based on a COTS solution. This, however, is expected to bring significant advantages in terms of simplifying communication protocol and reducing overheads.

- In this work we did not study a full mesh network configuration where ADCS sensors and actuators can directly communicate in absense of OBC. Instead our configuration uses spacecraft onboard computer as a relay and communication medium. However, this role can be ultimately removed to achieve a higher degree of robustness and autonomy by using capabilities of the IEEE 802.15.4 standard.

- A truly decentralized ADS architecture implies that the sensor nodes have specific computational power. We showed that this computation power can be used to run estimation algorithms and energy managers on each sensor to reduce the sensor activities without impacting the ADS performance. Furthermore we showed that this trade-off is very rewarding. A further step will be to identify the limits of this trade-off to optimize the system architecture.

- We showed that the sensor front end energy consumption has the largest contribution to the overall energy consumption of the ADS system. A future research direction can be exploring the possibility of applying MEMS design techniques to lower energy consumption of sensors and their startup time for space applications. This could result in a more efficient switching and larger flexibility in designing sensor scheduling solutions.

List of Publications

Patents

R. Amini, E.K.A.. Gill, G.N. Gaydadjiev. An Attitude Determination System Suitable for a Spacecraft. NL Patent no. 48.293-VB. (Issued Nov. 10, 2010)

Publications

1. R. Amini, G. T. Aalbers, R.J. Hamann, W. Jongkind. New Generations of Spacecraft Data Handling systems : Less Harness more Reliability. In *Proceedings of the* 57^{th} *International Astronautical Congress*, Valencia, Spain (2006).

2. F.M. Poppenk, R. Amini. Delfi-C3 control system development and verification. In *Proceedings of the* 57^{th} *International Astronautical Congress*, Valencia, Spain, (2006).

3. G.T. Aalbers, G.N. Gaydadijev, R. Amini. CDHS Design for a University Nanosatellite. In *Proceedings of the* 57^{th} *International Astronautical Congress*, Valencia, Spain, (2006).

4. W.J. Ubbels, A.R. Bonnema, R.J. Hamann, R. Amini, C.J. M. Verhoeven, J.A.P. Leijtens. The Delfi-C3 Student Nanosatellite, an Educational Testbed for Wireless Technology in Space, In *Proceedings of Wireless for Space Applications Workshop*, ESA/ESTEC, Noordwijk, The Netherlands, (2006).

5. R. Amini, E.K.A.. Gill, G.N. Gaydadjiev. The Challenges of Intra-Spacecraft Wireless Data Interfacing. In *Proceedings of the* 58^{th} *International Astronautical Congress*, Hyderabad, India, (2007).

6. J. Bowmeester, J., R. Amini, R. Hamann. Command and Data Handling Subsystem for a Satellite without Energy Storage: Delfi-C3. In *Proceedings of* 58^{th} *International Astronautical Congress*, Hyderabad, India, (2007).

7. F.M. Poppenk, R. Amini, G.F. Brouwer. Design and Application of a Helmholtz Cage for Testing Nano- satellites. In *Proceedings of* 58^{th} *International Astronautical Congress*, Hyderabad, India, (2007).

8. A.A. Vaartjes, R.J. Hamann, R. Amini. Integration and verification of a command and data handling subsystem for nano-satellite projects with critical time constraints: Delfi-C3, In *Proceedings of the* 58^{th} *International Astronautical Congress*, Hyderabad, India, (2007).

9. J. Elstak, R. Amini, R.J. Hamann. A comparative analysis of project management and systems engineering techniques in CubeSat projects. *INCOSE International Symposium*, Singapore, (2009).

10. S. Brak, R. Amini, P. Massioni. Student Nano-satellite Development: from Passive Stabilization to Three-Axis Active Attitude Control. In *Proceedings of the* 32^{nd} *Annual AAS Rocky Mountain Guidance and Control Conference*, Breckenridge, USA, (2009).

11. R. Amini, G.N. Gaydadjiev, E.K.A. Gill. Smart Power Management for an Onboard Wireless Sensors and Actuators Network. In *Proceedings of AIAA Space Conference & Exposition*, Pasadena, USA, (2009).

12. D. Torczynski, R. Amini, P. Massioni. Magnetorquer Based Attitude Control for a Nanosatellite Test Platform. In *Proceedings of AIAA Infotech@Aerospace Conference*, Atlanta, USA, (2010).

13. N.E. Cornejo, R. Amini, G.N. Gaydadjiev, Model-Based Fault Detection for the DELFI-N3XT Attitude Determination System, In *Proceedings of IEEE Aerospace Conference*, Big Sky, USA, (2010).

14. R. Amini, E.K.A.. Gill, G.N. Gaydadjiev. Decentralized Energy Management for Spacecraft Attitude Determination. In *Proceedings of the* 2^{nd} *CEAS European Conference on Guidance, Navigation & Control*, Delft, The Netherlands, (2013).

Bibliography

[Aalbers et al. 2006] G. Aalbers, G. Gaydadijev and R. Amini. CDHS design for a university nano-satellite. In *Proceedings of IAC 2006* (2006).

[Akyildiz et al. 2002] I. F. Akyildiz, W. Su, Y. Sankarasubramaniam and E. Cayirci. Wireless sensor networks: a survey. *Computer Networks*, 38:393–422 (2002).

[Alippi et al. 2009] C. Alippi, G. Anastasi, M. Di Francesco and M. Roveri. Energy management in wireless sensor networks with energy-hungry sensors. *Instrumentation Measurement Magazine, IEEE*, 12(2):16–23 (2009).

[Alippi et al. 2007] C. Alippi, G. Anastasi, C. Galperti, F. Mancini and M. Roveri. Adaptive sampling for energy conservation in wireless sensor networks for snow monitoring applications. In *Mobile Adhoc and Sensor Systems, 2007. MASS 2007. IEEE Internatonal Conference on*, pages 1–6 (2007).

[Alminde et al. 2004] L. Alminde, M. Bisgaard, D. Vinther, T. Viscor, and K. Z. Ostergard. The aau-cubesat student satellite project: architectural overview and lessons learned. In *16th IFAC Symposium on Automatic Control in Aerospace*, Russia (2004).

[Amini et al. 2005] R. Amini, J. A. Larsen, R. Izadi-Zamanabadi and D. Bhanderi. Design and implementation of a space environment simulation toolbox for small satellites. In *Proceedings of 25th International Astronautical Congress* (2005).

[Anderson 1998] D. Anderson. *FireWire system architecture, IEEE 1394*. PC system architecture series. MA Addison Wesley (1998).

[Andonovic et al. 2010] I. Andonovic, K. H. Kwong, C. Michie and M. Gilroy. Monitoring of farm animals with wireless sensor networks. In *Advanced Intelligence and Awarenss Internet (AIAI 2010), 2010 International Conference on* (2010).

[Araujo et al. 2009] J. Araujo, H. Sandberg and K. H. Johansson. Experimental validation of a localization system based on a heterogeneous sensor network. In *ASCC : 2009 7TH ASIAN CONTROL CONFERENCE*, pages 465–470. IEEE. QC 20110114 (2009).

[Arrawatia et al. 2011] M. Arrawatia, M. Baghini and G. Kumar. Rf energy harvesting system from cell towers in 900mhz band. In *Communications (NCC), 2011 National Conference on*, pages 1–5 (2011).

[Arruego et al. 2003] I. Arruego, S. Rodriguez, M. Michelena and H. G. (INTA). In-orbit experimen of intra-satellite optical wireless link onboard Nanosat-01. Presentation to the ESTEC wireless onboard spacecraft workshop (2003).

[Avazpour et al. 2014] I. Avazpour, T. Pitakrat, L. Grunske and J. Grundy. *Recommendation Systems in Software Engineering*, chapter 12. Springer (2014).

[AXON 2008] AXON. *AXON' CABLE - Cables and Harness for Space Applications*. AXON Cable & Interconnect, d edition (2008). `http://www.axon-cable.com/pdf/MILSTD1553%20DATABUS.pdf`, visited on: 15-11-2009.

[Bak 1999] T. Bak. *Spacecraft Attitude Determination : A Magnetometer Approach*. PhD thesis, Aalborg University (1999).

[Bandyopadhyay and Coyle 2005] S. Bandyopadhyay and E. J. Coyle. Spatio-temporal sampling rates and energy efficiency in wireless sensor networks. *IEEE/ACM Transaction on Networking (TON)*, 13(6):1339–1352 (2005).

[Bar-Itzhack and Oshman 1985] I. Y. Bar-Itzhack and Y. Oshman. Attitude determination from vector observations: Quaternion estimation. *IEEE Transactions on Aerospace and Electronic Systems*, AES-21:128–136 (1985).

[Barnes et al. 2002] C. Barnes, M. Ott, A. Johnston, K. Label, R. Reed, C. Marshall and T. Miyahira, editors. *Photonics for space environments VIII*, volume 4823, chapter Recent photonic activities under the NASA electronics parts and packaginf (NEPP) program. SPIE (2002).

[Berland 2003] B. Berland. Photovoltaic Technologies Beyond the Horizon: Optical Rectenna Solar Cell. Technical report, National Renewable Energy Laboratory (NREL) (2003).

[Bertsimas and Tsitsiklis 1997] D. Bertsimas and J. Tsitsiklis. *Introduction to Linear Optimization*. Athena Scientific, 1st edition (1997).

[Bevan et al. 2003] M. G. Bevan, M. A. G. Darrin, S. C. Walts, W. Schneider, C. S. Mills and R. F. Conde. Free-space optical data bus for spacecraft. In *Earth Science Technology Conference*. NASA (2003).

[Bever 1991] G. A. Bever. Digital signal conditioning for flight test instrumentation. Technical report, NASA (1991).

[Bierman 1977] G. J. Bierman. *Factorization Methods for Discrete Sequential Estimation*. Academic Press (1977).

[Blackburn et al. 1969] E. P. Blackburn, D. DeBra, B. Dorbrotin, J. Scull, R. E. Fischell, D. Fosth, J. Kelly, A. J. Fleig, H. Perkel, R. E. Roberson, J. Rodden, B. Tinling, S. O'Neil, F. J. Carroll and R. F. Bohling. Spacecraft mangetic torques. Technical Report SP-8018, NASA (1969).

[Boi et al. 2005] R. Boi, S. Brigati, F. Francesconi, C. Ghidini, P. Malcovati1, F. Maloberti1 and M. Poletti. A 0.8 μm soi cmos on-board data handling bus modem for satellite applications. In *Proceedings of the 26th European Solid-State Circuits Conference ESSCIRC '00*, Italy (2005).

[Bouffard et al. 1995] M. Bouffard, J. P. Gardelle, M. L. Moine and P. Temporelli. Soho: A modular spacecraft concept to allow flexible payload integration and efficient development. *Acta Astronautica*, 37:277– 291 (1995).

[Brouwer et al. 2000] M. Brouwer, A. Castelijn, H. van Ingen Schenau, B. Oving, L. Timmermans and T. Zwartbol. Developments in test and verification equipment for spacecraft. Technical Report NLR-TP-2000-658, NLR (2000).

[BU67401L 2011] BU67401L. Ultra compact & low power +3.3v dual mil-std-1553 transceiver (2011). `http://www.ddc-web.com/Products/248/Default.aspx`.

[Busch et al. 2004] C. Busch, M. Magdon-Ismail, F. Sivrikaya and B. Yener. Contention-free mac protocols for wireless sensor networks. In *IN DISC*, pages 245–259 (2004).

[Carayon et al. 2002] J. Carayon, V. Dubourg, P. Danto and G. Galea. An innovative onboard computer for cnes microsatellites. In *21^{th} IEEE Digital Avionics Systems Conference (DASC)*, pages 1–5 (2002).

[Carlson et al. 2010] E. Carlson, K. Strunz and B. Otis. A 20 mv input boost converter with efficient digital control for thermoelectric energy harvesting. *Solid-State Circuits, IEEE Journal of*, 45(4):741–750 (2010).

[Carmo et al. 2010] J. Carmo, L. Goncalves and J. Correia. Thermoelectric microconverter for energy harvesting systems. *Industrial Electronics, IEEE Transactions on*, 57(3):861–867 (2010).

[Carruthers and Kahn 1998] J. Carruthers and J. Kahn. Angle diversity for nondirected wireless infrared communication. In *Communications, 1998. ICC 98. Conference Record.1998 IEEE International Conference on*, volume 3, pages 1665–1670 (1998).

[Cayirci et al. 2005] E. Cayirci, T. Coplu and O. Emiroglu. Power aware many to many routing in wireless sensor and actuator networks. In *Wireless Sensor Networks, 2005. Proceeedings of the Second European Workshop on*, pages 236–245 (2005).

[CC2420] CC2420 *CC2420 2.4 GHz IEEE 802.15.4 /ZigBee-ready RF Transceiver*. Chipcon Products.

[CCSDS Secretariat 2013] CCSDS Secretariat. Recommendation for space data system practice. spacecraft onboard interface systems-low data-rate wireless communications for spacecraft monitoring and control. Technical report, NASA (2013).

[Chai and Draxler 2014] T. Chai and R. R. Draxler. Root mean square error (rmse) or mean absolute error (mae)? arguments against avoiding rmse in the literature. *Geoscientific Model Development*, 7(3):1247–1250 (2014).

[Champaigne 2003] K. Champaigne. Wireless sensors onboard spacecraft. Technical report, Presentation to the ESTEC wireless onboard spacecraft workshop (2003).

[Chau et al. 1999] S. Chau, L. Alkalai, A. Tai and J. Burt. Design of a fault-tolerant cots-based bus architecture. *Reliability, IEEE Transactions on*, 48(4):351–359 (1999).

[Chen et al. 2002] B. Chen, K. Jamieson, H. Balakrishnan and R. Morris. Span: an energy-efficient coordination algorithm for topology maintenance in ad hoc wireless networks. *Wirel. Netw.*, 8:481–494 (2002).

[Chen and Trajkovic 2004] H. Chen and L. Trajkovic. Trunked radio systems: traffic prediction based on user clusters. In *Wireless Communication Systems, 2004. 1st International Symposium on*, pages 76–80 (2004).

[Chu et al. 2006] D. Chu, A. Deshpande, J. M. Hellerstein and W. Hong. Approximate data collection in sensor networks using probabilistic models. In *Proceedings of the 22nd International Conference on Data Engineering*, ICDE '06, pages 48–48, Washington, DC, USA. IEEE Computer Society (2006).

[CHU 2015] J. CHU. *Dynamics, distributed control and autonomous cluster operations of fractionated spacecraft*. PhD thesis, Delft University of Technology (2015).

[Chung et al. 1999] E.-Y. Chung, L. Benini and G. De Micheli. Dynamic power management using adaptive learning tree. In *Proceedings of the 1999 IEEE/ACM international conference on Computer-aided design*, ICCAD '99, pages 274–279, Piscataway, NJ, USA. IEEE Press (1999).

[Condor Engineering Inc. 2004] Condor Engineering Inc. ML-STD-1553 protocol tutorial. Technical report, Condor Engineering Inc. (2004).

[Culp 1979] A. W. Culp. *Principles of Energy Conversion*. McGraw-Hill, New York (1979).

[Department of Defense (DoD) 1999] Department of Defense (DoD), editor. *Parametric Cost Estimating Handbook - Joint Government/Industry Initiative*. DoD, second edition (1999).

[Eckerley et al. 2005] S. Eckerley, J. Schalk, O. Coumar and K. Haira. The eads micropack. In *5th round table on micro/nano technologies for space, ESA-ESTEC* (2005).

[ECSS 2005] ECSS. Space engineering standards. recommendations for can bus in spacecraft onboard applications. Technical report, European Cooperation for Space Standardization (ECSS) at ESA-ESTEC, The Netherlands (2005).

[ECSS 2008] ECSS. Ecss-e-st-50-12c - spacewire - links, nodes, routers and networks. Technical Report ECSS-E-50-12 Draft 4, ESA, Netherlands (2008).

[Elias 2000] M. Elias. Development of a low cost, fault tolerant, and highly reliable command and data handling computer (pulse^{TM}). In *The 19th Digital Avionics Systems Conference*, pages 8B4/1–8B4/8 (2000).

[Emrich 2005] A. Emrich. Can application in avionics. Technical report, Omnisys Instruments AB, Sweden (2005).

[ESA 1979] ESA. *Spacecraft Data Handling Interface Standards*, ttc.b.01 issue 1 edition (1979).

[ESA 1983] ESA. Service manipulator subsystem. Technical Report TPA/SPEC/48 issue 1, European Space Agency (1983).

[ESA 1998] ESA, editor. *ENVISAT - Europe's Earth Observation Mission for the new Millennium*, volume 60, The Netherlands. ESA, European Space Agency (1998).

[Etschberge 2001] K. Etschberge. *Controller Area Network*. IXXAT Automation GmbH (2001).

[Euler 1770] L. Euler. Problema algebraicum ob affectiones prorsus singulares memorabile. *Novi Commentarii Academiae Scientarum Petropolitanae*, 15(33):101 (1770).

[Faridani 1986] H. M. Faridani. Performance of kalman filter with missing measurements. *Automatica*, 22:117–120 (1986).

[Farrel and Stuelpnagel 1966] J. L. Farrel and J. C. Stuelpnagel. A least squares estimate of spacecraft attitude. *SIAM review*, 8(3) (1966).

[Feriencik et al. 2006] M. Feriencik, K. Wehrle, A. A. Hutter and L. Garcia. Rf intra-satellite communication demonstrator. In *Wireless for space applications workshop* (2006).

[FireWire 2008] FireWire. Ieee standard for a high-performance serial bus. *IEEE Std 1394-2008*, pages 1–906 (2008).

[Futron Corp. 2002] Futron Corp. Space transportation costs: Trends in price per pound to orbit 1990-2000. Technical report, Futron (2002).

[Gantois et al. 2006] K. Gantois, F. Teston, O. Montenbruck, P. Vuilleumier, P. V. D. Braembussche and M. Markgraf. Mission and new technologies overview. In *Proceedings of The 4S Symposium*, Italy (2006).

[Gao et al. 2011] H. Gao, P. Baltus, R. Mahmoudi and A. van Roermund. 2.4ghz energy harvesting for wireless sensor network. In *Wireless Sensors and Sensor Networks (WiSNet), 2011 IEEE Topical Conference on*, pages 57–60 (2011).

[Gauss 1900] C. F. Gauss. *Werke*, volume VIII, pages 357–362. Konigliche Gesellschafr der Wisssenscafren (1900).

[Gayrard et al. 2003] J. D. Gayrard, M. Maignan, M. Sotom, B. Benazet and N. Venet. Applications of optical techniques in future communication payloads. In *Proceedings of 21st International Communications Satellite Systems Conf. and Exhibit (AIAA 2003-2297)*, Yokohama, Japan (2003).

[Gfeller and Bapst 1979] F. Gfeller and U. Bapst. Wireless in-house data communication via diffuse infrared radiation. *Proceedings of the IEEE*, 67(11):1474–1486 (1979).

[Gill et al. 2001] E. Gill, O. Montenbruck and H. Kayal. The BIRD satellite mission as a milestone toward gps based autonomous navigation. *Journal of the institute of navigation*, 48(2) (2001).

[Gill et al. 2006] E. Gill, O. Montenbruck, S. D. S. and S. Persson. Autonomous satellite formation flying for the prisma technology demonstration mission. In 16^{th} *AAS/AIAA Space Flight Mechanics Conference*, Florida (2006).

[Gill et al. 2010] E. Gill, P. Sundaramoorthy, J. Bouwmeester, B. Zandbergen and R. Reinhard. Formation flying within a constellation of nano-satellites: The qb50 mission. In *6th International Workshop on Satellite Constellation and Formation Flying*, Taiwan (2010).

[Goetzberger and Hoffmann 2005] A. Goetzberger and V. U. Hoffmann. *Photovoltaic Solar Energy Generation*. Springer (2005).

[Goldstein 1950] H. Goldstein. *Classical Mechanics*. Addison-Wesley (1950).

[Guerrero 2003] H. Guerrero. Trends and evolution of microsensors: Towards the 21st century transducing principles. In *Proceedings of 2nd Int. Conf. Integrated Micro/Nano-Technologies for Space*, Pasadena, USA (2003).

[Guo et al. 2009] P. Guo, T. Jiang, K. Zhang and H. H. Chen. Clustering algorithm in initialization of multi-hop wireless sensor networks. *Wireless Communications, IEEE Transactions on*, 8(12):5713–5717 (2009).

[Guo et al. 2006] Y. Guo, P. Corke, G. Poulton, T. Wark, G. Bishop-Hurley and D. Swain. Animal behaviour understanding using wireless sensor networks. In *Local Computer Networks, Proceedings 2006 31st IEEE Conference on*, pages 607–614 (2006).

[Guyomar et al. 2009] D. Guyomar, G. Sebald, E. Lefeuvre and A. Khodayari. Toward heat energy harvesting using pyroelectric material. *Journal of Intelligent Material Systems and Structures*, 20(3):265–271 (2009).

[Haartsen 2000] J. Haartsen. The bluetooth radio system. *Personal Communications, IEEE*, 7(1):28–36 (2000).

[Haebel 2004] W. Haebel. A new approach to provide high-reliability data systems without using space-qualified electronic components. *Acta Astronautica*, 55(3-9):563–571. New Opportunities for Space. Selected Proceedings of the 54th International Astronautical Federation Congress (2004).

[Hamann 1985] R. Hamann. Design techniques for robots: Space applications. *Robotics*, 1(4):223–250 (1985).

[Hamilton 1844] W. R. Hamilton. On quaternions; or a new system of imaginaries in algebra. *Philosophical Magazine*, 25:489–495 (1844).

[Han et al. 2004] Q. Han, S. Mehrotra and N. Venkatasubramanian. Energy efficient data collection in distributed sensor environments. In *Distributed Computing Systems, 2004. Proceedings. 24th International Conference on*, pages 590–597 (2004).

[Harte and Ofrane 2006] L. Harte and A. Ofrane. *Telecom Systems, PSTN, PBX, Datacom, IP Telephony, IPTV, Wireless and Billing*. Althos (2006).

[Hashemipour et al. 1988] H. Hashemipour, S. Roy and A. Laub. Decentralized structures for parallel kalman filtering. *Automatic Control, IEEE Transactions on*, 33(1):88–94 (1988).

[Havard et al. 2008] T. Havard, M. Sutton and D. Armon. Spacecraft functional sensitivity study. In *Proceedings of AIAA/6th Responsive Space Conference* (2008).

[Hill et al. 2000] J. Hill, R. Szewczyk, A. Woo, S. Hollar, D. Culler and K. Pister. System architecture directions for networked sensors. *SIGPLAN Not.*, 35:93–104 (2000).

[Hoffmeyer 2000] P. Hoffmeyer. The orsted satellite project. *Air & Space Europe*, 2(5):74–79 (2000).

[Hou et al. 2009] R. Hou, W. Ren and Y. Zhang. A wireless sensor network clustering algorithm based on energy and distance. In *Computer Science and Engineering, 2009. WCSE '09. Second International Workshop on*, volume 1, pages 439–442 (2009).

[Howard and Hardage 1999] J. Howard and D. Hardage. Spacecraft environments interactions: Space radiation and its effects on electronic systems. Technical Report NASA/TP-1999-209373, NASA Marshall Space Flight Center (1999).

[IEEE 1996] IEEE. IEEE standard for heterogeneous interconnect (hic) (low-cost, low-latency scalable serial interconnect for parallel system construction). *IEEE Std 1355-1995* (1996).

[IEEE 2000] IEEE. IEEE std 1394a-2000, IEEE standard for a high performance serial bus. Technical report, IEEE (2000).

[IEEE 2010] IEEE. Draft standard for information technology-telecommunications and information exchange between systems-local and metropolitan area networks-specific requirements part 3: Carrier sense multiple access with collision detection (csma/cd) access method and physical layer specifications amendment: Physical layer and management parameters for serial 40 gb/s ethernet operation over single mode fiber. *IEEE P802.3bg/D2.0, July 2010 (Amendment of IEEE Std 802.3-2008)*, pages 1–51 (2010).

[Incledon 2005] S. Incledon. A power converter for manned spacecraft from cots components. In 3^{rd} *International Energy Conversion Engineering Conference*, USA (2005).

[ISO11898 2003] ISO11898. *ISO 11898-1:2003(E) Road Vehicles - Controller Area Network (CAN) - Part 1: Data Link Layer and Physical Signalling*. International Organization for Standardization (ISO) (2003).

[Jain and Chang 2004] A. Jain and E. Y. Chang. Adaptive sampling for sensor networks. In *Proc. DMSNâĂŹ04*, pages 10–16 (2004).

[Johannessen and Aguirre-Martinez 1999] J. J. Johannessen and M. Aguirre-Martinez. Gravity field and steady-state ocean circulation mission. Technical Report ESA SP- 1233(1), European Space Agency, The Netherlands (1999).

[Kalman 1960] R. E. Kalman. A new approach to linear filtering and prediction problems. *Transactions of the ASME-Journal of Basic Engineering*, 82(Series D):35–45 (1960).

[Kamgarpour and Tomlin 2008] M. Kamgarpour and C. Tomlin. Convergence properties of a decentralized kalman filter. In *Decision and Control, 2008. CDC 2008. 47th IEEE Conference on*, pages 3205–3210 (2008).

[Kane et al. 1983] T. R. Kane, P. W. Likins and D. A. Levinson. *Spacecraft Dynamics*. McGraw-Hill (1983).

[Kayali 2002] S. Kayali. Utilization of cots electronics in space application, reliability challenges and reality. Technical report, NASA Jet Propulstion Labortory (2002).

[Keshavarzian et al. 2006] A. Keshavarzian, H. Lee and L. Venkatraman. Wakeup scheduling in wireless sensor networks. In *Proceedings of the 7th ACM international symposium on Mobile ad hoc networking and computing*, MobiHoc '06, pages 322–333, New York, NY, USA. ACM (2006).

[Kho et al. 2007] J. Kho, A. Rogers and N. R. Jennings. Decentralised adaptive sampling of wireless sensor networks. In *1st Int Workshop on Agent Technology for Sensor Networks,*, Hawaii, USA (2007).

[Kim et al. 2000] G. Kim, X. Han and R. Chen. An 8-gb/s optical backplane bus based on microchannel interconnects: Design, fabrication and performance measurements. *Lightwave Technology*, 18(11):1477–1486 (2000).

[Kim and Han 2000] J. Kim and J. Han. Development of a distributed OBDH system with MIL-STD-1553B and its applications. In *IEEE Aerospace Conference Proceedings*, pages 243–249 (2000).

[Kimura et al. 2004] S. Kimura, H. Yamamoto, Y. Nagai, H. Hashimoto, N. Takahashi and K. Yoshihara. Single event performance of a cots processor. In 22^{nd} *AIAA International Communications Satellite Systems Conference & Exhibit (ICSSC)*, USA (2004).

[Koelle 1984] D. E. Koelle. Cost reduction trends in space communications by larger satellites/platforms. *Acta Astronautica*, 11(12):785–794 (1984).

[Kopetz 1991] H. Kopetz. Event-triggered versus time-triggered real-time systems. Research Report 8/1991, Technische Universität Wien, Institut für Technische Informatik, Treitlstr. 1-3/182-1, 1040 Vienna, Austria (1991).

[Kopetz and Bauer 2003] H. Kopetz and G. Bauer. The time-triggered architecture. *Proceedings of the IEEE*, 91(1):112–126 (2003).

[Krishnan and Mazzuchi 2001] G. S. Krishnan and T. A. Mazzuchi. Reliability assessment for cots components in space flight applications. Technical report, NASA (2001).

[Lane and Hoots 1979] M. H. Lane and F. R. Hoots. General perturbations theories derived from the 1965 lane drag theory. *NASA STI/Recon Technical Report N*, 80:23347 (1979).

[Lane and Murphy 1962] M. H. Lane and P. M. F. J. J. Murphy. On the representation of air density in satellite deceleration equations by power functions with integral exponents. Technical Report Project Space Track Technical Report No. APGC-TDR-62-15, Air Force Systems Command, Eglin AFB, FL. (1962).

[Lao et al. 1998] N. Y. Lao, T. J. Mosher and J. M. Neff. *Small Satellite Cost Model*. The Aorospace Corporation (1998).

[Lappas et al. 2006] V. Lappas, G. Prassinos, A. Baker and R. Magnuss. Wireless sensor motes for small satellite applications. *IEEE Antennas and Propagation Magazine*, 48(5):175–179 (2006).

[Larson and Wertz 1992] W. J. Larson and J. R. Wertz. *Space Mission Analysis and Design*. Space Technology Library (1992).

[Layton et al. 1998] P. Layton, H. Anthony, R. Boss and P. Hsu. Radiation testing results of cots based space microcircuits. In *Radiation Effects Data Workshop, 1998. IEEE*, pages 170–176 (1998).

[Lee et al. 2003] J. Lee, K. Di Filippo, A. Ng and C. Ribe. Modeling and simulation of a commercial medium sun sensor. In *Control and Automation, 2003. ICCA '03. Proceedings. 4th International Conference on*, pages 728–732 (2003).

[Lee 2005] W. Lee. *Wireless and Cellular Telecommunications*. McGraw-Hill Professional, 3 edition (2005).

[Li et al. 2009] S. Li, G. Fan and G. Xu. Application of wireless satellite bus in micro-satellite design. In *Mechatronics and Automation, 2009. ICMA 2009. International Conference on*, pages 2612–2616 (2009).

[Li et al. 1992] Y. Li, T. Jaing and J. Sharon. Massively parallel free-space optical Clos network using wavelength-division multiple access. *Electrical Letters*, 28(21):2002–2003 (1992).

[Liu 2000] J. W. S. W. Liu. *Real-Time Systems*. Prentice Hall PTR, Upper Saddle River, NJ, USA, 1st edition (2000).

[Liu and Goldsmith 2004] X. Liu and A. Goldsmith. Kalman filtering with partial observation losses. In *Decision and Control, 2004. CDC. 43rd IEEE Conference on*, volume 4, pages 4180–4186 (2004).

[Lockheed Martin 1998] Lockheed Martin. Koreasat 3 cdr. Technical report, Lockheed Martin (1998).

[Lopez et al. 2004] F. T. Lopez, P. Roos, L. Stagnaro, C. Plummer and B. Storni. The can bus in spacecraft on board applications. In *Proceedings of DASIA Conference*, France (2004).

[Lorenz et al. 2004] E. Lorenz, W. Borwald, K. Briess, H. Kayal, M. Schneller and H. Wuensten. Resumes of the bird mission. In *Proceedings of The 4S Symposium: Small Satellites, Systems and Services (ESA SP-571)*, page 31.1 (2004).

[Maeusli 1994] D. Maeusli. *Towards and upgraded ESA On Board Data Handling Subsytem (ESA OBDH-9x). Motivation and Upgrades summary*. ESA-ESTEC On-board Information Management Section, 1 edition (1994).

[Magness 2003] R. Magness. A comparison of can and bluetooth protocols a study for application of can over bluetooth for wireless on-board data handling for a spacecraft sensor network. In *DASIA 2003*, volume 532 of *ESA Special Publication* (2003).

[Magness 2006] R. Magness. TEC-E wireless technology dossier - wireless onboard spacecraft and in space exploration. Technical Report REF. TOSE-1B-DOS-4, ESA/ESTEC (2006).

[Magness et al. 2004] R. Magness, P. Plancke, I. Hernandez and C. Plummer. Current activities and status of the esa/estec-industry wireless onboard spacecraft working group. In *4th Space Internet Workshop*, Baltimore, USA. ESA (2004).

[Mahr and Richardson 2003] E. Mahr and G. Richardson. Development of the small satellite cost model (SSCM) edition 2002. In *Aerospace Conference, 2003. Proceedings. 2003 IEEE*, volume 8, pages 3831–3841 (2003).

[MAI400] MAI400 *MAI-400 Single Axis Reaction Wheel Assembly*. Maryland Aerospace, Hampshire,, UK.

[Mane et al. 2011] P. Mane, J. Xie, K. K. Leang and K. Mossi. Cyclic energy harvesting from pyroelectric materials. *IEEE Transactions on Ultrasonics, Ferroelectrics and Frequency Control*, 58(1):10–17 (2011).

[Marbini and Sacks 2003] A. D. Marbini and L. E. Sacks. Adaptive sampling mechanisms in sensor networks. Technical report, University College London (2003).

[Markley 1988] F. L. Markley. Attitude determination using vector observations and the singular value decomposition. *Journal of the Astonautical Sciences*, 38:245–258 (1988).

[Markley 1993] F. L. Markley. Attitude determination using vector observations: a fast optimal matrix algorithm. *Journal of the Astonautical Sciences*, 41(2):261–280 (1993).

[Markley 2004] F. L. Markley. Attitude estimation or quaternion estimation? *The Journal of the Astronautical Sciences*, 52(1&2):221–238 (2004).

[Maybeck 1979] P. S. Maybeck. *Stochastics Models, Estimation, and Control*, volume 1. Academic Press (1979).

[Meltzer 2015] M. Meltzer. *The Cassini-Huygens visit to Saturn: An Historic Mission to the Ringed Planet*. Springer (2015).

[Menichelli et al. 2000] M. Menichelli, R. Battiston, S. Bizzaglia, S. Blasko, G. Castellini, L. D. D. Masso, A. Gabbanini, A. Papi, G. Scolieri and M. Tesi. Total dose test of commercial off-the-shelf components to be used in power supply for space experiments. *IEEE Transactions on Nuclear Science*, 47:1879–1884 (2000).

[Menichelli et al. 2002] M. Menichelli, R. Battiston, S. Bizzaglia, S. Blasko, L. di Masso, A. Papi, G. Scolieri, G. Castellini, A. Gabbanini and M. Tesi. Total Dose Test for Commercial Off-The Components to BE Used in a Space Experiment:. a Survey on Current Technologies. In M. Barone, E. Borchi, J. Huston, C. Leroy, P. G. Rancoita, P. Riboni, & R. Ruchti, editor, *Advanced Technology - Particle Physics*, pages 792–799 (2002).

[Miler et al. 2002] J. Miler, J.Guerrero, D. Goldstein and T. Robinson. Modular spacecraft building blocks for plug and play spacecraft. In *16th Annual AIAA/USU Conference on Small Satellites*, Utah, USA (2002).

[Misic and Misic 2008] J. Misic and V. Misic. *Wireless Personal Area Networks: Performance, Interconnection, and Security with IEEE 802.15.4*. Wiley, 1 edition (2008).

[Montenbruck and Eberhard 2000] O. Montenbruck and G. Eberhard. *Satellite Orbits: Models, Methods, and Applications*. Physics and Astronomy Online Library. Springer London, Limited (2000).

[Morita et al. 2007] K. Morita, K. Watanabe, N. Hayashibara and M. Takizawa. An efficient data transmission protocol in a wireless sensor-actuator network. In *Complex, Intelligent and Software Intensive Systems, 2007. CISIS 2007. First International Conference on*, pages 11–18 (2007).

[Murthy and Manoj 2004] C. S. R. Murthy and B. S. Manoj. *Ad Hoc Wireless Networks: Architectures and Protocols*. Prentice Hall, 1 edition (2004).

[Mutazono et al. 2010] A. Mutazono, M. Sugano and M. Murata. Energy efficient sleep scheduling in wireless sensor networks inspired by satellite behavior of frogs. In *Pervasive Computing and Communications Workshops (PERCOM Workshops), 2010 8th IEEE International Conference on*, pages 450–455 (2010).

[Naik and Sivalingam 2004] P. Naik and K. M. Sivalingam. *A survey of MAC protocols for sensor networks*, pages 93–107. Kluwer Academic Publishers, Norwell, MA, USA (2004).

[Narvaez 2003] P. Narvaez. System level emc testing of spacecraft. In *EMC IEEE 2003 Symposium* (2003).

[NASA 2009] NASA. *National Polar-Orbiting Operational Environmental Satellite System (NPOESS) Preparatory Project (NPP) Mission Data Format Control Book (MDFCB)*. NASA Goddard Space Flight Center, USA, revision A edition (2009).

[NLR 1993] NLR. Annual report 1993. Technical report, Nationaal Lucht- en Ruimtevaartlaboratorium (1993).

[Nolas et al. 2001] G. S. Nolas, J. Sharp and H. J. Goldsmid. *Thermoelectrics : basic principles and new materials developments / G.S. Nolas, J. Sharp, H.J. Goldsmid*. Springer (2001).

[Nuwayhid and Hamade 2005] R. Nuwayhid and R. Hamade. Design and testing of a locally made loop-type thermosyphonic heat sink for stove-top thermoelectric generators. *Renewable Energy*, 30(7):1101–1116 (2005).

[Oria et al. 2006] C. Oria, A. Torralba, V. Baena, J. Granado and J. ChÃČÂąvez. Power line communications: Application to space. In *Wireless for Space Applications Workshop 2006*, Noordwijk, The Netherlands. ESA/ESTEC (2006).

[Park 2011] P. Park. *Modeling, Analysis and Design of Wireless Sensor Network Protocols*. PhD thesis, KTH School of Electrical Engineering (2011).

[Parkes 2001] S. Parkes. Spacewire: a satellite on-board data-handling network. *Aircraft Engineering and Aerospace Technology: An International*, 73(4):374–379 (2001).

[Patel 1999] M. Patel. *ind and Solar Power Systems*. CRC Press LLC (1999).

[Paulson et al. 1969] D. C. Paulson, D. B. Jackson and C. D. Brown. Spars algorithms and simulation results. In *Symposium on Spacecraft Attitude Estimation*, volume 1, pages 293–317 (1969).

[Pelissou et al. 2005] P. Pelissou, A. S. adn Francisco Jose Lopez Hernandez, P. Plancke and I. H. Velasco. Validation of a wireless optical layer for on-board data communications. Technical report, EADS ASTRIUM (2005).

[Philips Semiconductor 2000] Philips Semiconductor. *THE I^2C BUS SPECIFICATION VERSION 2.1*. Philips Semiconductor (2000).

[Plummer 1996] C. Plummer. *4-255 Data Bus Specification*. Cotectic Ltd., draft 1.1.f edition (1996).

[Plummer and Planck 2001] C. Plummer and P. Planck. Spacecraft harness reduction study. Technical Report RE-01247-CP/009, Cotectic Ltd. (2001).

[Plummer et al. 2003] C. Plummer, P. Roos and L. Stagnaro. Can bus as a spacecraft onboard bus. In *Proceedings of DASIA 2003 (ESA SP-532)*, page 51.1, Czech Republic. ESA (2003).

[Polastre et al. 2004] J. Polastre, J. Hill and D. Culler. Versatile low power media access for wireless sensor networks. In *Proceedings of the 2nd international conference on Embedded networked sensor systems*, SenSys '04, pages 95–107, New York, NY, USA. ACM (2004).

[Quwaider and Biswas 2010] M. Quwaider and S. Biswas. *Wireless Body Area Networks: A Framework of Network-integrated Sensing and Energy-aware Protocols for Resource- constrained Applications in Wireless Body Area Networks*. VDM Verlag Dr. Müller (2010).

[Raghunathan et al. 2002] V. Raghunathan, C. Schurgers, S. Park, M. Srivastava and B. Shaw. Energy-aware wireless microsensor networks. In *IEEE Signal Processing Magazine*, pages 40–50 (2002).

[Rahimi et al. 2005] M. Rahimi, R. Baer, O. I. Iroezi, J. C. Garcia, J. Warrior, D. Estrin and M. Srivastava. Cyclops: in situ image sensing and interpretation in wireless sensor networks. In *Proceedings of the 3rd international conference on Embedded networked sensor systems*, SenSys '05, pages 192–204, New York, NY, USA. ACM (2005).

[Rakow et al. 2006] G. Rakow, R. Schnurr and S. Parkes. Spacewire protocol ID: What does it means to you? In *IEEE Aerospace Conference 2006*, pages 1–7 (2006).

[Ravichandran et al. 2009] P. Ravichandran, S. Kulkarni, S. Sharma, H. Vasudevamurthy, M. Vanitha and P. Lakshminarsimhan. Wireless telecommand and telemetry systems for satellite communication using zigbee network. *Advances in Recent Technologies in Communication and Computing, International Conference on*, pages 274–278 (2009).

[Rhee et al. 2005] I. Rhee, A. Warrier, M. Aia and J. Min. Z-mac: a hybrid mac for wireless sensor networks. In *Proceedings of the 3rd international conference on Embedded networked sensor systems*, SenSys '05, pages 90–101, New York, NY, USA. ACM (2005).

[Rhee and Lyou 2012] S.-H. Rhee and J. Lyou. Development of a fine digital sun sensor for stsat-2. *International Journal of Aeronautics & Space Science*, 13(2):260–265 (2012).

[Rockwell Collins 1997] Rockwell Collins. Specifications for the rockwell collins 60J-3 gps embedded module-phase III (GEM III) receiver cpn 822-0453-001 and 822-0453-005 for use in the user equipment segment of the NAVSTAR global positioning system. Technical Report CPN 752-9085-001, Rev. F, Rockwell Collins (1997).

[Roming et al. 2005] P. W. A. Roming, T. E. Kennedy, K. O. Mason, J. A. Nousek, L. Ahr, R. E. Bingham, P. S. Broos, M. J. Carter, B. K. Hancock, H. E. Huckle, S. D. Hunsberger, H. Kawakami, R. Killough, T. S. Koch, M. K. McLelland, K. Smith, P. J. Smith, J. C. Soto, P. T. Boyd, A. A. Breeveld, S. T. Holland, M. Ivanushkina, M. S. Pryzby, M. D. Still and J. Stock. The swift ultraviolet/optical telescope. *AIP Conf. Proc.*, 727:651–654 (2005).

[Roshan 2004] P. Roshan. *802.11 Wireless LAN Fundamentals*. Cisco Press (2004).

[Rouault 2006] H. Rouault. Self-powering techniques for wireless intra satellite communication. In *Wireless for Space Applications Workshop 2006*, Noordwijk, The Netherlands. ESA/ESTEC (2006).

[Rushby 2003] J. Rushby. A comparison of bus architectures for safety-critical embedded systems. Technical Report NASA/CR-2003-212161, NASA (2003).

[Russek 1994] L. G. Russek. Alarm for patient monitor and life support equipment system. US Patent (1994).

[Sakano et al. 1991] T. Sakano, K. Noguchi and T. Matsumoto. Performance of lightwave interconnection using spatial addressing (LISA) and its application for multiprocessor systems. *Lightwave Technology*, 9(12):1733–1741 (1991).

[Santamaria et al. 2003] A. Santamaria, F. Lopez-Hernandez, H. Guerrero, I. Arruego and S. Rodriguez. Wireless infra-red links for intra-satellite communications. In *DASIA 2003*, volume 532 of *ESA Special Publication* (2003).

[Santini and Römer 2006] S. Santini and K. Römer. An adaptive strategy for quality-based data reduction in wireless sensor networks. In *Proceedings of the 3rd International Conference on Networked Sensing Systems (INSSâĂŹ06*, pages 29–36 (2006).

[Scheler and Schröder-Preikschat 2006] F. Scheler and W. Schröder-Preikschat. Time-triggered vs. event-triggered: A matter of configuration? In *Proceedings of the GI/ITG Workshop on non-Functional Properties of Embedded Systems*, pages 107–112. VDE Verlag GmbH (2006).

[Schild and Würtz 1997] K. Schild and J. Würtz. Off-line scheduling of a real-time system. In *Proceedings of CP97 Workshop on Industrial Constraint-Directed Scheduling*, pages 29–38. ACM Press (1997).

[Schurgers et al. 2002] C. Schurgers, V. Tsiatsis and M. Srivastava. Stem: Topology management for energy efficient sensor networks. In *Aerospace Conference Proceedings, 2002. IEEE*, volume 3, pages 1099–1108 (2002).

[Schuster et al. 2002] R. Schuster, I. Walter, D. Hundertmark and F. Schrandt. Design and calibration of the BIRD payload platform. In *Pecora 15/Land Satellite Information IV Conference, ISPRS Commission I Mid-term Symposium/FIEOS (Future Intelligent Earth Observing Satellites)* (2002).

[Seah et al. 2009] W. Seah, Z. A. Eu and H.-P. Tan. Wireless sensor networks powered by ambient energy harvesting (wsn-heap) - survey and challenges. In *Wireless Communication, Vehicular Technology, Information Theory and Aerospace Electronic Systems Technology, 2009. Wireless VITAE 2009. 1st International Conference on*, pages 1–5 (2009).

[Shuster 1993] M. D. Shuster. Survey of attitude representations. *Journal of the Astronautical Sciences*, 41:439–517 (1993).

[Shuster 2006] M. D. Shuster. The generelized wahba problem. *The Journal of Astronautical Sciences*, 54:245–259 (2006).

[Silberstein et al. 2006] A. Silberstein, R. Braynard and J. Yang. Constraint chaining: on energy-efficient continuous monitoring in sensor networks. In *Proceedings of the 2006 ACM SIGMOD international conference on Management of data*, SIGMOD '06, pages 157–168, New York, NY, USA. ACM (2006).

[Singla et al. 2004] P. Singla, D. Mortari, and J. Junkins. How to avoid singularity for Euler angle set? In *2004 Space Flight Mechanics Meeting Conference*, Hawaii (2004).

[Sinha and Chandrakasan 2001] A. Sinha and A. Chandrakasan. Dynamic power management in wireless sensor networks. *Design Test of Computers, IEEE*, 18(2):62–74 (2001).

[Sinopoli et al. 2003] B. Sinopoli, L. Schenato, M. Franceschetti, K. Poolla, M. Jordan and S. Sastry. Kalman filtering with intermittent observations. In *Decision and Control, 2003. Proceedings. 42nd IEEE Conference on*, volume 1, pages 701–708 (2003).

[Smith et al. 2003] J. Smith, C. Plummer and P. Plancke. Standardization activity for spacecraft onboard interfaces. In *Proceedings of IEEE Aerospace Conference*, volume 3, pages 1281–1289 (2003).

[Soltero et al. 2002] M. Soltero, J. Zhang and C. Cockril. 422 and 485 standards overview and system configurations. Technical report, Texas Instruments (2002).

[Sontag 1998] E. Sontag. *Mathematical Control Theory: Deterministic Finite Dimensional Systems*. Texts in Applied Mathematics. Springer (1998).

[Stone et al. 2012] T. Stone, R. Alena, J. Baldwin and P. Wilson. A viable cots based wireless architecture for spacecraft avionics. In *Aerospace Conference, 2012 IEEE*, pages 1–11 (2012).

[Stuelpnagel 1964] J. Stuelpnagel. On the parametrization of the three-dimensional rotation group. *Siam Review*, 6 (1964).

[Sundaramoorthy et al. 2010] P. Sundaramoorthy, E. Gill and C. Verhoeven. Formation flying within a constellation of nano-satellites: The qb50 mission. In *61st International Astronautical Congress*, Prague (2010).

[Szerdahelyi 2003] L. Szerdahelyi. Secondary AOCS design. Technical Report HYP-2-01, Astrium Gmbh (2003).

[Tai et al. 1999] A. Tai, S. Chau and L. Alkalai. COTS-based fault tolerance in deep space: qualititative and quantitative analyses of a bus network architecture. In *IEEE International Symposium on High Assurance Systems Engineering*, pages 97–104 (1999).

[Tang and Cao 2008] M. Tang and J. Cao. An energy-efficient data-driven power management for wireless sensor networks. In *Proceedings of the 5th workshop on Data management for sensor networks*, DMSN '08, pages 21–27, New York, NY, USA. ACM (2008).

[Taylor et al. 2005] J. Taylor, A. Makovsky, A. Barbieri, R. Tung, P. Estabrook and A. G. Thomas. Mars exploration rover telecommunications. Technical report, NASA Jet Propulsion Laboratory (2005).

[Texas Instruments 2010] Texas Instruments. *CC2533: An Optimized System-on-Chip Solution for 2.4-GHz IEEE 802.15.4 Remote Control* (2010). `http://www.ti.com/lit/ds/swrs087/swrs087.pdf`.

[Thorpe and Labs 2009] D. Thorpe and T. Labs. Economics of launch vehicles & two configurations for tremendous cost reductions. In 45^th *AIAA/ASME/SAE/ASEE Joint Propulsion Conference & Exhibit*. AIAA (2009).

[Trautner et al. 2008] R. Trautner, P. Armbruster, P. Fabry, A. Fernandez-Leon, J. Ilstad, D. Jameux, M. Suess and R. Weigand. Avionics architectures and components for planetary entry probe payloads and systems. In *Proceedings of International Planetary Probe Workshop* (2008).

[Tulone and Madden 2006] D. Tulone and S. Madden. Paq: time series forecasting for approximate query answering in sensor networks. In *In EWSN*, pages 21–37 (2006).

[Ubbels et al. 2005] W. Ubbels, A. Bonnema, E. van Breukelen, J. Doorn, R. van den Eikhoff, E. V. der Linden, G. Aalbers, J. Rotteveel, R. Hamann and C. Verhoeven. Delfi-C3: a student nanosatellite as a test-bed for thin film solar cells and wireless onboard communication. In *Recent Advances in Space Technologies 2005 (RAST 2005)*, pages 167–172 (2005).

[Umehira et al. 2008] M. Umehira, H. Saito, O. Kagami, T. Fujita and Y. Fujino. Design and experiments of wide area wireless network for sensors and actuators. In *Information and Telecommunication Technologies, 2008. APSITT. 7th Asia-Pacific Symposium on*, pages 263–268 (2008).

[Underwood 2003] C. I. Underwood. Observations of radiation in the space radiation environment and its effect on commercial off-the-shelf electronics in low-earth orbit. *Philosophical Transactions of the Royal Society of London. Series A: Mathematical, Physical and Engineering Sciences*, 361(1802):193–197 (2003).

[van der Ha and Shuster 2009] J. van der Ha and M. Shuster. A tutorial on vectors and attitude [focus on education]. *Control Systems, IEEE*, 29(2):94–107 (2009).

[van Ingen Schenau et al. 1998] H. van Ingen Schenau, L. van Rijn and J. Spaa. Test and verigication equipment for the attitude & orbit contorl system of the xmm satellite. Technical Report NLR-TP-98236, Nationaal Lucht- en Ruimtevaartlaboratorium (1998).

[Verdone 2004] R. Verdone. An energy-efficient decentralised communication protocol for a network of uniformly distributed sensors polled by a wireless transceiver. In *IEEE International Conference on Communications*, volume 6, pages 3491–3498 (2004).

[Vuran et al. 2004] M. C. Vuran, O. B. Akan and I. F. Akyildiz. Spatio-temporal correlation: theory and applications for wireless sensor networks. *Comput. Netw.*, 45:245–259 (2004).

[Wagner and Barton 2012] R. Wagner and R. Barton. Performance comparison of wireless sensor network standard protocols in an aerospace environment:

Isa100.11a and zigbee pro. In *Aerospace Conference, 2012 IEEE*, pages 1–14 (2012).

[Wahba 1965] G. Wahba. A least squares estimate of satellite attitude. 7(3):409–409 (1965).

[Walts et al. 2001] S. C. Walts, W. Schneider, M. A. G. Darrin, B. G. Boone and P. J. Luers. Infrared communications for small spacecraft: from a wireless bus to cluster concepts. In *Society of Photo-Optical Instrumentation Engineers (SPIE) Conference Series*, volume 4395, pages 200–213 (2001).

[Webb 2002] E. Webb. Ethernet for space flight applications. In *Aerospace Conference Proceedings, 2002. IEEE*, volume 4, pages 1927–1934 (2002).

[Wie 1998] B. Wie. *Space Vehicle Dynamics and Control*. American Institute of Aeronautics and Astronautics (1998).

[Willett et al. 2004] R. Willett, A. Martin and R. Nowak. Backcasting: adaptive sampling for sensor networks. In *Proceedings of the 3rd international symposium on Information processing in sensor networks*, IPSN '04, pages 124–133, New York, NY, USA. ACM (2004).

[Wilson and Atkinson 2013] W. Wilson and G. Atkinson. Wireless sensor applications in extreme aeronautical environments. In *Wireless for Space and Extreme Environments (WiSEE), 2013 IEEE International Conference on*, pages 1–6 (2013).

[Wilson and Juarez 2014] W. C. Wilson and P. D. Juarez. Emerging needs for pervasive passive wireless sensor networks on aerospace vehicles. In *The 5th International Conference on Emerging Ubiquitous Systems and Pervasive Networks (EUSPN-2014)/ The 4th International Conference on Current and Future Trends of Information and Communication Technologies in Healthcare (ICTH 2014)/ Affiliated Workshops, September 22-25, 2014, Halifax, Nova Scotia, Canada*, pages 101–108 (2014).

[Wojtczuk et al. 2010] S. Wojtczuk, P. Chiu, X. Zhang, D. Derkacs, C. Harris, D. Pulver and M. Timmons. Ingap/gaas/ingaas 41 In *Photovoltaic Specialists Conference (PVSC), 2010 35th IEEE*, pages 1259–1264 (2010).

[Wolfram and Bloom 2004] K. Wolfram and H. Bloom. New radiation-hardened high-speed serial data bus for satellite onboard communication. In *Geoscience and Remote Sensing Symposium, 2004. IGARSS '04. Proceedings. 2004 IEEE International*, volume 1, pages 7 vol. (cviii+4896) (2004).

[Woodroffe and Madle 2004] A. M. Woodroffe and P. Madle. Application and experience of can as a low cost obdh bus system. In *Proceedings of MAPLD conference*, USA (2004).

[Xie 2014] S. Xie. Wireless sensor network for satellite applications: A survey and case study. *Unmanned Systems*, 2(3) (2014).

[Xing et al. 2008] F. Xing, Z. You, G. Zhang and J. Sun. A novel active pixels sensor (aps) based sun sensor based on a feature extraction and image correlation (feic) technique. *Measurement Science and Technology*, 19(12):125203 (2008).

[Xu et al. 2001] Y. Xu, J. Heidemann and D. Estrin. Geography-informed energy conservation for ad hoc routing. In *Proceedings of the 7th annual international conference on Mobile computing and networking*, MobiCom '01, pages 70–84, New York, NY, USA. ACM (2001).

[Ye and Heidemann 2004] W. Ye and J. Heidemann. *Medium access control in wireless sensor networks*, pages 73–91. Kluwer Academic Publishers, Norwell, MA, USA (2004).

[Ye et al. 2004] W. Ye, J. Heidemann and D. Estrin. Medium access control with coordinated adaptive sleeping for wireless sensor networks. *IEEE/ACM Trans. Netw.*, 12:493–506 (2004).

[Ye et al. 2002] W. Ye, J. Heidemann, D. Estrin and A. P. P. S-mac. An energy-efficient mac protocol for wireless sensor networks. In *Proceedings of the IEEE INFOCOM*, volume 3, pages 1567–1576 (2002).

[Yuanyuan et al. 2008] L. Yuanyuan, M. Wei, S. Donglin and T. Bihua. Emc test and frequency allocation of wsn used in spacecraft. In *Antennas, Propagation and EM Theory, 2008. ISAPE 2008. 8th International Symposium on*, pages 1131–1134 (2008).

[Zhang et al. 2009] J. Zhang, W. Li, Z. Yin, S. Liu and X. Guo. Forest fire detection system based on wireless sensor network. In *Industrial Electronics and Applications, 2009. ICIEA 2009. 4th IEEE Conference on*, pages 520–523 (2009).

[Zhang et al. 2004] K. L. Zhang, S. K. Chou and S. S. Ang. Development of a solid propellant microthruster with chamber and nozzle etched on a wafer surface. *Journal of Micromechanics and Microengineering*, 14:785–792 (2004).

[Zheng et al. 2003] R. Zheng, J. C. Hou and L. Sha. Asynchronous wakeup for ad hoc networks. In *Proceedings of the 4th ACM international symposium on Mobile ad hoc networking & computing*, MobiHoc '03, pages 35–45, New York, NY, USA. ACM (2003).

[Zuquim et al. 2003] A. Zuquim, L. Vieira, M. Vieira, A. Vieira, H. Carvalho, J. Nacif, J. C.N. Coelho, J. D.C. da Silva, A. Fernandes and A. Loureiro. Efficient power management in real-time embedded systems. In *Emerging Technologies and Factory Automation, 2003. Proceedings. ETFA '03. IEEE Conference*, volume 1, pages 496–505 (2003).

Index

Curriculum Vitae

Rouzbeh Amini was born in Ahvaz, Iran. In 2003, he received his B.Sc. in Electrical and Control Engineering from Sharif University of Technology, Tehran, Iran. In Summer 2003, he was admitted to Master of Science program at Aalborg University (AAU) in Denmark to continue his education in Electrical Engineering with focus on Intelligent Autonomous Systems. During the course of his study at AAU, Rouzbeh worked on modeling and control of advanced systems, fault detection, fault diagnosis and attitude determination and control for spacecraft. He worked on AAUSAT-II CubeSat and designed its attitude determination system with his team. AAUSAT-II was successfully launched on April 28, 2008. He also worked on fault diagnosis for spacecraft in re-entry mode as a research assistant. Rouzbeh's MS thesis was on modeling and defect detection of a novel multilayer piezoelectric motor. Rouzbeh's MS graduation thesis was recognized as an exceptionally independent and excellent performance which is most rarely given in Danish universities and requires a performance far beyond the expected.

In Fall 2005, Rouzbeh joined Space Systems Engineering (SSE) chair of Faculty of Aerospace Engineering at Delft University of Technology as a PhD student. His research was on feasibility of using wireless communication onboard spacecraft to reduce the onboard harness. He was also appointed as a researcher and supervisor to help Delfi-C3 CubeSat program which was successfully launched on April 28, 2008 along with AAUSAT-II CubeSat. He later contributed to Delfi-n3Xt three-unit CubeSat program as a supervisor which was successfully launched on November 21, 2013.

Rouzbeh currently works in home automation and control industry with focus on system architecture, integration and wireless solutions.

His research interests are in system design and integration, wireless sensor networks and navigation technologies.